HHS Public Access

Author manuscript

Chem Rev. Author manuscript; available in PMC 2021 April 22.

Published in final edited form as:

Chem Rev. 2020 April 22; 120(8): 3787–3851. doi:10.1021/acs.chemrev.9b00738.

ImmunoPET: Concept, Design, and Applications

Weijun Wei,
Department of Nuclear Medicine, Renji Hospital, School of Medicine, Shanghai Jiao Tong University, Shanghai 200127, China;

Departments of Radiology and Medical Physics, University of Wisconsin—Madison, Madison, Wisconsin 53705, United States

Zachary T. Rosenkrans,
Department of PharmaceuticalSciences, University of Wisconsin—Madison, Madison, Wisconsin 53705, United States

Jianjun Liu,
Department of Nuclear Medicine, Renji Hospital, School of Medicine, Shanghai Jiao Tong University, Shanghai 200127, China

Gang Huang,
Department of Nuclear Medicine, Renji Hospital, School of Medicine, Shanghai Jiao Tong University, Shanghai 200127, China;

Shanghai Key Laboratory of Molecular Imaging, Shanghai University of Medicine and Health Sciences, Shanghai 201318, China

Quan-Yong Luo,
Department of Nuclear Medicine, Shanghai Jiao Tong University Affiliated Sixth People's Hospital, Shanghai 200233, China

Weibo Cai
Departments of Radiology and Medical Physics and Department of Pharmaceutical Sciences, University of Wisconsin—Madison, Madison, Wisconsin 53705, United States;

University of Wisconsin Carbone Cancer Center, Madison, Wisconsin 53705, United States

Abstract

Immuno-positron emission tomography (immunoPET) is a paradigm-shifting molecular imaging modality combining the superior targeting specificity of monoclonal antibody (mAb) and the inherent sensitivity of PET technique. A variety of radionuclides and mAbs have been exploited to develop immunoPET probes, which has been driven by the development and optimization of radiochemistry and conjugation strategies. In addition, tumor-targeting vectors with a short circulation time (e.g., Nanobody) or with an enhanced binding affinity (e.g., bispecific antibody) are being used to design novel immunoPET probes. Accordingly, several immunoPET probes,

Corresponding Authors: Weibo Cai – Phone: (608)262-1749; wcai@uwhealth.org, **Quan-Yong Luo** – luoqy@sjtu.edu.cn, **Gang Huang** – huanggang@sumhs.edu.cn.
Complete contact information is available at: https://pubs.acs.org/10.1021/acs.chemrev.9b00738

The authors declare no competing financial interest.

such as ^{89}Zr-Df-pertuzumab and ^{89}Zr-atezolizumab, have been successfully translated for clinical use. By noninvasively and dynamically revealing the expression of heterogeneous tumor antigens, immunoPET imaging is gradually changing the theranostic landscape of several types of malignancies. ImmunoPET is the method of choice for imaging specific tumor markers, immune cells, immune checkpoints, and inflammatory processes. Furthermore, the integration of immunoPET imaging in antibody drug development is of substantial significance because it provides pivotal information regarding antibody targeting abilities and distribution profiles. Herein, we present the latest immunoPET imaging strategies and their preclinical and clinical applications. We also emphasize current conjugation strategies that can be leveraged to develop next-generation immunoPET probes. Lastly, we discuss practical considerations to tune the development and translation of immunoPET imaging strategies.

Graphical Abstract

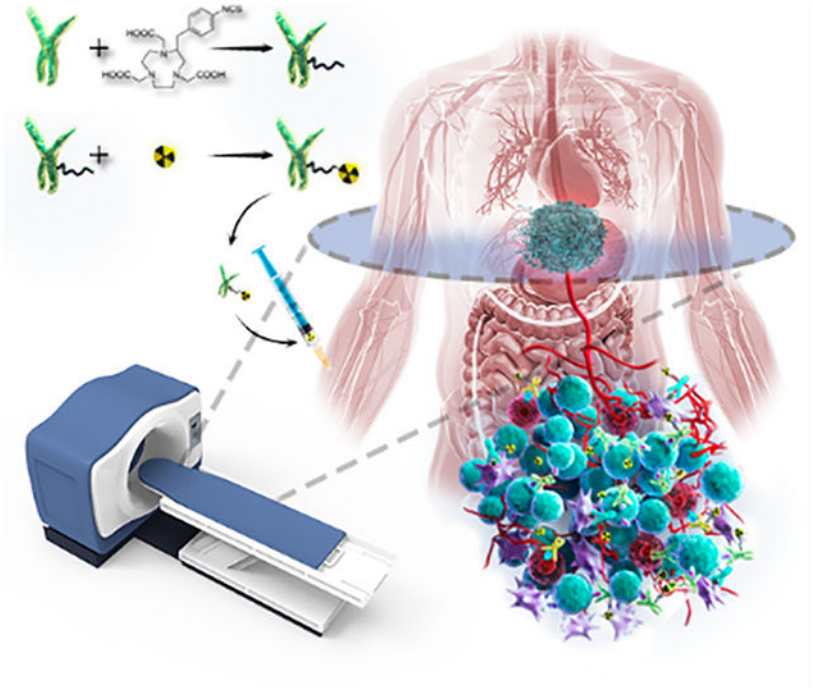

1. INTRODUCTION

Molecular imaging is defined as “visualization, characterization, and measurement of biological processes at the molecular and cellular levels in humans and other living systems” by using molecular imaging agents and tools.[1] Positron emission tomography (PET) imaging is the foundation of molecular imaging and has drastically improved global healthcare since its inception in the clinical practice.[2–4] With the gradual discovery of the molecular pathogenesis of cancers and contemporaneous understanding of the host immune system, molecularly targeted therapies (e.g., small-molecule inhibitors and monoclonal antibodies [mAbs]) and immunotherapies (e.g., immune checkpoint inhibitors) have been developed. The clinical use of these novel regimens is changing the therapeutic landscape

for numerous cancers.[5–7] In the era of molecularly targeted therapy and cancer immunotherapy, it is clear that PET imaging with traditional radiotracers is inadequate.[8] For instance, 18F-fluorodeoxyglucose (^{18}F-FDG) PET/computed tomography (CT) has been integrated into several criteria in predicting and assessing responses to targeted therapies or immunotherapies.[9,10] However, several studies have reported that 18F-FDG PET/CT parameters, such as SUVmax and SUVmean, did not correlate with clinical responses for immunotherapy regimens.[11,12] Additionally, it is challenging to differentiate immune-related adverse events (e.g., sarcoidosis) and pseudoprogression on ^{18}F-FDG PET images,[13,14] leading to misinterpretation.

To further improve the clinical management of cancers and noncancerous diseases, the integration of novel molecular imaging approaches into routine diagnostic toolbox is critically important.[15] Antibody-derived molecular imaging probes have been instrumental in visualizing target expression and pharmacokinetics of therapeutic mAbs in living subjects. Although several antibody-based tracers for single-photon emission computed tomography (SPECT) imaging exist in the clinic,[16] PET imaging with antibody-based tracers has distinct advantages in terms of image quality, spatial resolution, and quantification.[17]

2. CONCEPT OF IMMUNOPET

Immuno-positron emission tomography (immunoPET or iPET), which exquisitely fuses the extraordinary targeting specificity of mAb and the superior sensitivity and resolution of PET, is a paradigm shift for molecular imaging modalities.[18] The concept of immunoPET was manifested more than two decades ago,[19,20] but its development rapidly accelerated in recent years with the increasing approval of therapeutic antibodies and the more widespread production of long half-life radionuclides. Meanwhile, the concept of immunoPET has evolved over the years with the incorporation of antibody fragments or mimetics as targeting moieties. More importantly, the clinical application of immunoPET imaging has increased our understanding of tumor heterogeneity and refined clinical disease management. For instance, the status of programmed death ligand-1 (PD-L1) assessed by ^{89}Zr-atezolizumab immunoPET, but not by immunohistochemistry (IHC) or RNA sequencing, predicted the therapeutic response of atezolizumab in patients with three types of tumors.[21]

Despite the existence of several reviews on immunoPET, there are none that comprehensively describe the design strategies and the application landscape of this novel imaging modality. In this review, we first elaborate on the development of immunoPET imaging strategies by introducing positron-emitting radionuclides, associated chelators, targeting vectors (e.g., mAbs and antibody fragments), as well as traditional and novel conjugation strategies. We then introduce the role of immunoPET in imaging cancers and noncancerous diseases, followed by a recapitulation of how immunoPET imaging aids in the development of antibody and antibody-based therapeutics. In the last part of the review, we discuss practical considerations for future development and translation of immunoPET imaging tracers.

3. DESIGN AND CONJUGATION STRATEGIES OF IMMUNOPET

ImmunoPET applications require simple, fast, and specific radiolabeling of antibody vectors under mild conditions. Optimal immunoPET imaging is attributed to a highly specific tumor uptake and low background retention. Toward this end, it is essential for a tracer to specifically saturate its target as fast as possible, with the unbound tracer cleared out rapidly from the blood circulation. Generally, the successful development of immunoPET probes is highly dependent on the choice of tumor-targeting vectors, radionuclides, bifunctional chelators, and conjugation strategies as discussed below.

3.1. Antibodies, Antibody Fragments, and VHHs

3.1.1. Full-Length Antibodies.—The development and use of mAbs have achieved considerable success, and various kinds of mAbs have been adapted to treat solid tumors, hematological malignancies, as well as noncancerous diseases.[5,22–24] In 2018, the Food and Drug Administration (FDA) and European Medicines Agency (EMA) approved 13 antibody therapeutics for clinical use.[25] Although only five new antibody therapeutics were approved in 2019, it is anticipated that at least 13 products will be granted approval in 2020.[26] The therapeutic mechanisms of mAbs mainly include antibody-dependent cell-mediated cytotoxicity (ADCC), antibody-dependent cellular phagocytosis (ADCP), complement-dependent cytotoxicity (CDC), interruption of a signaling pathway, inhibition of enzymatic activity, and inhibition of immune checkpoint, which are discussed extensively in other reviews.[27,28] For therapeutic purposes, immunoglobulin G (IgG) is considered to have the most favorable balance between clearance and tumor uptake.[29] Over the past decade, immunoPET imaging with radiolabeled mAbs has progressed rapidly together with the development of antibody engineering and production of long-lived PET radionuclides.[18] Currently, mAb-based immunoPET imaging is being actively investigated in preclinical models and has attracted considerable attention in clinical practice. The tumor-targeting and treatment efficacy of mAbs can be maximized by generating bispecific antibodies (BsAb) or trispecific antibodies.[30,31] By targeting multiple tumor antigens, these novel polyspecific antibodies are alternatives for developing immunoPET probes.[32]

3.1.2. Limitations of Full-Length mAbs in Immuno-PET Imaging.—Despite the clinical success, mAb-derived immunoPET probes suffer from several disadvantages. First, the size of mAb (150 kDa; Figure 1a) exceeds the clearance cutoff value (60 kDa) of glomerular filtration. Additionally, the interaction between the Fc domain of IgG and the neonatal Fc receptor (FcRn) in endothelial cells further protects serum IgG from degradation.[33–35] Consequently, long-lived radionuclides that match the serum half-life of mAbs are required to develop the radiotracers. These factors synergistically contribute to the typical features of mAb-based immunoPET imaging, such as slow blood clearance, less optimal target-to-background [T/B] ratio, and the necessity to image repeatedly after administration of a single dose of the tracer. In addition, the pharmacology of antibody–antigen binding and the internalization of the antibody–antigen complex must also be considered when developing mAb-derived PET imaging tracers.[36–38] To maximize tumor uptake and detect liver malignancies or metastases, preloading or coadministration of unlabeled antibody is required in the course of immunoPET imaging.[39] However, the

required blocking dose differs in a target- and antibody-dependent manner[40] and is greatly affected by the antibody treatment schedule at the time of tracer injection.[41] Therefore, a feasible and reproducible imaging protocol needs to be carefully established before carrying out regular immunoPET scanning. Antibodies are produced in eukaryotic cell lines due to their complex expression and post-translational modifications.[42] Because of this, the use of large amounts of antibodies is costly, further increased from the expenses of producing radiometals. Therefore, high costs may limit the widespread use of mAb-based immunoPET imaging tracers.

3.1.3. VHHs.—Because mAbs tend to circulate in the blood and deposit in normal organs such as the liver, spleen, and bone marrow, smaller antibody constructs have been employed to accelerate the clearance of unbound radiotracer from systemic circulation and correspondingly achieve higher T/B ratios. Furthermore, small antibody fragments may penetrate solid tumors more efficiently and homogeneously.[43] Several types of smaller targeting vectors are available, including camelid heavy-chain-only antibodies (HCAbs) and shark-derived immunoglobulin new antigen receptors (IgNARs).[44] HCAbs (Figure 1b) are naturally occurring antigen-binding antibodies in *Camelidae*. HCAbs can be obtained by immunization of camels, llamas, or dromedaries or from näive or synthetic phage libraries.[45] HCAbs have only two constant domains, as opposed to the three constant domains of an IgG. HCAbs are generally humanized for theranostic purposes.[46,47]

The variable domain of the heavy chain of a HCAb (VHH, Figure 1c), often referred to as Nanobody (a trade name of Ablynx) or single-domain antibody (sdAb), is the smallest antigen-binding derivative. With its molecular weight around 15 kDa and diameter <4 nm, VHH can penetrate deeply into tumor tissues while retaining its antigen recognition ability.[48] VHHs targeting various cellular or subcellular receptors or oncogenic proteins have also been generated.[49,50] Manifold techniques are available to achieve chemical functionalization of VHHs, which indubitably facilitates more sophisticated applications of VHHs.[51,52] Specifically, strategies like PEGylation and albumin hitchhiking may be used to prolong the circulatory half-life of VHH,[53–55] enabling more thorough and efficient targeting of the targets.

It has been suggested that VHHs are “magic bullets” for molecular cancer imaging.[56] For radiometal labeling, cysteine (Cys) or lysine (Lys) residues on VHHs are chemically modified with bifunctional chelators. Whereas for radio-iodination of VHHs, either direct electrophilic radioiodination or indirect radiolabeling methods can be used.[57] Because of the variable number of Lys or Cys residues in the complementary-determining region 3 (CDR3) of VHHs, it is challenging to radiolabel VHHs homogeneously using these standard methods. Methodologies that enable site-specific radiolabeling are readily available to prepare homogeneous VHH-based radiotracers (described in section 3.3.3.).[58,59] Despite the favorable pharmacokinetics, radiotracers based on VHHs have very high kidney accumulation due to the renal clearance of the excess material, limiting their role in detecting lesions located in the urinary system or in the vicinity of kidneys. Several factors (e.g., the sequence of the VHH, conjugation method, as well as specific receptors in the glomeruli) may all contribute to the high kidney retention of the developed radiotracers.[60,61] However, there are strategies to circumvent this phenomenon, including coinfusion of

gelofusine and Lys,[62] removal of polyhistidine tag (His-tag),[63] PEGylation,[64] and site-specific radiohalogen labeling.[65] Furthermore, VHHs are also being actively exploited for therapeutic purposes,[66] either in the form of radioimmunotherapy (RIT),[67–69] or in the form of photoimmunotherapy (PIT).[70,71]

3.1.4. Other Engineered Antibody Fragments and Proteins.—Several other antibody fragments have been engineered for imaging purposes.[72] In general, these antibody fragments lack the Fc region and are smaller in size. Single-chain variable fragment (scFv, Figure 1d) is one of the most popular antibody fragments with a molecular size of ~25 kDa. A scFv clears exceptionally fast from the bloodstream and creates much higher T/B ratios compared with an intact IgG. scFv is composed of variable light and variable heavy chains that are joined by a flexible peptide linker. As such, the length and amino acid composition of the peptide linker between the two domains significantly affect the binding affinity and size of the engineered scFv.[73] A significant drawback of scFv molecules is their monovalent antigen-binding specificity. In certain cases, engineering a monovalent scFv into multivalent constructs may enhance the avidity and optimize the tumor-targeting capability. Diabody (~60 kDa, Figure 1e) is a divalent variant of the monovalent scFv. Typically, a Cysmodified diabody (Cys-diabody) is constructed and used for site-specific radiolabeling.[74] Similar to radiolabeled VHHs, radiolabeled scFv, and diabody are rapidly cleared by the urinary system, resulting in high accumulation of the radiotracers in the kidneys. Other larger divalent forms, such as minibody (Mb, Figure 1f) and $(scFv)_2$-Fc constructs, have also been developed as targeting vectors.[75,76] Several multivalent scFv fragments, such as triabody (~90 kDa) and trimerbody (110 kDa), also showed potential as ligands for immunoPET imaging.[77,78]

In the pursuit of proteins with enhanced or novel functions, a multitude of protein scaffolds has been generated and used in the field of molecular imaging. These low-molecular-weight proteins lack disulfide bonds and glycosylation, so they can be expressed in bacterial systems with proper conformation rapidly.[79] Currently, one of the most commonly engineered protein scaffolds for PET imaging is the Affibody (6 kDa).[80] For instance, $Z_{HER2:342}$ is an Affibody molecule targeting human epidermal growth factor receptor 2 (HER2) and has been widely studied for PET imaging. The most attractive advantages of HER2-targeting Affibodies are their unique binding sites on HER2, which are distinct from HER2-targeted therapeutics (e.g., trastuzumab).[81,82] Therefore, novel imaging approaches employing these Affibodies may help discriminate the downregulation and saturation of HER2 following HER2-targeted therapies. Other similar molecules that have already been used for molecular imaging include adnectins,[83] fibronectin,[84] knottins,[85,86] and anticalins.[87,88] Like VHHs, the primary benefits of these small antigen-targeting moieties are to permit same-day molecular imaging.[89] The advantages from accelerated clearance are compensated by lower tumor uptake, yielding modest imaging quality. To enhance tumor retention and decrease kidney retention, several approaches (e.g., PEGylation) can be used to modify the targeting vectors.[90–92]

Of the BsAbs, bispecific T-cell engager (BiTE) antibody constructs (~55 kDa) are designed to induce context-dependent anticancer immune responses by cross-linking tumor cells with cytotoxic T cells.[93–95] One successful example is the blinatumomab, which simultaneously

targets CD19-positive B cells and then recruits CD3-positive cytotoxic T cells.[96] It is much more challenging to design T-cell-dependent BsAb constructs because each arm of the antibody has a different antigen-binding affinity. Moreover, the T-cell-targeting arm substantially affects the in vivo distribution of the antibody and, therefore, the fate of the developed molecular imaging tracers.[97,98]

3.2. Radionuclides and Chelators

In recent years, various antibodies targeting diverse antigens have been labeled with gamma-emitting radionuclides (e.g., ^{131}I, ^{123}I, ^{111}In, or ^{99m}Tc) and used for diagnosis by SPECT or planar imaging or for therapeutic applications. Because of their poor diagnostic performance, very few are routinely used in the clinic. With the global installation of cyclotrons, a variety of novel positron-emitting radionuclides is being produced.[99,100] High-purity radiometals, a fundamental component in immunoPET imaging probes, are increasingly being produced and used in recent years.[101,102] Traditionally, radiometals are eluted from generators or produced using solid targets with cyclotrons.[103] As a supplement to solid targets, liquid targets (solution targets) can also be used to produce radiometals upon optimization.[104] Several factors need to be considered before exploiting them for radiolabeling, which include physical properties (e.g., half-life [$T_{1/2}$] and decay mode), chemical properties, production efficiency, safety profiles, and price. The $T_{1/2}$ of a chosen positron emitter has to closely match the biological half-life of the targeting vector. In conjugating immunoPET imaging probes, the positron emitter is generally complexed with an inert chelator that is attached to the targeting antibody. The major principle is that the binding affinity, stability, and pharmacokinetic characteristics of the final radiopharmaceutical are in concert with the naive antibody. There are several review articles describing various radiometals and their coordination chemistry[101,105,106] and ^{18}F radiolabeling of heat-sensitive molecules.[107] In this section, we will confine to the most promising radionuclides and related chelators used for immunoPET imaging (Table 1).

3.2.1. Zirconium-89.—Zirconium-89 (^{89}Zr, $T_{1/2}$ = 78.4 h) has been extensively used in the biomedical imaging field due to its fitting emission energy properties and long half-life, which matches the circulation half-life of mAbs.[108,109] ^{89}Zr can be produced via several different nuclear reaction pathways, such as the ^{nat}Sr(α,xn)^{89}Zr reaction, ^{89}Y(d,2n)^{89}Zr reaction, or ^{89}Y(p,n)^{89}Zr reaction.[110] However, the production of ^{89}Zr using solid targets with a small medical cyclotron might still be challenging. Recent studies have reported the production of ^{89}Zr via solution targets, which are filled with a yttrium nitrate solution ($Y(NO_3)_3{\cdot}6H_2O$). [111,112] Further refinement of the irradiation procedures of liquid targets may potentially broaden the availability of ^{89}Zr and therefore the development of ^{89}Zr-based PET imaging. In developing ^{89}Zr-mAb conjugates, ^{89}Zroxalate (^{89}Zr–Zr(ox)$_2$) can be converted to 89Zr-chloride (^{89}Zr-$ZrCl_4$), which tends to undergo aquation and chelation with chelator-modified mAbs more rapidly.[113,114] Moreover, ^{89}Zr-chloride lacks the toxic oxalic acid of ^{89}Zr-oxalate.[115]

^{89}Zr is coupled to a mAb of interest through a bifunctional chelator, which possesses a ligand for capturing ^{89}Zr and a reactive group for conjugating Lys or Cys residues on the mAb surface. Desferrioxamine (Figure 2a), denoted as Df or DFO, is a clinically used

chelator for complexation of ^{89}Zr. Traditionally, the preparation of 89Zr-mAb conjugates involves a multistep synthesis, in which a succinylated-derivative of desferrioxamine B (N-sucDf) was used to modify mAbs.[116–118] This pioneering work paved the way for subsequent preclinical and more importantly, the clinical success of ^{89}Zr-mAb immunoPET imaging. The development of a novel *p*-isothiocyanatobenzyl-derivative of desferrioxamine B (known variously as *p*-SCN-Bn-deferoxamine, Df-Bz-NCS or DFO-*p*Phe-NCS; Figure 2b) further allowed efficient and rapid preparation of ^{89}Zr-mAb conjugates. This process involves the first coupling of Df–Bz–NCS to the lysine-NH_2 groups of a mAb under alkaline conditions (pH 8.9–9.1) followed by radiolabeling with ^{89}Zr-oxalate.[119,120]

Despite their attractive characteristics, such chelators are unable to saturate the octavalent demands of the Zr^{4+} cation,[121] which results in less stable ^{89}Zr-immunoconjugates as indicated by accumulation of free 89Zr in the bone. Preclinical studies suggested that ^{89}Zr's tropism for bone may introduce undesirable radiation to bone marrow and confound imaging conclusions of bone malignancies or joint inflammation.[122,123] The clinical impact of unbound ^{89}Zr remains to be determined. A family of novel bifunctional chelators that impart enhanced stabilities has been developed to surmount this problem. One of these, the tetrahydroxamate chelator called DFO* (Figure 2c) and its derivative DFO*-*p*Phe-NCS (Figure 2d) were synthesized successfully.[124,125] ^{89}Zr-DFO*-trastuzumab was thermodynamically more stable and had significantly lower bone uptake compared to the DFO modified mAb.[125] More recently, DFOcyclo*-*p*Phe-NCS (Figure 3a), a novel DFO* derivative, was developed.[126] When competed with excess DFO, this novel chelator was more stable than DFO and DFO* for chelating 89Zr. ImmunoPET imaging and biodistribution studies further demonstrated significantly lower bone uptake of 89Zr-DFOcyclo*-trastuzumab than ^{89}Zr-DFO-trastuzumab. Despite this, ^{89}Zr-DFOcyclo*-trastuzumab and ^{89}Zr-DFO*-trastuzumab showed comparable imaging performance (Figure 3b). Desferrichromes (DFC) and related compounds have also been explored for coordinating ^{89}Zr, but the DFC system did not show a dramatic advantage over DFO in in vivo imaging studies.[127]

Other novel ^{89}Zr chelators include those that do not contain hydroxamate moieties, such as *p*-SCN-Bn-H6phospa,[128] 3,4,3-(LI-1,2-HOPO),[129] *p*-SCN-Bn-HOPO,[130,131] and many other novel chelators containing hydroxamate moieties.[132–137] For instance, DFO-1-hydroxy-2-pyridone ligand (DFO-HOPO) is an octadentate chelator for ^{89}Zr. ^{89}Zr-DFO-HOFO showed excellent renal clearance and significantly lower bone uptake compared with ^{89}Zr-DFO.[135] Meanwhile, other novel ^{89}Zr chelators with cyclic structures have been developed.[136,138,139] Most recently, ligands containing carboxylate or amino donors have been tested as ^{89}Zr chelators.[140] Of these, 1,4,7,10-tetraazacyclododecane-1,4,7,10-tetraacetic acid (DOTA, vide infra) has been shown to outperform other analogues because ^{89}Zr-DOTA demonstrated exceptional stability and more rapid systemic clearance. However, the high temperature (90 °C), longer reaction duration (45 min), and the need to use ^{89}Zr-$ZrCl_4$ may hinder its application in the immunoPET imaging field.

3.2.2. Copper-64.—Copper-64 (^{64}Cu, $T_{1/2}$ = 12.7 h) stands out as an immunoPET imaging radionuclide because of its ready availability and favorable properties. ^{64}Cu is typically produced by bombardment of an enriched nickel target via the ^{64}Ni(p,n)^{64}Cu

nuclear reaction.[141] Interestingly, a recent study reported the possibility of ^{64}Cu production using a liquid target.[142] Because ^{64}Cu undergoes β^- emission in addition to β^+ emission, it is a promising theranostic radionuclide. Furthermore, the combination of ^{64}Cu and ^{67}Cu ($T_{1/2}$ = 61.8 h, β^-: 100%) results in an attractive theranostic pair.[143] To avoid nonspecific deposition of ^{64}Cu in healthy tissues, various macrocyclic ligands and their derivatives have been developed. DOTA and its derivatives (Figure 4a–d) are the most commonly used ones to chelate ^{64}Cu for PET imaging.[144,145] However, it has been shown that DOTA is not the chelator of choice to develop immunoPET tracers.[146,147] NOTA (1,4,7-triazacyclononane-1,4,7-triacetic acid)-based chelators (Figure 4e,f) are the most successful for chelating both ^{64}Cu and ^{68}Ga (vide infra) and are well-suited for radiolabeling of heat-sensitive antibody vectors at room temperature (rt). A comparison of the NOTA derivative 1,4,7-triazacyclononane,1-glutaric acid-4,7-acetic acid (NODAGA, Figure 4g) and DOTA for labeling a mAb with ^{64}Cu demonstrated better in vivo performance of ^{64}Cu-NODAGA-mAb than that of ^{64}Cu-DOTA-mAb.[148] *p*-SCN-Bz-MANOTA (Figure 4h), another NOTA derivative, outperformed DOTA and NODAGA as ^{64}Cu-MANOTA-Fab showed the highest stability and the lowest background uptake in immunoPET imaging studies.[149]

In addition, a series of cyclam-based macrocycles have been devised for ^{64}Cu-labeling of antibodies. One of such agents, CB - TE2A (4, 11 - bis (carboxymethyl) - 1, 4, 8, 11 - tetraazabicyclo[6.6.2]hexadecane, Figure 4i), has shown its merits as an effective chelator for ^{64}Cu.[150] Unfortunately, the unfriendly labeling conditions (95 °C, 60 min, pH 6–7) limit the use of CB-TE2A in applications with antibody-based agents.[151] CB-TE1A1P [(1,4,8,11-tetraazacyclotetradecane-1-(methanephosphonic acid)-8-(methanecarboxylic acid), Figure 4j] bearing a methanephosphonic acid and a carboxymethyl pendant arm can be radiolabeled with ^{64}Cu at rt.[152,153] While CB-TE2P [1,4,8,11-tetraazacyclotetradecane-1,8-di-(methanephosphonic acid), Figure 4k] can also be used for ^{64}Cu-labeling at mild conditions,[154] CB-TE1A1P is more favorable for antibody labeling because the carboxylate group allows for facile bioconjugation. Indeed, several studies have used ^{64}Cu-CB-TE1A1P for immunoPET imaging.[155,156] To further capitalize the better radiochemical yield (RCY) of cyclam derivatives, several other cyclam-based bis-(phosphinate)-bearing ligands for conventional or click chemistry-based ^{64}Cu-labeling were developed.[157,158] These novel cyclam-based bifunctional ligands are highly promising for developing immunoPET probes with ^{64}Cu under mild conditions (25–37 °C, 10–20 min, pH 5.5–6.2).[158] SarAr (Figure 4l) is a sarcophagine-based chelator used for developing immunoPET probes and can be labeled with radiometals under mild conditions (20–37 °C, 5–30 min, pH 5–5.5).[159,160]

The use of different chelators may result in varied accumulation patterns of the ^{64}Cu-labeled mAb in the blood pool and in other healthy organs (e.g., liver) despite the similar tumor uptake.[161] Generally, ^{64}Cu undergoes hepatobiliary clearance which may result in increased liver and intestine signals, limiting the detection of diseases at these sites as well as diseases at the adjacent organs or tissues (e.g., pancreas). However, this problem can be resolved with 64Cu-labeled VHHs, which precisely detected small pancreatic tumors with clarity and high T/B ratio.[162]

3.2.3. Yttrium-86.—Yttrium-86 (^{86}Y, $T_{1/2}$ = 14.7 h) decays via electron capture (ec) and positron emission, accompanied by the emission of γ rays. Several nuclear reactions have

been explored to produce ^{86}Y. To date, the recommended reaction is ^{86}Sr(p,n)^{86}Y reaction,[163–165] where the target material $SrCO_3$ or SrO is enriched for irradiation with energies from 8–15 MeV. Although a liquid target has also been used to produce ^{86}Y,[104] the yield is generally low and methods for separating radiation-induced chemical species need to be established. With the refinement of methods for separating radioyttrium,[166] the large scale production of ^{86}Y is feasible with hospital-based cyclotrons. The most appealing application of ^{86}Y is in tandem with yttrium-90 (^{90}Y, $T_{1/2}$ = 64.1 h), which is a pure beta emitter with excellent therapeutic properties.[167,168] The advantage of this theranostic pair is that quantitative PET imaging with ^{86}Y allows precise dosimetry of ^{90}Y-based radiopharmaceuticals.[169] Both clinical and preclinical studies have suggested that sequential use of ^{86}Y and ^{90}Y is an attractive theranostic pair if proper targeting vectors are used.[170,171] Derivatives of ethylenediaminetetraacetic acid (EDTA, Figure 5a,b), diethylenetriamine pentaacetic acid (DTPA, Figure 5c), and DOTA are the most widely used chelators for yttrium radiolabeling of mAbs.[172,173] Several studies have shown that incorporating the isothiocyanatobenzyl group (SCN-Bz) into the backbone of DTPA (Figure 5d) may sterically hinder the release of yttrium from the radiopharmaceuticals.[174,175] To further improve the coordination efficiency of DTPA derivatives, CHX-A′′-DTPA (Figure 5e) and *p*-SCN-Bn-CHX-A′′-DTPA (Figure 5f) bearing a cyclohexyl were developed, and these chelators possessed improved stability over DTPA in radiolabeling mAbs.[176–179]

3.2.4. Radioiodine-124.—Radioisotopes of iodine have long been used as theranostic agents in the field of thyroid cancer.[180] One among these, 124I ($T_{1/2}$ = 4.18 d) can be produced through the 124Te(p,n)^{124}I reaction.[181,182] Iodine-124 has gained interest in radiolabeling mAbs since the clinical feasibility of immunoPET imaging with a ^{124}I-labeled HMFGI mAb was first demonstrated in 1991.[183–186] ImmunoPET imaging with ^{124}I-labeled antibody agents are useful for evaluating bone metastases, another major benefit compared to those labeled with bone-seeking radiometals (e.g., ^{89}Zr). It is important to mention that ^{124}I-labeled immunoPET probes may not be appropriate for detecting primary thyroid cancers, stomach cancers, and urinary malignancies (e.g., bladder cancer and prostate cancer) because thyroid and stomach can scavenge iodide produced by deiodination and iodide is cleared via the urinary system. In addition to its role in PET imaging, ^{124}I is a theranostic agent because of Auger electrons produced during its decay.[187] ImmunoPET imaging using ^{124}I-mAb is fully concordant with 131I-mAb RIT, where immunoPET imaging acts as a scouting procedure prior to RIT.[188] Currently, the IODO-GEN method is the method of choice for radioiodination of noninternalizing mAbs.[189] In an attempt to trap radioiodinated mAbs inside the tumor cells for improved molecular imaging, residualizing prosthetic agents for radioiodination have been developed and used by several groups.[190–195]

3.2.5. Fluorine-18.—With a high positron yield of 97%, a low mean positron range of 0.5 mm, and no simultaneous γ ray emission, fluorine-18 (^{18}F, $T_{1/2}$ = 110 min) is an ideal radionuclide for PET imaging.[196] Diabodies and VHHs labeled with ^{18}F have short plasma half-lives and can permit same-day imaging,[197] a practical advantage over mAb-based imaging tracers. However, 18F has not been used to develop immunoPET probes until recently due to the harsh radio-labeling conditions and low RCY.

With the development of automated chemistry stations, several prosthetic groups for radiofluorination have been reported.[198] [^{18}F]Fluorobenzaldehyde ([^{18}F]FBA, Figure 6a) is among the most popular prosthetic groups used for radio-fluorination of biomolecules.[199] *N*-Succinimidyl-4-[^{18}F]-fluorobenzoate ([^{18}F]SFB, Figure 6b) is another prosthetic group which can form a stable amide bond with the Lys residue on proteins or peptides.[200–202] Generally, an average RCY of 30%–35% will be obtained when [^{18}F]SFB is used for labeling proteins or peptides.[203] *N*-[2-(4-[^{18}F]-Fluorobenzamido)-ethyl]maleimide ([^{18}F]FBEM, Figure 6c) is a thiol-reactive ^{18}F-labeling agent that can be site-specifically conjugated to Cys residues.[204–207] However, the radiosynthesis of [^{18}F]FEBM is a multistep and time-consuming process and often results in low RCY. It has been reported that the preparation of [^{18}F]FBEM using automated radiochemical procedures requires less time and provides higher RCY (~17%).[208] Another prosthetic group that facilitates radio-labeling of biomolecules under mild conditions (37–40 °C, 15 min, pH 8.5–9.0) is 2,3,5,6-tetrafluorophenyl 6-[^{18}F]-fluoronicotinate ([^{18}F]TFPFN, Figure 6d).[209,210] Recent studies simplified the synthesis of [^{18}F]TFPFN without drying [^{18}F]fluoride,[211,212] but the unfavorable RCY (~5%) in labeling VHHs may limit its applications.[213] Direct ^{18}F-labeling approaches include the silicon–fluoride acceptor approach (^{18}F-SiFA),[214–217] and the organotrifluoroborate ([^{18}F]BF_3) method,[218] but one concern is that the solvents (e.g., acetonitrile) or the acidic conditions (pH 2.0–2.5) used in these methods are detrimental for sensitive antibodies.

In 2009, McBride et al. reported the aluminum-fluoride (Al^{18}F) chelation strategy where fluorine is firmly bound to Al^{3+} by forming Al^{18}F, which is complexed to NOTA with the resultant complex conjugated to the biomolecule of interest.[219] This method has since been widely used for radiofluorination of various biomolecules.[220] Although this procedure allows rapid fluorination of peptides, the high temperature (~100 °C) necessary for the complexation is unsuitable for most antibodies and some peptides. To overcome this drawback, a facile two-step procedure was described,[221] where [^{18}F]AlF was first complexed to NODA-MPAEM at high temperature (105–109 °C, 15–20 min; Figure 6e) and the purified intermediate then conjugated to antibodies via the maleimide–thiol reaction at rt for 10 min. Building upon this work, a series of novel acyclic polydentate ligands permitting facile Al^{18}F radiolabeling of antibodies have been developed.[222,223] RESCA-tetrafluorophenyl ester ((±)-H_3RESCA-TFP, Figure 6f) and RESCA-maleimide ((±)-H_3RESCA-Mal, Figure 6g) are two chelators that can be used to conjugate biomolecules via the Lys or Cys residues, respectively.[224] Future studies are warranted to evaluate the diagnostic value of Al^{18}F-RESCA-labeled antibodies.

3.2.6. Gallium-68.—Gallium-68 (^{68}Ga, $T_{1/2}$ = 1.1 h) is an attractive positron-emitting radionuclide because it is readily available from an affordable in-house ^{68}Ge/^{68}Ga generator. Because ^{68}Ge has a half-life of 270.8 days, the shelf life of the generator is about 6–12 months based on elution schedules.[225] Meanwhile, other means have been explored to produce ^{68}Ga on a large scale.[226–228] Although extensively studied for ^{67}Ga/^{68}Ga complexation, the DOTA-Gallium complex is less stable than its counterpart NOTA analogue. Currently, NOTA and its derivatives are the “gold standard” for ^{67}Ga/^{68}Ga complexation because of their fast and efficient radiolabeling at rt and high in vivo stability.

[229] HBED and its derivatives (Figure 7a–c) enabled ^{68}Ga-labeling of heat-labile antibodies and antibody fragments at ambient temperatures.[230,231] H2dedpa and its bifunctional derivative *p*-SCN-Bn-H2dedpa (Figure 7d,e) were developed for labeling peptides with ^{68}Ga or 64Cu and tracers based on these chelators have shown promising imaging potentials.[232–234] CP256 (Figure 7f) and YM103 (Figure 7g) are two other acyclic ligands that have yielded encouraging imaging results.[235] PCTA and its derivative (Figure 7h,i) were superior with respect to kinetics and RCY for radiolabeling mAbs with ^{64}Cu.[236,237] Similarly, ^{68}Ga-PCTA complex also showed improvement over ^{68}Ga-NOTA for conjugating peptides.[238] TRAP-Pr, a derivative of NOTA bearing phosphinic acid groups, showed significantly improved specificity for Ga^{3+} in radiolabeling peptides,[239] but the harsh radiolabeling conditions (95 °C, pH 3.2) prohibit its use in radiolabeling of antibody vectors. To the best of our knowledge, many of the chelators mentioned above (e.g., *p*-SCN-Bn-H2dedpa, YM103, and PCTA) have not been utilized in developing immunoPET probes, but it is plausible that these chelators may have a certain value for ^{68}Ga-based immunoPET probes.

3.2.7. Other Radiometals.—Scandium-44 (^{44}Sc, $T_{1/2}$ = 3.9h) is a positron-emitting isotope and can be produced from a generator or a cyclotron source.[240–242] Our team showed that CHX-A”-DTPA as opposed to other conventional chelators(i.e., DOTA, NOTA, DTPA), achieved ^{44}Sc-labeling of a Fab fragment at rt.[243] We are positive that the development of novel chelation strategies will further expand applications of ^{44}Sc in the biomedical imaging field.[244,245]

Manganese-52 (^{52}Mn, $T_{1/2}$ = 5.591 d) can be produced via several nuclear reactions including the natCr(p,x)^{52}Mn reaction.[246,247] Manganese-52 has a higher β^+ branching ratio of 29.4% and a lower β^+ energy of 575 keV when compared to ^{89}Zr (β^+: 22.8%, $E_{\beta+\max}$ = 901 keV), making it a promising alternative to ^{89}Zr for immunoPET imaging. In a proof-of-concept study, we reported that the chelation of ^{52}Mn via DOTA is possible and immunoPET imaging with 52Mn-DOTA-mAb is feasible over the course of several days.[248] Other radiometals that can be incorporated into immunoPET imaging include ^{152}Tb ($T_{1/2}$ = 17.5 h),[249] ^{76}Br ($T_{1/2}$ = 16.2h),[250,251] and ^{132}La ($T_{1/2}$ = 4.59 h).[252,253]

3.3. New Conjugation Strategies

Lysine-based random conjugation is the most prevalent method used for chemical modification of antibodies, followed by nonspecific Cys-based conjugation. Indeed, many clinical-grade radiolabeled antibodies have been produced via lysine functionalization. However, modification of antibodies at undesirable sites may compromise the immunoreactivity and distribution profiles of the radiolabeled antibodies. Hence, continuous efforts have been devoted to developing site-specific conjugation strategies to produce well-defined radio-tracers for high-quality imaging.[254]

3.3.1. Conventional Site-Specific Conjugation.—For site-specific modification purposes, proteins and antibodies are produced with short peptide tags via standard protein engineering and recombinant expression protocols. Generally, tags are introduced at the C-terminal end of the mAbs or sdAbs to avoid antigen-binding interference. Cys engineering is the most frequently used method for site-specific radiolabeling of antibody vectors (Figure

8a).[255,256] The most commonly used strategy for Cys modification is via the maleimide conjugation, which is reversible and may result in the release of the maleimide scaffold in plasma (retro-Michael reaction).[257] Recently, a novel strategy that may realize irreversible Cys bioconjugation was described.[258] Thanks to the continuous advancement of the biomedical field, more sophisticated techniques are being exponentially developed for site-specific modification of proteins.[259] Future studies may synthesize novel immunoPET agents taking advantage of these emerging techniques.

3.3.2. Click Chemistry-Mediated Radiolabeling.—Click chemistry has been increasingly applied to develop new molecular imaging probes.[260,261] Of various click chemistry reactions, the Cu(I)-catalyzed 1,3-dipolar cycloaddition between azides and alkynes (CuAAC) is frequently used to develop radiopharmaceuticals. 18F-labeled small-molecule probes prepared via the CuAAC reaction are actively assessed in clinical settings.[262,263] If it is necessary to avoid the use of Cu(I) catalyst, particularly when developing immunoPET probes with radiometals, the catalyst-free strain-promoted azide–alkyne cycloaddition (SPAAC) reaction is a bioorthogonal alternative (Figure 8b).[264,265] However, the synthetic complexity and hydrophobicity of the cyclooctyne precursors in the SPAAC system may potentially limit its widespread application. The inverse electron demand Diels–Alder (IEDDA) reaction between strained *trans*-cyclooctene (TCO) and electron-deficient tetrazine (Tz) is a giant step forward in the field of bioorthogonal chemistry in terms of reactivity and application possibilities (Figure 8c).[266] As such, this chemistry has been applied in a myriad of uses developing molecular imaging probes.[267–269] Moreover, the axial TCO isomers were found to be more reactive than their equatorial analogues.[270]

Photoclick chemistry has been used in the field of chemical biology for years.[271,272] On the basis of the previous success, several groups have used photochemical methods to develop immunoPET probes recently.[273–275] Upon further refinement, these novel bioconjugation methods may eliminate time-consuming purification steps and maximize RCY, which is particularly needed for short-lived radionuclides such as ^{11}C ($T_{1/2} \approx 20$ min) and ^{68}Ga ($T_{1/2} = 1.1$ h).

3.3.3. Enzyme-Mediated Radiolabeling.—Enzymatic methods are well suited to achieve site-specific labeling of antibody vectors. Prominent one among them utilizes sortase A (SrtA), an enzyme derived primarily from Gram-positive *Staphylococcus aureus*. Typically, SrtA recognizes substrates containing C-terminal LP*X*TG motifs (where X = any amino acid except proline) and cleaves the peptide between threonine and glycine (Gly), leading to loss of the downstream part of the substrates (e.g., His-tag) and formation of new peptide bonds with nucleophilic substrates containing N-terminal Gly residues.[276] While SrtA is a well-established enzyme responsible for anchoring LP*X*TG-containing proteins to the growing cell wall and pili of various Gram-positive bacteria, recombinant SrtA has been developed into a valuable protein engineering tool in recent years.[277] By employing sortase-mediated transpeptidation, it is facile to install functional moieties (e.g., chelator and dye) onto the N- or C-terminus of an antibody in a site-specific fashion (Figure 9). The use of SrtA has facilitated site-specific radiolabeling of VHHs using either ^{18}F[55,278] or radiometals.[64,162] A unique two-step modular system is also available to conjugate immunoPET probes.

In this system, SrtA is used to incorporate the strained cyclooctyne functional groups into the targeting vector of interest, followed by azide–alkyne cycloaddition reaction between the click chemistry handles.[279,280] With further improvement of the catalytic activity of SrtA and evolution of Ca^{2+} independent SrtA mutants,[281–283] SrtA will serve as a versatile platform for developing more sophisticated immuno-PET probes.

Butelase-1 is another transpeptidase found in *Clitoria ternatea* (butterfly pea) and recognizes a tripeptide motif, Asn-His-Val.[284,285] Butelase-1 efficiently cyclizes peptides and proteins with a high yield. Although it is the fastest peptide ligase, its biological applications are limited because it cannot be produced as of now using recombinant techniques. Theoretically, a combination of butelase-1 and SrtA may facilitate the labeling of proteins at two distinct sites. This was proven in a recent work by Harmand et al.,[286] which reported that the combination of SrtA and butelase 1 allowed facile preparation of C-to-C fusion proteins and dual-labeling of an IgG1 molecule with two fluorescent dyes. A combination of butelase-1 with other transpeptidases may be possible in the future.

Recently, a chemoenzymatic strategy combining glycan engineering and click chemistry was invented. The combination of these strategies allowed site-specific attachment of molecules to the heavy chain glycans. This methodology involves the following steps: (1) removal of galactose residues on the C_H2 domain of the heavy chains of an antibody using β−1,4-galactosidase, (2) attachment of azide-modified monosaccharide to the heavy chain glycans using β-galactosyltransferase mutant to Gal-T(Y289L), (3) synthesis of chelator or dye-containing cyclic dibenzocyclooctyne (DIBO or DBCO), (4) catalyst-free click chemistry between azide-bearing antibody and DIBO-bearing payload (e.g., chelator or dye), and (5) radiolabeling of the site selectively modified antibody using radionuclides of interest (Figure 10).[287] This method has been applied to design dual-labeled agents for PET and optical imaging of colorectal cancers.[288] A recent study demonstrated that ^{89}Zr-DFO-trastuzumab developed using this chemoenzymatic strategy outperformed its counterpart developed by random conjugation method because the site-specifically modified ^{89}Zr-DFO-trastuzumab showed enhanced immunoreactivity and stability in immunoPET imaging studies.[289] Although being able to yield homogeneous and well-defined products, this method suffers from a lengthy and relatively tedious protocol.

HaloTag is a genetic construct with multifunctional and versatile capabilities. The molecular mechanism of this system is based on a mutant bacterial haloalkane dehalogenase enzyme, which is obtained from *Rhodococcus rhodochrous*.[290,291] Use of the HaloTag technology begins with the fusion of the HaloTag (33 kDa) to the protein of interest. A HaloTag-specific ligand is then introduced, resulting in the formation of an irreversible covalent bond between the HaloTag-modified protein and the ligand.[292,293] As we all know, His-tag is ubiquitously introduced in protein production, but its role is merely limited to the isolation and purification of proteins.[294,295] In comparison, HaloTag can be employed to rapidly purify proteins and the isolated proteins may further enable multimodal molecular imaging. Preliminary evidence has demonstrated the feasibility of HaloTag-based pretargeted imaging. This strategy involves first administering a HaloTag-modified antibody for pretargeting and then a small radiolabeled molecule with a short circulation time for imaging.[296]

Analogous to these, Schibli et al. reported that microbial transglutaminase (mTGase) can modify mAbs in a stoichio-metric manner and the site-specifically engineered mAbs are of particular interest for molecular imaging.[297,298] Another bacterial enzyme lipoic acid ligase (LplA) was also used with [^{18}F]fluorooctanoic acid ([^{18}F]FA) for site-specific radio-labeling of a Fab fragment.[299] Although mTGase and LplA have shown potential in mediating site-specific radiolabeling of biomolecules, their robustness needs to be confirmed by future studies.

3.3.4. Pretargeted ImmunoPET Imaging Strategies.—The slow blood clearance of mAb is problematic because it leads to high background activity and radiation exposure, especially to the red bone marrow. Aside from reducing the molecular size and removing or blocking the Fcγ receptors (FcγRs), pretargeted immunoPET imaging holds promise to improve the imaging quality while decreasing radiation exposure.[300] In addition, this imaging approach enables the use of short-lived PET radionuclides (e.g., the widely available ^{68}Ga and ^{18}F).[301] Pretargeted imaging was initially achieved using the biotin–streptavidin interaction and BsAbs.[302,303] In the avidin–biotin pretargeting approach, a streptavidinmodified immunoconjugate, and radiolabeled biotin were used.[304,305] Streptavidin and biotin-based pretargeting systems have been investigated in several clinical studies.[306–308] However, the bacterially derived streptavidin constructs are prone to have immunogenicity, which may limit repeated imaging or therapy.[309] A second concern for this system is that endogenous biotin in patient blood and tissues may competitively occupy and block the binding sites of streptavidin, thus preventing the binding of radiolabeled biotin.

In a BsAb-based pretargeted imaging system, a BsAb that can bind to target antigen and radiolabeled hapten is first injected, enabling the saturation of the target and washing out of the unbound antibodies. Once the unbound antibody is cleared from the blood and normal tissues, a radiolabeled chelate is injected and a portion will be captured by the BsAbs at the tumor sites with the remainder eliminated rapidly from the body. This strategy has been refined over the years and used in clinical studies for pretargeted radioimmunotherapy (pRIT),[310] as well as for pretargeted immunoSPECT and immunoPET imaging.[311–314] Traditionally, BsAbs used for pretargeted imaging and therapy were produced by chemical methods[315,316] or by recombinant expression from *Escherichia coli* or myeloma cell cultures.[317,318] Although several clinical studies have validated the therapeutic effect of pRIT using the antibodies produced this way,[319,320] the murine or chimeric property of such agents limit their clinical use. To further advance the clinical translation and application of pretargeted imaging and therapy, a more innovative Dock-and-Lock method is now being used to develop humanized recombinant BsAbs on a large scale.[321] One such example is the anti-CEA × anti-HSG TF2 BsAb, which contains a humanized antihist-amine-succinyl-glycine (HSG) Fab fragment from the anti-HSG mAb 679 and two humanized anti-CEA Fab fragments derived from the hMN14 mAb (labetuzumab).[219,321] As the hapten peptides of the pretargeted system, the radiolabeled small molecules bear two HSG groups and various chelators (Figure 11), allowing versatile labeling with radionuclides of interest (e.g., ^{68}Ga and [^{18}F]AlF). Currently, several other such BsAbs (e.g., TF4 for CD20 and TF10 for a mucin antigen) produced via this approach are also being actively investigated for theranostic purposes.[322–324] Using the directed evolution and yeast surface display,[325]

Orcutt and coauthors at the Massachusetts Institute of Technology (MIT) constructed another pretargeted system,[326,327] which exploits a principle similar to the streptavidin–biotin system but replaces streptavidin with a C825 scFv capturing benzyl(Bn)-DOTA-radiometal complex. In this system, use of a clearing agent (e.g., dextran-(Y)-DOTA-Bn conjugate) further improved the imaging quality and therapeutic outcome.[328,329]

In recent years, bioorthogonal chemical reactions have been developed as alternatives to biologic pretargeting interactions for recruiting radiolabeled probes to the tumor-bound mAb, as excellently described in several reviews.[330–332] Since its initial report,[266] the IEDDA reaction has been widely used for pretargeted tumor imaging. Various TCO-conjugated antibodies and ^{111}In-, ^{18}F-, or ^{64}Cu-labeled Tz probes have been used to achieve pretargeted imaging.[333–335] These novel strategies substantially improved T/B ratios and reduced radiation dose to the bone marrow. Ideal imaging results were achieved when the tagged biomolecules (e.g., TCO-modified mAb) were completely cleared from the circulation before injecting the radiolabeled Tz, which could be accomplished by injecting a clearing agent (e.g., Tz-galactose-albumin).[336,337] Furthermore, sequential use of the enzyme-mediated site-specific modification and click chemistry produced improved imaging results.[338] On the basis of the available evidence, the added value of this strategy is confined to the production of homogeneous immunoconjugate and reduced use of the antibody because the imaging performance was comparable to that of the randomly labeled analogous construct.[339] Along with this, several other Tz-modified chelators have been developed for labeling peptides with radiometals,[340,341] but their performance with antibodies remains to be determined. It is also notable that some chemical reactions are not suitable for in vivo pretargeted imaging due either to the interactions of the radioligand with serum albumin or to the slow reaction kinetics.[342,343]

As discussed above, high-affinity Affibodies have been successfully applied for molecular imaging of cancers. The unfavorable part is that their rapid renal clearance, reabsorption, and internalization unavoidably lead to high accumulation of the radiotracers in the proximal tubule of the kidneys. Pretargeted imaging approaches have been harnessed to overcome this disadvantage.[344–347] One such approach is the peptide nucleic acid (PNA)-mediated hybridization system, where the primary PNA strand used for tumor targeting can selectively and rapidly hybridize with the secondary complementary PNA strand equipped with radionuclides. For instance, Vorobyeva et al. developed a modular system consisting of $Z_{HER2:342}$-SR-HP1 (primary targeting agent) and 68Ga-HP2 (secondary targeting agent).[348] They reported that this Affibody-based imaging approach yielded increased tumor uptake and decreased kidney uptake in preclinical ovary cancer models.

3.3.5. Clearance-Enhanced ImmunoPET Imaging.—Other than the above-mentioned methods for increasing image contrast and improving image quality, use of urokinase and a urokinase-cleavable bifunctional chelator (CB-TE1A1PUSL-DBCO) is a promising radionuclide clearance enhancement system.[349] This system has been used to develop ^{64}Cu-CB-TE1A1P-USL-trastuzumab,[156] where injection of urokinase triggers urokinase-responsive cleavage of the radiotracer, leading to enhanced elimination of radioactivity from the blood circulation, enhanced hepatic radioactivity clearance, and significantly increased tumor-to-blood ratio. These studies indicate that urokinase and

urokinase substrate linkers can be used to induce clearance of radioactivity from the nontargeted tissues and shorten the time required to obtain optimal immunoPET imaging contrast.

4. IMMUNOPET IMAGING OF CANCERS

The major application of immunoPET imaging is to facilitate better management of cancer patients. According to several clinical reports, immunoPET imaging provided excellent specificity and sensitivity in detecting primary tumors.[184,186] ImmunoPET imaging is also an appealing option for detecting lymph node and distant metastases.[118,350] More importantly, accumulating clinical evidence suggests that immunoPET can detect previously unknown lymph node and distant meta-stases.[39,41] These impressive results indicate that immunoPET may complement IHC staining in clinical dilemmas when suspected lesions are inaccessible for biopsy. However, suboptimal imaging conditions (e.g., imaging protocol and facility performance) and low expression of the target in small tumor lesions may lead to underestimation of the tumor burden and target abundance. Following immunoPET imaging, patients with positive findings can be selected for subsequent therapies (e.g., antibody therapy and antibody-based RIT), whereas patients with negative or heterogeneous findings may need multidisciplinary treatments. ImmunoPET is a useful diagnostic tool but also a theranostic companion for radiation dosimetry prior to administering the therapeutic radiopharmaceuticals (discussed in section 8). Moreover, immunoPET imaging is useful for improved triage during early disease stages and to facilitate image-guided surgery.[351,352] The information provided by immunoPET will significantly enhance the existing diagnostic methods for better tumor characterization. One can envision that tumors may be classified not only according to their origins and mutation status but also according to the expression of specific tumor antigens in the future.

4.1. Receptor Tyrosine Kinases

Receptor tyrosine kinases (RTKs) are often overexpressed and/or mutated in a variety of cancers.[353] As the best-studied oncogenic drivers, RTKs have been among the most explored targets for developing anticancer therapeutics. Indeed, mAbs and small-molecule tyrosine kinase inhibitors (TKIs) suppressing RTKs or their ligands are the most typical examples of targeted cancer therapies. Along with this success, substantial efforts have been dedicated to developing immunoPET imaging approaches for revealing the heterogeneous status of RTKs in cancers.[354]

4.1.1. Epidermal Growth Factor Receptor.—Human epidermal growth factor receptor (EGFR) is a RTK regulated by at least seven activating ligands in humans.[355] Several mAbs (e.g., cetuximab, panitumumab, and nimotuzumab) targeting the extracellular domain of EGFR and TKIs (e.g., erlotinib) targeting the intracellular domain of EGFR have been approved for treating EGFR-positive cancers. An initial clinical study demonstrated that ^{89}Zr-Df-cetuximab immunoPET imaging could visualize EGFR expression and predict the treatment efficacy of cetuximab in advanced colorectal cancers.[356] However, a follow-up study showed that ^{89}Zr-Dfcetuximab uptake failed to predict the efficacy of cetuximab monotherapy in patients with RAS wild-type metastatic colorectal cancer.[357] ^{89}Zr-Df-

cetuximab was further investigated in nine patients with head and neck squamous cell carcinoma (HNSCC) or nonsmall-cell lung cancer (NSCLC). The results showed no direct relationship between EGFR expression and tumor uptake of the radiotracer in terms of the T/B ratio,[358] which was in concert with the results reported by two other studies.[359,360] Because cetuximab irreversibly binds to EGFR expressed in liver cells, van Loon et al. reasoned that an optimal preloading of unlabeled cetuximab is needed to first saturate liver EGFRs.[358] In addition, Pool et al. found that shed EGFR ectodomain levels in liver and plasma interfere with EGFR-targeted immunoPET imaging agents, and increased administration of radiotracer could improve tumor visualization.[361]

Panitumumab is a fully human mAb targeting EGFR.[362] Niu et al. initially reported that ^{64}Cu-DOTA-panitumumab immunoPET imaging failed to quantify EGFR protein expression in three different HNSCC xenografts,[363] probably due to the poor penetration of the antibody and varying tumor vasculature in the used models. However, several other studies showed that uptake of ^{89}Zr-panitumumab was associated with EGFR expression in other tumor models.[364–366] Additionally, a group reported the clinical safety and feasibility of ^{89}Zrpanitumumab immunoPET in noninvasively characterizing EGFR expression.[367,368] Scott et al. screened a variety of mouse mAbs and found that mAb 806 specifically targets the overexpressed or activated forms of EGFR.[369,370] ch806, a chimeric form of mAb 806, has been validated as an effective therapeutic antibody and ch806-based molecular imaging showed specific accumulation of the antibody at multiple tumor sites.[371,372] In an attempt to trap the radioiodinated ch806 in lysosomes, ch806 was further radiolabeled with residualizing peptides ^{124}I-IMP-R4 and ^{124}I-PEG$_4$-tptddYddtpt. The tumor uptake of ^{124}I-IMP-R4-ch806 (Figure 12) and ^{124}I PEG$_4$-tptddYddtpt-ch806 was apparent in preclinical glioma models.[373,374] More recently, two other preclinical studies have demonstrated the value of ^{89}Zr-Df-nimotuzumab immunoPET diagnosing epidermoid carcinomas and gliomas.[375,376]

Affibody-based PET imaging probes are also being developed to image EGFR expression.[377–381] Burley et al. developed two Affibody-based EGFR-targeting radioligands (^{89}Zr-DFO-Z$_{EGFR:03115}$ and ^{18}F-AlF-NOTA-Z$_{EGFR:03115}$).[382] The authors found that 18F-AlF-NOTA-Z$_{EGFR:03115}$ PET imaging could correlate EGFR downregulation in response to cetuximab treatment in preclinical HNSCC models. These probes may have clinical utility because of the poor performance of ^{89}Zr-Df-cetuximab and the dichotomous role ^{64}Cu-DOTA-panitumumab in mapping EGFR levels. Although the development of next-generation EGFR-targeting mAbs may overcome cetuximab-induced resistance,[383,384] VHH-based EGFR-targeting therapeutics may also overcome cetuximab-induced resistance. One such VHH, 7D12, penetrates more deeply and homogeneously into tumors than cetuximab.[385,386] Therefore, 7D12-based nuclear medicine imaging approaches may serve as promising tools in selecting patients suitable for VHH-based therapies.[387,388]

4.1.2. Human Epidermal Growth Factor Receptor 2.—

Human epidermal growth factor receptor 2 (HER2/ErbB2) has attracted much interest as a molecular imaging target in the past two decades. Along with the clinical approval of HER2-targeted antibody therapeutics (e.g., trastuzumab, trastuzumab emtansine [T-DM1], and pertuzumab), several antibody-based radiotracers have been developed for imaging HER2 expression.[389] Of them,

two initial clinical studies using ^{111}In-DTPA-trastuzumab reported uptake of the tracer in the myocardial wall and detection of new HER2-positive breast cancer lesions.[16,390] Since ^{89}Zr became clinically available,[118] successive translational studies have reported the value of ^{89}Zr-Df-trastuzumab immunoPET in detecting both previously known and unknown metastatic breast cancer lesions,[41] detecting heterogeneous HER2 expression in breast cancer lesions before T-DM1 treatment and predicting T-DM1 treatment outcomes.[391–393] ^{64}Cu-DOTA-trastuzumab is an alternative that has also been tested in the clinic.[394,395] In addition to trastuzumab, pertuzumab is another FDA-approved mAb targeting HER2. ^{89}Zr-Df-pertuzumab has been successfully translated into the clinic and ^{89}Zr-Df-pertuzumab immunoPET imaging was able to detect primary breast cancers and distant breast cancer metastases including brain metastases (Figure 13a–d).[396] However, no clinical studies have directly compared the diagnostic efficacies of ^{89}Zr-Dftrastuzumab and ^{64}Cu-DOTA-trastuzumab.

Increasing evidence supports HER2 as a broad tumor biomarker beyond its established role in breast cancers.[397] Preliminary studies have reported the value of HER2-specific immunoPET in elucidating HER2 expression levels in gastric cancer and esophagogastric adenocarcinoma.[398–400] Because HER2 serves as a biomarker for ovarian cancer and also potentially for advanced thyroid cancers, it is rational that HER2-targeted immunoPET imaging was able to map HER2 expression in these solid tumors.[401–404]

Although a combination of 18F-FDG PET and ^{89}Zr-Dftrastuzumab immunoPET robustly predicted the treatment efficacy of T-DM1, ^{89}Zr-Df-trastuzumab did not accumulate in a proportion of HER2-positive lesions.[391] Temporal modulation of HER2 expression with mucolytic treatment enhanced tumor uptake of ^{89}Zr-Df-trastuzumab in a preclinical breast cancer model.[405] Moreover, it has been shown that caveolin-1 mediates HER2 internalization and depletion of caveolin-1 with lovastatin increased tumor uptake of ^{89}Zr-DFO-trastuzumab.[406] This effect was further validated by a more recent study where oral administration of lovastatin enhanced tumor accumulation of ^{89}Zr-DFO-pertuzumab in preclinical gastric cancer models.[407] More importantly, image-guided modulation of HER2 expression and internalization could improve the efficacy of trastuzumab treatment.[408] These results together demonstrate that modulation of HER2 expression or internalization could increase tumor uptake of HER2-targeted immunoPET probes and also the efficacies of HER2-targeted therapeutic regimens.

Small biomolecules (e.g., antibody fragments, sdAbs, and Affibodies) are also being used as HER2-targeting vectors.[409,410] Beylergil et al. developed 68Ga-DOTA-F(ab′)$_2$-trastuzumab and investigated the diagnostic utility of this radiotracer in 15 patients with breast cancer. Although less optimal than radiolabeled trastuzumab, this imaging approach detected diseases in 4/8 patients with HER2-positive breast cancers.[411] 2Rs15d is a sdAb developed against HER2 and has shown excellent targeting of HER2 in both preclinical settings,[63] and clinical settings.[412] In both cases, 68Ga was randomly conjugated on Lys residues of 2Rs15d without compromising the targeting affinity of 2Rs15d, in part due to the absence of Lys residues in its antigen-binding domains. (*Note: 2Rs15d contains six lysines that are dispersed in the framework and away from the receptor-binding regions.*) A recent study revealed that SrtA-mediated site-specific radiolabeling of 2Rs15d yielded homogeneous

^{68}Ga-NOTA-2Rs15d, and immunoPET imaging with this radiotracer readily visualized HER2-positive breast cancers.[413] However, the renal clearance of ^{68}Ga-NOTA-2Rs15d and the resultant high tracer retention in bilateral kidneys is problematic, which was also observed in several other 18F-labeled VHHs.[202,414] In this setting, two HER2-specific VHHs (i.e., 2Rs15d and 5F7) were radiolabeled with [^{18}F]TFPFN and subsequent immunoPET imaging with the synthesized probes successfully detected tumors with prominent tumor uptake and substantially lower renal uptake.[415] Furthermore, [^{18}F]AlF-NOTA-Tz-TCO-GK-2Rs15d was developed by the IEDDA reaction and incorporation of a renal brush border enzyme-cleavable Gly-Lys (GK) linker in the prosthetic moiety. This strategy achieved quite high RCY (~17%) while also maintaining high T/B ratios (Figure 13e,f).[416] 2Rs15d has been validated useful as a vehicle for RIT after labeling with ^{177}Lu or ^{131}I,[67,417] providing valuable therapeutic options accompanying the above-mentioned immunoPET imaging. A clinical trial evaluating the safety and distribution of ^{131}I-SGMIB-2Rs15d in breast cancers has completed patient recruitment (NCT02683083).

$Z_{HER2:342}$ is a second-generation HER2-targeting Affibody and has been radiolabeled nonselectively with ^{125}I and ^{111}In[418,419] or site-specifically with ^{18}F-FBEM.[205,420,421] Xu et al. further modified $Z_{HER2:342}$ with a hydrophilic linker (Cys-Gly-Gly-Gly-Arg-Asp-Asn) that is conjugated with maleimidomonoamide-NOTA and radiolabeled the derivative with Al^{18}F.[422] The authors found that this modification produced excellent imaging contrast and low abdomen uptake of the developed tracer. DOTA-$Z_{HER2:342-pep2}$ (ABY-002) is a chemically synthesized derivative of $Z_{HER2:342}$ with a DOTA coupled to its NH_2 terminus. Therefore, this agent could be site-specifically radiolabeled with 111In or 68Ga.[423–425] Furthermore, 111In-ABY-002 and 68Ga-ABY-002 demonstrated the potential in visualizing HER2-expressing metastatic lesions in patients with breast cancer.[426] Another group of HER2-specific molecular imaging tracers is based on the Affibody MMA-DOTA-Cys^{61}-$Z_{HER2:2891}$-Cys (ABY-025).[427–429] Of them, ^{68}Ga-ABY-025 can be produced in compliance with Good Manufacturing Practice (GMP)[430] and can be used to accurately image HER2 expression in metastatic breast cancers.[431–434] Because ^{18}F is a radionuclide validated for clinical use and its longer half-life enables imaging over a longer time window compared to ^{68}Ga, Glaser et al. used three methods (i.e., ^{18}F-SiFA, ^{18}F-AlF-NOTA, and ^{18}F-FBA) to radiolabel ABY-025. They found that ^{18}F-FBA-ZHER2:2891 (GE226) emerged as a highly specific candidate for imaging HER2 expression in pre- and post-treatment settings.[435,436] $Z_{HER2:2395}$ is another variant of $Z_{HER2:342}$ and has a C-terminal Cys.[437] This Affibody molecule was site-specifically labeled with Al^{18}F-NOTA (90 °C, 15 min) with an acceptable RCY (21% ± 5.7%).[438]

Aiming to improve the therapeutic effect of HER2-targeted therapies, BsAbs are being increasingly produced,[439–442] which may serve as appealing immunoPET imaging components. Because of the progress in preclinical and clinical studies, we are optimistic that HER2-targeted immunoPET imaging will provide a noninvasive and dynamic visualization and quantification of HER2 expression in heterogeneous tumors, which will refine clinical management of HER2-targeted therapeutics. Apart from detecting the heterogeneous HER2 expression in tumor tissues for initial patient selection,[443] HER2-specific immunoPET may serve as a useful tool in predicting therapeutic responses following HER2-targeted therapies.[444,445] This will be especially useful when the applied

HER2-specific vector binds to epitopes different from that of the clinically approved antibodies (e.g., trastuzumab and pertuzumab).[446]

4.1.3. Human Epidermal Growth Factor Receptor 3.—

Human epidermal growth factor receptor 3 (HER3/ErbB3) has weak intracellular kinase activity and does not form homodimers, but it is a signal amplifier after forming heterodimers with other EGFR family members (i.e., HER2 and EGFR). It has been well established that HER3 is related to the development and progression of several types of cancers.[447] With the broad clinical application of HER2- and EGFR-targeting agents, increasing evidence indicates that HER3 is also implicated in the resistance of HER2- or EGFR-targeting therapeutics.[448] As such, more than 13 HER3-targeting mAbs (e.g., patritumab, lumretuzumab, KTN3379, REGN1400) are under clinical investigation as either monotherapy agents or components of combination therapies.[449] Additionally, duligotuzumab (MEHD7945A) is a human IgG1 mAb dually targeting HER3 and EGFR.[450,451]

Patritumab is a fully human anti-HER3 mAb and has shown to have an excellent safety profile in clinical trials. Although a preclinical study showed the feasibility of ^{64}Cu-DOTA-patritumab immunoPET in imaging HER3 expression,[452] the clinical use of ^{64}Cu-DOTA-patritumab was not satisfactory because tumor uptake of 64Cu-DOTA-patritumab was not robust.[453] The discrepancy observed in these two studies may possibly be caused by the substantial uptake of the radiotracer in human livers and less potent targeting property of the antibody. GSK2849330 is another fully human HER3-specific mAb and dose-dependent, saturable uptake of the agent was reported in a preclinical study where ^{89}Zr-GSK2849330 was employed.[454] More recently, van Oordt et al. characterized the value of ^{89}Zr-GSK2849330 immunoPET in clinical settings.[455] The authors validated ^{89}Zr-Df-GSK2849330 saturation after preloading with unlabeled GSK2849330 and also observed a significant uptake of the tracer in the liver and spleen. Lumretuzumab (RG7116) is a humanized mAb targeting the extracellular domain of HER3.[456] ImmunoPET imaging with ^{89}Zr-lumretuzumab provided useful information on HER3 expression in multiple tumor-bearing mouse models.[457] A follow-up clinical study using ^{89}Zr-lumretuzumab further demonstrated tumor uptake of the tracer.[458] The study also revealed significant liver uptake of the tracer, which was partially caused by Kupffer cell-mediated capture and clearance of the glycoengineered antibody.

Several other HER3-targeting vectors, including HER3 specific antibody fragments and Affibody, have been developed and employed as PET and fluorescent imaging probes.[459–462] However, probes of long retention time are favored for imaging HER3 because this receptor has a low density on the tumor cells but high abundance in the normal organs and tissues, such as the small intestine. Furthermore, Affibody-based imaging probes have very fast blood clearance due to their small sizes (~7 kDa), which results in substantial kidney retention that interferes with image interpretation.[463,464] To this end, a biparatopic VHH construct MSB0010853 (39.5 kDa), which blocks two different HER3 epitopes, was developed (Figure 14a).[465] Warnders et al. reported that tumor uptake of ^{89}Zr-MSB0010853 correlated with HER3 expression (Figure 14b), and its uptake in tissues was dose-dependent. Owing to the relatively larger size and the albumin-binding capacity of ^{89}Zr-MSB0010853,

bloodstream circulation of this tracer was relatively longer and renal uptake is relatively lower (<15% ID/g).[465]

4.1.4. Vascular Endothelial Growth Factor Receptor.—

Vascular endothelial-derived growth factor (VEGF)/VEGF receptor (VEGFR) signaling pathway is the key pathway regulating vasculogenesis and angiogenesis during physiologic homeostasis and diseases.[466] A number of therapeutic agents targeting VEGF (e.g., bevacizumab and ramucirumab) and VEGFR (e.g., sorafenib and sunitinib) have been approved for clinical use around the world.[467] As a neutralizing mAb targeting VEGF-A, the benefits of bevacizumab have been validated for different oncological indications.[468] To date, clinical immunoPET studies using ^{89}Zr-Df-bevacizumab were performed in a variety of tumors, including breast cancer,[469] neuroendocrine tumors,[470] renal cell carcinoma (RCC),[471] NSCLC,[472] and glioma.[473,474] ^{89}Zr-Df-bevacizumab immuno-PET imaging detected VEGF-A downregulation induced either by the mammalian target of rapamycin inhibitor (everolimus) in patients with neuroendocrine tumors,[470] or by the HSP90 inhibitor, luminespib (NVP-AUY922), in ovarian cancer xenografts.[475] However, clinical ^{89}Zr-Df-bevacizumab immunoPET imaging failed to monitor VEGF reduction in patients with breast cancer following NVP-AUY922 treatment.[476] To enhance the penetration of bevacizumab across the blood–brain barrier (BBB), intra-arterial administration and blood–brain barrier opening (BBBO) are two emerging strategies.[477] In agreement with this clinical evidence, BBBO with mannitol followed by intra-arterial administration of ^{89}Zr-Df-bevacizumab resulted in significantly higher accumulation of the tracer in the ipsilateral hemisphere.[478]

To gain a more thorough insight into tumor response following antiangiogenic treatment, ranibizumab (a humanized Fab fragment targeting all isoforms of VEGF-A) was radiolabeled with ^{89}Zr.[479] Uptake of ^{89}Zr-ranibizumab in the tumor center reduced substantially following sunitinib treatment. However, immunoPET scanning performed 7 days after the termination of the treatment showed that tracer accumulation in the tumor centers increased and returned to baseline. It is worthwhile to note that uptake of ^{89}Zr-Dfbevacizumab in RCC and normal organs may also rebound following sunitinib treatment,[471] but a similar phenomenon was not observed following sorafenib or everolimus treatment of RCC.[480,481] All of the clinical evidence indicates that expression of VEGF not only varies in different patients but also among the metastases and within the tumor in a single patient. VEGF-directed immunoPET is useful for visualizing the dynamic changes of VEGF before and after VEGF-targeted therapies. It has been postulated that antiangiogenic therapies induce the apoptosis of the endothelial cells and “normalize” the hyper-permeability of the tumor vasculature.[482] Therefore, disruption of the tumor vasculature may lead to reduced tumor uptake of the radiotracer, regardless of the VEGF levels. This factor should be taken into consideration when interpreting the imaging results.

Although VEGF-A binds to both VEGFR-1 and VEGFR-2, VEGFR-2 plays a key role in regulating angiogenesis and vascular permeability. Results from several preclinical studies demonstrated that it was also feasible to image tumor vasculature by targeting VEGFR-2.[483–485]

4.1.5. Other Receptor Tyrosine Kinases.—Other than the EGFR family members, there are many other RTKs implicated in the pathogenesis and progression of cancers and non-cancerous diseases.[486] Of them, c-MET (also known as mesenchymal–epithelial transition factor), platelet-derived growth factor (PDGF) receptor (PDGFR), and insulin-like growth factor-1 receptor (IGF-1R) are emerging therapeutic and diagnostic targets.

c-MET is the receptor for the hepatocyte growth factor (HGF). The HGF/c-MET pathway is vital for the development and metastatic progression of gastrointestinal cancers,[487] NSCLC,[488] and several other malignancies.[489] Furthermore, c-MET is closely related to the acquired resistance of EGFR-targeted or VEGFR2-targeted therapies in a broad range of solid tumors.[490] Current efforts are directed to validate c-MET as a biomarker and HGF/c-MET pathway inhibitors as anticancer therapeutics. However, several clinical trials have failed to demonstrate the synergistic effect of c-MET or HGF inhibitors in combination therapies, such as onartuzumab plus erlotinib in NSCLC,[491] and rilotumumab plus epirubicin, cisplatin, and capecitabine in gastric or gastro-esophageal junction adenocarcinoma.[492] Therefore, development and clinical translation of companion diagnostic probes may underpin clinical investigation of HGF/c-MET pathway inhibition for cancer therapies. Luo et al. produced a recombinant human HGF (rh-HGF) and demonstrated that ^{64}Cu-NOTA-rh-HGF PET imaging indirectly visualized c-MET-positive human glioblastoma in mouse models.[493] Using a fully human mAb rilotumumab (AMG102) which selectively targets HGF, Price et al. developed ^{89}Zr-DFO-AMG102 and reported that immunoPET imaging with this tracer determined HGF in the local tumor microenvironment (TME).[494] To directly delineate c-MET abundance, several radiotracers have been developed and tested in preclinical mouse models.[495,496] Onartuzumab is a one-armed monovalent antibody targeting the c-MET.[497] Pool et al. demonstrated that ^{89}Zr-Dfonartuzumab immunoPET imaging could visualize erlotinib-induced c-MET upregulation and luminespib-induced c-MET downregulation in NSCLC models.[498] Escorcia et al. reported the theranostic value of ^{89}Zr-Df-onartuzumab and 177Lu-DTPA-onartuzumab in pancreatic ductal adenocarcinoma (PDAC) xenograft models. In this theranostic scenario, immunoPET imaging with ^{89}Zr-Df-onartuzumab identified c-MET-positive PDAC xenografts and targeted radioligand therapy with ^{177}Lu-DTPA-onartuzumab efficiently delayed the growth of the selected tumors.[499] A more recent study by Klingler et al. reported the synthesis of ^{89}Zr-DFO-azepinonartuzumab within 10 min via the one-pot photoradiochemical conjugation reaction.[500] When compared to the conventional ^{89}Zr-DFO-Bn-NCS-onartuzumab, immunoPET imaging with ^{89}Zr-DFO-azepin-onartuzumab resulted in comparable T/B ratios but a lower uptake in the liver. These results highlight the feasibility of immunoPET in assessing the dynamics of the HGF/c-MET signaling pathway and selecting candidates most likely to benefit from HGF/c-MET-targeted therapies.

PDGF and PDGF receptors (i.e., PDGFRα and PDGFRβ) stimulate the growth of tumor cells and regulate tumor angiogenesis as well as tumor stromal fibroblasts.[501,502] Although no PDGF-specific TKIs have been approved, olaratumab (LY3012207, IMC-3G3), a human IgG1 mAb targeting PDGFRα, was approved by the FDA in 2016 for treating soft-tissue sarcomas.[503] To directly image stromal PDGFR, PDGFRβ-targeting Affibodies have been radiolabeled with ^{111}In or ^{68}Ga and tested in preclinical glioma models.[504–506] By using a

dual cysteine disulfide bond linker, a dimeric Affibody molecule $Z_{PDGFR\beta}$ was produced and ^{89}Zr-DFO-$Z_{PDGFR\beta}$ immunoPET imaging visualized PDGFRβ-expressing colorectal adenocarcinomas.[507] Overexpression of PDGFRa has been reported to be associated with lymph node metastases of papillary thyroid cancers.[508–511] Accordingly, Wagner et al. developed ^{64}Cu-NOTA-D13C6 and reported that immunoPET imaging with this tracer identified papillary thyroid cancers that have the potential to metastasize (Figure 15).[512]

IGF-1R is universally expressed in hematologic and solid tumors.[513,514] Insulin-like growth factors and IGF-1R are attractive targets for cancer therapy and imaging.[515] R1507 is a mAb targeting IGF-1R and molecular imaging with R1507-based radiotracers, ^{111}In-R1507 and ^{89}Zr-Df-R1507, successfully determined IGF-1R expression in breast cancer xenografts.[516] We screened an IGF-1R-specific mAb 1A2G11 and developed an immunoPET probe ^{89}Zr-Df-1A2G11,[517] which specifically accumulated in IGF-1R-positive pancreatic cancers.[518] In accordance with the antibody-based imaging findings, an Affibody-based immunoPET tracer also specifically delineated U87MG tumors with enhanced clearance from the renal-urine system.[519] These preclinical results imply that IGF-1R-specific immunoPET may help identify patients that would benefit from anti-IGF-1R therapies and enable dynamic monitoring of the IGF-1R expression following the therapies.[520]

4.2. Clusters of Differentiation

Clusters of differentiation (CD) antigens have long been investigated as either diagnostic or therapeutic targets for a broad spectrum of diseases. In this review, we will describe in-depth some selected markers (i.e., CD20, CD38, CD146, and CD105). However, there are many other CD antigens that have shown potential as molecular imaging targets, including CD54 (known as intercellular adhesion molecule, ICAM-1),[521] CD44,[118,522–524] CD47,[525–527] and CD138.[528,529]

4.2.1. CD20.—Lymphoma is an umbrella term for a large group of cancers that often arise from the lymph nodes. CD20 and CD30 are two common biomarkers for molecular imaging of lymphoma.[530–532] Rituximab, a CD20-specific chimeric mAb, was approved by the FDA for the treatment of non-Hodgkin's lymphoma (NHL) in 1997 and rheumatoid arthritis (RA) in 2006.[533] Studies have reported the feasibility of ^{64}Cu-DOTA-rituximab and ^{89}Zr-rituximab immunoPET in revealing CD20 expression in NHL-bearing humanized mouse models.[534,535] Of them, ^{89}Zr-rituximab has been translated for clinical use. Muylle et al. have reported that ^{89}Zr-rituximab immunoPET/CT scanning without preloading of cold rituximab enabled clearer tumor visualization and higher tumor uptake (Figure 16).[536]

Recently, antibody fragments targeting human CD20 have been engineered and investigated after being labeled with ^{124}I, ^{89}Zr, or ^{64}Cu. Olafsen et al. engineered two rituximab fragments of different sizes (a Mb of 80 kDa and a scFv-Fc fragment of 105 kDa). The authors reported that both fragments offered CD20-specific imaging, but the Mb-based radiotracer resulted in images of higher contrast.[537] Humanized obinutuzumab (GA101) and fully human ofatumumab are two other CD20-targeting mAbs showing superior activity when compared to rituximab.[538] Yoon et al. radiolabeled these two mAbs with ^{89}Zr and compared their diagnostic efficacies with ^{89}Zr-rituximab.[539] The authors reported that both

^{89}Zrobinituzumab and 89Zr-ofatumumab localized lymphoma xenografts more clearly than 89Zr-rituximab. Zettlitz et al. further engineered antibody fragments from obinutuzumab and radiolabeled these CD20-specific vectors with ^{89}Zr, ^{124}I, and ^{18}F.[197,540] Similarly, the authors found that obinutuzumab-based radiotracers outperformed rituximab-based radiotracers in delineating CD20 expression.[540] To further conquer the poor tumor penetration and undesirable pharmacokinetics of full-length antibodies, a set of hCD20-targeting sdAbs were generated.[68] One of these sdAbs, sdAb 9079 was radiolabeled with ^{68}Ga and ^{177}Lu and used for immunoPET imaging and targeted therapy of lymphoma, respectively.

Both 124I-rituximab and ^{89}Zr-rituximab immunoPET/CT imaging was able to visualize CD20 expression in patients with RA.[541,542] In addition to imaging NHL and RA, recent studies have reported the value of ^{89}Zr-rituximab immunoPET imaging in diagnosing orbital inflammatory diseases and interstitial pneumonitis,[543–545] but rituximab treatment has not been approved for these diseases.

4.2.2. CD38.—CD38 is a transmembrane glycoprotein highly and uniformly expressed on multiple myeloma (MM), NHL, and several types of solid tumor cells.[546,547] Several CD38-specific mAbs (e.g., daratumumab, isatuximab, and MOR202) have been developed. Daratumumab is a fully human mAb and has been proven a clinical success for treating MM.[548] Recently, both 64Cu- and 89Zr-labeled daratumumab have shown excellent imaging attributes for detecting subcutaneous and disseminated MM (Figure 17a–c).[549,550] Preclinical applications of CD38-targeted immunoPET imaging has also been extended to detecting lung cancer, hepatocellular carcinoma, and lymphoma (Figure 17d).[551–553] Additionally, CD38-specific sdAbs were generated for imaging and treating MM.[554,555] Small agents like sdAbs penetrate more effectively into the disseminated MM lesions than the conventional mAbs. Because daratumumab administration interferes with CD38 detection and some of the sdAbs binds to CD38 independently of daratumumab,[555,556] immunoPET probes derived from sdAbs will be very useful for detecting MM at early stages and evaluating the efficacy of daratumumab treatment.

Accompanying the above imaging success, substantial preclinical evidence has demonstrated that CD38-targeted RIT could achieve the eradication of disseminated MM.[557–559] Using a less immunogenic two-step pRIT strategy consisting of a novel 028-Fc-C825 bispecific protein (targeting CD38 antigen and yttrium-DOTA ligand) and a ^{90}Y-DOTA-biotin dramatically reduced tumor growth and increased survival in both MM and NHL models.[560] These results indicate the superiority of CD38 for both immunoPET imaging and pRIT. Clinical translation of these CD38-targeted theranostic agents will likely improve the management of patients with MM (NCT03665155).[561]

4.2.3. CD146.—CD146, also known as MUC18 or MCAM, was originally identified as a marker for melanoma and now is a novel biomarker for several cancers.[562] Recently, Jiang et al. demonstrated that CD146 interacts with VEGFR-2 in the endothelium and promotes angiogenesis. Additionally, they found that an anti-CD146 mAb (AA98) or CD146 siRNA could successfully inhibit the CD146/VEGFR-2 pathway.[563] It has been proven that AA98 has anticancer effects in several types of cancer, including leiomyosarcoma, pancreatic

cancer, hepatocellular carcinoma, breast cancer, among others.[564–567] The work is of importance because intrinsic or acquired resistance to bevacizumab occurs in clinical practice,[568] and novel agents targeting CD146 may have therapeutic benefits.

Our group initially generated a murine anti-CD146 mAb (denoted as YY146) and radiolabeled it for immunoPET imaging of glioblastoma multiforme.[569] In the work, we reported that ^{64}Cu-NOTA-YY146 immunoPET imaging could delineate U87MG tumors as small as 2 mm in diameter. Additionally, we explored the potential therapeutic effects of YY146 on U87MG cells. Another immunoPET imaging agent based on YY146 was developed by labeling the YY146 with ^{89}Zr.[570] Follow-up studies from our group revealed that ^{64}Cu-NOTA-YY146 immunoPET could clearly visualize both subcutaneous and metastatic lung cancer xenografts.[571,572] Furthermore, ^{89}Zr-Df-YY146-ZW800, a dual-modality imaging tool, enabled immunoPET and near-infrared fluorescence (NIRF) imaging of CD146-positive hepatocellular carcinomas (Figure 18a,b).[573] The prominent and persistent uptake of ^{89}Zr-Df-YY146-ZW800 also facilitated image-guided resection of the orthotopic HepG2 tumors (Figure 18c). On the basis of the previous success, a more recent study further developed a theranostic pair consisting of ^{89}Zr-Df-YY146 and IR700-YY146.[122] While immunoPET imaging with ^{89}Zr-Df-YY146 precisely diagnosed CD146-positive melanomas, PIT with IR700-YY146 efficiently eradicated a large portion of CD146-positive small melanomas in an image-guided manner. These promising results imply that the development of humanized YY146 (huYY146) would be worthwhile. In future clinical scenarios, immunoPET imaging with ^{64}Cu-NOTA-huYY146 or ^{89}Zr-Df-huYY146 may identify patients with an increased likelihood of responding to CD146-targeted therapies. CD146-targeted immunoPET imaging will be able to monitor early treatment responses to such therapies.

4.2.4. CD105.—Endoglin (CD105) is a transforming growth factor-β (TGF-β) coreceptor expressed on proliferating vascular endothelium in solid tumors.[574,575] A recent study elucidated that increased tumoral cytoplasmic and endothelial expression of CD105 was significantly associated with advanced stage, renal vein invasion, and microvascular invasion of RCC.[576] TRC105, a therapeutic mAb that binds to human CD105 with high avidity, has been demonstrated to be safe and effective in patients with advanced solid tumors such as RCC and hepatocellular carcinoma.[577–581]

The first successful immunoPET imaging of CD105 expression in murine breast tumor models was reported by our group in 2011.[582,583] ^{64}Cu-DOTA-TRC105 and ^{89}Zr-Df-TRC105 were used in these two studies. ^{66}Ga-NOTATRC105,[584] and multimodality imaging probes targeting CD105,[585–587] have since been developed and validated in various solid tumor models. Of note, ^{89}Zr-Df-TRC105–800CW immunoPET imaging could noninvasively monitor lung metastases from breast cancer and facilitate straightforward image-guided surgical removal of the tumors.[585] We also generated and characterized a Fab fragment from the TRC105 and then investigated its potential utility for PET imaging of tumor angiogenesis in breast cancer models.[588,589] To develop highly specific noninvasive imaging probes for pancreatic cancer, we synthesized a bispecific heterodimer by conjugating an antitissue factor (TF) Fab with an anti-CD105 Fab and then labeled the heterodimer with ^{64}Cu. This dual-targeting technique provided synergistic improvements in binding affinity,

and immunoPET imaging with the developed ^{64}Cu-NOTA-heterodimer clearly delineated both subcutaneous and orthotopic pancreatic tumors (Figure 18d,e).[590] After dual-labeling of the heterodimer with ^{64}Cu and fluorescent dye, dual-modality PET/NIRF imaging using ^{64}Cu-NOTA-heterodimer-ZW800 also specifically and readily detected pancreatic tumors.[591]

These studies strongly demonstrated the feasibility of noninvasive imaging of CD105 expression using PET or PET/NIRF technologies. Broad clinical applications of TRC105-based imaging will enable noninvasive detection of both primary and small metastatic tumor nodules, intra-operative guidance for tumor removal, selective patient stratification for TRC105 therapy, and image-guided RIT.[592] In addition, CD105 expression is upregulated on tumor endothelial cells following inhibition of the VEGF signaling pathway.[593,594] As such, TRC105-based immunoPET imaging may select patients who will potentially benefit from the combinational therapy with TRC105 and VEGF inhibitors or antibodies.

4.3. Carbohydrate Antigens

4.3.1. Carbohydrate Antigen 19.9.—Carbohydrate antigen 19.9 (CA19.9) is an established biomarker for several epithelial tumors, lung cancer, breast cancer, and PDAC. 5B1 is a fully human IgG targeting CA19.9 and has been widely used for theranostic purposes.[595–597] In a first-in-human clinical trial, immunoPET imaging with ^{89}Zr-DFO-5B1 detected known PDACs, metastases, and small LN metastases,[39] which remained undetected on conventional imaging studies.

By using the chemoenzymatic methodology described above,[287] 5B1 was also site-specifically modified with DFO and radiolabeled with 89Zr. ImmunoPET imaging with ^{89}Zr-^{ss}DFO-5B1 showed exceptional uptake of the radiotracer in the CA19.9-positive BxPC-3 models but not the CA19.9-negative MIAPaCa-2 models. Moreover, dual-modal imaging with ^{89}Zr-^{ss}dual-5B1 delineated both primary and metastatic tumors in an orthotopically implanted PDAC model.[598] Because tumors shed CA19.9 into the bloodstream, it is sometimes necessary to inject cold antibody to saturate the shed antigen.[599] By utilizing the IEDDA reaction with TCO-conjugated antibodies and Tz-conjugated radioligands, several pretargeted immunoPET imaging strategies have been explored. One such system with 5B1-TCO and Tz-PEG$_{11}$-Al[^{18}F]-NOTA resulted in clear delineation of the CA19.9-expressing PDAC xenografts. However, radioactivity in the intestine retained over the imaging course. Another pretargeting approach consisting of 5B1-TCO and ^{64}Cu-NOTA-PEG$_7$-Tz or ^{64}Cu-NOTA-Tz showed improved diagnostic value, with the former combination showed better T/B contrast at the earlier imaging time-points (Figure 19).[600]

4.3.2. Carbohydrate Antigen 125.—Mucin 16 (MUC16) is a glycoprotein highly expressed in several types of cancers (e.g., ovarian, endometrial, and fallopian tube cancers). Carbohydrate antigen 125 (CA-125) is the released extracellular region of MUC16 following proteolytic cleavage and is regularly used to screen for ovarian cancer, to monitor cancer treatment efficacy, and to check for cancer recurrence.[601] B43.13 (oregovomab) is a high-affinity murine mAb and has been employed as an immunotherapeutic agent in the treatment of advanced ovarian cancers. To facilitate early detection of ovarian cancers, 64Cu-NOTA-

mAb-B43.13 and ^{89}Zr-DFO-mAb-B43.13 were developed sequentially.[602,603] ImmunoPET imaging with these two tracers clearly delineated CA125-positive OVCAR3 tumors. ^{89}Zr-DFO-mAb-B43.13 immunoPET imaging is particularly attractive because it also detected LN involvement with high contrast and accuracy.[603] REGN4018 is a human BsAb that specifically binds to MUC16 and CD3.[604] Although circulating CA-125 serves as an antigen sink and interferes with MUC16-targeted therapies, the potency of REGN4018 is not hampered by the circulating CA-125. It has been shown that the site-specifically labeled ^{89}Zr-DFO-REGN4018 localized to the spleen and lymph nodes of nontumor-bearing mice. The imaging capabilities of ^{89}Zr-DFO-REGN4018 was further investigated in humanized mouse models with two humanized targets (CD3 and MUC16). In these models, the bispecific ^{89}Zr-DFOREGN4018 specifically accumulated in the secondary lymphoid organs as well as the MUC16-expressing tumors (Figure 20). Currently, REGN4018 is undergoing a phase I clinical trial (NCT03564340) either as a monotherapy agent or in combination with cemiplimab (an anti-PD-1 antibody).

4.4. Prostate-Specific Membrane Antigen

Using ^{18}F-FDG or ^{11}C-choline PET tracers to image prostate cancer (PCa) often yields false negative or false positive uptake due to the slow growth and the low glycolytic rate of most PCas. Interpretation of ^{18}F-FDG PET images in PCa is often difficult or even impossible because of the spillover effects from the accumulation of the tracer in the bladder and the intestine.[605] Prostate-specific membrane antigen (PSMA) is a transmembrane glycoprotein that is highly expressed on most prostate adenocarcinomas and has gained increasing interest as a target molecule for imaging and therapy in the past five years.[606–608] A recent study has elucidated a novel oncogenic signaling role of PSMA and reported that suppression of PSMA inhibited the PI3K signaling pathway and promoted tumor regression in preclinical PCa models.[609] Studies using both antibodies and small-molecule agents have been conducted to develop PSMA-targeted SPECT and PET imaging platforms. PSMA-targeted theranostic approaches have been extensively reviewed elsewhere.[610–613] Herein, we only focus on PSMA-specific immunoPET imaging probes.

A variety of mAbs specific for intracellular and extracellular epitopes of PSMA have been developed.[605,614–616] J591, a humanized mAb which binds to an extracellular domain of PSMA, has been clinically investigated for both imaging and therapy.[617–621] Recently, Fung et al. demonstrated that ^{124}IJ591 and ^{89}Zr-J591 had comparable surface binding and internalization rates in preclinical prostate models.[622] These studies imply that PCa theranostics using ^{177}Lu- and ^{124}I-or ^{89}Zr- labeled J591 is feasible, safe and may have superior targeting toward bone lesions relative to conventional imaging modalities. This may refine management strategies for patients with PSMA-positive PCas. Capromab (7E11) is a murine mAb, which has been investigated clinically as a SPECT imaging agent for recurrent and metastatic PCas[623] and a therapeutic agent after labeling with ^{90}Y.[624] Because capromab binds to an epitope on the intracellular domain of PSMA, tracers derived from this mAb are limited to detecting dead cells and do not possess advantages in imaging soft-tissue and bone metastases from PCas when compared to tracers binding to the extracellular domain.[625] D2B is another PSMA-specific murine mAb for developing theranostic agents.[626,627] More recently, Barinka and co-workers reported the characterization of four novel

murine PSMA-specific mAbs. One of these, 5D3, demonstrated 10-fold higher affinity compared to J591.[628] A follow-up study further revealed that 5D3 may serve as a promising surrogate for imaging PSMA expression.[629]

When compared to mAbs, VHHs and engineered antibody fragments offer faster delivery and similar tumor delineating properties.[630,631] Viola-Villegas et al. engineered a Mb and a diabody from the intact antibody J591 and reported that immunoPET imaging with these smaller antibody fragments offered rapid tumor accumulation and accelerated clearance in PSMA-expressing PCas.[632] One such radiotracer, ^{89}Zr-IAB2M, was further translated in a dose-escalation clinical trial that included 18 patients with metastatic PCas.[633] In this clinical study, immunoPET imaging with ^{89}Zr-IAB2M delineated metastatic PCa lesions in 17 of 18 patients 48 h after the intravenous injection of the radiotracer (10 mg). Moreover, ^{89}Zr-IAB2M immunoPET outperformed ^{99m}Tc-MDP and CT in detecting bone lesions and magnetic resonance imaging (MRI) and ^{18}F-FDG PET in detecting LN/soft tissue metastases (Figure 21).[633] A phase I/IIa trial further confirmed the diagnostic efficacy of ^{89}Zr-IAB2M.[634] Another advantage of this probe was its negligible accumulation in lacrimal and salivary glands because a major side effect of PSMA-targeting agents is the xerostomia.[635] Beile et al. initially generated three mAbs against cell-adherent PSMA from spleen cells of mice[636–638] and more recently developed multimeric antibody fragments from these murine antibodies.[639] They showed that the radiolabeled antibody fragments had stable tumor uptake and faster serum clearance.

Amassing clinical studies investigating PSMA-targeted PET imaging have demonstrated uptake of the tracers in non-prostate malignancies.[640,641] It has been proposed that uptake of PSMA-targeted tracer in nonprostate malignancies is due to the significant angiogenesis in tumor tissues.[642] Indeed, PSMA is expressed by the neovasculature endothelium but not by the tumor cells or the normal vasculature endothelium in most solid tumors.[643,644] In this context, several clinical studies have suggested that PSMA is another promising surrogate for molecular imaging of tumor neovasculature.[645,646] As such, PSMA-targeted PET and immunoPET imaging will help select patients for subsequent PSMA-targeted therapies and/or antiangiogenesis therapies (e.g., bevacizumab).

4.5. Carcinoembryonic Antigen

As a key member of carcinoembryonic antigen-related cell adhesion molecules (CEACAMs), carcinoembryonic antigen (CEA) serves as a vital tumor antigen and a serum tumor marker.[647] Arcitumomab (CEAScan) is a ^{99m}Tc-labeled hapten-peptide pretargeted imaging probe approved by the FDA and EMA for detecting colonic cancer metastases.[648] However, this agent was withdrawn from the market because of competition from the more cost-effective ^{18}F-FDG. To improve the imaging quality and specificity, several CEA-specific pretargeted immunoSPECT imaging agents were investigated. These efforts are exemplified in a study by Sharkey et al.,[649] in which a superior tumor-to-blood ratio (~100:1) was obtained in human colon cancer xenografts. Alternatively, CEA-directed pretargeted immunoPET imaging was designed by first pretargeting CEA with a multivalent BsAb (which also targets HSG) followed by the injection of a radiolabeled hapten peptide. In this strategy, the DOTA-containing IMP288 peptide allowed ^{68}Ga complexation and the

NOTA-containing IMP-449 peptide allowed facile [^{18}F]AlF chelation.[311,650] In addition to detecting subcutaneous tumors, two recent studies demonstrated that TF2/^{68}Ga-IMP288 pretargeted immunoPET outperformed ^{18}F-FDG PET in detecting disseminated human colorectal cancers (Figure 22).[651,652] Moreover, this highly sensitive pretargeting technique could be used to visualize CEA-containing human colorectal cancer tissues and normal epithelial cells.[653] The study also demonstrated that pretargeted immunoPET has superior accuracy than ^{18}F-FDG PET in delineating CEA$^+$ tumors due to the highly specific tumor uptake and low background activity. Upon clinical translation, this novel imaging method may be useful to identify tumor lesions during surgical dissection. A recent first-in-human clinical trial has reported that TF2/^{68}Ga-IMP288 pretargeted immunoPET imaging revealed abnormal foci in all patients with relapsed medullary thyroid cancer.[654] This study also demonstrated that a 30 h time lag between the injection of TF2 and ^{68}Ga-IMP288 and a TF2-to-IMP288 molar ratio of 20 were the most favorable conditions for imaging. Moreover, an ongoing clinical trial is evaluating the diagnostic role of TF2/^{68}Ga-IMP288 pretargeted immunoPET imaging in patients with HER2-negative but CEA$^+$ breast cancers (NCT01730612).

Along with this progress, a series of antibody fragments were engineered from a murine mAb T84.66 and have been radiolabeled with radiometals such as ^{64}Cu and ^{124}I.[655–657] To improve the T/B ratio of the engineered antibody fragments, mutation of the residues in the Fc fragment essential for FcRn binding can be performed. For instance, Kenanova et al. formatted a series of anti-CEA scFv-Fc fragments[658,659] and found that PET imaging with a ^{124}I-labeled scFv-Fc bearing one double mutation (H310A/H435Q) showed the highest imaging quality.[658] To further permit same-day immunoPET imaging, several types of labetuzumab fragments have been radiolabeled with [^{18}F]AlF using the chelating ligand NODAMPAEM.[660] Despite the facile and rapid procedure, high kidney and liver accumulation of the developed tracers may hinder the clinical translation.[660]

AMG 211 (MEDI-565) is a BiTE composed of a humanized anti-CEA arm and a deimmunized anti-CD3 arm. AMG 211 could efficiently activate human T cells which lysed CEA$^+$ colorectal tumor cells in a preclinical model.[661] However, this treatment effect was not observed in patients with advanced gastrointestinal adenocarcinoma.[662] To uncover the underlying reasons for the poor efficacy, the in vivo biodistribution and tumor targeting ability of AMG 211 was investigated with ^{89}Zr-AMG 211 immunoPET imaging.[663,664] The results revealed the accumulation of the tracer in CD3-rich lymphoid organs (e.g., spleen and bone marrow). Tumor uptake of ^{89}Zr-AMG 211 was evident yet varied strikingly within and between patients, attributed to the heterogeneous expression of CEA in different tumor lesions and varying tumor vasculature and tissue permeability.[664] To specifically deliver interleukin-2 (IL-2) to CEA$^+$ tumors and overcome the adverse effects of IL-2 monotherapy, cergutuzumab amunaleukin (CEA-IL2v) has been designed and is actively undergoing a clinical investigation in combination with the anti-PD-L1 atezolizumab in CEA-expressing advanced solid tumors (NCT02350673).[665] Recently, a pilot immunoPET imaging study with ^{89}Zr-CEAIL2v showed a preferential drug accumulation in CEA$^+$ tumors, and two cycles of CEA-IL2v administration reduced the number of tumor lesions and tumor uptake of the radiotracer (Figure 23).[666] This exploratory study also indicated nonspecific uptake of ^{89}Zr-CEA-IL2 in nonmalignant lymphoid organs, suggesting the in vivo distribution of

CEA-IL2v is driven by the synergistic effect of CEA targeting and IL-2 binding on immune cells.

4.6. Carbonic Anhydrase IX

Carbonic anhydrase IX (CAIX) is a cytosolic and trans-membrane enzyme belonging to the zinc-containing metal-loenzyme family.[667] By catalyzing the conversion of carbon dioxide and water to carbonic acid ($CO_2 + H_2O \rightleftarrows HCO_3^- + H^+$), CAIX contributes to the acidic extracellular environment of hypoxic tissues, predominantly hypoxic tumors and metastases.[668] CAIX is homogeneously overexpressed in 95% of clear cell renal cell carcinoma (ccRCC) cases, so it is an optimal theranostic target for ccRCC. Several mAbs (e.g., cG250 or girentuximab) targeting CAIX are undergoing clinical investigations.[669,670] On the basis of preclinical studies, where 124I-cG250 and ^{89}Zr-cG250 immunoPET imaging clearly visualized CAIX-expressing ccRCC xenografts,[671–673] a recent clinical study reported that ^{89}Zr-girentuximab immunoPET imaging precisely predicted the pathology of all the immunoPET-positive primary renal lesions. This result changed the clinical decision for 36% of patients with recurrent/metastatic ccRCC (Figure 24).[674] Several proof-of-concept clinical studies have also validated the safety and superior diagnostic value of ^{124}I-cG250 in ccRCC,[184,186,675] with an average sensitivity and specificity of 86.2% and 85.9%, respectively.[186] Additionally, multimodal imaging with ^{124}I-cG250 could realize precise intraoperative localization of ccRCC, which further guided and confirmed complete surgical resection of the diseases.[676] In contrast to ^{124}I-cG250, which rapidly releases ^{124}I after being internalized into tumor cells, the residual radiometal ^{89}Zr from ^{89}Zr-cG250 will be trapped inside the tumor cells.[672]

M75, another mAb targeting CAIX, is regularly used in IHC studies to detect CAIX.[677] In recent studies this mAb has been radiolabeled with ^{64}Cu and ^{61}Cu, and the developed radiotracers revealed specific binding in CAIX-expressing colorectal cancer models.[678,679] Moreover, several other CAIX targeting mAbs have shown preliminary anticancer effects.[680–682] Up to now, they have not been used for immunoPET imaging. Lastly, it is worthwhile to note that CAIX is highly expressed in a plethora of other tumor cells, tumor-associated stromal cells, and cancer stem cells.[668] Because of the above-described merits and limited presence of CAIX in normal tissues, CAIX may serve as an ideal target for developing advanced theranostic agents.

4.7. Trophoblast Cell Surface Antigen 2

Trophoblast cell surface antigen 2 (TROP-2), a 46 kDa transmembrane glycoprotein, is overexpressed in a broad range of cancers.[683,684] Sacituzumab govitecan (IMMU-132) is an antibody–drug conjugate (ADC) targeting TROP-2 and has been approved as a third-line therapy for metastatic triple-negative breast cancers.[685] Moreover, its application is being extended for the treatment of several other malignancies. hRS7 is a humanized IgG1 mAb targeting TROP-2. hRS7-based immunoPET or immunoSPECT imaging clearly visualized TROP2 expression in PCa models.[686] TF12 (157 kDa) is a trivalent BsAb composed of an anti-HSG Fab and two anti-TROP-2 Fabs derived from the hRS7.[687] Using TF12, pretargeted immunoPET imaging, pRIT, and image-guided surgery of human PCas have all been achieved.[688–690] While TROP-2 immunoPET imaging is of clinical interest for

selecting TROP-2-positive patients, its value in evaluating the therapeutic response following IMMU-132 treatment is limited because TROP-2 is not a predictive biomarker for response.[691]

4.8. Stem Cell Antigens

Cancer stem cells (CSCs) are characterized by undifferentiated features, which may include self-renewal, long-term replication, and diverse differentiation abilities.[692] It has been proposed that CSCs are a major driving force of tumor occurrence and metastasis.[693] Additionally, chemotherapy and radiotherapy resistances are mediated in part by CSCs.[694] Therefore, noninvasive imaging of CSCs is clinically relevant and may aid the identification and eradication of CSCs. Of the various stem cell markers, leucine-rich repeat-containing G-protein coupled receptor 5 (LGR5), prostate stem cell antigen (PSCA), and CD133 are three attractive biomarkers that have been exploited for immunoPET imaging.

LGR5, a marker of adult stem cells, is highly expressed in some human cancers.[695] Noninvasive LGR5 assessment was achieved with two LGR5-targeting immunoPET probes (i.e., ^{89}Zr-DFO-8F2 and ^{89}Zr-DFO-9G5). ^{89}Zr-DFO-8F2 showed higher specificity over ^{89}Zr-DFO-9G5 in visualizing LGR5 expression in colorectal tumors.[696] While PSMA-targeting agents have shown great promise in patients with PCas, PSCA is an alternative target for designing theranostic agents. Using an anti-PSCA mAb, 7F5, and a newly developed chelator, L^5-NCS, David et al. showed that ^{64}Cu-L^5-7F5 immunoPET imaging clearly visualized PSCA-positive PC3 tumors with minute activity in the liver. In comparison, ^{64}Cu-NODAGA-7F5 immunoPET imaging showed much less tumor accumulation but significantly higher liver uptake (Figure 25).[158] A11 is a humanized anti-PSCA Mb and ^{124}I or ^{89}Zr-labeled A11 was able to detect PSCA-expressing PCas[697] as well as to evaluate the treatment response.[698] Additionally, PSCA-targeted fluorescence or dual-modal immunoPET/fluorescence imaging agents hold great promise for intraoperatively visualizing PSCA-positive PCas and pancreatic cancers.[699–701]

AC133, an epitope of the second extracellular loop of CD133, is one of the most extensively investigated markers for CSCs.[702] An initial study showed that anti-AC133 mAb-based fluorescence imaging agents visualized CD133-overexpressing tumors.[703] More recently, immunoPET imaging with an AC133-targeted radiotracer (^{64}Cu-NOTA-AC133 mAb) permitted successful detection of CD133$^+$ U251 tumors and glioma stem cells. More importantly, the ^{64}Cu-NOTA-AC133 mAb immunoPET imaging patterns correlated well with the cytoarchitecture of the orthotopically growing gliomas.[704] In the efforts for imaging CSCs, one recurring concern is that CSCs are not abundant in the TME. Taking this fact into consideration, we advocate the use of PET imaging over other imaging modalities for detecting and quantifying CSCs.

4.9. Proteases

Proteases are a group of evolutionarily conserved enzymes and can be classified into six groups by their mechanisms of action: Cys, serine, threonine, aspartate, glutamic acid proteases, and metalloprotease. Proteases play essential roles in tumor angiogenesis, invasion, and metastasis.[705] Therefore, proteases are attractive targets for developing

molecular imaging probes. Urokinase plasminogen activator (uPA) receptor (uPAR) is one of the validated targets. AE105, a high-affinity peptide antagonist against uPAR, has been radiolabeled and investigated extensively in preclinical studies.[706] Inspired by the preclinical success, ^{64}Cu-DOTA-AE105 and ^{68}Ga-NOTA-AE105 have been successfully translated into the clinic for PET imaging of uPAR in patients with solid tumors.[707,708] Using an IgG1 mAb (ATN-291) specifically targeting human uPA, Yang and co-workers developed a radiotracer ^{89}Zr-Df-ATN-291.[709] The authors reported the utility of ^{89}Zr-Df-ATN-291 immunoPET in monitoring the expression of uPA/uPAR in several mouse xenografts. Matrix metalloproteinases (MMPs) have been heralded as attractive targets for cancer therapy for decades.[710] LEM-2/15 is a mAb specific for membrane type 1-matrix metalloproteinase (MT1-MMP, MMP14), and immunoPET imaging with ^{89}Zr-DFO-LEM 2/15 specifically localized the intracranial patient-derived xenograft tumors.[711] Moreover, ^{89}Zr-DFO-LEM 2/15 immunoPET imaging showed a higher specificity than ^{68}Ga-DOTAAF7p, a MT1-MMP-specific peptide-based tracer, in identifying PDACs.[712]

Prostate-specific antigen (PSA) is a target in the androgen receptor (AR) pathway. PSA level in the blood is a reliable readout of AR pathway activity. “Free” PSA (fPSA) is a catalytically active serine protease and has been exploited as an immunoPET imaging target. 5A10 is a mAb that selectively binds fPSA. ^{89}Zr-5A10 immunoPET detected intratumoral fPSA expression following different pharmacological interventions.[713] However, ^{89}Zr-5A10 immunoPET yielded less favorable imaging contrast because ^{89}Zr-5A10 targeted secreted PSA with only a small proportion of the tracer directed to the tumor sites. Therefore, an immunoPET probe with increased internalization into tumor cells would image the AR pathway activity more clearly. To achieve this, two mAbs (i.e., 11B6 and its humanized version hu11B6) targeting human kallikrein-related peptidase 2 (hK2), another serine protease regulated by the AR pathway, were used for immunoPET imaging.[714] In contrast to the transient uptake of ^{89}Zr-5A10 in tumors, ^{89}Zr-11B6 internalized into the tumor cells and showed steadily increasing tumor uptake. Moreover, ^{89}Zr-11B6 immunoPET imaging delineated AR-driven hK2 expression in mice bearing subcutaneous or metastatic human PCa xenografts.[714]

4.10. Membrane-Bound Surface Glycoprotein Mesothelin

Membrane-bound surface glycoprotein mesothelin (MSLN) is overexpressed in mesothelioma and several other solid tumors such as ovarian, lung, breast, and pancreatic cancers.[715,716] It is worth mentioning that soluble mesothelin is a superior tumor marker for monitoring tumor burden and therapeutic response in patients with malignant pleural mesothelioma.[717] Substantial studies have reported the feasibility of MSLN imaging using several MSLN-targeting mAbs such as a murine mAb 11–25, a chimeric mAb amatuximab, and an ADC DMOT4039A (composed of MMOT0530A and MMAE).[718–720] In a clinical study evaluating the treatment efficacy of DMOT4039A in patients with pancreatic or ovarian cancer, Lamberts et al. found that uptake of ^{89}Zr-MMOT0530A correlated with MSLN expression from IHC staining.[721] These results indicate that this imaging technique may guide individualized antibody-based therapies. As observed in a previous study,[361] several recent studies have demonstrated that shed antigen MSLN in blood circulation negatively regulates the circulation and tumor-targeting efficacy of amatuximab.[722,723]

These results indicate the role of MSLN-targeted immunoPET in assessing the performance of mesothelin-targeted therapeutic antibodies and selecting patients for mesothelin-targeted therapies.[724]

4.11. Glycoprotein A33

Glycoprotein A33 (GPA33) is a cell surface target uniformly overexpressed in over 90% of colorectal cancers and a subset of gastric and pancreatic cancers.[725] This antigen has been extensively studied as a target for both RIT and SPECT imaging using a murine mAb A33.[726,727] Following the humanization of A33 (huA33) and preclinical evaluation of huA33-based immunoPET tracers,[728,729] recent studies have translated ^{124}I-huA33 to the clinic. This immunoPET imaging technique enabled the quantitative assessment of GPA33 status in colorectal cancers.[185,730] Pretargeted immunoPET imaging has been successfully employed to delineate GPA33-expressing human colorectal carcinoma xenografts. In such a work by Zeglis et al., huA33-TCO was administered 24 h prior to ^{64}Cu-Tz-SarAr to reach the tumors and permit blood clearance.[339] Owing to the superior stability and exclusive renal clearance of ^{64}Cu-Tz-SarAr, the in vivo pretargeting yielded specific uptake of the radioligand in the colorectal tumors with high T/B ratios (Figure 26). This imaging strategy also outperformed a previous pretargeted imaging strategy, in which substantial uptake of ^{64}Cu-Tz-NOTA was observed in the gastrointestinal tract.[335] In the future, the combination of GPA33-specific immunoPET imaging and pRIT may allow precise diagnosis and treatment of colorectal cancers.[329,731,732]

4.12. Other Promising Tumor Biomarkers

Several other cell surface antigens have shown promise for imaging cancers at the cellular and molecular levels in either preclinical or clinical settings, such as folate receptor alpha,[733,734] tumor vascular markers,[735–737] death receptor 5,[738–740] glypican-3,[741–743] cell adhesion molecules,[744,745] six-transmembrane epithelial antigen of prostate-1 (STEAP1),[746–749] hormone receptors,[750–752] TGF-β pathway,[753–755] chemokine receptors,[756,757] and extracellular matrix-like fibronectin.[162,188] Here, we also discuss some of the promising targets briefly.

Tumor-associated glycoprotein (TAG)-72 is another glyco-protein highly expressed in the majority of adenocarcinomas. 3E8 is a humanized mAb against TAG-72 and has shown theranostic potential in colorectal cancer xenografts.[758] For antibody fragment-based immunoPET imaging of TAG-72, PEGylated targeting vectors may serve as favorable surrogates for efficiently delivering the radionuclide to the tumor site while lowering kidney uptake.[759–761] Delta-like 3 (DLL3), a Notch pathway ligand, has been identified as a marker for pulmonary neuroendocrine tumors (i.e., small cell lung cancer and large cell neuroendocrine carcinoma) and neuroendocrine PCas.[762–764] As such, DLL3 may also serve as a tractable immunoPET imaging target.[765,766] Similar to the GPA33-targeted theranostic scenario, GD2-specific immunoPET imaging may help assess GD2 expression in patients with neuroblastomas.[767,768] Along with the clinical use of GD2-targeted antibody therapy and RIT,[769–771] and future implementation of pRIT,[772] GD2-targeted immunoPET imaging may guide precise anti-GD2 therapies and complement other imaging modalities to refine the management of neuroblastomas.

5. IMMUNOPET IMAGING OF IMMUNE SYSTEM

Cancer immunotherapy is increasingly becoming the standard-of-care treatment for a broad spectrum of cancers. IHC, polymerase-chain-reaction (PCR)-based assays and serum or blood biomarkers are regularly used to predict the therapeutic responses of immunotherapy regimens. Despite these approaches, it is still very challenging to properly select patients suitable for immunotherapy and precisely evaluate the treatment responses. Furthermore, immune-related adverse events are increasingly being reported. Currently, there are no reliable surveillance strategies to diagnose those unexpected complications.[773,774] Accumulating evidence has suggested that immunoPET imaging may substantially improve the clinical immunotherapy by dynamically visualizing immune responses across the whole body.[775–777] To achieve this goal, radiotracers have been developed to image interleukins and specific immune cells, including B cells,[778] natural killer cells,[779,780] macrophages,[781–783] myeloid cells,[278,784] and T cells. In this section, we mainly present the most recent evidence of immunoPET strategies in delineating T cells by targeting lineage-associated antigens, immune checkpoint molecules, OX40, and interferon gamma (IFN γ).

5.1. Lineage-Associated Antigens

In addition to tracking T cells via ex vivo direct labeling or reporter gene imaging,[785–787] it is advantageous to track T cells using novel immunoPET techniques by targeting general T cell markers (e.g., CD3, CD4, CD8, CD2, and CD7). ImmunoPET imaging with a ^{89}Zr-labeled antimouse CD3 antibody (clone 17A2; R&D Systems) revealed a correlation between high tumor uptake of the radiotracer and better therapeutic response of anticytotoxic T lymphocyte antigen 4 (CTLA-4) therapy in a preclinical colorectal cancer model.[788] However, significant liver accumulation of the radiotracer was found on immunoPET images, which was explained as liver clearance of the radiolabeled antibody. Another study also labeled the same clone (clone 17A2; Bio X Cell) with ^{89}Zr and confirmed the uptake of the developed radiotracer in lymphoid organs (i.e., spleen, lymph nodes, and thymus) and tumor-infiltrating lymphocytes (TILs) in syngeneic bladder cancer models.[789] But what was different in this study was that the tracer was largely deposited in the spleen rather than in the liver, similar to that reported in another study.[790] CD2 and CD7 are pan T cell markers and immunoPET tracers targeting these two markers have been developed to track adoptively transferred T cells.[791] However, the safety profiles, long-term effects, and impact of these tracers on the functionality of T cells remain to be determined.

To noninvasively detect CD8$^+$ T cells, two Mbs (i.e., 2.43 Mb and YTS169 Mb) were engineered from two parental rat antimouse CD8 mAbs. Both ^{64}Cu-NOTA-Mbs retained high antigen specificity in imaging CD8$^+$ T cells.[792] IAB22M2C is a clinical-stage Mb that targets human CD8 with high affinity. A recent phase I study has demonstrated the safety profile of ^{89}Zr-Df-IAB22M2C immunoPET imaging in patients with solid tumors.[793] This study also reported a specific accumulation of the radiotracer in CD8$^+$ T cell-rich tissues, such as lymph nodes, spleen, and tumors. A phase II clinical trial with this immunoPET probe investigating the correlation between 89Zr-Df-IAB22M2C immunoPET signal and CD8 status assessed by IHC in patients with metastatic cancers is currently underway (NCT03802123).

Two diabody-based anti-CD4 and anti-CD8 tracers, ^{89}ZrmalDFO-GK1.5 cDb and ^{89}Zr-malDFO-2.43 cDb, also specifically targeted various lymphoid organs and allowed longitudinal monitoring of transplanted T cells.[794] To thoroughly assess CD8-targeted immunoPET imaging, ^{89}ZrmalDFO-169 cDb binding to CD8a of all mouse strains was assessed.[795] ImmunoPET imaging with this radiotracer detected intratumoral CD8$^+$ T cells after anti-CD137 or anti-PD-L1 therapy in immune-competent mice bearing CT26 tumors. Afterward, ^{64}Cu-TETA-169 cDb was developed and used to image CD8$^+$ T cells after immunotherapy using different treatment protocols.[796] As reported by the work, serial ^{64}Cu-TETA-169 cDb immunoPET imaging mapped T cell distribution and also detected treatment-associated hypertrophy of liver and spleen following multiple cycles of immunotherapy.

Other types of antibody vectors used for imaging T cells include VHH and monovalent antibody. Rashidian et al. produced a CD8-specific mouse VHH (VHH-X118) and fabricated ^{89}Zr-PEGylatedVHH-X118 using sortase-catalyzed site-specific conjugation.[64] This immunoPET probe robustly detected thymus, secondary lymphoid structures as well as CD8$^+$ T cells in B16 melanomas. This study also highlighted the value of CD8-targeted immunoPET in predicting the treatment response of anti-CTLA-4 immunotherapy, where the homogeneous distribution of immunoPET signal within the tumors predicted a favorable response to the anti-CTLA-4 immunotherapy. Moreover, another recent study radiolabeled a CD8-specific monovalent antibody with ^{89}Zr and immuno-PET imaging with the developed agent (denoted as ZED8) efficiently detected human CD8-expressing tumors.[797] This tracer was developed under quality standards appropriate for regulatory approval and is currently under clinical investigation (NCT04029181).

5.2. Immune Checkpoints

Immune checkpoints are critical components of inhibitory immune signaling pathways. The first-generation immune checkpoint inhibitors are immunomodulatory mAbs that block immune checkpoints. Notably, immune checkpoint inhibitors blocking CTLA-4, programmed death receptor 1 (PD1), and PD-L1 have emerged as trailblazers in treating various kinds of cancers.[6] Accordingly, immunoPET probes targeting CTLA-4, PD1, or PD-L1, are extensively investigated.

CTLA-4 is a negative immune regulator highly expressed on regulatory T cells (Treg) and on activated T cells. Recent studies have elucidated that CTLA-4 and PD-1 may share one pathway by inhibiting signaling through CD28, which is a costimulatory receptor that promotes T cell activation and proliferation.[798] Several studies have reported the feasibility of CTLA-4-targeted immunoPET in imaging T cells in humanized mice[799] and in immune-competent mice.[800] H11 is a VHH targeting mouse CTLA-4 and immunoPET with ^{89}Zr-H11-PEG clearly delineated CTLA-4 expression within the TME.[801] Moreover, several studies have shown the expression of CTLA-4 on tumor cells,[802] which was corroborated by an imaging study where ^{64}Cu-DOTA-ipilimumab showed persistent accumulation in the CTLA-4-expressing A549 tumors.[803]

PD1 is a characteristic marker expressed on exhausted CD8$^+$ T cells. Pembrolizumab and nivolumab are anti-PD-1 checkpoint inhibitors used for treating a variety of solid tumors.

Several immunoPET probes using pembrolizumab/ nivolumab and ^{89}Zr/^{64}Cu have been developed and investigated in preclinical studies.[804–808] Of them, ^{89}Zr-pembrolizumab and 64Cu-pembrolizumab PET/CT examinations showed prominent uptake of the radiotracers in the humanized mice bearing A375 melanomas, indicating infiltration of PD-1-positive human lymphocytes into the tumors.[806] Similarly, ^{89}Zr-Df-nivolumab immunoPET imaging delineated PD-1-positive human lymphocytes in A549 tumors and salivary glands in humanized mice.[808] More recently, a seminal study by Niemeijer et al. investigated the clinical value of ^{89}Zr-Dfnivolumab immunoPET imaging in 13 patients with NSCLC prior to the nivolumab treatment.[809] For the first time, this study reported a correlation between ^{89}Zr-Df-nivolumab uptake and PD-1 expression in the TILs assessed by IHC in clinical settings (Figure 27a,b). This study also indicated the value of ^{89}Zr-Df-nivolumab uptake in predicting the treatment efficacy of nivolumab. However, this predictive value needs to be confirmed in a larger patient cohort.

Two IHC methods for determining PD-L1 expression have been approved to predict patient response before anti–PD-L1 therapies. However, sampling limitations and multifaceted expression of PD-L1 may lead to underestimation of the target. Substantial preclinical evidence has suggested that immuno-PET imaging can assess the heterogeneous status of PD-L1 throughout the whole body and thus can overcome above drawbacks.[810–813] In a recent first-in-human clinical trial (NCT02478099), 89Zr-atezolizumab was assessed in 22 patients with progressive bladder cancer, NSCLC or triple-negative breast cancer.[21] ImmunoPET imaging with ^{89}Zratezolizumab showed deposition of the radiotracer in non-malignant lymph nodes, spleens, and sites of inflammation. More importantly, ^{89}Zr-atezolizumab immunoPET visualized all the metastatic tumor lesions by imaging heterogeneous PD-L1 expression. High tumor uptake of ^{89}Zr-atezolizumab correlated with better response to atezolizumab treatment, whereas PD-L1 IHC failed to predict the treatment outcome. ^{89}Zr-atezolizumab immunoPET imaging could also select RCC patients who may benefit from nivolumab therapy.[814] Moreover, there are two ongoing clinical trials evaluating the diagnostic value of PD-L1-targeted immunoPET in advanced thoracic malignancies (NCT03746704) and in locally advanced or metastatic solid tumors (NCT02453984).

Engineered small proteins (e.g., fibronectin, ~10 kDa) are alternative targeting moieties that have been used for imaging PD-L1 expression.[815] Following a preclinical study which discovered the high binding affinity of ^{18}F-BMS-986192 (an ^{18}F-labeled adnectin) to human and cynomolgus PD-L1,[816] a recent clinical study reported that ^{18}F-BMS-986192 immuno-PET could noninvasively image the heterogeneous PD-L1 status in lung cancers (Figure 27c). High-affinity consensus (HAC) PD1 (14 kDa) is another high-affinity binder engineered from PD-1 protein and can be used for imaging human PD-L.[817] In the course of optimizing HAC-PD1 variants for PD-L1 imaging, aglycosylated HAC-PD1 showed increased tumor uptake and decreased glandular uptake.[818] Other targeting vectors that have been integrated into immunoPET for imaging PD-L1 include an Affibody molecule,[819] VHHs,[820–822] and a Fab fragment.[823]

Beyond imaging PD-L1 expression pre- and postimmuno-therapy, PD-L1-targeted immunoPET is an innovative approach to monitor PD-L1 upregulation following radiation

therapy[824,825] or PD-L1 downregulation after molecular-targeted therapy.[826] Although anti-PD-L1 therapy has become the first-line treatment option for patients with NSCLC, therapeutic resistance occurs in some patients. Among many potential reasons, secreted PD-L1 splicing variants may induce resistance to anti-PD-L1 therapy by acting as decoys in plasma.[827] Similar to that observed in other conditions,[722,723] PD-L1-targeted immunoPET may predict and assess anti-PDL1 resistance because soluble PD-L1 will relocate the radiotracer to the plasma and liver but not to the tumor sites. Besides its expression on tumor cells, PD-L1 is also expressed in normal lymphoid organs and is an independent marker for brown adipose tissue (BAT) (Figure 28),[828–830] indicating that PD-L1-targeted immunoPET may as serve as a cutting-edge imaging technique to aid basic research.

5.3. Other Emerging T Cell Markers

OX40, also known as CD134, is a 50 kDa type I membrane glycoprotein belonging to the tumor necrosis factor (TNF) receptor superfamily.[831] Binding of OX40 by its ligand OX40L results in the activation of T cells, indicating OX40 is a promising candidate for monitoring clinical immunotherapies. By radiolabeling a murine mAb (clone: OX-86; Bio X Cell) with ^{64}Cu, Alam et al. developed an OX40-targeted radiotracer ^{64}Cu-DOTA-AbOX40.[832] The authors found that early immunoPET imaging with ^{64}Cu-DOTA-AbOX40 characterized the spatiotemporal expression of OX40$^+$ T cells and also predicted the response of CpG vaccination in lymphoma models. These results demonstrated that OX40-targeted immunoPET could adequately visualize the heterogeneous dynamics of OX40$^+$ T cells in immune responses across different subjects. For further clinical translation, this murine antibody-based immunoPET imaging strategy needs to be optimized with human or humanized antibodies.

IFNγ is a soluble immunomodulatory factor that exerts effects on both innate and adaptive immunity. IFNγ is primarily secreted by activated lymphocytes such as CD4$^+$ and CD8$^+$ T cells.[833] Gibson et al. recently labeled an IFNγ-targeting rat mAb (AN-18) with ^{89}Zr and found that tumor cell uptake of ^{89}Zr-anti-IFNγ was IFNγ-dependent.[790] After a series of CpG vaccination and mAb treatment experiments, they further demonstrated the robust ability of ^{89}Zr-anti-IFNγ immunoPET in detecting T cell activation and exhaustion in spontaneous tumor models. These results together support the future development of IFNγ-targeted immunoPET for clinical use. In addition to the targets discussed above, there are several other targets successfully leveraged for imaging T cells, including granzyme B[834,835] and IL-2 receptor.[836] However, peptides and interleukins rather than antibodies were used as the targeting vectors in these platforms.

6. IMMUNOPET IMAGING OF INFLAMMATION

Although 18F-FDG PET is a clinically viable method to noninvasively quantify inflammation, it lacks specificity due to the uptake of the tracer by metabolically active tissues. Inflammation is decisive in tumor progression, and inflammation and cancer share certain signaling molecules.[837] Therefore, some of the aforementioned immunoPET probes could reasonably be extended to detect and evaluate inflammatory diseases.[838] In this section, we highlight the role of immunoPET in detecting several inflammatory diseases.

6.1. Rheumatoid Arthritis

Rheumatoid arthritis (RA) is a polygenic and multifactorial joint disease characterized by autoantibodies to various molecules such as IgG and citrullinated proteins.[839] Treatment strategies for RA mainly include disease-modifying antirheumatic drugs, which can be further categorized into small molecules (e.g., methotrexate) and biologic agents (e.g., anti-TNFα mAbs).[840] Although RA is incurable, it is important to identify and treat RA patients at earlier stages to delay the joint damage.

To track autoantibody to glucose-6-phosphate isomerase (GPI), Wipke et al. initially radiolabeled an anti-GPI IgG with ^{64}Cu and found that the developed probe specifically localized to the diseased joints.[841] This highlighted the possibility that immunoPET imaging may help us understand the sophisticated autoimmunity responses involved in human RA. F8-IL10 is a novel treatment option for RA patients. F8-IL10 was developed by fusing the Fv fragment of the human antibody F8 with the anti-inflammatory cytokine IL10, resulting in selective delivery of IL10 to the fibronectin-expressing inflammatory sites.[842] A translational study investigating [^{124}I]I-F8-IL10 found that this radiotracer accumulated readily in the arthritic joints of RA patients. However, this immunoPET study also revealed very rapid blood clearance of the radiotracer and unexpected high uptake in the liver and spleen.[843] Certolizumab pegol (CZP) is a PEGylated fab fragment targeting TNFα and has shown remarkable efficacy in controlling the symptoms of RA. ^{89}Zr-DFO-CZP was recently synthesized and immunoPET imaging with this tracer specifically located diseased joints and paws of transgenic mice expressing human TNFα.[844]

Fibroblast activation protein (FAP) is a type II trans-membrane glycoprotein belonging to the family of serine prolyl oligopeptidases. In addition to being a theranostic target for cancers,[845–847] FAP is closely associated with the progression of RA. A fully human noninternalizing anti-FAP antibody 28H1 that binds to both murine and human FAP has been reported.[848] When labeled with ^{89}Zr, it specifically visualized inflamed joints of RA models (Figure 29).[849] More importantly, 28H1-based molecular imaging tracers could monitor the response of RA to different treatment options at molecular levels.[850–852]

6.2. Inflammatory Bowel Disease

Inflammatory bowel disease (IBD) is a chronic inflammatory disorder composed of two major subtypes: Crohn's disease and ulcerative colitis.[853] In current clinical practice, endoscopy is the most commonly applied technique to diagnose and monitor IBD. However, this invasive examination fails to provide information regarding molecular markers involved in the development and progression of IBD. By targeting integrins and immune mediators, immunoPET imaging approaches have been adapted to sensitively grade the disease severity.[854] An initial study radiolabeled a β_7 integrin-specific mAb (FIB504.64) and showed specific uptake of ^{64}Cu-DOTAFIB504.64 in the gut of mice with dextran sulfate sodium (DSS)-induced colitis.[855] To lower background signals in nontarget organs, immunoPET probes were developed using FIB504.64 fragments.[856] In these studies, ^{64}Cu-NOTA-FIB504.64-F(ab′)$_2$ outperformed ^{64}Cu-NOTA-FIB504.64-Fab in detecting DSS-induced colitis. Moreover, ^{64}Cu-NOTA-FIB504.64-F(ab′)$_2$ immunoPET also demonstrated better

imaging contrast than ^{64}Cu-DOTA-DATK32, a mAb-derived tracer targeting the integrin heterodimer $\alpha_4\beta_7$.

More recently, several immunoPET tracers targeting innate immune cells, interleukins, and CD4$^+$ T cells have been characterized in murine models of colitis. Dmochowska et al. reported increased IL-1β and increased infiltration of CD11b$^+$ CD3$^-$ innate immune cells in the inflamed colon of colitic mice.[857] ImmunoPET imaging studies in this work further corroborated the above observations. While ^{89}Zr-α-CD11b (clone M1/70) immunoPET detected colonic inflammation with higher sensitivity than MRI, ^{89}Zr-α-IL-1β (clone B122) immunoPET correlated the disease severity, although less robustly than ^{18}F-FDG (Figure 30a–c). ^{89}Zr-malDFO-GK1.5 cDb is an antimouse CD4 radiotracer initially used for imaging immune system reconstitution.[794] Freise et al. recently assessed the diagnostic value of ^{89}Zr-malDFO-GK1.5 cDb in tracking CD4$^+$ T cell infiltration in DSS-induced colitis mouse models.[858] ImmunoPET imaging showed radiotracer uptake in mesenteric lymph nodes and colons of the colitic mice (Figure 30d,e), which correlated with increased infiltration of CD4$^+$ T cells into the inflamed colons revealed by IHC staining. Taken together, immunoPET is less intrusive and could provide useful information regarding the dynamics of immune cells throughout the intestines. This may in turn help monitor the disease severity and predict the treatment responses.

6.3. Other Inflammatory Diseases

With the development of specific mAbs for various inflammation-related antigens, immunoPET probes have been developed to image several other inflammatory diseases such as graft versus host disease,[859,860] atherosclerotic plaques,[861–863] and inflammation-induced lymphangiogenesis.[864,865] In addition, immunoPET or immunoPET/MRI hybrid imaging are being used to detect bacterial, fungal, or viral infections.[866–870] In the case of invasive pulmonary aspergillosis, a mouse mAb mJF5 and its humanized derivative hJF5 have proven to be highly specific to mannoprotein antigens produced by *Aspergillus*. Preclinical studies have validated the accuracy of ^{64}Cu-DOTA-mJF5 and ^{64}Cu-NODAGA-hJF5 in detecting *Aspergillus* lung infection.[871–873] From these preclinical reports, it is conceivable that upon continuous investigation and clinical translation, immunoPET imaging holds enormous potential to diagnose the abovementioned inflammatory diseases.

7. IMMUNOPET IMAGING OF BETA CELL MASS

Diabetes mellitus (DM) is a metabolic disease characterized by a functional loss of beta cell mass (β cell mass, BCM) or the insufficient response of beta cells to insulin. It has been estimated that over 550 million people will suffer from diabetes by 2030.[874] To monitor the early and dynamic change of BCM, various molecular imaging probes have been developed, including several antibody-based probes.[875] Transmembrane protein 27 (TMEM27) is a validated BCM biomarker, and TMEM27-targeted immunoPET and fluorescent imaging probes have shown promise in imaging BCM.[876] Dipeptidyl peptidase 6 (DPP6) is a newly identified biomarker for pancreatic alpha and beta cells. A VHH (i.e., 4hD29) targeting DPP6 was produced, initially radiolabeled with 99mTc, and used for immunoSPECT imaging of endocrine cell mass (ECM).[877] More recently, ^{68}Ga-NOTA-4hD29 was

developed and immunoPET imaging with this agent successfully detected DPP6-positive tumors.[878] Upon clinical translation, this agent holds promise for detecting ECM, transplanted human islets, and DPP6-positive tumors.

ImmunoPET imaging of BCM is advantageous compared to other imaging modalities because of its targeting sensitivity and specificity. In preclinical models, beta cell-specific immunoPET has been used to image insulinomas and grafted human islets. However, it is very challenging for immunoPET to detect islets scattered across the pancreas in preclinical models, due either to the high background signal or to the restricted species reactivity of the antibodies. It remains to be determined whether immunoPET imaging can visualize beta cell islets in humans. If so, this novel imaging modality may improve the management of diabetes by monitoring the dynamic change of BCM over time. As we mentioned above, ^{52}Mn is a relatively new radiometal used for immunoPET. Two interesting studies have elucidated that ^{52}Mn alone serves as a sensitive tracer for measuring and quantifying BCM.[879,880] Clinical trials are warranted to confirm the unique application of ^{52}Mn PET in quantifying and monitoring BCM.

8. IMMUNOPET IMAGING-GUIDED ADVANCED THERAPEUTICS

The landscape of theranostics has evolved over time. The management of thyroid diseases (e.g., differentiated thyroid cancer and hyperthyroidism) has been revolutionized since the use of theranostic radioiodine isotopes in the 1940s.[881,882] With the identification of highly specific cancer antigens and the concomitant development of radiopharmaceuticals, PSMA-targeted and somatostatin-derived theranostic agents have achieved remarkable success in diagnosing and treating advanced PCas and neuroendocrine tumors, respectively.[883,884] This trend is expected to flourish with the discovery of newer molecular targets and synchronous advance in radiochemistry.[885]

ImmunoPET imaging can visualize the spatial heterogeneity of target expression and thus predict the responses of therapeutic antibodies, including the immune checkpoint inhibitors.[21,809,814] Besides selecting patients for antibody therapies, immunoPET imaging is a robust approach to select patients for antibody-based therapies, particularly RIT. Most of the aforementioned biomarkers can be leveraged to develop RIT agents. Traditional RIT has proven useful for treating radiosensitive tumors and disseminated hematologic malignancies.[886–888] However, it is less effective for radioresistant or bulky tumors. It is anticipated that innovative pRIT (e.g., agents produced via the Dock-and-Lock technology) may deliver a higher therapeutic dose to the tumor while reducing hematologic toxicity. Several exemplary targets with clinical theranostic evidence are discussed below.

B7-H3 (CD276) is an immunoregulatory glycoprotein that is also overexpressed in a broad spectrum of solid tumors.[889] Preclinical studies have reported that immunoPET imaging was able to delineate CD276 expression on tumor cells and blood vessels.[890,891] 8H9 (Omburtamab) is a murine mAb against B7-H3,[892] and ^{131}I-8H9 has been used to treat several types of solid tumors after intrathecal administration.[893,894] A recent study elucidated that pretherapy immunoPET imaging with ^{124}I-8H9 allowed for noninvasive estimation of the therapeutic index of ^{131}I-8H9.[895] Interestingly, ^{124}I itself may serve as a

theranostic radioisotope due to the emission of high-energy positrons. To test the clinical feasibility, a phase I clinical trial was carried out to assess the theranostic value of ^{124}I-8H9 in patients with diffuse intrinsic pontine glioma.[896] The results demonstrated that ^{124}I-8H9 was precisely delivered to the brainstem lesions after intratumoral infusion (Figure 31). Moreover, immunoPET/MR imaging following ^{124}I-8H9 infusion quantitated the absorbed dose in the tumors and other organs. These clinical studies together demonstrate that intrathecal administration of ^{124}I-8H9 and ^{131}I-8H9 in tandem (or ^{124}I-8H9 alone) may maximize the therapeutic outcome while limiting the systemic toxicity.

CEA is another biomarker extensively studied for cancer theranostics over the years. CEA-directed pRIT was initially investigated in patients with primary colorectal cancer[897] and then in patients with medullary thyroid cancer.[319,320] However, the frequent hematological toxicity and immune responses of these first-generation approaches limited their broad applications. The IMP288 peptide allows facile radiolabeling with either therapeutic (such as ^{177}Lu, ^{90}Y, and ^{213}Bi) or diagnostic (such as ^{68}Ga, ^{111}In, and ^{86}Y) radiometals, providing a perfect platform for designing theranostic agents. A preclinical study has shown the survival benefit of TF2/^{177}Lu-IMP288 pRIT in colorectal cancer models.[898] A follow-up clinical trial further reported that TF2/^{177}Lu-IMP288 pRIT was feasible in patients with colorectal cancer, but the efficacy was limited because all the patients showed progressive disease eight weeks later.[899,900] Use of ^{213}Bi ($T_{1/2}$ = 45.6 min) instead of ^{177}Lu in this pretargeted system showed comparable therapeutic efficacy in colorectal cancer models, but the dosing schedule needs to be optimized to reduce nephrotoxicity before clinical translation.[901] With further development of humanized antibodies,[902] dual-modal imaging probes,[903] and the pRIT system,[904] CEA-targeted theranostic toolbox holds excellent prospects for improving the management of CEA-positive human malignancies.

As mentioned earlier (section 4.3.1), a recent clinical trial has demonstrated the clinical feasibility of CA19.9-targeted immunoPET in localizing PDAC.[39] This study also indicated that 5B1 might deliver therapeutic doses to PDAC after labeled with beta emitters. A preclinical study explored the therapeutic benefit of CA19.9-directed pRIT, in which 5B1-TCO was administered 72 h before the injection of ^{177}Lu-DOTA-PEG$_7$-Tz or ^{177}Lu-CHX-A′′-DTPA-PEG$_7$ -Tz.[905] The results demonstrated that the former combination showed a dose-dependent therapeutic response in PDAC models. Along with this preclinical evidence, an ongoing clinical trial (NCT03118349) is evaluating the safety and dosimetry of ^{177}Lu-CHX-A′′-DTPA-5B1 in patients with CA19.9-positive malignancies. 5B1 as a standalone monotherapy or in combination with chemotherapy is also under clinical investigation (NCT02672917). On the basis of the reported evidence and future clinical trial results, the 5B1-based theranostic toolbox may hopefully improve the clinical management of CA19.9-positive malignancies.

RIT is an established tool in the treatment of hematologic malignancies, such as NHL.[906,907] CD20 is a classical theranostic target since two radiolabeled murine mAbs (^{131}I-tositumomab, Bexxar; ^{90}Y-ibritumomab tiuxetan, Zevalin) were approved for the treatment of B-cell NHL.[908] Nonetheless, the clinical use of Bexxar and Zevalin is stagnant. Bexxar has not been commercially available since 2014 for multiple reasons (mainly due to the disappointing profits). In two recent studies, researchers reported the feasibility and

satisfactory treatment efficacy of ^{90}Y-rituximab in patients with relapsed or refractory NHL.[909,910] Furthermore, several preclinical and clinical studies have reported the superior effectiveness of pRIT or RIT in treating lymphomas by targeting several targets, such as CD20,[911,912] CD38,[560] and CD45.[913] CD33 is another alternative target for RIT of hematological malignancies[914,915] and for immunoPET imaging.[916] Continuous innovation of the pRIT systems and incorporation of immunoPET techniques may reinvigorate the enthusiasm for managing hematologic malignancies with nuclear medicine approaches. Readers are recommended to refer to an excellent review parsing RIT for more information.[167]

9. IMMUNOPET IMAGING-GUIDED DRUG DEVELOPMENT

In the development of antibody- and antibody-based therapeutics, iterative approaches are needed, including the identification of antigens and screening and selection of optimal antibodies. Traditionally, several analytical and structural techniques (e.g., mass spectrometry, liquid chromatography, and electrophoresis) are used to assess the developed antibody therapeutics. Apart from these procedures, it is necessary to examine the pharmacodynamic properties and safety profiles of antibodies before clinical translation for human use.[917] Complementary to their role as diagnostic methods in the clinic, molecular imaging approaches are increasingly being used for fundamental research and antibody drug development.[918–920] Molecular imaging can assist antibody drug discovery (e.g., target selection and antibody optimization) as well as the clinical assessment of antibody drugs (e.g., distribution, clearance, safety profile, and therapeutic efficacy). As a result, the translation of promising antibody candidates can be accelerated from preclinical prototype to bedside reality.[921,922]

With the development and use of total-body PET scanners, immunoPET imaging will facilitate the thorough assessment of mAb pharmacokinetics up to 30 days at the preclinical stage.[923–925] ImmunoPET imaging can reveal both dose-dependent and dose-independent uptake of mAb in normal organs and in tumors. This is particularly useful when the target antigen is expressed in tumors as well as normal tissues.[926] While the dose-dependent uptake is largely mediated by relevant receptors expressed on the surface of tumor cells, the dose-independent uptake is mainly caused by osmosis and retention of mAb in the TME. ImmunoPET imaging will help estimate the therapeutic effect of antibody therapeutics in phase I dose-escalation studies and calculate the amount of unlabeled antibody required for preloading or coadministration,[41,927] which will saturate target antigens in normal organs and maximize the binding of mAb to the target antigens in tumors.

In addition to mAbs, ADCs are among the most effective targeted cancer therapeutics. Third-generation ADCs with increased potency and stability are under clinical investigation.[928] During ADC development, cytotoxic drugs are linked to mAbs via bifunctional linkers. ImmunoPET imaging has shown its value in assessing the in vivo stability of novel linkers. This was exemplified by two recent studies where a novel platinum(II) linker was developed for ADC conjugates.[929,930] More importantly, immunoPET imaging can characterize the effect of drug-to-antibody ratio on the overall blood retention and tumor-targeting efficacies of the developed ADCs (Figure 32).[930–932] As another therapeutic alternative, RIT delivers

therapeutic radionuclides to the tumor site by taking advantage of antibody specificity.[933] ImmunoPET imaging permits dosimetry calculations for these therapies and further predicts dose-limiting organs prior to the RIT,[934] optimizing the development and use of RIT agents.

ImmunoPET-guided drug development provides insightful information regarding the distribution and targeting potential of new antibody drugs or antibody-based therapeutics. However, it should not be ignored that radionuclides, chelators, and radiolabeling methods may alter the inferred pharmacokinetics of the conjugated antibody tracers.

10. FUTURE PERSPECTIVES AND CONCLUSIONS

As described in this review, immunoPET is an invaluable companion diagnostic tool actively changing the management of cancers and noncancerous diseases (Table 2). However, it must be noted that most of the immunoPET probes have only been assessed in preclinical stages or in small cohorts of patients. Further studies are needed to translate some of the promising immunoPET probes and to confirm the diagnostic value of the clinically used ones. The development of antibody therapeutics will continue to reshape the therapeutic landscape of human diseases, and more sophisticated immunoPET imaging strategies will be designed accordingly. By making the right diagnoses and optimizing subsequent therapeutic decisions, immunoPET will hopefully help clinicians refine clinical practice and realize truly personalized medicine. The ultimate purpose of designing and using immunoPET is to facilitate better management of patients and lessen the financial burden for them and society.[935,936]

There are several concerns about the immunoPET technique. A fundamental question that needs to be addressed is under which settings immunoPET may be integrated into the clinical diagnostic toolbox. In our view, immunoPET is a companion diagnostic tool that should be used together with clinically approved or clinical-stage therapeutic regimens. An initial immunoPET imaging is preferred to be performed before the commencement of targeted antibody or small-molecule inhibitor treatment because it will provide pivotal information on the baseline expression level of the target. The unique information obtained at the baseline will further allow adequate restaging and evaluation of the disease. Repeated immunoPET imaging after the treatments will help evaluate the therapeutic response and also the change of the target, especially for patients with multiple biopsy-inaccessible tumor lesions. Several other concerns might be gradually resolved with the progress of the field. Specifically speaking, the development of GMP-compliant production and purification processes may spur the clinical use of this imaging technique while minimizing unnecessary radiation dose to the health care staff.[937,938] ImmunoPET imaging with total-body PET scanners will further decrease radiation exposure without compromising the image quality.[939–941] Furthermore, advances in PET technology and reconstruction algorithms will lead to improved spatial and temporal resolution of immunoPET images.[942] In most instances, immunoPET imaging is performed for patients with metastatic diseases. Consequently, another misgiving is the lack of histochemical confirmation of some of the tracer-avid lesions. However, the primary purpose of the initial immunoPET imaging is to stratify patients by mapping the expression of a specific biomarker. If the uptake or sizes of the

tracer-avid lesions decrease on post-treatment immunoPET images, it is rational to consider these lesions as histopathology-positive.

For developing antibody-based radiopharmaceuticals, we would like to emphasize the importance of multidisciplinary collaboration. Specifically, multiple approaches (e.g., genomic, serological, proteomic, biological, and bioinformatical approaches) should be leveraged to identify antigens highly or exclusively overexpressed on the surface of the tumor cells, tumor stromal cells, tumor vasculature endothelial cells, immune cells, or beta cells.[943] While the abundance and specificity are key factors when selecting suitable imaging targets, the function and stability of the targets need also to be considered.[944] Of the diverse targets that are currently being investigated in preclinical studies or in clinical trials, some are relatively specific for certain tumor types (for example, TROP-2 for breast cancer and PCa, and CD138 for MM). When using antibodies as targeting vectors, it is important to remember that different IgG types have varying circulation time,[945] and the interactions between the Fc domain and FcγR/FcRn dynamically regulate the immunological functions of the developed antibody.[946–948] For instance, tislelizumab (BGBA317) is a humanized IgG4 that binds to PD-1 but not to FcγRI.[949] This improvement results in enhanced tumor growth inhibition when compared to BGB-A317/IgG4S228P, which has a high affinity to FcγR. Thus, Fc engineering could be used to introduce mutations that may abrogate the binding of IgG with FcγR. This strategy could also be exploited to increase the cellular accumulation of an antibody–antigen complex when targeting secreted antigens[714] or to enhance the persistence of VHHs in circulation.[950] In addition, strategies like deglycosylation of antibodies may further improve the immunoPET imaging quality.[951,952] A high-affinity antibody does not always guarantee high tumor uptake because other factors such as circulating antigens and tumor vasculature may affect the accessibility of the radiolabeled antibody. Aside from the singly targeted imaging probes, antibody-based heterodimers, or dual-targeting probes may have higher targeting efficacy and superior specificity than their monospecific peers.[30,32,953] With the advent and evolvement of click chemistry,[261] future studies may further harness this powerful method to synthesize modular immunoPET probes with improved in vivo performance. Furthermore, pretargeting strategies may also be harnessed to optimize the imaging quality.[954,955]

In the characterization of antibody-based diagnostic or theranostic probes, attention should be paid whether immunodeficient strains of animals are used in the imaging studies and how this may impact the imaging performance of the investigated probes. For example, a recent study reported that immunoPET radiotracers had inefficient tumor targeting and high off-target binding to the spleen in the highly immunodeficient mouse strains.[766] This was consistent with a previous study which reported that ADCs had limited antitumor activity in the ultra immunodeficient NSG mice.[956] In this setting, the use of humanized mouse models or nonhuman primates is very necessary to assess the imaging performance of the immunoPET probes prior to pilot clinical investigations.[957] In addition, antibodies cross-reactive with human, nonhuman primate, and mouse antigens would be beneficial in preclinical immunoPET imaging studies.

Other than their use in immunoPET, antibodies are actively investigated as either monotherapy agents or antibody conjugates for effective cancer treatment. Antibodies can be

modified with therapeutic radionuclides and photosensitizers for RIT[167] and PIT,[958,959] respectively, as novel treatment options. Two radiolabeled therapeutic anti-CD20 antibodies, ^{131}I-tositumomab and ^{90}Y-ibritumomab tiuxetan, have been approved by the FDA for the treatment of B-cell lymphoma.[531,960] To maximize the therapeutic index, pRIT strategies may be used. For detailed information on RIT, readers are recommended to refer to other excellent reviews.[302,954,961] RTKs and oncogenic proteins are ideal candidates for RIT.[237,618,962] For instance, a recent study reported that pRIT with anti-HER2-DOTA-pRIT + ^{177}Lu-DOTA-Bn inhibited HER-2 positive breast cancers and substantially improved survival without inducing toxicity in normal tissues.[963] Therefore, radiolabeled antibodies or antibody fragments targeting some of the selected makers discussed above may provide additional therapeutic options for cancer patients in the era of precision medicine.[964,965] The use of pairs of β^+ and β^- emitting radionuclides (e.g., ^{86}Y/^{90}Y) is desirable as a promising theranostic platform for sequential imaging, dosimetry, and therapy. In addition to the traditional β-emitting therapeutic isotopes, accumulating evidence is supporting the clinical application of targeted alpha therapy, where mAbs or small molecules are labeled with therapeutic α-emitters. ^{225}Ac ($T_{1/2}$ = 10.0 d) and ^{213}Bi are both attractive therapeutic α-emitters, but the therapeutic index of ^{213}Bilabeled agents was inferior to ^{225}Ac-labeled agents.[966,967] In translating these radiotherapeutics to the clinic, the safety profiles of the agents need to be carefully assessed. For therapeutic radionuclides without intrinsic imaging capabilities, immunoPET imaging may help estimate the pharmacokinetics of the therapeutic radiopharmaceuticals and evaluate the dose-limiting organs.

Optical fluorescence imaging using dye-labeled mAbs or sequential PET/NIR imaging with dual-labeled mAbs has the potential to improve cancer surgery outcomes.[968–970] However, the payload of fluorophores needs to be carefully determined because the ratio of the fluorophore to mAb greatly affects both the pharmacokinetics and tumor-targeting efficiency of the developed probes.[971,972] Besides, the emission of charged particles from radionuclides traveling through dielectric materials, such as in living subjects, results in the production of Cerenkov luminescence.[973] Cerenkov luminescence has been validated effective for triggering photodynamic therapy.[974,975] More interestingly, Cerenkov luminescence imaging (CLI) with optical imaging systems after the administration of radioactive tracers is an emerging imaging paradigm and can be exploited for image-guided surgery.[976] While applications involving Cerenkov luminescence are still in their infancy, they hold great potential.[977,978]

While several advantages exist over other imaging modalities, the broad application of immunoPET may be restrained by a scarcity of radiometals and antibodies in less-developed countries. Therefore, immunoSPECT imaging may alternatively fill the gap. To this end, γ-emitting radionuclides like ^{99m}Tc, ^{123}I, and ^{111}In may be used to develop immunoSPECT imaging probes.[979] It should be noted that the high-energy γ emission from ^{131}I makes it unfavorable for developing immunoSPECT probes. The use of novel radiolabeling methods may improve the stability, binding affinity, internalization, and intracellular track of the radioiodinated mAbs.[980]

In summary, the development of immunoPET imaging strategies has achieved great success in the past decade. With continuous improvement and clinical translation, immunoPET

imaging holds great promise in optimizing clinical management of human diseases, especially cancers.

ACKNOWLEDGMENTS

We apologize to authors whose work we could not cite due to the limited space of this review. We thank Zhoumi Hu and Dawei Jiang for their insightful comments on this paper. We also appreciate all the reviewers for their input and insightful comments. The study was supported by research grants from the Natural Science Foundation of China (grant nos. 81830052, 81530053, and 81974271), Shanghai Key Laboratory of Molecular Imaging (grant no. 18DZ2260400), University of Wisconsin—Madison, and the National Institutes of Health (P30 CA014520).

Biographies

Weijun Wei obtained his M.D. and Ph.D. degrees with distinction in nuclear medicine and molecular imaging from the School of Medicine, Shanghai Jiao Tong University, in 2019. Dr. Wei was a joint graduate at the University of Wisconsin–Madison under the supervision of Prof. Weibo Cai during 09/2017–09/2018. Currently, Dr. Wei serves as a nuclear medicine physician at Renji Hospital, School of Medicine, Shanghai Jiao Tong University, where he is focusing on developing novel antibody- and nanobody-based probes for imaging and treating cancers. Dr. Wei has published more than 20 articles in several world-renowned journals.

Zachary Rosenkrans is currently a Ph.D. student in the Pharmaceutical Sciences program at the University of Wisconsin–Madison under the supervision of Dr. Weibo Cai. He previously received a B.S. in Chemical Engineering from the University of Kansas in Lawrence, KS. His research is focused on developing nanomaterial-based platforms for image-guided drug delivery and theranostics.

Prof. Jianjun Liu is the chief nuclear medicine physician at Renji Hospital, School of Medicine, Shanghai Jiao Tong University. As the director of the department, Prof. Liu leads a multidisciplinary team exploring novel therapeutic approaches for cancers on one hand and developing next-generation molecular imaging probes on the other hand. One of his specific interests is to design, validate, and translate antibody- and nanobody-based immunoPET imaging tracers. Prof. Liu has authored more than 40 research papers and tutored over 10 graduates.

Prof. Gang Huang is a well-recognized professor and leader of nuclear medicine and molecular imaging in China. His research and clinical work are focused on the diagnosis and treatment of malignancies, especially theranostics using nuclear medicine and molecular imaging approaches. He is the Elected President of the Asia Oceania Federation of Nuclear Medicine and Biology, Dean of the Asia Oceania School of Nuclear Medicine, the Ninth President of the Chinese Nuclear Medicine Society, and Editor-in-Chief of the *Chinese Journal of Nuclear Medicine and Molecular Imaging*. Prof. Huang has authored more than 200 articles, edited more than 30 books, given over 500 talks and received over 10 awards, such as the State Scientific and Technological Progress Award (the second place) and the Shanghai Medical Science and Technology Award (the first place), etc.

Prof. Quan-Yong Luo obtained his M.D. degree in nuclear medicine and molecular imaging from Shanghai Jiao Tong University in 2006. Currently, he is the director and chief physician at the Department of Nuclear Medicine, Shanghai Jiao Tong University Affiliated Sixth People's Hospital. Besides his interest in clinical PET and SPECT imaging, he has been actively involved in radioiodine treatment of differentiated thyroid cancers for two decades. Prof. Luo has published more than 70 articles, in which his team has thoroughly investigated the diagnostic efficacies of SPECT and PET imaging, as well as the treatment efficacy of radioiodine in patients with differentiated thyroid cancer.

Prof. Weibo Cai is a Vilas Distinguished Achievement Professor of Radiology/Medical Physics/Biomedical Engineering/Materials Science & Engineering/Pharmaceutical Sciences at the University of Wisconsin–Madison, USA. He received a Ph.D. degree in Chemistry from UCSD in 2004. Prof. Cai's research at UW–Madison (http://mi.wisc.edu/) is mainly focused on antibody-based molecular imaging and nanotechnology. He has authored more than 300 articles (H-index: 79), edited three books, and received many awards (e.g., Fellow of AIMBE in 2018 and Fellow of SNMMI in 2019). Prof. Cai's trainees at UW–Madison have received over 100 awards.

ABBREVIATIONS USED

ADCP	antibody-dependent cellular phagocytosis
ADCC	antibody-dependent cell-mediated cytotoxicity
ADC	antibody–drug conjugate
AR	androgen receptor
BBB	blood–brain barrier
BiTE	bispecific T-cell engager
BCM	beta cell mass
CDC	complement-dependent cytotoxicity
CB-TE2A	4,11-bis(carboxymethyl)-1,4,8,11-tetraazabicyclo[6.6.2]hexadecane
CA19.9	carbohydrate antigen 19.9
CA-125	carbohydrate antigen 125
CEA	carcinoembryonic antigen
CAIX	carbonic anhydrase IXcc
RCC	clear cell renal cell carcinoma
CSC	cancer stem cell
CTLA-4	cytotoxic T lymphocyte antigen 4

CLI	Cerenkov luminescence imaging
CuAAC	Cu(I)-catalyzed 1,3-dipolar cycloaddition between azides and alkynes
DSS	dextran sulfate sodium
DLL3	delta-like 3
EDTA	ethylenediaminetetraacetic acid
EGFR	human epidermal growth factor receptor
FcγR	Fcγ receptor
FcRn	neonatal Fc receptor
^{18}F-FDG	^{18}F-fluorodeoxyglucose
GPI	glucose-6-phosphate isomerase
GPA33	glycoprotein A33
HNSCC	head and neck squamous cell carcinoma
HCAb	heavy-chain-only antibody
HER2/ErbB2	human epidermal growth factor receptor 2
HER3/ErbB3	Human epidermal growth factor receptor 3
HGF	hepatocyte growth factor
IHC	immunohistochemistry
IGF-1R	insulin-like growth factor-1 receptor
IBD	inflammatory bowel disease
ImmunoPET	immuno-positron emission tomography
LGR5	leucine-rich repeat-containing G-protein coupled receptor 5
mAb	monoclonal antibody
MM	multiple myeloma
MSLN	membrane-bound surface glycoprotein mesothelin
NSCLC	nonsmall-cell lung cancer
NHL	non-Hodgkin’s lymphoma
NOTA	1,4,7-triazacyclononane-1,4,7-triacetic acid
NODAGA	1,4,7-triazacyclononane,1-glutaric acid-4,7-acetic acid

PDGFR	platelet-derived growth factor receptor
PD-L1	programmed death ligand-1
PET	positron emission tomography
pRIT	pretargeted radioimmunotherapy
PDAC	pancreatic ductal adenocarcinoma
PSCA	prostate stem cell antigen
PSA	prostate-specific antigen
PD1	programmed death receptor 1
PIT	photoimmunotherapy
PSMA	prostate-specific membrane antigen
RCY	radiochemical yield
RTKs	receptor tyrosine kinases
RIT	radioimmunotherapy
RA	rheumatoid arthritis
SPECT	single-photon emission computed tomography
sdAb	single-domain antibody
scFv	single-chain variable fragment
SPAAC	strain-promoted azide–alkyne cycloaddition
SrtA	sortase A
STEAP1	six-transmembrane epithelial antigen of prostate-1
TKIs	tyrosine kinase inhibitors
TME	tumor microenvironment
TGF-β	transforming growth factor-β
TROP-2	trophoblast cell-surface antigen 2
TAG-72	tumor-associated glycoprotein-72
Treg	regulatory T cells
VHH	variable domain of the heavy chain of a HCAb
VEGF	vascular endothelial-derived growth factor
VEGFR	vascular endothelial-derived growth factor receptor

REFERENCES

(1). Mankoff DA A definition of molecular imaging. J. Nucl. Med 2007, 48, 18N–21N.

(2). Ametamey SM; Honer M; Schubiger PA Molecular imaging with PET. Chem. Rev 2008, 108, 1501–1516. [PubMed: 18426240]

(3). James ML; Gambhir SS A molecular imaging primer: modalities, imaging agents, and applications. Physiol. Rev 2012, 92, 897–965. [PubMed: 22535898]

(4). Rahmim A; Lodge MA; Karakatsanis NA; Panin VY; Zhou Y; McMillan A; Cho S; Zaidi H; Casey ME; Wahl RL Dynamic whole-body PET imaging: principles, potentials and applications. Eur. J. Nucl. Med. Mol. Imaging 2019, 46, 501–518. [PubMed: 30269154]

(5). Scott AM; Wolchok JD; Old LJ Antibody therapy of cancer. Nat. Rev. Cancer 2012, 12, 278–287. [PubMed: 22437872]

(6). Khalil DN; Smith EL; Brentjens RJ; Wolchok JD The future of cancer treatment: immunomodulation, CARs and combination immunotherapy. Nat. Rev. Clin. Oncol 2016, 13, 273–290. [PubMed: 26977780]

(7). Sanmamed MF; Chen L A paradigm shift in cancer immunotherapy: from enhancement to normalization. Cell 2018, 175, 313–326. [PubMed: 30290139]

(8). Pimlott SL; Sutherland A Molecular tracers for the PET and SPECT imaging of disease. Chem. Soc. Rev 2011, 40, 149–162. [PubMed: 20818455]

(9). Cho SY; Lipson EJ; Im HJ; Rowe SP; Gonzalez EM; Blackford A; Chirindel A; Pardoll DM; Topalian SL; Wahl RL Prediction of response to immune checkpoint inhibitor therapy using early-Time-Point (18)F-FDG PET/CT imaging in patients with advanced melanoma. J. Nucl. Med 2017, 58, 1421–1428. [PubMed: 28360208]

(10). Aide N; Hicks RJ; Le Tourneau C; Lheureux S; Fanti S; Lopci E FDG PET/CT for assessing tumour response to immunotherapy: Report on the EANM symposium on immune modulation and recent review of the literature. Eur. J. Nucl. Med. Mol. Imaging 2019, 46, 238–250. [PubMed: 30291373]

(11). Sachpekidis C; Anwar H; Winkler J; Kopp-Schneider A; Larribere L; Haberkorn U; Hassel JC; Dimitrakopoulou-Strauss A The role of interim (18)F-FDG PET/CT in prediction of response to ipilimumab treatment in metastatic melanoma. Eur. J. Nucl. Med. Mol. Imaging 2018, 45, 1289–1296. [PubMed: 29478079]

(12). Anwar H; Sachpekidis C; Winkler J; Kopp-Schneider A; Haberkorn U; Hassel JC; Dimitrakopoulou-Strauss A Absolute number of new lesions on (18)F-FDG PET/CT is more predictive of clinical response than SUV changes in metastatic melanoma patients receiving ipilimumab. Eur. J. Nucl. Med. Mol. Imaging 2018, 45, 376–383. [PubMed: 29124281]

(13). Wong ANM; McArthur GA; Hofman MS; Hicks RJ The Advantages and challenges of using FDG PET/CT for response assessment in melanoma in the era of targeted agents and immunotherapy. Eur. J. Nucl. Med. Mol. Imaging 2017, 44, 67–77. [PubMed: 28389693]

(14). Rossi S; Toschi L; Castello A; Grizzi F; Mansi L; Lopci E Clinical characteristics of patient selection and imaging predictors of outcome in solid tumors treated with checkpoint-inhibitors. Eur. J. Nucl. Med. Mol. Imaging 2017, 44, 2310–2325. [PubMed: 28815334]

(15). de Vries EGE; Kist de Ruijter L; Lub-de Hooge MN; Dierckx RA; Elias SG; Oosting SF Integrating molecular nuclear imaging in clinical research to improve anticancer therapy. Nat. Rev. Clin. Oncol 2019, 16, 241–255. [PubMed: 30479378]

(16). Behr TM; Behe M; Wormann B Trastuzumab and breast cancer. N. Engl. J. Med 2001, 345, 995–998. [PubMed: 11575295]

(17). Rahmim A; Zaidi H PET versus SPECT: strengths, limitations and challenges. Nucl. Med. Commun 2008, 29, 193–207. [PubMed: 18349789]

(18). Knowles SM; Wu AM Advances in immuno-positron emission tomography: antibodies for molecular imaging in oncology. J. Clin. Oncol 2012, 30, 3884–3892. [PubMed: 22987087]

(19). Philpott GW; Schwarz SW; Anderson CJ; Dehdashti F; Connett JM; Zinn KR; Meares CF; Cutler PD; Welch MJ; Siegel BA RadioimmunoPET: detection of colorectal carcinoma with positron-emitting copper-64-labeled monoclonal antibody. J. Nucl. Med 1995, 36, 1818–1824. [PubMed: 7562049]

(20). Goldenberg DM; Nabi HA Breast cancer imaging with radiolabeled antibodies. Semin. Nucl. Med 1999, 29, 41–48. [PubMed: 9990682]

(21). Bensch F; van der Veen EL; Lub-de Hooge MN; Jorritsma-Smit A; Boellaard R; Kok IC; Oosting SF; Schroder CP; Hiltermann TJN; van der Wekken AJ; et al. 89)Zratezolizumab imaging as a non-invasive approach to assess clinical response to PD-L1 blockade in cancer. Nat. Med 2018, 24, 1852–1858. [PubMed: 30478423]

(22). Ribas A; Wolchok JD Cancer immunotherapy using checkpoint blockade. Science 2018, 359, 1350–1355. [PubMed: 29567705]

(23). Carter PJ; Lazar GA Next generation antibody drugs: pursuit of the 'high-hanging fruit. Nat. Rev. Drug Discovery 2018, 17, 197–223. [PubMed: 29192287]

(24). Sehlin D; Syvanen S Engineered antibodies: new possibilities for brain PET? Eur. J. Nucl. Med. Mol. Imaging 2019, 46, 2848–2858. [PubMed: 31342134]

(25). Kaplon H; Reichert JM Antibodies to watch in 2019. MAbs 2019, 11, 219–238. [PubMed: 30516432]

(26). Kaplon H; Muralidharan M; Schneider Z; Reichert JM Antibodies to watch in 2020. MAbs 2020, 12, 1703531. [PubMed: 31847708]

(27). Bournazos S; Wang TT; Dahan R; Maamary J; Ravetch JV Signaling by antibodies: Recent Progress. Annu. Rev. Immunol 2017, 35, 285–311. [PubMed: 28446061]

(28). Hafeez U; Gan HK; Scott AM Monoclonal antibodies as immunomodulatory therapy against cancer and autoimmune diseases. Curr. Opin. Pharmacol 2018, 41, 114–121. [PubMed: 29883853]

(29). Wittrup KD; Thurber GM; Schmidt MM; Rhoden JJ Practical theoretic guidance for the design of tumor-targeting agents. Methods Enzymol 2012, 503, 255–268. [PubMed: 22230572]

(30). Brinkmann U; Kontermann RE The making of bispecific antibodies. MAbs 2017, 9, 182–212. [PubMed: 28071970]

(31). Runcie K; Budman DR; John V; Seetharamu N Bi-specific and tri-specific antibodies- the next big thing in solid tumor therapeutics. Mol. Med 2018, 24, 50. [PubMed: 30249178]

(32). Luo H; Hong H; Yang SP; Cai W Design and applications of bispecific heterodimers: molecular imaging and beyond. Mol. Pharmaceutics 2014, 11, 1750–1761.

(33). Ward ES; Zhou J; Ghetie V; Ober RJ Evidence to support the cellular mechanism involved in serum IgG homeostasis in humans. Int. Immunol 2003, 15, 187–195. [PubMed: 12578848]

(34). Ober RJ; Martinez C; Vaccaro C; Zhou J; Ward ES Visualizing the site and dynamics of IgG salvage by the MHC class I-related receptor, FcRn. J. Immunol 2004, 172, 2021–2029. [PubMed: 14764666]

(35). Suzuki T; Ishii-Watabe A; Tada M; Kobayashi T; Kanayasu-Toyoda T; Kawanishi T; Yamaguchi T Importance of neonatal FcR in regulating the serum half-life of therapeutic proteins containing the Fc domain of human IgG1: a comparative study of the affinity of monoclonal antibodies and Fc-fusion proteins to human neonatal FcR. J. Immunol 2010, 184, 1968–1976. [PubMed: 20083659]

(36). Graff CP; Wittrup KD Theoretical analysis of antibody targeting of tumor spheroids: importance of dosage for penetration, and affinity for retention. Cancer Res 2003, 63, 1288–1296. [PubMed: 12649189]

(37). Rudnick SI; Lou J; Shaller CC; Tang Y; Klein-Szanto AJ; Weiner LM; Marks JD; Adams GP Influence of affinity and antigen internalization on the uptake and penetration of Anti-HER2 antibodies in solid tumors. Cancer Res 2011, 71, 2250–2259. [PubMed: 21406401]

(38). Bergstrom M The use of microdosing in the development of small organic and protein therapeutics. J. Nucl. Med 2017, 58, 1188–1195. [PubMed: 28546333]

(39). Lohrmann C; O'Reilly EM; O'Donoghue JA; Pandit-Taskar N; Carrasquillo JA; Lyashchenko SK; Ruan S; Teng R; Scholz W; Maffuid PW; et al. Retooling a blood-based biomarker: phase I assessment of the high-affinity CA19–9 antibody HuMab-5B1 for immuno-PET imaging of pancreatic cancer. Clin. Cancer Res 2019, 25, 7014–7023. [PubMed: 31540979]

(40). Bensch F; Smeenk MM; van Es SC; de Jong JR; Schroder CP; Oosting SF; Lub-de Hooge MN; Menke-van der Houven van Oordt CW; Brouwers AH; Boellaard R; et al. Comparative

biodistribution analysis across four different (89)Zrmonoclonal antibody tracers-The first step towards an imaging warehouse. Theranostics 2018, 8, 4295–4304. [PubMed: 30214621]

(41). Dijkers EC; Oude Munnink TH; Kosterink JG; Brouwers AH; Jager PL; de Jong JR; van Dongen GA; Schroder CP; Lub-de Hooge MN; de Vries EG Biodistribution of 89Zr-trastuzumab and PET imaging of HER2-positive lesions in patients with metastatic breast cancer. Clin. Pharmacol. Ther 2010, 87, 586–592. [PubMed: 20357763]

(42). Steinmeyer DE; McCormick EL The art of antibody process development. Drug Discovery Today 2008, 13, 613–618. [PubMed: 18598918]

(43). Orcutt KD; Adams GP; Wu AM; Silva MD; Harwell C; Hoppin J; Matsumura M; Kotsuma M; Greenberg J; Scott AM; et al. Molecular simulation of receptor occupancy and tumor penetration of an antibody and smaller scaffolds: application to molecular Imaging. Mol. Imaging Biol 2017, 19, 656–664. [PubMed: 28213834]

(44). Konning D; Zielonka S; Grzeschik J; Empting M; Valldorf B; Krah S; Schroter C; Sellmann C; Hock B; Kolmar H Camelid and shark single domain antibodies: structural features and therapeutic potential. Curr. Opin. Struct. Biol 2017, 45, 10–16. [PubMed: 27865111]

(45). Yan J; Li G; Hu Y; Ou W; Wan Y Construction of a synthetic phage-displayed Nanobody library with CDR3 regions randomized by trinucleotide cassettes for diagnostic applications. J. Transl. Med 2014, 12, 343. [PubMed: 25496223]

(46). Vincke C; Loris R; Saerens D; Martinez-Rodriguez S; Muyldermans S; Conrath K General strategy to humanize a camelid single-domain antibody and identification of a universal humanized nanobody scaffold. J. Biol. Chem 2009, 284, 3273–3284. [PubMed: 19010777]

(47). Huang H-F; Zhu H; Li G-H; Xie Q; Yang X-T; Xu X-X; Tian X-B; Wan Y-K; Yang Z Construction of anti-hPD-L1 HCAb Nb6 and in situ (124)I labeling for noninvasive detection of PD-L1 expression in human bone sarcoma. Bioconjugate Chem 2019, 30, 2614–2623.

(48). Muyldermans S Nanobodies: natural single-domain antibodies. Annu. Rev. Biochem 2013, 82, 775–797. [PubMed: 23495938]

(49). Ingram JR; Schmidt FI; Ploegh HL Exploiting nanobodies' singular traits. Annu. Rev. Immunol 2018, 36, 695–715. [PubMed: 29490163]

(50). Heukers R; De Groof TWM; Smit MJ Nanobodies detecting and modulating GPCRs outside in and inside out. Curr. Opin. Cell Biol 2019, 57, 115–122. [PubMed: 30849632]

(51). Holliger P; Hudson PJ Engineered antibody fragments and the rise of single domains. Nat. Biotechnol 2005, 23, 1126–1136. [PubMed: 16151406]

(52). Schumacher D; Helma J; Schneider AFL; Leonhardt H; Hackenberger CPR Nanobodies: chemical functionalization strategies and intracellular applications. Angew. Chem., Int. Ed 2018, 57, 2314–2333.

(53). Tijink BM; Laeremans T; Budde M; Stigter-van Walsum M; Dreier T; de Haard HJ; Leemans CR; van Dongen GA Improved tumor targeting of anti-epidermal growth factor receptor Nanobodies through albumin binding: taking advantage of modular Nanobody technology. Mol. Cancer Ther 2008, 7, 2288–2297. [PubMed: 18723476]

(54). Vugmeyster Y; Entrican CA; Joyce AP; Lawrence-Henderson RF; Leary BA; Mahoney CS; Patel HK; Raso SW; Olland SH; Hegen M; et al. Pharmacokinetic, biodistribution, and biophysical profiles of TNF nanobodies conjugated to linear or branched poly(ethylene glycol). Bioconjugate Chem 2012, 23, 1452–1462.

(55). Rashidian M; Wang L; Edens JG; Jacobsen JT; Hossain I; Wang Q; Victora GD; Vasdev N; Ploegh H; Liang SH Enzyme-mediated modification of single-domain antibodies for imaging modalities with different characteristics. Angew. Chem., Int. Ed 2016, 55, 528–533.

(56). Chakravarty R; Goel S; Cai W Nanobody: the "magic bullet" for molecular imaging? Theranostics 2014, 4, 386–398. [PubMed: 24578722]

(57). Pruszynski M; Koumarianou E; Vaidyanathan G; Revets H; Devoogdt N; Lahoutte T; Lyerly HK; Zalutsky MR Improved tumor targeting of anti-HER2 nanobody through N-succinimidyl 4-guanidinomethyl-3-iodobenzoate radiolabeling. J. Nucl. Med 2014, 55, 650–656. [PubMed: 24578241]

(58). De Vos J; Devoogdt N; Lahoutte T; Muyldermans S Camelid single-domain antibody-fragment engineering for (pre)-clinical in vivo molecular imaging applications: adjusting the bullet to its target. Expert Opin. Biol. Ther 2013, 13, 1149–1160. [PubMed: 23675652]

(59). Crauwels M; Massa S; Martin C; Betti C; Ballet S; Devoogdt N; Xavier C; Muyldermans S Site-specific radioactive labeling of nanobodies. Methods Mol. Biol 2018, 1827, 505–540. [PubMed: 30196514]

(60). Behr TM; Goldenberg DM; Becker W Reducing the renal uptake of radiolabeled antibody fragments and peptides for diagnosis and therapy: present status, future prospects and limitations. Eur. J. Nucl. Med. Mol. Imaging 1998, 25, 201–212.

(61). Vegt E; de Jong M; Wetzels JF; Masereeuw R; Melis M; Oyen WJ; Gotthardt M; Boerman OC Renal toxicity of radiolabeled peptides and antibody fragments: mechanisms, impact on radionuclide therapy, and strategies for prevention. J. Nucl. Med 2010, 51, 1049–1058. [PubMed: 20554737]

(62). Tchouate Gainkam LO; Caveliers V; Devoogdt N; Vanhove C; Xavier C; Boerman O; Muyldermans S; Bossuyt A; Lahoutte T Localization, mechanism and reduction of renal retention of technetium-99m labeled epidermal growth factor receptor-specific nanobody in mice. Contrast Media Mol. Imaging 2011, 6, 85–92. [PubMed: 20936711]

(63). Xavier C; Vaneycken I; D'Huyvetter M; Heemskerk J; Keyaerts M; Vincke C; Devoogdt N; Muyldermans S; Lahoutte T; Caveliers V Synthesis, preclinical validation, dosimetry, and toxicity of 68Ga-NOTA-anti-HER2 Nanobodies for iPET imaging of HER2 receptor expression in cancer. J. Nucl. Med 2013, 54, 776–784. [PubMed: 23487015]

(64). Rashidian M; Ingram JR; Dougan M; Dongre A; Whang KA; LeGall C; Cragnolini JJ; Bierie B; Gostissa M; Gorman J; et al. Predicting the response to CTLA-4 blockade by longitudinal noninvasive monitoring of CD8 T cells. J. Exp. Med 2017, 214, 2243–2255. [PubMed: 28666979]

(65). Vaneycken I; D'huyvetter M; Hernot S; De Vos J; Xavier C; Devoogdt N; Caveliers V; Lahoutte T Immuno-imaging using nanobodies. Curr. Opin. Biotechnol 2011, 22, 877–881. [PubMed: 21726996]

(66). Debie P; Devoogdt N; Hernot S Targeted nanobody-based molecular tracers for nuclear imaging and image-guided surgery. Antibodies 2019, 8, 12.

(67). D'Huyvetter M; Vincke C; Xavier C; Aerts A; Impens N; Baatout S; De Raeve H; Muyldermans S; Caveliers V; Devoogdt N; et al. Targeted radionuclide therapy with A 177Lu-labeled anti-HER2 nanobody. Theranostics 2014, 4, 708–720. [PubMed: 24883121]

(68). Krasniqi A; D'Huyvetter M; Xavier C; Van der Jeught K; Muyldermans S; Van Der Heyden J; Lahoutte T; Tavernier J; Devoogdt N Theranostic radiolabeled anti-CD20 sdAb for targeted radionuclide therapy of non-Hodgkin lymphoma. Mol. Cancer Ther 2017, 16, 2828–2839. [PubMed: 29054987]

(69). Pruszynski M; D'Huyvetter M; Bruchertseifer F; Morgenstern A; Lahoutte T Evaluation of an anti-HER2 nanobody labeled with (225)Ac for targeted alpha-particle therapy of cancer. Mol. Pharmaceutics 2018, 15, 1457–1466.

(70). Heukers R; van Bergen en Henegouwen PM; Oliveira S Nanobody-photosensitizer conjugates for targeted photodynamic therapy. Nanomedicine 2014, 10, 1441–1451. [PubMed: 24394212]

(71). van Driel P; Boonstra MC; Slooter MD; Heukers R; Stammes MA; Snoeks TJA; de Bruijn HS; van Diest PJ; Vahrmeijer AL; van Bergen En Henegouwen PMP; et al. EGFR targeted nanobody-photosensitizer conjugates for photodynamic therapy in a pre-clinical model of head and neck cancer. J. Controlled Release 2016, 229, 93–105.

(72). Kenanova V; Wu AM Tailoring antibodies for radionuclide delivery. Expert Opin. Drug Delivery 2006, 3, 53–70.

(73). Long NE; Sullivan BJ; Ding H; Doll S; Ryan MA; Hitchcock CL; Martin EW Jr.; Kumar K; Tweedle MF; Magliery TJ Linker engineering in anti-TAG-72 antibody fragments optimizes biophysical properties, serum half-life, and high-specificity tumor imaging. J. Biol. Chem 2018, 293, 9030–9040. [PubMed: 29669811]

(74). Olafsen T; Cheung CW; Yazaki PJ; Li L; Sundaresan G; Gambhir SS; Sherman MA; Williams LE; Shively JE; Raubitschek AA; et al. Covalent disulfide-linked anti-CEA diabody allows site-

specific conjugation and radiolabeling for tumor targeting applications. Protein Eng., Des. Sel 2004, 17, 21–27. [PubMed: 14985534]

(75). Hu S; Shively L; Raubitschek A; Sherman M; Williams LE; Wong JY; Shively JE; Wu AM Minibody: A novel engineered anti-carcinoembryonic antigen antibody fragment (single-chain Fv-CH3) which exhibits rapid, high-level targeting of xenografts. Cancer Res 1996, 56, 3055–3061. [PubMed: 8674062]

(76). Wu AM Engineered antibodies for molecular imaging of cancer. Methods 2014, 65, 139–147. [PubMed: 24091005]

(77). Eder M; Knackmuss S; Le Gall F; Reusch U; Rybin V; Little M; Haberkorn U; Mier W; Eisenhut M 68Ga-labelled recombinant antibody variants for immuno-PET imaging of solid tumours. Eur. J. Nucl. Med. Mol. Imaging 2010, 37, 1397–1407. [PubMed: 20157706]

(78). Rios X; Compte M; Gomez-Vallejo V; Cossio U; Baz Z; Morcillo MA; Ramos-Cabrer P; Alvarez-Vallina L; Llop J Immuno-PET imaging and pharmacokinetics of an anti-CEA scFv-based trimerbody and its monomeric counterpart in human gastric carcinoma-bearing mice. Mol. Pharmaceutics 2019, 16, 1025–1035.

(79). Banta S; Dooley K; Shur O Replacing antibodies: engineering new binding proteins. Annu. Rev. Biomed. Eng 2013, 15, 93–113. [PubMed: 23642248]

(80). Stahl S; Graslund T; Eriksson Karlstrom A; Frejd FY; Nygren PA; Lofblom J Affibody molecules in biotechnological and medical applications. Trends Biotechnol 2017, 35, 691–712. [PubMed: 28514998]

(81). Kramer-Marek G; Kiesewetter DO; Capala J Changes in HER2 expression in breast cancer xenografts after therapy can be quantified using PET and (18)F-labeled affibody molecules. J. Nucl. Med 2009, 50, 1131–1139. [PubMed: 19525458]

(82). Orlova A; Wallberg H; Stone-Elander S; Tolmachev V On the selection of a tracer for PET imaging of HER2-expressing tumors: direct comparison of a 124I-labeled affibody molecule and trastuzumab in a murine xenograft model. J. Nucl. Med 2009, 50, 417–425. [PubMed: 19223403]

(83). Lipovsek D Adnectins: engineered target-binding protein therapeutics. Protein Eng., Des. Sel 2011, 24, 3–9. [PubMed: 21068165]

(84). Hackel BJ; Kimura RH; Gambhir SS Use of (64)Cu-labeled fibronectin domain with EGFR-overexpressing tumor xenograft: molecular imaging. Radiology 2012, 263, 179–188. [PubMed: 22344401]

(85). Kimura RH; Cheng Z; Gambhir SS; Cochran JR Engineered knottin peptides: a new class of agents for imaging integrin expression in living subjects. Cancer Res 2009, 69, 2435–2442. [PubMed: 19276378]

(86). Kintzing JR; Cochran JR Engineered knottin peptides as diagnostics, therapeutics, and drug delivery vehicles. Curr. Opin. Chem. Biol 2016, 34, 143–150. [PubMed: 27642714]

(87). Terwisscha van Scheltinga AG; Lub-de Hooge MN; Hinner MJ; Verheijen RB; Allersdorfer A; Hulsmeyer M; Nagengast WB; Schroder CP; Kosterink JG; de Vries EG; et al. In vivo visualization of MET tumor expression and anticalin biodistribution with the MET-specific anticalin 89Zr-PRS-110 PET tracer. J. Nucl. Med 2014, 55, 665–671. [PubMed: 24614223]

(88). Schiefner A; Skerra A The menagerie of human lipocalins: a natural protein scaffold for molecular recognition of physiological compounds. Acc. Chem. Res 2015, 48, 976–985. [PubMed: 25756749]

(89). Krasniqi A; D'Huyvetter M; Devoogdt N; Frejd FY; Sorensen J; Orlova A; Keyaerts M; Tolmachev V Same-day imaging using small proteins: Clinical Experience and Translational Prospects in Oncology. J. Nucl. Med 2018, 59, 885–891. [PubMed: 29545374]

(90). Tsai SW; Li L; Williams LE; Anderson AL; Raubitschek AA; Shively JE Metabolism and renal clearance of 111In-labeled DOTA-conjugated antibody fragments. Bioconjugate Chem 2001, 12, 264–270.

(91). Yang K; Basu A; Wang M; Chintala R; Hsieh MC; Liu S; Hua J; Zhang Z; Zhou J; Li M; et al. Tailoring structure-function and pharmacokinetic properties of single-chain Fv proteins by site-specific PEGylation. Protein Eng., Des. Sel 2003, 16, 761–770.

(92). Kontermann RE Strategies for extended serum half-life of protein therapeutics. Curr. Opin. Biotechnol 2011, 22, 868–876. [PubMed: 21862310]

(93). Klinger M; Benjamin J; Kischel R; Stienen S; Zugmaier G Harnessing T cells to fight cancer with BiTE(R) antibody constructs–past developments and future directions. Immunol. Rev 2016, 270, 193–208. [PubMed: 26864113]

(94). Yuraszeck T; Kasichayanula S; Benjamin JE Translation and clinical development of bispecific T-cell engaging antibodies for cancer treatment. Clin. Pharmacol. Ther 2017, 101, 634–645. [PubMed: 28182247]

(95). Krishnamurthy A; Jimeno A Bispecific antibodies for cancer therapy: A review. Pharmacol. Ther 2018, 185, 122–134. [PubMed: 29269044]

(96). Topp MS; Gokbuget N; Stein AS; Zugmaier G; O'Brien S; Bargou RC; Dombret H; Fielding AK; Heffner L; Larson RA; et al. Safety and activity of blinatumomab for adult patients with relapsed or refractory B-precursor acute lymphoblastic leukaemia: a multicentre, single-arm, phase 2 study. Lancet Oncol 2015, 16, 57–66. [PubMed: 25524800]

(97). Warnders FJ; Waaijer SJ; Pool M; Lub-de Hooge MN; Friedrich M; Terwisscha van Scheltinga AG; Deegen P; Stienen SK; Pieslor PC; Cheung HK; et al. Biodistribution and PET imaging of labeled bispecific T Cell-engaging antibody targeting EpCAM. J. Nucl. Med 2016, 57, 812–817. [PubMed: 26848172]

(98). Mandikian D; Takahashi N; Lo AA; Li J; Eastham-Anderson J; Slaga D; Ho J; Hristopoulos M; Clark R; Totpal K; et al. Relative target affinities of T-cell-dependent bispecific antibodies determine biodistribution in a solid tumor mouse model. Mol. Cancer Ther 2018, 17, 776–785. [PubMed: 29339550]

(99). Zhou Y; Baidoo KE; Brechbiel MW Mapping biological behaviors by application of longer-lived positron emitting radio-nuclides. Adv. Drug Delivery Rev 2013, 65, 1098–1111.

(100). Boros E; Packard AB Radioactive transition metals for imaging and therapy. Chem. Rev 2019, 119, 870–901. [PubMed: 30299088]

(101). Price EW; Orvig C Matching chelators to radiometals for radiopharmaceuticals. Chem. Soc. Rev 2014, 43, 260–290. [PubMed: 24173525]

(102). Kostelnik TI; Orvig C Radioactive main group and rare earth metals for imaging and therapy. Chem. Rev 2019, 119, 902–956. [PubMed: 30379537]

(103). Aluicio-Sarduy E; Ellison PA; Barnhart TE; Cai W; Nickles RJ; Engle JW PET radiometals for antibody labeling. J. Labelled Compd. Radiopharm 2018, 61, 636–651.

(104). Oehlke E; Hoehr C; Hou X; Hanemaayer V; Zeisler S; Adam MJ; Ruth TJ; Celler A; Buckley K; Benard F; et al. Production of Y-86 and other radiometals for research purposes using a solution target system. Nucl. Med. Biol 2015, 42, 842–849. [PubMed: 26264926]

(105). Cutler CS; Hennkens HM; Sisay N; Huclier-Markai S; Jurisson SS Radiometals for combined imaging and therapy. Chem. Rev 2013, 113, 858–883. [PubMed: 23198879]

(106). Wadas TJ; Wong EH; Weisman GR; Anderson CJ Coordinating radiometals of copper, gallium, indium, yttrium, and zirconium for PET and SPECT imaging of disease. Chem. Rev 2010, 110, 2858–2902. [PubMed: 20415480]

(107). Morris O; Fairclough M; Grigg J; Prenant C; McMahon A A review of approaches to (18) F radiolabelling affinity peptides and proteins. J. Labelled Compd. Radiopharm 2019, 62, 4–23.

(108). Zhang Y; Hong H; Cai W PET tracers based on Zirconium-89. Curr. Radiopharm 2011, 4, 131–139. [PubMed: 22191652]

(109). Dilworth JR; Pascu SI The chemistry of PET imaging with zirconium-89. Chem. Soc. Rev 2018, 47, 2554–2571. [PubMed: 29557435]

(110). La MT; Tran VH; Kim HK Progress of coordination and utilization of Zirconium-89 for positron emission tomography (PET) studies. Nucl. Med. Mol. Imaging 2019, 53, 115–124. [PubMed: 31057683]

(111). Pandey MK; Bansal A; Engelbrecht HP; Byrne JF; Packard AB; DeGrado TR Improved production and processing of (8)(9)Zr using a solution target. Nucl. Med. Biol 2016, 43, 97–100. [PubMed: 26471714]

(112). Dias GM; Ramogida CF; Rousseau J; Zacchia NA; Hoehr C; Schaffer P; Lin KS; Benard F 89)Zr for antibody labeling and in vivo studies - a comparison between liquid and solid target production. Nucl. Med. Biol 2018, 58, 1–7. [PubMed: 29291493]

(113). Graves SA; Kutyreff C; Barrett KE; Hernandez R; Ellison PA; Happel S; Aluicio-Sarduy E; Barnhart TE; Nickles RJ; Engle JW Evaluation of a chloride-based (89)Zr isolation strategy using a tributyl phosphate (TBP)-functionalized extraction resin. Nucl. Med. Biol 2018, 64–65, 1–7.

(114). Pandya DN; Bhatt NB; Almaguel F; Rideout-Danner S; Gage HD; Solingapuram Sai KK; Wadas TJ 89)Zr-chloride can be used for immuno-PET radiochemistry without loss of antigen reactivity in vivo. J. Nucl. Med 2019, 60, 696–701. [PubMed: 30442753]

(115). Holland JP; Sheh Y; Lewis JS Standardized methods for the production of high specific-activity zirconium-89. Nucl. Med. Biol 2009, 36, 729–739. [PubMed: 19720285]

(116). Verel I; Visser GWM; Boellaard R; Stigter-van Walsum M; Snow GB; van Dongen GAMS 89Zr immuno-PET: comprehensive procedures for the production of 89Zr-labeled monoclonal antibodies. J. Nucl. Med 2003, 44, 1271–1281. [PubMed: 12902418]

(117). Verel I; Visser GW; Boerman OC; van Eerd JE; Finn R; Boellaard R; Vosjan MJ; Stigter-van Walsum M; Snow GB; van Dongen GA Long-lived positron emitters zirconium-89 and iodine-124 for scouting of therapeutic radioimmunoconjugates with PET. Cancer Biother.Radiopharm 2003, 18, 655–661. [PubMed: 14503961]

(118). Borjesson PK; Jauw YW; Boellaard R; de Bree R; Comans EF; Roos JC; Castelijns JA; Vosjan MJ; Kummer JA; Leemans CR; et al. Performance of immuno-positron emission tomography with zirconium-89-labeled chimeric monoclonal antibody U36 in the detection of lymph node metastases in head and neck cancer patients. Clin. Cancer Res 2006, 12, 2133–2140. [PubMed: 16609026]

(119). Perk LR; Vosjan MJ; Visser GW; Budde M; Jurek P; Kiefer GE; van Dongen GA p-Isothiocyanatobenzyl-desferrioxamine: a new bifunctional chelate for facile radiolabeling of monoclonal antibodies with zirconium-89 for immuno-PET imaging. Eur. J. Nucl. Med. Mol. Imaging 2010, 37, 250–259. [PubMed: 19763566]

(120). Vosjan MJ; Perk LR; Visser GW; Budde M; Jurek P; Kiefer GE; van Dongen GA Conjugation and radiolabeling of monoclonal antibodies with zirconium-89 for PET imaging using the bifunctional chelate p-isothiocyanatobenzyl-desferrioxamine. Nat. Protoc 2010, 5, 739–743. [PubMed: 20360768]

(121). Holland JP; Divilov V; Bander NH; Smith-Jones PM; Larson SM; Lewis JS 89Zr-DFO-J591 for immunoPET of prostate-specific membrane antigen expression in vivo. J. Nucl. Med 2010, 51, 1293–1300. [PubMed: 20660376]

(122). Wei W; Jiang D; Ehlerding EB; Barnhart TE; Yang Y; Engle JW; Luo QY; Huang P; Cai W CD146-targeted multimodal image-guided photoimmunotherapy of melanoma. Adv. Sci. (Weinh) 2019, 6, 1801237. [PubMed: 31065511]

(123). Bailly C; Gouard S; Guerard F; Chalopin B; Carlier T; Faivre-Chauvet A; Remaud-Le Saec P; Bourgeois M; Chouin N; Rbah-Vidal L What is the best radionuclide for immuno-PET of multiple myeloma? a comparison study between (89)Zr- and (64)Cu-labeled anti-CD138 in a preclinical syngeneic model. Int. J. Mol. Sci 2019, 20, 2564.

(124). Patra M; Bauman A; Mari C; Fischer CA; Blacque O; Haussinger D; Gasser G; Mindt TL An octadentate bifunctional chelating agent for the development of stable zirconium-89 based molecular imaging probes. Chem. Commun. (Cambridge, U. K.) 2014, 50, 11523–11525.

(125). Vugts DJ; Klaver C; Sewing C; Poot AJ; Adamzek K; Huegli S; Mari C; Visser GWM; Valverde IE; Gasser G; et al. Comparison of the octadentate bifunctional chelator DFO*-pPhe-NCS and the clinically used hexadentate bifunctional chelator DFO-pPhe-NCS for (89)Zr-immuno-PET. Eur. J. Nucl. Med. Mol. Imaging 2017, 44, 286–295. [PubMed: 27573793]

(126). Raave R; Sandker G; Adumeau P; Jacobsen CB; Mangin F; Meyer M; Moreau M; Bernhard C; Da Costa L; Dubois A; et al. Direct comparison of the in vitro and in vivo stability of DFO, DFO* and DFOcyclo* for (89)Zr-immunoPET. Eur. J. Nucl. Med. Mol. Imaging 2019, 46, 1966–1977. [PubMed: 31161258]

(127). Adams CJ; Wilson JJ; Boros E Multifunctional desferrichrome analogues as versatile (89)Zr(IV) chelators for immunoPET probe development. Mol. Pharmaceutics 2017, 14, 2831–2842.

(128). Price EW; Zeglis BM; Lewis JS; Adam MJ; Orvig C H6phospa-trastuzumab: bifunctional methylenephosphonate-based chelator with 89Zr, 111In and 177Lu. Dalton Trans 2014, 43, 119–131. [PubMed: 24104523]

(129). Deri MA; Ponnala S; Zeglis BM; Pohl G; Dannenberg JJ; Lewis JS; Francesconi LC Alternative chelator for (8)(9)Zr radiopharmaceuticals: radiolabeling and evaluation of 3,4,3-(LI-1,2-HOPO). J. Med. Chem 2014, 57, 4849–4860. [PubMed: 24814511]

(130). Deri MA; Ponnala S; Kozlowski P; Burton-Pye BP; Cicek HT; Hu C; Lewis JS; Francesconi LC p-SCN-Bn-HOPO: A superior bifunctional chelator for (89)Zr immunoPET. Bioconjugate Chem 2015, 26, 2579–2591.

(131). Tinianow JN; Pandya DN; Pailloux SL; Ogasawara A; Vanderbilt AN; Gill HS; Williams SP; Wadas TJ; Magda D; Marik J Evaluation of a 3-hydroxypyridin-2-one (2,3-HOPO) based macrocyclic chelator for (89)Zr(4+) and its use for immunoPET imaging of HER2 positive model of ovarian carcinoma in mice. Theranostics 2016, 6, 511–521. [PubMed: 26941844]

(132). Guérard F; Lee Y-S; Tripier R; Szajek LP; Deschamps JR; Brechbiel MW Investigation of Zr(iv) and89Zr(iv) complexation with hydroxamates: progress towards designing a better chelator than desferrioxamine B for immuno-PET imaging. Chem. Commun 2013, 49, 1002–1004.

(133). Guerard F; Lee YS; Brechbiel MW Rational design, synthesis, and evaluation of tetrahydroxamic acid chelators for stable complexation of zirconium(IV). Chem. - Eur. J 2014, 20, 5584–5591. [PubMed: 24740517]

(134). Boros E; Holland JP; Kenton N; Rotile N; Caravan P Macrocycle-based hydroxamate ligands for complexation and immunoconjugation of (89)Zirconium for positron emission tomography (PET) imaging. ChemPlusChem 2016, 81, 274–281. [PubMed: 27630807]

(135). Allott L; Da Pieve C; Meyers J; Spinks T; Ciobota D; Kramer-Marek G; Smith G Evaluation of DFO-HOPO as an octadentate chelator for zirconium-89. Chem. Commun 2017, 53, 8529–8532.

(136). Zhai C; Summer D; Rangger C; Franssen GM; Laverman P; Haas H; Petrik M; Haubner R; Decristoforo C Novel bifunctional cyclic chelator for (89)Zr labeling-radiolabeling and targeting properties of RGD Conjugates. Mol. Pharmaceutics 2015, 12, 2142–2150.

(137). Rudd SE; Roselt P; Cullinane C; Hicks RJ; Donnelly PSJCC A desferrioxamine B squaramide ester for the incorporation of zirconium-89 into antibodies. Chem. Commun 2016, 52, 11889–11892.

(138). Summer D; Garousi J; Oroujeni M; Mitran B; Andersson KG; Vorobyeva A; Lofblom J; Orlova A; Tolmachev V; Decristoforo C Cyclic versus noncyclic chelating scaffold for (89)Zr-Labeled ZEGFR:2377 affibody bioconjugates targeting epidermal growth factor receptor overexpression. Mol. Pharmaceutics 2018, 15, 175–185.

(139). Zhai C; He S; Ye Y; Rangger C; Kaeopookum P; Summer D; Haas H; Kremser L; Lindner H; Foster J; et al. Rational design, synthesis and preliminary evaluation of novel fusarinine C-based chelators for radiolabeling with Zirconium-89. Biomolecules 2019, 9, 91.

(140). Pandya DN; Bhatt N; Yuan H; Day CS; Ehrmann BM; Wright M; Bierbach U; Wadas TJ Zirconium tetraazamacro-cycle complexes display extraordinary stability and provide a new strategy for zirconium-89-based radiopharmaceutical development. Chem. Sci 2017, 8, 2309–2314. [PubMed: 28451334]

(141). McCarthy DW; Shefer RE; Klinkowstein RE; Bass LA; Margeneau WH; Cutler CS; Anderson CJ; Welch MJ Efficient production of high specific activity 64Cu using a biomedical cyclotron. Nucl. Med. Biol 1997, 24, 35–43. [PubMed: 9080473]

(142). Alves F; Alves VHP; Do Carmo SJC; Neves ACB; Silva M; Abrunhosa AJ Production of copper-64 and gallium-68 with a medical cyclotron using liquid targets. Mod. Phys. Lett. A 2017, 32, 1740013.

(143). Smith NA; Bowers DL; Ehst DA The production, separation, and use of 67Cu for radioimmunotherapy: a review. Appl. Radiat. Isot 2012, 70, 2377–2383. [PubMed: 22871441]

(144). Cai W; Wu Y; Chen K; Cao Q; Tice DA; Chen X In vitro and in vivo characterization of 64Cu-labeled Abegrin, a humanized monoclonal antibody against integrin alpha v beta 3. Cancer Res 2006, 66, 9673–9681. [PubMed: 17018625]

(145). Cai W; Chen K; He L; Cao Q; Koong A; Chen X Quantitative PET of EGFR expression in xenograft-bearing mice using 64Cu-labeled cetuximab, a chimeric anti-EGFR monoclonal antibody. Eur. J. Nucl. Med. Mol. Imaging 2007, 34, 850–858. [PubMed: 17262214]

(146). Ferreira CL; Yapp DT; Lamsa E; Gleave M; Bensimon C; Jurek P; Kiefer GE Evaluation of novel bifunctional chelates for the development of Cu-64-based radiopharmaceuticals. Nucl. Med. Biol 2008, 35, 875–882. [PubMed: 19026949]

(147). Cooper MS; Ma MT; Sunassee K; Shaw KP; Williams JD; Paul RL; Donnelly PS; Blower PJ Comparison of (64)Cu-complexing bifunctional chelators for radioimmunoconjugation: labeling efficiency, specific activity, and in vitro/in vivo stability. Bioconjugate Chem 2012, 23, 1029–1039.

(148). Ghosh SC; Pinkston KL; Robinson H; Harvey BR; Wilganowski N; Gore K; Sevick-Muraca EM; Azhdarinia A Comparison of DOTA and NODAGA as chelators for (64)Cu-labeled immunoconjugates. Nucl. Med. Biol 2015, 42, 177–183. [PubMed: 25457653]

(149). Moreau M; Poty S; Vrigneaud JM; Walker P; Guillemin M; Raguin O; Oudot A; Bernhard C; Goze C; Boschetti F; et al. MANOTA: a promising bifunctional chelating agent for copper-64 immunoPET. Dalton Trans 2017, 46, 14659–14668. [PubMed: 28861553]

(150). Wong EH; Weisman GR; Hill DC; Reed DP; Rogers ME; Condon JS; Fagan MA; Calabrese JC; Lam K-C; Guzei IA; et al. Synthesis and characterization of cross-bridged cyclams and pendant-armed derivatives and structural studies of their copper(II) complexes. J. Am. Chem. Soc 2000, 122, 10561–10572.

(151). Wadas TJ; Anderson CJ Radiolabeling of TETA- and CBTE2A-conjugated peptides with copper-64. Nat. Protoc 2006, 1, 3062–3068. [PubMed: 17406569]

(152). Ferdani R; Stigers DJ; Fiamengo AL; Wei L; Li BT; Golen JA; Rheingold AL; Weisman GR; Wong EH; Anderson CJ Synthesis, Cu(II) complexation, 64Cu-labeling and biological evaluation of cross-bridged cyclam chelators with phosphonate pendant arms. Dalton Trans 2012, 41, 1938–1950. [PubMed: 22170043]

(153). Guo Y; Ferdani R; Anderson CJ Preparation and biological evaluation of (64)Cu labeled Tyr(3)-octreotate using a phosphonic acid-based cross-bridged macrocyclic chelator. Bioconju-gate Chem 2012, 23, 1470–1477.

(154). Stigers DJ; Ferdani R; Weisman GR; Wong EH; Anderson CJ; Golen JA; Moore C; Rheingold AL A new phosphonate pendant-armed cross-bridged tetraamine chelator accelerates copper(ii) binding for radiopharmaceutical applications. Dalton Trans 2010, 39, 1699–1701. [PubMed: 20449406]

(155). Zeng D; Guo Y; White AG; Cai Z; Modi J; Ferdani R; Anderson CJ Comparison of conjugation strategies of cross-bridged macrocyclic chelators with cetuximab for copper-64 radiolabeling and PET imaging of EGFR in colorectal tumor-bearing mice. Mol. Pharmaceutics 2014, 11, 3980–3987.

(156). Ren Q; Mohri K; Warashina S; Wada Y; Watanabe Y; Mukai H Improved immuno-PET imaging of HER2-positive tumors in mice: urokinase injection-triggered clearance enhancement of(64)Cu-trastuzumab. Mol. Pharmaceutics 2019, 16, 1065–1073.

(157). David T; Kubicek V; Gutten O; Lubal P; Kotek J; Pietzsch HJ; Rulisek L; Hermann P Cyclam derivatives with a bis(phosphinate) or a phosphinato-phosphonate pendant arm: ligands for fast and efficient copper(II) complexation for nuclear medical applications. Inorg. Chem 2015, 54, 11751–11766. [PubMed: 26615961]

(158). David T; Hlinova V; Kubicek V; Bergmann R; Striese F; Berndt N; Szollosi D; Kovacs T; Mathe D; Bachmann M; et al. Improved conjugation, 64-Cu radiolabeling, in vivo stability, and imaging using nonprotected bifunctional macrocyclic ligands: bis-(Phosphinate) cyclam (BPC) chelators. J. Med. Chem 2018, 61, 8774–8796. [PubMed: 30180567]

(159). Di Bartolo N; Sargeson AM; Smith SV New 64Cu PET imaging agents for personalised medicine and drug development using the hexa-aza cage, SarAr. Org. Biomol. Chem 2006, 4, 3350–3357. [PubMed: 17036125]

(160). Voss SD; Smith SV; DiBartolo N; McIntosh LJ; Cyr EM; Bonab AA; Dearling JL; Carter EA; Fischman AJ; Treves ST; et al. Positron emission tomography (PET) imaging of neuroblastoma and melanoma with 64Cu-SarAr immunoconjugates. Proc. Natl. Acad. Sci. U. S. A 2007, 104, 17489–17493. [PubMed: 17954911]

(161). Dearling JL; Voss SD; Dunning P; Snay E; Fahey F; Smith SV; Huston JS; Meares CF; Treves ST; Packard AB Imaging cancer using PET–the effect of the bifunctional chelator on the biodistribution of a (64)Cu-labeled antibody. Nucl. Med. Biol 2011, 38, 29–38. [PubMed: 21220127]

(162). Jailkhani N; Ingram JR; Rashidian M; Rickelt S; Tian C; Mak H; Jiang Z; Ploegh HL; Hynes RO Noninvasive imaging of tumor progression, metastasis, and fibrosis using a nanobody targeting the extracellular matrix. Proc. Natl. Acad. Sci. U.S. A 2019, 116, 14181–14190. [PubMed: 31068469]

(163). Yoo J; Tang L; Perkins TA; Rowland DJ; Laforest R; Lewis JS; Welch MJ Preparation of high specific activity (86)Y using a small biomedical cyclotron. Nucl. Med. Biol 2005, 32, 891–897. [PubMed: 16253815]

(164). Avila-Rodriguez MA; Nye JA; Nickles RJ Production and separation of non-carrier-added 86Y from enriched 86Sr targets. Appl. Radiat. Isot 2008, 66, 9–13. [PubMed: 17869530]

(165). Qaim SM; Spahn I Development of novel radionuclides for medical applications. J. Labelled Compd. Radiopharm 2018, 61, 126–140.

(166). Aluicio-Sarduy E; Hernandez R; Valdovinos HF; Kutyreff CJ; Ellison PA; Barnhart TE; Nickles RJ; Engle JW Simplified and automatable radiochemical separation strategy for the production of radiopharmaceutical quality (86)Y using single column extraction chromatography. Appl. Radiat. Isot 2018, 142, 28–31. [PubMed: 30245439]

(167). Larson SM; Carrasquillo JA; Cheung NK; Press OW Radioimmunotherapy of human tumours. Nat. Rev. Cancer 2015, 15, 347–360. [PubMed: 25998714]

(168). Hernandez R; Walker KL; Grudzinski JJ; Aluicio-Sarduy E; Patel R; Zahm CD; Pinchuk AN; Massey CF; Bitton AN; Brown RJ; et al. (90)Y-NM600 targeted radionuclide therapy induces immunologic memory in syngeneic models of T-cell Non-Hodgkin's Lymphoma. Commun. Biol 2019, 2, 79. [PubMed: 30820474]

(169). Rosch F; Herzog H; Qaim SM The beginning and development of the theranostic approach in nuclear medicine, as exemplified by the radionuclide pair (86)Y and (90)Y. Pharmaceuticals 2017, 10, 56.

(170). Herzog H; Rosch F; Stocklin G; Lueders C; Qaim SM; Feinendegen LE Measurement of pharmacokinetics of yttrium-86 radiopharmaceuticals with PET and radiation dose calculation of analogous yttrium-90 radiotherapeutics. J. Nucl. Med 1993, 34, 2222–2226. [PubMed: 8254415]

(171). Ehlerding EB; Ferreira CA; Aluicio-Sarduy E; Jiang D; Lee HJ; Theuer CP; Engle JW; Cai W 86/90Y-based theranostics targeting angiogenesis in a murine breast cancer model. Mol. Pharmaceutics 2018, 15, 2606–2613.

(172). Ikotun OF; Lapi SE The rise of metal radionuclides in medical imaging: copper-64, zirconium-89 and yttrium-86. Future Med. Chem 2011, 3, 599–621. [PubMed: 21526898]

(173). Nayak TK; Brechbiel MW 86Y based PET radiopharmaceuticals: radiochemistry and biological applications. Med. Chem 2011, 7, 380–388. [PubMed: 21711222]

(174). Roselli M; Schlom J; Gansow OA; Raubitschek A; Mirzadeh S; Brechbiel MW; Colcher D Comparative biodistributions of yttrium- and indium-labeled monoclonal antibody B72.3 in athymic mice bearing human colon carcinoma xenografts. J. Nucl. Med 1989, 30, 672–682. [PubMed: 2785585]

(175). Camera L; Kinuya S; Garmestani K; Brechbiel MW; Wu C; Pai LH; McMurry TJ; Gansow OA; Pastan I; Paik CH; et al. Comparative biodistribution of indium- and yttrium-labeled B3 monoclonal antibody conjugated to either 2-(p-SCN-Bz)-6-methyl-DTPA (1B4M-DTPA) or 2-(p-SCN-Bz)-1,4,7,10-tetraazacyclododecane tetraacetic acid (2B-DOTA). Eur. J. Nucl. Med 1994, 21, 640–646. [PubMed: 7957350]

(176). Palm S; Enmon RM Jr.; Matei C; Kolbert KS; Xu S; Zanzonico PB; Finn RL; Koutcher JA; Larson SM; Sgouros G Pharmacokinetics and biodistribution of (86)Y-trastuzumab for(90)Y dosimetry in an ovarian carcinoma model: correlative MicroPET and MRI. J. Nucl. Med 2003, 44, 1148–1155. [PubMed: 12843231]

(177). Parry R; Schneider D; Hudson D; Parkes D; Xuan JA; Newton A; Toy P; Lin R; Harkins R; Alicke B; et al. Identification of a novel prostate tumor target, mindin/RG-1, for antibody-based radiotherapy of prostate cancer. Cancer Res 2005, 65, 8397–8405. [PubMed: 16166318]

(178). Nayak TK; Regino CA; Wong KJ; Milenic DE; Garmestani K; Baidoo KE; Szajek LP; Brechbiel MW PET imaging of HER1-expressing xenografts in mice with 86Y-CHX-A′′-DTPA-cetuximab. Eur. J. Nucl. Med. Mol. Imaging 2010, 37, 1368–1376. [PubMed: 20155263]

(179). Nayak TK; Garmestani K; Milenic DE; Baidoo KE; Brechbiel MW HER1-targeted 86Y-panitumumab possesses superior targeting characteristics than 86Y-cetuximab for PET imaging of human malignant mesothelioma tumors xenografts. PLoS One 2011, 6, e18198. [PubMed: 21464917]

(180). Silberstein EB Radioiodine: the classic theranostic agent. Semin. Nucl. Med 2012, 42, 164–170. [PubMed: 22475425]

(181). Sajjad M; Bars E; Nabi HA Optimization of 124I production via 124Te(p,n)124I reaction. Appl. Radiat. Isot 2006, 64, 965–970. [PubMed: 16725332]

(182). Nye JA; Avila-Rodriguez MA; Nickles RJ A new binary compound for the production of 124I via the 124Te(p,n)124I reaction. Appl. Radiat. Isot 2007, 65, 407–412. [PubMed: 17174098]

(183). Wilson CB; Snook DE; Dhokia B; Taylor CV; Watson IA; Lammertsma AA; Lambrecht R; Waxman J; Jones T; Epenetos AA Quantitative measurement of monoclonal antibody distribution and blood flow using positron emission tomography and 124iodine in patients with breast cancer. Int. J. Cancer 1991, 47, 344–347. [PubMed: 1847121]

(184). Divgi CR; Pandit-Taskar N; Jungbluth AA; Reuter VE; Gonen M; Ruan S; Pierre C; Nagel A; Pryma DA; Humm J; et al. Preoperative characterisation of clear-cell renal carcinoma using iodine-124-labelled antibody chimeric G250 (124I-cG250) and PET in patients with renal masses: a phase I trial. Lancet Oncol 2007, 8, 304–310. [PubMed: 17395103]

(185). Carrasquillo JA; Pandit-Taskar N; O'Donoghue JA; Humm JL; Zanzonico P; Smith-Jones PM; Divgi CR; Pryma DA; Ruan S; Kemeny NE; et al. (124)I-huA33 antibody PET of colorectal cancer. J. Nucl. Med 2011, 52, 1173–1180. [PubMed: 21764796]

(186). Divgi CR; Uzzo RG; Gatsonis C; Bartz R; Treutner S; Yu JQ; Chen D; Carrasquillo JA; Larson S; Bevan P; et al. Positron emission tomography/computed tomography identification of clear cell renal cell carcinoma: results from the REDECT trial. J. Clin. Oncol 2013, 31, 187–194. [PubMed: 23213092]

(187). Cascini GL; Niccoli Asabella A; Notaristefano A; Restuccia A; Ferrari C; Rubini D; Altini C; Rubini G 124 Iodine: a longer-life positron emitter isotope-new opportunities in molecular imaging. BioMed Res. Int 2014, 2014, 672094. [PubMed: 24895600]

(188). Tijink BM; Perk LR; Budde M; Stigter-van Walsum M; Visser GW; Kloet RW; Dinkelborg LM; Leemans CR; Neri D; van Dongen GA (124)I-L19-SIP for immuno-PET imaging of tumour vasculature and guidance of (131)I-L19-SIP radioimmuno-therapy. Eur. J. Nucl. Med. Mol. Imaging 2009, 36, 1235–1244. [PubMed: 19259661]

(189). Visser GW; Klok RP; Gebbinck JW; ter Linden T; van Dongen GA; Molthoff CF Optimal quality (131)I-monoclonal antibodies on high-dose labeling in a large reaction volume and temporarily coating the antibody with IODO-GEN. J. Nucl. Med 2001, 42, 509–519. [PubMed: 11337531]

(190). Foulon CF; Reist CJ; Bigner DD; Zalutsky MR Radioiodination via D-amino acid peptide enhances cellular retention and tumor xenograft targeting of an internalizing anti-epidermal growth factor receptor variant III monoclonal antibody. Cancer Res 2000, 60, 4453–4460. [PubMed: 10969792]

(191). Stein R; Govindan SV; Mattes MJ; Chen S; Reed L; Newsome G; McBride BJ; Griffiths GL; Hansen HJ; Goldenberg DM Improved iodine radiolabels for monoclonal antibody therapy. Cancer Res 2003, 63, 111–118. [PubMed: 12517786]

(192). Govindan SV; Griffiths GL; Stein R; Andrews P; Sharkey RM; Hansen HJ; Horak ID; Goldenberg DM Clinical-scale radiolabeling of a humanized anticarcinoembryonic antigen monoclonal antibody, hMN-14, with residualizing 131I for use in radioimmunotherapy. J. Nucl. Med 2005, 46, 153–159. [PubMed: 15632046]

(193). Vaidyanathan G; Alston KL; Bigner DD; Zalutsky MR Nepsilon-(3-[*I]Iodobenzoyl)-Lys5-Nalpha-maleimido-Gly1-GEEEK ([*I]IB-Mal-D-GEEEK): a radioiodinated prosthetic group containing negatively charged D-glutamates for labeling internalizing monoclonal antibodies. Bioconjugate Chem 2006, 17, 1085–1092.

(194). Vaidyanathan G; Zalutsky MR Synthesis of N-succinimidyl 4-guanidinomethyl-3-[*I]iodobenzoate: a radio-iodination agent for labeling internalizing proteins and peptides. Nat. Protoc 2007, 2, 282–286. [PubMed: 17406587]

(195). Boswell CA; Marik J; Elowson MJ; Reyes NA; Ulufatu S; Bumbaca D; Yip V; Mundo EE; Majidy N; Van Hoy M; et al. Enhanced tumor retention of a radiohalogen label for site-specific modification of antibodies. J. Med. Chem 2013, 56, 9418–9426. [PubMed: 24131491]

(196). Fowler JS; Ido T Initial and subsequent approach for the synthesis of 18FDG. Semin. Nucl. Med 2002, 32, 6–12. [PubMed: 11839070]

(197). Zettlitz KA; Tavare R; Tsai WK; Yamada RE; Ha NS; Collins J; van Dam RM; Timmerman JM; Wu AM 18)F-labeled anti-human CD20 cys-diabody for same-day immunoPET in a model of aggressive B cell lymphoma in human CD20 transgenic mice. Eur. J. Nucl. Med. Mol. Imaging 2019, 46, 489–500. [PubMed: 30456475]

(198). Krishnan HS; Ma L; Vasdev N; Liang SH (18)F-labeling of sensitive biomolecules for positron emission tomography. Chem. - Eur. J 2017, 23, 15553–15577. [PubMed: 28704575]

(199). Speranza A; Ortosecco G; Castaldi E; Nardelli A; Pace L; Salvatore M Fully automated synthesis procedure of 4-[18F]fluorobenzaldehyde by commercial synthesizer: amino-oxi peptide labelling prosthetic group. Appl. Radiat. Isot 2009, 67, 1664–1669. [PubMed: 19443231]

(200). Cai W; Olafsen T; Zhang X; Cao Q; Gambhir SS; Williams LE; Wu AM; Chen X PET imaging of colorectal cancer in xenograft-bearing mice by use of an 18F-labeled T84.66 anti-carcinoembryonic antigen diabody. J. Nucl. Med 2007, 48, 304–310. [PubMed: 17268029]

(201). Sharma SK; Wuest M; Way JD; Bouvet VR; Wang M; Wuest FR Synthesis and pre-clinical evaluation of an (18)F-labeled single-chain antibody fragment for PET imaging of epithelial ovarian cancer. Am. J. Nucl. Med. Mol. Imaging 2016, 6, 185–198. [PubMed: 27508105]

(202). Vaidyanathan G; McDougald D; Choi J; Koumarianou E; Weitzel D; Osada T; Lyerly HK; Zalutsky MR Preclinical evaluation of 18F-labeled anti-HER2 nanobody conjugates for imaging HER2 receptor expression by immuno-PET. J. Nucl. Med 2016, 57, 967–973. [PubMed: 26912425]

(203). Vaidyanathan G; Zalutsky MR Synthesis of N-succinimidyl 4-[18F]fluorobenzoate, an agent for labeling proteins and peptides with 18F. Nat. Protoc 2006, 1, 1655–1661. [PubMed: 17487148]

(204). Cai W; Zhang X; Wu Y; Chen X A thiol-reactive 18F-labeling agent, N-[2-(4–18F-fluorobenzamido)ethyl]maleimide, and synthesis of RGD peptide-based tracer for PET imaging of alpha v beta 3 integrin expression. J. Nucl. Med 2006, 47, 1172–1180. [PubMed: 16818952]

(205). Kramer-Marek G; Kiesewetter DO; Martiniova L; Jagoda E; Lee SB; Capala J [18F]FBEM-Z(HER2:342)-affibody molecule-a new molecular tracer for in vivo monitoring of HER2 expression by positron emission tomography. Eur. J. Nucl. Med. Mol. Imaging 2008, 35, 1008–1018. [PubMed: 18157531]

(206). Li W; Niu G; Lang L; Guo N; Ma Y; Kiesewetter DO; Backer JM; Shen B; Chen X PET imaging of EGF receptors using [18F]FBEM-EGF in a head and neck squamous cell carcinoma model. Eur. J. Nucl. Med. Mol. Imaging 2012, 39, 300–308. [PubMed: 22109665]

(207). Lim K; Ropchan J; Kiesewetter DO; Chen X; Huang Y Automated radiosynthesis of [(18)F]FBEM, a sulfhydryl site specific labeling agent for peptides and proteins. Appl. Radiat. Isot 2018, 140, 294–299. [PubMed: 30098587]

(208). Kiesewetter DO; Jacobson O; Lang L; Chen X Automated radiochemical synthesis of [18F]FBEM: a thiol reactive synthon for radiofluorination of peptides and proteins. Appl. Radiat. Isot 2011, 69, 410–414. [PubMed: 20965741]

(209). Olberg DE; Arukwe JM; Grace D; Hjelstuen OK; Solbakken M; Kindberg GM; Cuthbertson A One step radiosynthesis of 6-[(18)F]fluoronicotinic acid 2,3,5,6-tetrafluorophenyl ester ([(18)F]F-Py-TFP): a new prosthetic group for efficient labeling of biomolecules with fluorine-18. J. Med. Chem 2010, 53, 1732–1740. [PubMed: 20088512]

(210). Basuli F; Li C; Xu B; Williams M; Wong K; Coble VL; Vasalatiy O; Seidel J; Green MV; Griffiths GL; et al. Synthesis of fluorine-18 radio-labeled serum albumins for PET blood pool imaging. Nucl. Med. Biol 2015, 42, 219–225. [PubMed: 25533724]

(211). Basuli F; Zhang X; Jagoda EM; Choyke PL; Swenson RE Facile room temperature synthesis of fluorine-18 labeled fluoronicotinic acid-2,3,5,6-tetrafluorophenyl ester without azeotropic drying of fluorine-18. Nucl. Med. Biol 2016, 43, 770–772. [PubMed: 27693671]

(212). Basuli F; Zhang X; Woodroofe CC; Jagoda EM; Choyke PL; Swenson RE Fast indirect fluorine-18 labeling of protein/peptide using the useful 6-fluoronicotinic acid-2,3,5,6-tetrafluorophenyl prosthetic group: A method comparable to direct fluorination. J. Labelled Compd. Radiopharm 2017, 60, 168–175.

(213). Zhou Z; McDougald D; Devoogdt N; Zalutsky MR; Vaidyanathan G Labeling single domain antibody fragments with fluorine-18 using 2,3,5,6-tetrafluorophenyl 6-[18F]fluoronicotinate resulting in high tumor-to-kidney ratios. Mol. Pharmaceutics 2019, 16, 214–226.

(214). Schirrmacher E; Wangler B; Cypryk M; Bradtmoller G; Schafer M; Eisenhut M; Jurkschat K; Schirrmacher R Synthesis of p-(di-tert-butyl[(18)F]fluorosilyl)benzaldehyde ([(18)F]SiFA-A) with high specific activity by isotopic exchange: a convenient labeling synthon for the (18)F-labeling of N-amino-oxy derivatized peptides. Bioconjugate Chem 2007, 18, 2085–2089.

(215). Iovkova L; Könning D; Wängler B; Schirrmacher R; Schoof S; Arndt H-D; Jurkschat K SiFA-modified phenylalanine: a key compound for the efficient synthesis of 18F-labelled peptides. Eur.J. Inorg. Chem 2011, 2011, 2238–2246.

(216). Wangler B; Kostikov AP; Niedermoser S; Chin J; Orchowski K; Schirrmacher E; Iovkova-Berends L; Jurkschat K; Wangler C; Schirrmacher R Protein labeling with the labeling precursor [(18)F]SiFA-SH for positron emission tomography. Nat. Protoc 2012, 7, 1964–1969. [PubMed: 23037311]

(217). Wangler C; Niedermoser S; Chin J; Orchowski K; Schirrmacher E; Jurkschat K; Iovkova-Berends L; Kostikov AP; Schirrmacher R; Wangler B One-step (18)F-labeling of peptides for positron emission tomography imaging using the SiFA methodology. Nat. Protoc 2012, 7, 1946–1955. [PubMed: 23037309]

(218). Liu Z; Lin KS; Benard F; Pourghiasian M; Kiesewetter DO; Perrin DM; Chen X One-step (18)F labeling of biomolecules using organotrifluoroborates. Nat. Protoc 2015, 10, 1423–1432. [PubMed: 26313478]

(219). McBride WJ; Sharkey RM; Karacay H; D'Souza CA; Rossi EA; Laverman P; Chang CH; Boerman OC; Goldenberg DM A novel method of 18F radiolabeling for PET. J. Nucl. Med 2009, 50, 991–998. [PubMed: 19443594]

(220). Kumar K; Ghosh A (18)F-AlF Labeled Peptide and Protein conjugates as positron emission tomography imaging pharmaceuticals. Bioconjugate Chem 2018, 29, 953–975.

(221). McBride WJ; D'Souza CA; Sharkey RM; Goldenberg DM The radiolabeling of proteins by the [18F]AlF method. Appl. Radiat. Isot 2012, 70, 200–204. [PubMed: 21890371]

(222). Cleeren F; Lecina J; Billaud EM; Ahamed M; Verbruggen A; Bormans GM New chelators for low temperature Al(18)F-labeling of biomolecules. Bioconjugate Chem 2016, 27, 790–798.

(223). Cleeren F; Lecina J; Ahamed M; Raes G; Devoogdt N; Caveliers V; McQuade P; Rubins DJ; Li W; Verbruggen A; et al. 18)F-labeling of heat-sensitive biomolecules for positron emission tomography imaging. Theranostics 2017, 7, 2924–2939. [PubMed: 28824726]

(224). Cleeren F; Lecina J; Bridoux J; Devoogdt N; Tshibangu T; Xavier C; Bormans G Direct fluorine-18 labeling of heat-sensitive biomolecules for positron emission tomography imaging using the Al(18)F-RESCA method. Nat. Protoc 2018, 13, 2330–2347. [PubMed: 30250289]

(225). Zhernosekov KP; Filosofov DV; Baum RP; Aschoff P; Bihl H; Razbash AA; Jahn M; Jennewein M; Rosch F Processing of generator-produced 68Ga for medical application. J. Nucl. Med 2007, 48, 1741–1748. [PubMed: 17873136]

(226). Pandey MK; Byrne JF; Jiang H; Packard AB; DeGrado TR Cyclotron production of (68)Ga via the (68)Zn(p,n)(68)Ga reaction in aqueous solution. Am. J. Nucl. Med. Mol. Imaging 2014, 4, 303–310. [PubMed: 24982816]

(227). Alves F; Alves VH; Neves ACB; do Carmo SJC; Nactergal B; Hellas V; Kral E; Gonçalves-Gameiro C; Abrunhosa AJ Cyclotron production of Ga-68 for human use from liquid targets: From theory to practice. AIP Conf. Proc 2011, 1845, 020001.

(228). Tieu W; Hollis CA; Kuan KKW; Takhar P; Stuckings M; Spooner N; Malinconico M Rapid and automated production of [(68)Ga]gallium chloride and [(68)Ga]Ga-DOTA-TATE on a medical cyclotron. Nucl. Med. Biol 2019, 74–75, 12–18.

(229). Fani M; Andre JP; Maecke HR 68Ga-PET: a powerful generator-based alternative to cyclotron-based PET radiopharmaceuticals. Contrast Media Mol. Imaging 2008, 3, 67–77. [PubMed: 18383558]

(230). Eder M; Wangler B; Knackmuss S; LeGall F; Little M; Haberkorn U; Mier W; Eisenhut M Tetrafluorophenolate of HBED-CC: a versatile conjugation agent for 68Ga-labeled small recombinant antibodies. Eur. J. Nucl. Med. Mol. Imaging 2008, 35, 1878–1886. [PubMed: 18509635]

(231). Fay R; Gut M; Holland JP Photoradiosynthesis of(68)Ga-labeled HBED-CC-Azepin-MetMAb for immuno-PET of c-MET receptors. Bioconjugate Chem 2019, 30, 1814–1820.

(232). Boros E; Ferreira CL; Cawthray JF; Price EW; Patrick BO; Wester DW; Adam MJ; Orvig C Acyclic chelate with ideal properties for (68)Ga PET imaging agent elaboration. J. Am. Chem. Soc 2010, 132, 15726–15733. [PubMed: 20958034]

(233). Boros E; Ferreira CL; Yapp DT; Gill RK; Price EW; Adam MJ; Orvig C RGD conjugates of the H2dedpa scaffold: synthesis, labeling and imaging with 68Ga. Nucl. Med. Biol 2012, 39, 785–794. [PubMed: 22381779]

(234). Boros E; Cawthray JF; Ferreira CL; Patrick BO; Adam MJ; Orvig C Evaluation of the H2)dedpa scaffold and its cRGDyK conjugates for labeling with 64Cu. Inorg. Chem 2012, 51, 6279–6284. [PubMed: 22583103]

(235). Berry DJ; Ma Y; Ballinger JR; Tavare R; Koers A; Sunassee K; Zhou T; Nawaz S; Mullen GE; Hider RC; et al. Efficient bifunctional gallium-68 chelators for positron emission tomography: tris(hydroxypyridinone) ligands. Chem. Commun. (Cambridge, U. K.) 2011, 47, 7068–7070.

(236). Ferreira CL; Yapp DT; Crisp S; Sutherland BW; Ng SS; Gleave M; Bensimon C; Jurek P; Kiefer GE Comparison of bifunctional chelates for (64)Cu antibody imaging. Eur. J. Nucl. Med. Mol. Imaging 2010, 37, 2117–2126. [PubMed: 20552190]

(237). Song IH; Lee TS; Park YS; Lee JS; Lee BC; Moon BS; An GI; Lee HW; Kim KI; Lee YJ; et al. Immuno-PET imaging and radioimmunotherapy of 64Cu-/177Lu-labeled anti-EGFR antibody in esophageal squamous cell carcinoma model. J. Nucl. Med 2016, 57, 1105–1111. [PubMed: 26917708]

(238). Ferreira CL; Lamsa E; Woods M; Duan Y; Fernando P; Bensimon C; Kordos M; Guenther K; Jurek P; Kiefer GE Evaluation of bifunctional chelates for the development of gallium-based radiopharmaceuticals. Bioconjugate Chem 2010, 21, 531–536.

(239). Notni J; Pohle K; Wester HJ Comparative gallium-68 labeling of TRAP-, NOTA-, and DOTA-peptides: practical consequences for the future of gallium-68-PET. EJNMMI Res 2012, 2,28. [PubMed: 22682112]

(240). Hernandez R; Valdovinos HF; Yang Y; Chakravarty R; Hong H; Barnhart TE; Cai W (44)Sc: an attractive isotope for peptide-based PET imaging. Mol. Pharmaceutics 2014, 11, 2954–2961.

(241). Singh A; van der Meulen NP; Muller C; Klette I; Kulkarni HR; Turler A; Schibli R; Baum RP First-in-human PET/CT imaging of metastatic neuroendocrine neoplasms with cyclotron-produced (44)Sc-DOTATOC: a proof-of-concept study. Cancer Biother.Radiopharm 2017, 32, 124–132. [PubMed: 28514206]

(242). Chaple IF; Lapi SE Production and use of the first-row transition metal PET radionuclides (43,44)Sc, (52)Mn, and (45)Ti. J. Nucl. Med 2018, 59, 1655–1659. [PubMed: 30262514]

(243). Chakravarty R; Goel S; Valdovinos HF; Hernandez R; Hong H; Nickles RJ; Cai W Matching the decay half-life with the biological half-life: ImmunoPET imaging with (44)Sc-labeled cetuximab Fab fragment. Bioconjugate Chem 2014, 25, 2197–2204.

(244). Nagy G; Szikra D; Trencsenyi G; Fekete A; Garai I; Giani AM; Negri R; Masciocchi N; Maiocchi A; Uggeri F; et al. AAZTA: an ideal chelating agent for the development of (44) Sc PET imaging agents. Angew. Chem., Int. Ed 2017, 56, 2118–2122.

(245). Li L; Jaraquemada-Peláez M. d. G.; Aluicio-Sarduy E; Wang X; Jiang D; Sakheie M; Kuo H-T; Barnhart TE; Cai W; Radchenko V; et al. [nat/44Sc(pypa)]–: thermodynamic stability,

radiolabeling, and biodistribution of a prostate-specific-membrane-antigen-targeting conjugate. Inorg. Chem 2020, 59, 1985–1995.

(246). Fonslet J; Tietze S; Jensen AI; Graves SA; Severin GW Optimized procedures for manganese-52: Production, separation and radiolabeling. Appl. Radiat. Isot 2017, 121, 38–43. [PubMed: 28024217]

(247). Brandt M; Cardinale J; Rausch I; Mindt TL Manganese in PET imaging: opportunities and challenges. J. Labelled Compd. Radiopharm 2019, 62, 541–551.

(248). Graves SA; Hernandez R; Fonslet J; England CG; Valdovinos HF; Ellison PA; Barnhart TE; Elema DR; Theuer CP; Cai W; et al. Novel preparation methods of (52)Mn for immunoPET imaging. Bioconjugate Chem 2015, 26, 2118–2124.

(249). Cicone F; Gnesin S; Denoel T; Stora T; van der Meulen NP; Muller C; Vermeulen C; Benesova M; Koster U; Johnston K; et al. Internal radiation dosimetry of a (152)Tb-labeled antibody in tumor-bearing mice. EJNMMI Res 2019, 9, 53. [PubMed: 31187358]

(250). Hoglund J; Tolmachev V; Orlova A; Lundqvist H; Sundin A Optimized indirect (76)Br-bromination of antibodies using N-succinimidyl para-[76Br]bromobenzoate for radioimmuno PET. Nucl. Med. Biol 2000, 27, 837–843. [PubMed: 11150718]

(251). Rossin R; Berndorff D; Friebe M; Dinkelborg LM; Welch MJ Small-animal PET of tumor angiogenesis using a (76)Br-labeled human recombinant antibody fragment to the ED-B domain of fibronectin. J. Nucl. Med 2007, 48, 1172–1179. [PubMed: 17574989]

(252). Aluicio-Sarduy E; Hernandez R; Olson AP; Barnhart TE; Cai W; Ellison PA; Engle JW Production and in vivo PET/ CT imaging of the theranostic pair (132/135)La. Sci. Rep 2019, 9, 10658. [PubMed: 31337833]

(253). Aluicio-Sarduy E; Thiele NA; Martin KE; Vaughn BA; Devaraj J; Olson AP; Barnhart TE; Wilson JJ; Boros E; Engle JW Establishing radiolanthanum chemistry for targeted nuclear medicine applications. Chem. - Eur. J 2020, 26, 1238–1242.

(254). Fay R; Holland JP The impact of emerging bioconjugation chemistries on radiopharmaceuticals. J. Nucl. Med 2019, 60, 587–591. [PubMed: 30902878]

(255). Tinianow JN; Gill HS; Ogasawara A; Flores JE; Vanderbilt AN; Luis E; Vandlen R; Darwish M; Junutula JR; Williams SP; et al. Site-specifically 89Zr-labeled monoclonal antibodies for ImmunoPET. Nucl. Med. Biol 2010, 37, 289–297. [PubMed: 20346868]

(256). Tavare R; Wu WH; Zettlitz KA; Salazar FB; McCabe KE; Marks JD; Wu AM Enhanced immunoPET of ALCAM-positive colorectal carcinoma using site-specific (6)(4)Cu-DOTA conjugation. Protein Eng., Des. Sel 2014, 27, 317–324. [PubMed: 25095796]

(257). Ravasco J; Faustino H; Trindade A; Gois PMP Bioconjugation with maleimides: a useful tool for chemical biology. Chem. - Eur. J 2019, 25, 43–59. [PubMed: 30095185]

(258). Bernardim B; Matos MJ; Ferhati X; Companon I; Guerreiro A; Akkapeddi P; Burtoloso ACB; Jimenez-Oses G; Corzana F; Bernardes GJL Efficient and irreversible antibody-cysteine bioconjugation using carbonylacrylic reagents. Nat. Protoc 2019, 14, 86–99. [PubMed: 30470819]

(259). Boutureira O; Bernardes GJ Advances in chemical protein modification. Chem. Rev 2015, 115, 2174–2195. [PubMed: 25700113]

(260). Zeng D; Zeglis BM; Lewis JS; Anderson CJ The growing impact of bioorthogonal click chemistry on the development of radiopharmaceuticals. J. Nucl. Med 2013, 54, 829–832. [PubMed: 23616581]

(261). Meyer JP; Adumeau P; Lewis JS; Zeglis BM Click chemistry and radiochemistry: the first 10 years. Bioconjugate Chem 2016, 27, 2791–2807.

(262). Nguyen QD; Smith G; Glaser M; Perumal M; Arstad E; Aboagye EO Positron emission tomography imaging of drug-induced tumor apoptosis with a caspase-3/7 specific [18F]-labeled isatin sulfonamide. Proc. Natl. Acad. Sci. U. S. A 2009, 106, 16375–16380. [PubMed: 19805307]

(263). Dubash SR; Merchant S; Heinzmann K; Mauri F; Lavdas I; Inglese M; Kozlowski K; Rama N; Masrour N; Steel JF; et al. Clinical translation of [(18)F]ICMT-11 for measuring chemotherapy-induced caspase 3/7 activation in breast and lung cancer. Eur. J. Nucl. Med. Mol. Imaging 2018, 45, 2285–2299. [PubMed: 30259091]

(264). de Almeida G; Sletten EM; Nakamura H; Palaniappan KK; Bertozzi CR Thiacycloalkynes for copper-free click chemistry. Angew. Chem., Int. Ed 2012, 51, 2443–2447.

(265). Chen K; Wang X; Lin W-Y; Shen CK-F; Yap L-P; Hughes LD; Conti PS Strain-promoted catalyst-free click chemistry for rapid construction of 64Cu-labeled PET imaging probes. ACS Med. Chem. Lett 2012, 3, 1019–1023. [PubMed: 24900423]

(266). Blackman ML; Royzen M; Fox JM Tetrazine ligation: fast bioconjugation based on inverse-electron-demand Diels-Alder reactivity. J. Am. Chem. Soc 2008, 130, 13518–13519. [PubMed: 18798613]

(267). Zeglis BM; Mohindra P; Weissmann GI; Divilov V; Hilderbrand SA; Weissleder R; Lewis JS Modular strategy for the construction of radiometalated antibodies for positron emission tomography based on inverse electron demand Diels-Alder click chemistry. Bioconjugate Chem 2011, 22, 2048–2059.

(268). Kumar A; Hao G; Liu L; Ramezani S; Hsieh JT; Oz OK; Sun X Click-chemistry strategy for labeling antibodies with copper-64 via a cross-bridged tetraazamacrocyclic chelator scaffold. Bioconjugate Chem 2015, 26, 782–789.

(269). Shi X; Gao K; Huang H; Gao R Pretargeted immuno-PET based on bioorthogonal chemistry for imaging EGFR positive colorectal cancer. Bioconjugate Chem 2018, 29, 250–254.

(270). Rossin R; van den Bosch SM; Ten Hoeve W; Carvelli M; Versteegen RM; Lub J; Robillard MS Highly reactive transcyclooctene tags with improved stability for Diels-Alder chemistry in living systems. Bioconjugate Chem 2013, 24, 1210–1217.

(271). Lim RK; Lin Q Photoinducible bioorthogonal chemistry: a spatiotemporally controllable tool to visualize and perturb proteins in live cells. Acc. Chem. Res 2011, 44, 828–839. [PubMed: 21609129]

(272). Herner A; Lin Q Photo-triggered click chemistry for biological applications. Top Curr. Chem. (Cham) 2016, 374, 1. [PubMed: 27397964]

(273). Sun L; Ding J; Xing W; Gai Y; Sheng J; Zeng D Novel strategy for preparing dual-modality optical/PET imaging probes via photo-click chemistry. Bioconjugate Chem 2016, 27, 1200–1204.

(274). Patra M; Eichenberger LS; Fischer G; Holland JP Photochemical conjugation and one-pot radiolabelling of antibodies for immuno-PET. Angew. Chem., Int. Ed 2019, 58, 1928–1933.

(275). Patra M; Klingler S; Eichenberger LS; Holland JP Simultaneous photoradiochemical labeling of antibodies for immuno-positron emission tomography. iScience 2019, 13, 416–431. [PubMed: 30903963]

(276). Mazmanian SK; Liu G; Ton-That H; Schneewind OJS Staphylococcus aureus sortase, an enzyme that anchors surface proteins to the cell wall. Science 1999, 285, 760–763. [PubMed: 10427003]

(277). Pishesha N; Ingram JR; Ploegh HL Sortase A: a model for transpeptidation and its biological applications. Annu. Rev. Cell Dev. Biol 2018, 34, 163–188. [PubMed: 30110557]

(278). Rashidian M; Keliher EJ; Bilate AM; Duarte JN; Wojtkiewicz GR; Jacobsen JT; Cragnolini J; Swee LK; Victora GD; Weissleder R; et al. Noninvasive imaging of immune responses. Proc. Natl. Acad. Sci. U. S. A 2015, 112, 6146–6151. [PubMed: 25902531]

(279). Paterson BM; Alt K; Jeffery CM; Price RI; Jagdale S; Rigby S; Williams CC; Peter K; Hagemeyer CE; Donnelly PS Enzyme-mediated site-specific bioconjugation of metal complexes to proteins: sortase-mediated coupling of copper-64 to a single-chain antibody. Angew. Chem., Int. Ed 2014, 53, 6115–6119.

(280). Alt K; Paterson BM; Westein E; Rudd SE; Poniger SS; Jagdale S; Ardipradja K; Connell TU; Krippner GY; Nair AK; et al. A versatile approach for the site-specific modification of recombinant antibodies using a combination of enzyme-mediated bioconjugation and click chemistry. Angew. Chem., Int. Ed 2015, 54, 7515–7519.

(281). Chen I; Dorr BM; Liu DR A general strategy for the evolution of bond-forming enzymes using yeast display. Proc. Natl. Acad. Sci. U. S. A 2011, 108, 11399–11404. [PubMed: 21697512]

(282). Chen L; Cohen J; Song X; Zhao A; Ye Z; Feulner CJ; Doonan P; Somers W; Lin L; Chen PR Improved variants of SrtA for site-specific conjugation on antibodies and proteins with high efficiency. Sci. Rep 2016, 6, 31899. [PubMed: 27534437]

(283). Jeong HJ; Abhiraman GC; Story CM; Ingram JR; Dougan SK Generation of Ca2+-independent sortase A mutants with enhanced activity for protein and cell surface labeling. PLoS One 2017, 12, e0189068. [PubMed: 29200433]

(284). Nguyen GK; Wang S; Qiu Y; Hemu X; Lian Y; Tam JP Butelase 1 is an asx-specific ligase enabling peptide macro-cyclization and synthesis. Nat. Chem. Biol 2014, 10, 732–738. [PubMed: 25038786]

(285). Nguyen GK; Qiu Y; Cao Y; Hemu X; Liu CF; Tam JP Butelase-mediated cyclization and ligation of peptides and proteins. Nat. Protoc 2016, 11, 1977–1988. [PubMed: 27658013]

(286). Harmand TJ; Bousbaine D; Chan A; Zhang X; Liu DR; Tam JP; Ploegh HL One-pot dual labeling of IgG 1 and preparation of C-to-C fusion proteins through a combination of Sortase A and Butelase 1. Bioconjugate Chem 2018, 29, 3245–3249.

(287). Zeglis BM; Davis CB; Aggeler R; Kang HC; Chen A; Agnew BJ; Lewis JS Enzyme-mediated methodology for the site-specific radiolabeling of antibodies based on catalyst-free click chemistry. Bioconjugate Chem 2013, 24, 1057–1067.

(288). Zeglis BM; Davis CB; Abdel-Atti D; Carlin SD; Chen A; Aggeler R; Agnew BJ; Lewis JS Chemoenzymatic strategy for the synthesis of site-specifically labeled immunoconjugates for multimodal PET and optical imaging. Bioconjugate Chem 2014, 25, 2123–2128.

(289). Kristensen LK; Christensen C; Jensen MM; Agnew BJ; Schjoth-Frydendahl C; Kjaer A; Nielsen CH Site-specifically labeled (89)Zr-DFO-trastuzumab improves immuno-reactivity and tumor uptake for immuno-PET in a subcutaneous HER2-positive xenograft mouse model. Theranostics 2019, 9, 4409–4420. [PubMed: 31285769]

(290). Los GV; Encell LP; McDougall MG; Hartzell DD; Karassina N; Zimprich C; Wood MG; Learish R; Ohana RF; Urh M; et al. HaloTag: a novel protein labeling technology for cell imaging and protein analysis. ACS Chem. Biol 2008, 3, 373–382. [PubMed: 18533659]

(291). England CG; Luo H; Cai W HaloTag technology: a versatile platform for biomedical applications. Bioconjugate Chem 2015, 26, 975–986.

(292). Urh M; Rosenberg M HaloTag, a platform technology for protein analysis. Curr. Chem. Genomics 2013, 6, 72–78.

(293). Encell LP; Ohana RF; Zimmerman K; Otto P; Vidugiris G; Wood MG; Los GV; McDougall MG; Zimprich C; Karassina N Suppl 1: Development of a dehalogenase-based protein fusion tag capable of papid, selective and covalent attachment to customizable ligands. Curr. Chem. Genomics 2013, 6, 55.

(294). Young CL; Britton ZT; Robinson AS Recombinant protein expression and purification: a comprehensive review of affinity tags and microbial applications. Biotechnol. J 2012, 7, 620–634. [PubMed: 22442034]

(295). Wood DW New trends and affinity tag designs for recombinant protein purification. Curr. Opin. Struct. Biol 2014, 26, 54–61. [PubMed: 24859434]

(296). Knight JC; Mosley M; Uyeda HT; Cong M; Fan F; Faulkner S; Cornelissen B In vivo pretargeted imaging of HER2 and TAG-72 expression using the HaloTag enzyme. Mol. Pharmaceutics 2017, 14, 2307–2313.

(297). Jeger S; Zimmermann K; Blanc A; Grunberg J; Honer M; Hunziker P; Struthers H; Schibli R Site-specific and stoichiometric modification of antibodies by bacterial transglutaminase. Angew. Chem., Int. Ed 2010, 49, 9995–9997.

(298). Spycher PR; Amann CA; Wehrmuller JE; Hurwitz DR; Kreis O; Messmer D; Ritler A; Kuchler A; Blanc A; Behe M; et al. Dual, site-specific modification of antibodies by using solid-phase immobilized microbial transglutaminase. ChemBioChem 2017, 18, 1923–1927. [PubMed: 28771896]

(299). Drake CR; Sevillano N; Truillet C; Craik CS; VanBrocklin HF; Evans MJ Site-specific radiofluorination of biomolecules with 8-[(18)F]-fluorooctanoic acid catalyzed by lipoic acid ligase. ACS Chem. Biol 2016, 11, 1587–1594. [PubMed: 27008570]

(300). Goldenberg DM; Sharkey RM; Paganelli G; Barbet J; Chatal JF Antibody pretargeting advances cancer radioimmunodetection and radioimmunotherapy. J. Clin. Oncol 2006, 24, 823–834. [PubMed: 16380412]

(301). Summer D; Mayr S; Petrik M; Rangger C; Schoeler K; Vieider L; Matuszczak B; Decristoforo C Pretargeted imaging with Gallium-68-improving the binding capability by increasing the number of tetrazine motifs. Pharmaceuticals 2018, 11, 102.

(302). Goldenberg DM; Chang CH; Rossi EA; McBride WJ; Sharkey RM Pretargeted molecular imaging and radio-immunotherapy. Theranostics 2012, 2, 523–540. [PubMed: 22737190]

(303). Altai M; Membreno R; Cook B; Tolmachev V; Zeglis BM Pretargeted imaging and therapy. J. Nucl. Med 2017, 58, 1553–1559. [PubMed: 28687600]

(304). Hnatowich DJ; Virzi F; Rusckowski M Investigations of avidin and biotin for imaging applications. J. Nucl. Med 1987, 28, 1294–1302. [PubMed: 3612292]

(305). Sakahara H; Saga T Avidin-biotin system for delivery of diagnostic agents. Adv. Drug Delivery Rev 1999, 37, 89–101.

(306). Kalofonos HP; Rusckowski M; Siebecker DA; Sivolapenko GB; Snook D; Lavender JP; Epenetos AA; Hnatowich DJ Imaging of tumor in patients with indium-111-labeled biotin and streptavidin-conjugated antibodies: preliminary communication. J. Nucl. Med 1990, 31, 1791–1796. [PubMed: 2230992]

(307). Weiden PL; Breitz HB Pretargeted radioimmunotherapy (PRIT) for treatment of non-Hodgkin's lymphoma (NHL). Crit. Rev. Oncol. Hematol 2001, 40, 37–51. [PubMed: 11578915]

(308). Forero A; Weiden PL; Vose JM; Knox SJ; LoBuglio AF; Hankins J; Goris ML; Picozzi VJ; Axworthy DB; Breitz HB; et al. Phase 1 trial of a novel anti-CD20 fusion protein in pretargeted radioimmunotherapy for B-cell non-Hodgkin lymphoma. Blood 2004, 104, 227–236. [PubMed: 14996706]

(309). Paganelli G; Chinol M Radioimmunotherapy: is avidinbiotin pretargeting the preferred choice among pretargeting methods? Eur. J. Nucl. Med. Mol. Imaging 2003, 30, 773–776. [PubMed: 12557049]

(310). Chang CH; Sharkey RM; Rossi EA; Karacay H; McBride W; Hansen HJ; Chatal JF; Barbet J; Goldenberg DM Molecular advances in pretargeting radioimunotherapy with bispecific antibodies. Mol. Cancer Ther 2002, 1, 553–563. [PubMed: 12479274]

(311). McBride WJ; Zanzonico P; Sharkey RM; Noren C; Karacay H; Rossi EA; Losman MJ; Brard PY; Chang CH; Larson SM; et al. Bispecific antibody pretargeting PET (immunoPET) with an 124I-labeled hapten-peptide. J. Nucl. Med 2006, 47, 1678–1688. [PubMed: 17015905]

(312). Sharkey RM; Karacay H; McBride WJ; Rossi EA; Chang C-H; Goldenberg DM Bispecific antibody pretargeting of radionuclides for immuno–single-photon emission computed tomography and immuno–positron emission tomography molecular imaging: An update. Clin. Cancer Res 2007, 13, 5577s–5585s. [PubMed: 17875792]

(313). Sharkey RM; Karacay H; Vallabhajosula S; McBride WJ; Rossi EA; Chang CH; Goldsmith SJ; Goldenberg DM Metastatic human colonic carcinoma: molecular imaging with pretargeted SPECT and PET in a mouse model. Radiology 2008, 246, 497–507. [PubMed: 18227543]

(314). Karacay H; Sharkey RM; McBride WJ; Rossi EA; Chang CH; Goldenberg DM Optimization of hapten-peptide labeling for pretargeted immunoPET of bispecific antibody using generator-produced 68Ga. J. Nucl. Med 2011, 52, 555–559. [PubMed: 21421724]

(315). Karacay H; Sharkey RM; McBride WJ; Griffiths GL; Qu Z; Chang K; Hansen HJ; Goldenberg DM Pretargeting for cancer radioimmunotherapy with bispecific antibodies: role of the bispecific antibody's valency for the tumor target antigen. Bioconjugate Chem 2002, 13, 1054–1070.

(316). Sharkey RM; McBride WJ; Karacay H; Chang K; Griffiths GL; Hansen HJ; Goldenberg DM A universal pretargeting system for cancer detection and therapy using bispecific antibody. Cancer Res 2003, 63, 354–363. [PubMed: 12543788]

(317). Rossi EA; Sharkey RM; McBride W; Karacay H; Zeng L; Hansen HJ; Goldenberg DM; Chang CH Development of new multivalent-bispecific agents for pretargeting tumor localization and therapy. Clin. Cancer. Res 2003, 9, 3886S–3896S. [PubMed: 14506187]

(318). Rossi EA; Chang CH; Losman MJ; Sharkey RM; Karacay H; McBride W; Cardillo TM; Hansen HJ; Qu Z; Horak ID; et al. Pretargeting of carcinoembryonic antigen-expressing cancers with a trivalent bispecific fusion protein produced in myeloma cells. Clin. Cancer Res 2005, 11, 7122s–7129s. [PubMed: 16203811]

(319). Chatal JF; Campion L; Kraeber-Bodere F; Bardet S; Vuillez JP; Charbonnel B; Rohmer V; Chang CH; Sharkey RM; Goldenberg DM; et al. Survival improvement in patients with medullary thyroid carcinoma who undergo pretargeted anti-carcinoembryonic-antigen radioimmunotherapy: a collaborative study with the French Endocrine Tumor Group. J. Clin. Oncol 2006, 24, 1705–1711. [PubMed: 16549819]

(320). Salaun PY; Campion L; Bournaud C; Faivre-Chauvet A; Vuillez JP; Taieb D; Ansquer C; Rousseau C; Borson-Chazot F; Bardet S; et al. Phase II trial of anticarcinoembryonic antigen pretargeted radioimmunotherapy in progressive metastatic medullary thyroid carcinoma: biomarker response and survival improvement. J. Nucl. Med 2012, 53, 1185–1192. [PubMed: 22743249]

(321). Rossi EA; Goldenberg DM; Cardillo TM; McBride WJ; Sharkey RM; Chang CH Stably tethered multifunctional structures of defined composition made by the dock and lock method for use in cancer targeting. Proc. Natl. Acad. Sci. U. S. A 2006, 103, 6841–6846. [PubMed: 16636283]

(322). Goldenberg DM; Rossi EA; Sharkey RM; McBride WJ; Chang CH Multifunctional antibodies by the Dock-and-Lock method for improved cancer imaging and therapy by pretargeting. J. Nucl. Med 2007, 49, 158–163. [PubMed: 18077530]

(323). Karacay H; Sharkey RM; Gold DV; Ragland DR; McBride WJ; Rossi EA; Chang CH; Goldenberg DM Pretargeted radioimmunotherapy of pancreatic cancer xenografts: TF10–90Y-IMP-288 alone and combined with gemcitabine. J. Nucl. Med 2009, 50, 2008–2016. [PubMed: 19949026]

(324). Sharkey RM; Rossi EA; McBride WJ; Chang CH; Goldenberg DM Recombinant bispecific monoclonal antibodies prepared by the dock-and-lock strategy for pretargeted radio-immunotherapy. Semin. Nucl. Med 2010, 40, 190–203. [PubMed: 20350628]

(325). Boder ET; Wittrup KD Yeast surface display for directed evolution of protein expression, affinity, and stability. Methods Enzymol 2000, 328, 430–444. [PubMed: 11075358]

(326). Orcutt KD; Ackerman ME; Cieslewicz M; Quiroz E; Slusarczyk AL; Frangioni JV; Wittrup KD A modular IgG-scFv bispecific antibody topology. Protein Eng., Des. Sel 2010, 23, 221–228. [PubMed: 20019028]

(327). Orcutt KD; Slusarczyk AL; Cieslewicz M; Ruiz-Yi B; Bhushan KR; Frangioni JV; Wittrup KD Engineering an antibody with picomolar affinity to DOTA chelates of multiple radionuclides for pretargeted radioimmunotherapy and imaging. Nucl. Med. Biol 2011, 38, 223–233. [PubMed: 21315278]

(328). Orcutt KD; Rhoden JJ; Ruiz-Yi B; Frangioni JV; Wittrup KD Effect of small-molecule-binding affinity on tumor uptake in vivo: a systematic study using a pretargeted bispecific antibody. Mol. Cancer Ther 2012, 11, 1365–1372. [PubMed: 22491799]

(329). Cheal SM; Xu H; Guo HF; Lee SG; Punzalan B; Chalasani S; Fung EK; Jungbluth A; Zanzonico PB; Carrasquillo JA; et al. Theranostic pretargeted radioimmunotherapy of colorectal cancer xenografts in mice using picomolar affinity (8)(6)Y-or (1)(7)(7)Lu-DOTA-Bn binding scFv C825/GPA33 IgG bispecific immunoconjugates. Eur. J. Nucl. Med. Mol. Imaging 2016, 43, 925–937. [PubMed: 26596724]

(330). Knight JC; Cornelissen B Bioorthogonal chemistry: implications for pretargeted nuclear (PET/SPECT) imaging and therapy. Am. J. Nucl. Med. Mol. Imaging 2014, 4, 96–113. [PubMed: 24753979]

(331). Rossin R; Robillard MS Pretargeted imaging using bioorthogonal chemistry in mice. Curr. Opin. Chem. Biol 2014, 21, 161–169. [PubMed: 25159021]

(332). Bailly C; Bodet-Milin C; Rousseau C; Faivre-Chauvet A; Kraeber-Bodere F; Barbet J Pretargeting for imaging and therapy in oncological nuclear medicine. EJNMMI Radiopharm Chem 2017, 2, 6. [PubMed: 29503847]

(333). Rossin R; Renart Verkerk P; van den Bosch SM; Vulders RC; Verel I; Lub J; Robillard MS In vivo chemistry for pretargeted tumor imaging in live mice. Angew. Chem., Int. Ed 2010, 49, 3375–3378.

(334). Devaraj NK; Thurber GM; Keliher EJ; Marinelli B; Weissleder R Reactive polymer enables efficient in vivo bioorthogonal chemistry. Proc. Natl. Acad. Sci. U. S. A 2012, 109, 4762–4767. [PubMed: 22411831]

(335). Zeglis BM; Sevak KK; Reiner T; Mohindra P; Carlin SD; Zanzonico P; Weissleder R; Lewis JS A pretargeted PET imaging strategy based on bioorthogonal Diels-Alder click chemistry. J. Nucl. Med 2013, 54, 1389–1396. [PubMed: 23708196]

(336). Rossin R; Lappchen T; van den Bosch SM; Laforest R; Robillard MS Diels-Alder reaction for tumor pretargeting: in vivo chemistry can boost tumor radiation dose compared with directly labeled antibody. J. Nucl. Med 2013, 54, 1989–1995. [PubMed: 24092936]

(337). Rossin R; van Duijnhoven SM; Lappchen T; van den Bosch SM; Robillard MS Trans-cyclooctene tag with improved properties for tumor pretargeting with the diels-alder reaction. Mol. Pharmaceutics 2014, 11, 3090–3096.

(338). Cook BE; Adumeau P; Membreno R; Carnazza KE; Brand C; Reiner T; Agnew BJ; Lewis JS; Zeglis BM Pretargeted PET imaging using a site-specifically labeled immuno-conjugate. Bioconjugate Chem 2016, 27, 1789–1795.

(339). Zeglis BM; Brand C; Abdel-Atti D; Carnazza KE; Cook BE; Carlin S; Reiner T; Lewis JS Optimization of a pretargeted strategy for the PET imaging of colorectal carcinoma via the modulation of radioligand pharmacokinetics. Mol. Pharmaceutics 2015, 12, 3575–3587.

(340). Seibold U; Wangler B; Wangler C Rational design, development, and stability assessment of a macrocyclic four-hydroxamate-bearing bifunctional chelating agent for (89) Zr. ChemMedChem 2017, 12, 1555–1571. [PubMed: 28715615]

(341). Litau S; Seibold U; Wangler B; Schirrmacher R; Wangler C iEDDA Conjugation reaction in radiometal labeling of peptides with (68)Ga and (64)Cu: unexpected findings. ACS Omega 2018, 3, 14039–14053. [PubMed: 30411057]

(342). Vugts DJ; Vervoort A; Stigter-van Walsum M; Visser GW; Robillard MS; Versteegen RM; Vulders RC; Herscheid JK; van Dongen GA Synthesis of phosphine and antibody-azide probes for in vivo Staudinger ligation in a pretargeted imaging and therapy approach. Bioconjugate Chem 2011, 22, 2072–2081.

(343). van den Bosch SM; Rossin R; Renart Verkerk P; Ten Hoeve W; Janssen HM; Lub J; Robillard MS Evaluation of strained alkynes for Cu-free click reaction in live mice. Nucl. Med. Biol 2013, 40, 415–423. [PubMed: 23380519]

(344). Westerlund K; Honarvar H; Tolmachev V; Eriksson Karlstrom A Design, preparation, and characterization of PNA-based hybridization probes for affibody-molecule-mediated pretargeting. Bioconjugate Chem 2015, 26, 1724–1736.

(345). Honarvar H; Westerlund K; Altai M; Sandstrom M; Orlova A; Tolmachev V; Karlstrom AE Feasibility of affibody molecule-based PNA-mediated radionuclide pretargeting of malignant tumors. Theranostics 2016, 6, 93–103. [PubMed: 26722376]

(346). Altai M; Perols A; Tsourma M; Mitran B; Honarvar H; Robillard M; Rossin R; ten Hoeve W; Lubberink M; Orlova A; et al. Feasibility of affibody-based bioorthogonal chemistry-mediated radionuclide pretargeting. J. Nucl. Med 2016, 57, 431–436. [PubMed: 26659353]

(347). Westerlund K; Altai M; Mitran B; Konijnenberg M; Oroujeni M; Atterby C; de Jong M; Orlova A; Mattsson J; Micke P; et al. Radionuclide therapy of HER2-expressing human xenografts using affibody-based peptide nucleic acid-mediated pretargeting: in vivo proof of principle. J. Nucl. Med 2018, 59, 1092–1098. [PubMed: 29439013]

(348). Vorobyeva A; Westerlund K; Mitran B; Altai M; Rinne S; Sorensen J; Orlova A; Tolmachev V; Karlstrom AE Development of an optimal imaging strategy for selection of patients for affibody-based PNA-mediated radionuclide therapy. Sci. Rep 2018, 8, 9643. [PubMed: 29942011]

(349). Matsumura K; Zouda M; Wada Y; Yamashita F; Hashida M; Watanabe Y; Mukai H Urokinase injection-triggered clearance enhancement of a 4-arm PEG-conjugated (64)Cu-bombesin analog tetramer: a novel approach for the improvement of PET imaging contrast. Int. J. Pharm 2018, 545, 206–214. [PubMed: 29746998]

(350). Borjesson PK; Jauw YW; de Bree R; Roos JC; Castelijns JA; Leemans CR; van Dongen GA; Boellaard R Radiation dosimetry of 89Zr-labeled chimeric monoclonal antibody U36 as used for immuno-PET in head and neck cancer patients. J. Nucl. Med 2009, 50, 1828–1836. [PubMed: 19837762]

(351). Freise AC; Wu AM In vivo imaging with antibodies and engineered fragments. Mol. Immunol 2015, 67, 142–152. [PubMed: 25934435]

(352). Zhang RR; Schroeder AB; Grudzinski JJ; Rosenthal EL; Warram JM; Pinchuk AN; Eliceiri KW; Kuo JS; Weichert JP Beyond the margins: real-time detection of cancer using targeted fluorophores. Nat. Rev. Clin. Oncol 2017, 14, 347–364. [PubMed: 28094261]

(353). Du Z; Lovly CM Mechanisms of receptor tyrosine kinase activation in cancer. Mol. Cancer 2018, 17, 58. [PubMed: 29455648]

(354). Pool M; de Boer HR; Hooge MNL; van Vugt M; de Vries EGE Harnessing integrative omics to facilitate molecular imaging of the human epidermal growth factor receptor family for precision medicine. Theranostics 2017, 7, 2111–2133. [PubMed: 28638489]

(355). Lemmon MA; Schlessinger J; Ferguson KM The EGFR family: not so prototypical receptor tyrosine kinases. Cold Spring Harbor Perspect. Biol 2014, 6, a020768.

(356). Menke-van der Houven van Oordt CW; Gootjes EC; Huisman MC; Vugts DJ; Roth C; Luik M; Mulder ER; Schuit RC; Boellaard R; Hoekstra OS; et al. 89Zr-cetuximab PET imaging in patients with advanced colorectal cancer. Oncotarget 2015, 6, 30384–30393. [PubMed: 26309164]

(357). van Helden EJ; Elias SG; Gerritse SL; van Es SC; Boon E; Huisman MC; van Grieken NCT; Dekker H; van Dongen GAMS; Vugts DJ; et al. [89Zr]Zr-cetuximab PET/CT as biomarker for cetuximab monotherapy in patients with RAS wild-type advanced colorectal cancer. Eur. J. Nucl. Med. Mol. Imaging 2019, DOI: 10.1007/s00259-019-04555-6.

(358). van Loon J; Even AJG; Aerts H; Ollers M; Hoebers F; van Elmpt W; Dubois L; Dingemans AC; Lalisang RI; Kempers P; et al. PET imaging of zirconium-89 labelled cetuximab: a phase I trial in patients with head and neck and lung cancer. Radiother. Oncol 2017, 122, 267–273. [PubMed: 28012793]

(359). Aerts HJ; Dubois L; Perk L; Vermaelen P; van Dongen GA; Wouters BG; Lambin P Disparity between in vivo EGFR expression and 89Zr-labeled cetuximab uptake assessed with PET. J. Nucl. Med 2008, 50, 123–131. [PubMed: 19091906]

(360). Even AJ; Hamming-Vrieze O; van Elmpt W; Winnepenninckx VJ; Heukelom J; Tesselaar ME; Vogel WV; Hoeben A; Zegers CM; Vugts DJ; et al. Quantitative assessment of Zirconium-89 labeled cetuximab using PET/CT imaging in patients with advanced head and neck cancer: a theragnostic approach. Oncotarget 2017, 8, 3870–3880. [PubMed: 27965472]

(361). Pool M; Kol A; Lub-de Hooge MN; Gerdes CA; de Jong S; de Vries EG; Terwisscha van Scheltinga AGT Extracellular domain shedding influences specific tumor uptake and organ distribution of the EGFR PET tracer 89Zr-imgatuzumab. Oncotarget 2016, 7, 68111–68121. [PubMed: 27602494]

(362). Yang XD; Jia XC; Corvalan JR; Wang P; Davis CG Development of ABX-EGF, a fully human anti-EGF receptor monoclonal antibody, for cancer therapy. Crit. Rev. Oncol. Hematol 2001, 38, 17–23. [PubMed: 11255078]

(363). Niu G; Li Z; Xie J; Le QT; Chen X PET of EGFR antibody distribution in head and neck squamous cell carcinoma models. J. Nucl. Med 2009, 50, 1116–1123. [PubMed: 19525473]

(364). Chang AJ; De Silva RA; Lapi SE Development and characterization of 89Zr-labeled panitumumab for immuno-positron emission tomographic imaging of the epidermal growth factor receptor. Mol. Imaging 2013, 12, 17–27. [PubMed: 23348788]

(365). Bhattacharyya S; Kurdziel K; Wei L; Riffle L; Kaur G; Hill GC; Jacobs PM; Tatum JL; Doroshow JH; Kalen JD Zirconium-89 labeled panitumumab: a potential immuno-PET probe for HER1-expressing carcinomas. Nucl. Med. Biol 2013, 40, 451–457. [PubMed: 23454247]

(366). Nayak TK; Garmestani K; Milenic DE; Brechbiel MW PET and MRI of metastatic peritoneal and pulmonary colorectal cancer in mice with human epidermal growth factor receptor 1-targeted 89Zr-labeled panitumumab. J. Nucl. Med 2012, 53, 113–120. [PubMed: 22213822]

(367). Do K; Cao L; Kang Z; Turkbey B; Lindenberg ML; Larkins E; Holkova B; Steinberg SM; Raffeld M; Peer CJ; et al. A phase II study of sorafenib combined with cetuximab in EGFR-expressing, KRAS-mutated metastatic colorectal cancer. Clin. Colorectal Cancer 2015, 14, 154–161. [PubMed: 25861837]

(368). Lindenberg L; Adler S; Turkbey IB; Mertan F; Ton A; Do K; Kummar S; Gonzalez EM; Bhattacharyya S; Jacobs PM; et al. Dosimetry and first human experience with (89)Zrpanitumumab. Am. J. Nucl. Med. Mol. Imaging 2017, 7, 195–203. [PubMed: 28913158]

(369). Johns TG; Stockert E; Ritter G; Jungbluth AA; Huang HJ; Cavenee WK; Smyth FE; Hall CM; Watson N; Nice EC; et al. Novel monoclonal antibody specific for the de2–7 epidermal growth factor receptor (EGFR) that also recognizes the EGFR expressed in cells containing amplification of the EGFR gene. Int. J. Cancer 2002, 98, 398–408. [PubMed: 11920591]

(370). Jungbluth AA; Stockert E; Huang HJ; Collins VP; Coplan K; Iversen K; Kolb D; Johns TJ; Scott AM; Gullick WJ; et al. A monoclonal antibody recognizing human cancers with amplification/overexpression of the human epidermal growth factor receptor. Proc. Natl. Acad. Sci. U. S. A 2003, 100, 639–644. [PubMed: 12515857]

(371). Panousis C; Rayzman VM; Johns TG; Renner C; Liu Z; Cartwright G; Lee FT; Wang D; Gan H; Cao D; et al. Engineering and characterisation of chimeric monoclonal antibody 806 (ch806) for targeted immunotherapy of tumours expressing de2–7 EGFR or amplified EGFR. Br. J. Cancer 2005, 92, 1069–1077. [PubMed: 15770208]

(372). Scott AM; Lee FT; Tebbutt N; Herbertson R; Gill SS; Liu Z; Skrinos E; Murone C; Saunder TH; Chappell B; et al. A phase I clinical trial with monoclonal antibody ch806 targeting transitional state and mutant epidermal growth factor receptors. Proc. Natl. Acad. Sci. U. S. A 2007, 104, 4071–4076. [PubMed: 17360479]

(373). Lee FT; O'Keefe GJ; Gan HK; Mountain AJ; Jones GR; Saunder TH; Sagona J; Rigopoulos A; Smyth FE; Johns TG; et al. Immuno-PET quantitation of de2–7 epidermal growth factor receptor expression in glioma using 124I-IMP-R4-labeled antibody ch806. J. Nucl. Med 2010, 51, 967–972. [PubMed: 20484439]

(374). Lee FT; Burvenich IJ; Guo N; Kocovski P; Tochon-Danguy H; Ackermann U; O'Keefe GJ; Gong S; Rigopoulos A; Liu Z; et al. L-tyrosine confers residualizing properties to a d-amino acid-rich residualizing peptide for radioiodination of internalizing antibodies. Mol. Imaging 2016, 15, 153601211664753.

(375). Chekol R; Solomon VR; Alizadeh E; Bernhard W; Fisher D; Hill W; Barreto K; DeCoteau JF; Parada AC; Geyer CR; Fonge H 89)Zr-nimotuzumab for immunoPET imaging of epidermal growth factor receptor I. Oncotarget 2018, 9, 17117–17132. [PubMed: 29682209]

(376). Tang Y; Hu Y; Liu W; Chen L; Zhao Y; Ma H; Yang J; Yang Y; Liao J; Cai J; et al. A radiopharmaceutical [(89)Zr]Zr-DFO-nimotuzumab for immunoPET with epidermal growth factor receptor expression in vivo. Nucl. Med. Biol 2019, 70, 23–31. [PubMed: 30826708]

(377). Miao Z; Ren G; Liu H; Jiang L; Cheng Z Small-animal PET imaging of human epidermal growth factor receptor positive tumor with a 64Cu labeled affibody protein. Bioconjugate Chem 2010, 21, 947–954.

(378). Miao Z; Ren G; Liu H; Qi S; Wu S; Cheng Z PET of EGFR expression with an 18F-labeled affibody molecule. J. Nucl. Med 2012, 53, 1110–1118. [PubMed: 22689926]

(379). Su X; Cheng K; Jeon J; Shen B; Venturin GT; Hu X; Rao J; Chin FT; Wu H; Cheng Z Comparison of two site-specifically (18)F-labeled affibodies for PET imaging of EGFR positive tumors. Mol. Pharmaceutics 2014, 11, 3947–3956.

(380). Cheng Q; Wallberg H; Grafstrom J; Lu L; Thorell JO; Hagg Olofsson M; Linder S; Johansson K; Tegnebratt T; Arner ES; et al. Preclinical PET imaging of EGFR levels: pairing a targeting with a non-targeting Sel-tagged Affibody-based tracer to estimate the specific uptake. EJNMMI Res 2016, 6, 58. [PubMed: 27388754]

(381). Garousi J; Andersson KG; Mitran B; Pichl ML; Stahl S; Orlova A; Lofblom J; Tolmachev V PET imaging of epidermal growth factor receptor expression in tumours using 89Zr-labelled ZEGFR:2377 affibody molecules. Int. J. Oncol 2016, 48, 1325–1332. [PubMed: 26847636]

(382). Burley TA; Da Pieve C; Martins CD; Ciobota DM; Allott L; Oyen WJG; Harrington KJ; Smith G; Kramer-Marek G Affibody-based PET imaging to guide EGFR-targeted cancer therapy in Head and Neck squamous cell cancer models. J. Nucl. Med 2019, 60, 353–361. [PubMed: 30213849]

(383). Reilly EB; Phillips AC; Buchanan FG; Kingsbury G; Zhang Y; Meulbroek JA; Cole TB; DeVries PJ; Falls HD; Beam C; et al. Characterization of ABT-806, a humanized tumor-specific anti-EGFR monoclonal antibody. Mol. Cancer Ther 2015, 14, 1141–1151. [PubMed: 25731184]

(384). Phillips AC; Boghaert ER; Vaidya KS; Falls HD; Mitten MJ; DeVries PJ; Benatuil L; Hsieh CM; Meulbroek JA; Panchal SC; et al. Characterization of ABBV-221, a tumor-selective EGFR-targeting antibody drug conjugate. Mol. Cancer Ther 2018, 17, 795–805. [PubMed: 29483208]

(385). Oliveira S; van Dongen GA; Stigter-van Walsum M; Roovers RC; Stam JC; Mali W; van Diest PJ; van Bergen en Henegouwen, P. M. Rapid visualization of human tumor xenografts through optical imaging with a near-infrared fluorescent anti-epidermal growth factor receptor nanobody. Mol. Imaging 2012, 11, 33–46. [PubMed: 22418026]

(386). Tintelnot J; Baum N; Schultheiss C; Braig F; Trentmann M; Finter J; Fumey W; Bannas P; Fehse B; Riecken K; et al. Nanobody targeting of epidermal growth factor receptor (EGFR) ectodomain variants overcomes resistance to therapeutic EGFR antibodies. Mol. Cancer Ther 2019, 18, 823–833. [PubMed: 30824613]

(387). Vosjan MJ; Perk LR; Roovers RC; Visser GW; Stigter-van Walsum M; van Bergen En Henegouwen PM; van Dongen GA Facile labelling of an anti-epidermal growth factor receptor Nanobody with 68Ga via a novel bifunctional desferal chelate for immuno-PET. Eur. J. Nucl. Med. Mol. Imaging 2011, 38, 753–763. [PubMed: 21210114]

(388). Beltrán Hernández I; Rompen R; Rossin R; Xenaki KT; Katrukha EA; Nicolay K; van Bergen en Henegouwen P; Grüll H; Oliveira S Imaging of tumor spheroids, dual-isotope SPECT, and autoradiographic analysis to assess the tumor uptake and distribution of different nanobodies. Mol. Imag. Biol 2019, 21, 1079–1088.

(389). Wei W; Ni D; Ehlerding EB; Luo QY; Cai W PET imaging of receptor tyrosine kinases in cancer. Mol. Cancer Ther 2018, 17, 1625–1636. [PubMed: 30068751]

(390). Perik PJ; Lub-De Hooge MN; Gietema JA; van der Graaf WT; de Korte MA; Jonkman S; Kosterink JG; van Veldhuisen DJ; Sleijfer DT; Jager PL; et al. Indium-111-labeled trastuzumab scintigraphy in patients with human epidermal growth factor receptor 2-positive metastatic breast cancer. J. Clin. Oncol 2006, 24, 2276–2282. [PubMed: 16710024]

(391). Gebhart G; Lamberts LE; Wimana Z; Garcia C; Emonts P; Ameye L; Stroobants S; Huizing M; Aftimos P; Tol J; et al. Molecular imaging as a tool to investigate heterogeneity of advanced HER2-positive breast cancer and to predict patient outcome under trastuzumab emtansine (T-DM1): the ZEPHIR trial. Ann. Oncol 2016, 27, 619–624. [PubMed: 26598545]

(392). Ulaner GA; Hyman DM; Ross DS; Corben A; Chandarlapaty S; Goldfarb S; McArthur H; Erinjeri JP; Solomon SB; Kolb H; et al. Detection of HER2-positive metastases in patients with HER2-negative primary breast cancer using 89Zr-trastuzumab PET/CT. J. Nucl. Med 2016, 57, 1523–1528. [PubMed: 27151988]

(393). Ulaner GA; Hyman DM; Lyashchenko SK; Lewis JS; Carrasquillo JA 89Zr-trastuzumab PET/CT for detection of human epidermal growth factor receptor 2-positive metastases in patients with human epidermal growth factor receptor 2-negative primary breast cancer. Clin. Nucl. Med 2017, 42, 912–917. [PubMed: 28872549]

(394). Tamura K; Kurihara H; Yonemori K; Tsuda H; Suzuki J; Kono Y; Honda N; Kodaira M; Yamamoto H; Yunokawa M; et al. 64Cu-DOTA-trastuzumab PET imaging in patients with HER2-positive breast cancer. J. Nucl. Med 2013, 54, 1869–1875. [PubMed: 24029656]

(395). Mortimer JE; Bading JR; Park JM; Frankel PH; Carroll MI; Tran TT; Poku EK; Rockne RC; Raubitschek AA; Shively JE; et al. Tumor uptake of (64)Cu-DOTA-trastuzumab in patients with metastatic breast cancer. J. Nucl. Med 2018, 59, 38–43. [PubMed: 28637802]

(396). Ulaner GA; Lyashchenko SK; Riedl C; Ruan S; Zanzonico PB; Lake D; Jhaveri K; Zeglis B; Lewis JS; O'Donoghue JA First-in-human human epidermal growth factor receptor 2-targeted imaging using (89)Zr-pertuzumab PET/CT: dosimetry and clinical application in patients with breast cancer. J. Nucl. Med 2018, 59, 900–906. [PubMed: 29146695]

(397). Meric-Bernstam F; Johnson AM; Dumbrava EEI; Raghav K; Balaji K; Bhatt M; Murthy RK; Rodon J; Piha-Paul SA Advances in HER2-targeted therapy: novel agents and opportunities beyond breast and gastric Cancer. Clin. Cancer Res 2019, 25, 2033–2041. [PubMed: 30442682]

(398). Guo X; Zhu H; Zhou N; Chen Z; Liu T; Liu F; Xu X; Jin H; Shen L; Gao J; et al. Noninvasive detection of HER2 expression in gastric cancer by (64)Cu-NOTA-trastuzumab in PDX mouse model and in patients. Mol. Pharmaceutics 2018, 15, 5174–5182.

(399). O'Donoghue JA; Lewis JS; Pandit-Taskar N; Fleming SE; Schoder H; Larson SM; Beylergil V; Ruan S; Lyashchenko SK; Zanzonico PB; et al. Pharmacokinetics, biodistribution, and radiation dosimetry for (89)Zr-trastuzumab in patients with esophagogastric cancer. J. Nucl. Med 2018, 59, 161–166. [PubMed: 28637800]

(400). Guo X; Zhou N; Chen Z; Liu T; Xu X; Lei X; Shen L; Gao J; Yang Z; Zhu H Construction of (124)I-trastuzumab for noninvasive PET imaging of HER2 expression: from patient-derived xenograft models to gastric cancer patients. Gastric Cancer 2020, DOI: 10.1007/s10120-019-01035-6.

(401). Jiang D; Im HJ; Sun H; Valdovinos HF; England CG; Ehlerding EB; Nickles RJ; Lee DS; Cho SY; Huang P; et al. Radiolabeled pertuzumab for imaging of human epidermal growth factor receptor 2 expression in ovarian cancer. Eur. J. Nucl. Med. Mol. Imaging 2017, 44, 1296–1305. [PubMed: 28265738]

(402). Yanai A; Harada R; Iwata R; Yoshikawa T; Ishikawa Y; Furumoto S; Ishida T; Yanai K Site-specific labeling of F-18 proteins using a supplemented cell-free protein synthesis system and O-2-[(18)F]Fluoroethyl-L-Tyrosine: [(18)F]FET-HER2 affibody molecule. Mol. Imaging Biol 2019, 21, 529–537. [PubMed: 30112727]

(403). Qi S; Hoppmann S; Xu Y; Cheng Z PET imaging of HER2-positive tumors with Cu-64-Labeled affibody molecules. Mol. Imag. Biol 2019, 21, 907–916.

(404). Wei W; Jiang D; Rosenkrans ZT; Barnhart TE; Engle JW; Luo Q; Cai W HER2-targeted multimodal imaging of anaplastic thyroid cancer. Am. J. Cancer Res 2019, 9, 2413–2427. [PubMed: 31815043]

(405). Wimana Z; Gebhart G; Guiot T; Vanderlinden B; Morandini R; Doumont G; Sherer F; Van Simaeys G; Goldman S; Ghanem G; et al. Mucolytic agents can enhance HER2 receptor accessibility for [(89)Zr]trastuzumab, improving HER2 imaging in a mucin-overexpressing breast cancer xenograft mouse model. Mol. Imaging Biol 2015, 17, 697–703. [PubMed: 25761907]

(406). Pereira PMR; Sharma SK; Carter LM; Edwards KJ; Pourat J; Ragupathi A; Janjigian YY; Durack JC; Lewis JS Caveolin-1 mediates cellular distribution of HER2 and affects trastuzumab binding and therapeutic efficacy. Nat. Commun 2018, 9, 5137. [PubMed: 30510281]

(407). Pereira PMR; Mandleywala K; Ragupathi A; Carter LM; Goos J; Janjigian YY; Lewis JS Temporal modulation of HER2 membrane availability increases pertuzumab uptake and pretargeted molecular imaging of gastric tumors. J. Nucl. Med 2019, 60, 1569–1578. [PubMed: 31171598]

(408). Pereira PMR; Ragupathi A; Shmuel S; Mandleywala K; Viola NT; Lewis JS HER2-targeted PET imaging and therapy of hyaluronan-masked HER2-overexpressing breast cancer. Mol. Pharmaceutics 2020, 17, 327–337.

(409). Cheng Z; De Jesus OP; Namavari M; De A; Levi J; Webster JM; Zhang R; Lee B; Syud FA; Gambhir SS Small-animal PET imaging of human epidermal growth factor receptor type 2 expression with site-specific 18F-labeled protein scaffold molecules.J. Nucl. Med 2008, 49, 804–813. [PubMed: 18413392]

(410). Cheng Z; De Jesus OP; Kramer DJ; De A; Webster JM; Gheysens O; Levi J; Namavari M; Wang S; Park JM; et al. 64Cu-labeled affibody molecules for imaging of HER2 expressing tumors. Mol. Imaging Biol 2010, 12, 316–324. [PubMed: 19779897]

(411). Beylergil V; Morris PG; Smith-Jones PM; Modi S; Solit D; Hudis CA; Lu Y; O'Donoghue J; Lyashchenko SK; Carrasquillo JA; Larson SM; Akhurst TJ Pilot study of 68Ga-DOTA-F(ab′)2-trastuzumab in patients with breast cancer. Nucl. Med. Commun 2013, 34, 1157–1165. [PubMed: 24100444]

(412). Keyaerts M; Xavier C; Heemskerk J; Devoogdt N; Everaert H; Ackaert C; Vanhoeij M; Duhoux FP; Gevaert T; Simon P; et al. Phase I study of 68Ga-HER2-nanobody for PET/CT assessment of HER2 expression in breast carcinoma. J. Nucl. Med 2016, 57, 27–33. [PubMed: 26449837]

(413). Massa S; Vikani N; Betti C; Ballet S; Vanderhaegen S; Steyaert J; Descamps B; Vanhove C; Bunschoten A; van Leeuwen FW; et al. Sortase A-mediated site-specific labeling of camelid single-domain antibody-fragments: a versatile strategy for multiple molecular imaging modalities. Contrast Media Mol. Imaging 2016, 11, 328–339. [PubMed: 27147480]

(414). Zhou Z; Chitneni SK; Devoogdt N; Zalutsky MR; Vaidyanathan G Fluorine-18 labeling of an anti-HER2 VHH using a residualizing prosthetic group via a strain-promoted click reaction: chemistry and preliminary evaluation. Bioorg. Med. Chem 2018, 26, 1939–1949. [PubMed: 29534937]

(415). Zhou Z; McDougald D; Devoogdt N; Zalutsky MR; Vaidyanathan G Labeling single domain antibody fragments with fluorine-18 using 2,3,5,6-tetrafluorophenyl 6-[18 F]fluoronicotinate resulting in high tumor to kidney ratios. Mol. Pharmaceutics 2019, 16, 214–226.

(416). Zhou Z; Devoogdt N; Zalutsky MR; Vaidyanathan G An efficient method for labeling single domain antibody fragments with (18)F using tetrazine-trans-cyclooctene ligation and a renal brush border enzyme-cleavable linker. Bioconjugate Chem 2018, 29, 4090–4103.

(417). D'Huyvetter M; De Vos J; Xavier C; Pruszynski M; Sterckx YGJ; Massa S; Raes G; Caveliers V; Zalutsky MR; Lahoutte T; et al. (131)I-labeled anti-HER2 camelid sdAb as a theranostic tool in cancer treatment. Clin. Cancer Res 2017, 23, 6616–6628. [PubMed: 28751451]

(418). Orlova A; Magnusson M; Eriksson TL; Nilsson M; Larsson B; Höidén-Guthenberg I; Widström C; Carlsson J; Tolmachev V; Ståhl S. J. C. r.; Nilsson FY Tumor imaging using a picomolar affinity HER2 binding affibody molecule. Cancer Res 2006, 66, 4339–4348. [PubMed: 16618759]

(419). Tolmachev V; Nilsson FY; Widstrom C; Andersson K; Rosik D; Gedda L; Wennborg A; Orlova A 111In-benzyl-DTPAZHER2:342, an affibody-based conjugate for in vivo imaging of HER2 expression in malignant tumors. J. Nucl. Med 2006, 47, 846–853. [PubMed: 16644755]

(420). Kiesewetter DO; Kramer-Marek G; Ma Y; Capala J Radiolabeling of HER2 specific affibody(R) molecule with F-18. J. Fluorine Chem 2008, 129, 799–805.

(421). Kramer-Marek G; Bernardo M; Kiesewetter DO; Bagci U; Kuban M; Omer A; Zielinski R; Seidel J; Choyke P; Capala J PET of HER2-positive pulmonary metastases with 18F-ZHER2:342 affibody in a murine model of breast cancer: comparison with 18FFDG. J. Nucl. Med 2012, 53, 939–946. [PubMed: 22582046]

(422). Xu Y; Bai Z; Huang Q; Pan Y; Pan D; Wang L; Yan J; Wang X; Yang R; Yang M PET of HER2 expression with a novel(18)FAl labeled affibody. J. Cancer 2017, 8, 1170–1178. [PubMed: 28607591]

(423). Orlova A; Tolmachev V; Pehrson R; Lindborg M; Tran T; Sandstrom M; Nilsson FY; Wennborg A; Abrahmsen L; Feldwisch J Synthetic affibody molecules: a novel class of affinity ligands for molecular imaging of HER2-expressing malignant tumors. Cancer Res 2007, 67, 2178–2186. [PubMed: 17332348]

(424). Tolmachev V; Velikyan I; Sandstrom M; Orlova A A HER2-binding Affibody molecule labelled with 68Ga for PET imaging: direct in vivo comparison with the 111In-labelled analogue. Eur. J. Nucl. Med. Mol. Imaging 2010, 37, 1356–1367. [PubMed: 20130858]

(425). Tolmachev V; Wallberg H; Sandstrom M; Hansson M; Wennborg A; Orlova A Optimal specific radioactivity of anti-HER2 affibody molecules enables discrimination between xenografts with high and low HER2 expression levels. Eur. J. Nucl. Med. Mol. Imaging 2011, 38, 531–539. [PubMed: 21069318]

(426). Baum RP; Prasad V; Muller D; Schuchardt C; Orlova A; Wennborg A; Tolmachev V; Feldwisch J Molecular imaging of HER2-expressing malignant tumors in breast cancer patients using synthetic 111In- or 68Ga-labeled affibody molecules. J. Nucl. Med 2010, 51, 892–897. [PubMed: 20484419]

(427). Sorensen J; Sandberg D; Sandstrom M; Wennborg A; Feldwisch J; Tolmachev V; Astrom G; Lubberink M; Garske-Roman U; Carlsson J; et al. First-in-human molecular imaging of HER2 expression in breast cancer metastases using the 111In-ABY-025 affibody molecule. J. Nucl. Med 2014, 55, 730–735. [PubMed: 24665085]

(428). Ahlgren S; Orlova A; Wallberg H; Hansson M; Sandstrom M; Lewsley R; Wennborg A; Abrahmsen L; Tolmachev V; Feldwisch J Targeting of HER2-expressing tumors using 111In-ABY-025, a second-generation affibody molecule with a fundamentally reengineered scaffold. J. Nucl. Med 2010, 51, 1131–1138. [PubMed: 20554729]

(429). Feldwisch J; Tolmachev V; Lendel C; Herne N; Sjoberg A; Larsson B; Rosik D; Lindqvist E; Fant G; Hoiden-Guthenberg I; et al. Design of an optimized scaffold for affibody molecules. J. Mol. Biol 2010, 398, 232–247. [PubMed: 20226194]

(430). Sorensen J; Velikyan I; Sandberg D; Wennborg A; Feldwisch J; Tolmachev V; Orlova A; Sandstrom M; Lubberink M; Olofsson H; et al. Measuring HER2-receptor expression in metastatic breast cancer using [68Ga]ABY-025 affibody PET/CT. Theranostics 2016, 6, 262–271. [PubMed: 26877784]

(431). Velikyan I; Wennborg A; Feldwisch J; Lindman H; Carlsson J; Sorensen J Good manufacturing practice production of [(68)Ga]Ga-ABY-025 for HER2 specific breast cancer imaging. Am. J. Nucl. Med. Mol. Imaging 2016, 6, 135–153. [PubMed: 27186441]

(432). Sandstrom M; Lindskog K; Velikyan I; Wennborg A; Feldwisch J; Sandberg D; Tolmachev V; Orlova A; Sorensen J; Carlsson J; et al. Biodistribution and radiation dosimetry of the anti-HER2 aaffibody molecule 68Ga-ABY-025 in breast cancer patients. J. Nucl. Med 2016, 57, 867–871. [PubMed: 26912439]

(433). Sandberg D; Tolmachev V; Velikyan I; Olofsson H; Wennborg A; Feldwisch J; Carlsson J; Lindman H; Sorensen J Intra-image referencing for simplified assessment of HER2-expression in breast cancer metastases using the affibody molecule ABY-025 with PET and SPECT. Eur. J. Nucl. Med. Mol. Imaging 2017, 44, 1337–1346. [PubMed: 28261749]

(434). Velikyan I; Schweighofer P; Feldwisch J; Seemann J; Frejd FY; Lindman H; Sorensen J Diagnostic HER2-binding radiopharmaceutical, [(68)Ga]Ga-ABY-025, for routine clinical use in breast cancer patients. Am. J. Nucl. Med. Mol. Imaging 2019, 9, 12–23. [PubMed: 30911434]

(435). Glaser M; Iveson P; Hoppmann S; Indrevoll B; Wilson A; Arukwe J; Danikas A; Bhalla R; Hiscock D Three methods for 18F labeling of the HER2-binding affibody molecule Z(HER2:2891) including preclinical assessment. J. Nucl. Med 2013, 54, 1981–1988. [PubMed: 24115530]

(436). Trousil S; Hoppmann S; Nguyen QD; Kaliszczak M; Tomasi G; Iveson P; Hiscock D; Aboagye EO Positron emission tomography imaging with 18F-labeled ZHER2:2891 affibody for detection of HER2 expression and pharmacodynamic response to HER2-modulating therapies. Clin. Cancer Res 2014, 20, 1632–1643. [PubMed: 24493830]

(437). Ahlgren S; Wallberg H; Tran TA; Widstrom C; Hjertman M; Abrahmsen L; Berndorff D; Dinkelborg LM; Cyr JE; Feldwisch J; et al. Targeting of HER2-expressing tumors with a site-specifically 99mTc-labeled recombinant affibody molecule, ZHER2:2395, with C-terminally engineered cysteine. J. Nucl. Med 2009, 50, 781–789. [PubMed: 19372467]

(438). Heskamp S; Laverman P; Rosik D; Boschetti F; van der Graaf WT; Oyen WJ; van Laarhoven HW; Tolmachev V; Boerman OC Imaging of human epidermal growth factor receptor type 2 expression with 18F-labeled affibody molecule ZHER2:2395 in a mouse model for ovarian cancer. J. Nucl. Med 2012, 53, 146–153. [PubMed: 22173842]

(439). Yin W; Zhu J; Gonzalez-Rivas D; Okumura M; Rocco G; Pass H; Jiang G; Yang Y Construction of a novel bispecific antibody to enhance antitumor activity against lung cancer. Adv. Mater 2018, 30, 1805437.

(440). Slaga D; Ellerman D; Lombana TN; Vij R; Li J; Hristopoulos M; Clark R; Johnston J; Shelton A; Mai E Avidity-based binding to HER2 results in selective killing of HER2-overexpressing cells by anti-HER2/CD3. Sci. Transl. Med 2018, 10, eaat5775. [PubMed: 30333240]

(441). Rius Ruiz I; Vicario R; Morancho B; Morales CB; Arenas EJ; Herter S; Freimoser-Grundschober A; Somandin J; Sam J; Ast O; et al. p95HER2-T cell bispecific antibody for breast cancer treatment. Sci. Transl. Med 2018, 10, eaat1445. [PubMed: 30282693]

(442). Huang S; Li F; Liu H; Ye P; Fan X; Yuan X; Wu Z; Chen J; Jin C; Shen B; et al. Structural and functional characterization of MBS301, an afucosylated bispecific anti-HER2 antibody. MAbs 2018, 10, 864–875. [PubMed: 30081724]

(443). Bensch F; Brouwers AH; Lub-de Hooge MN; de Jong JR; van der Vegt B; Sleijfer S; de Vries EGE; Schroder CP89)Zr-trastuzumab PET supports clinical decision making in breast cancer patients, when HER2 status cannot be determined by standard work up. Eur. J. Nucl. Med. Mol. Imaging 2018, 45, 2300–2306. [PubMed: 30058029]

(444). Kramer-Marek G; Gijsen M; Kiesewetter DO; Bennett R; Roxanis I; Zielinski R; Kong A; Capala J Potential of PET to predict the response to trastuzumab treatment in an ErbB2-positive human xenograft tumor model. J. Nucl. Med 2012, 53, 629–637. [PubMed: 22410461]

(445). Lam K; Chan C; Reilly RM Development and preclinical studies of (64)Cu-NOTA-pertuzumab F(ab′)2 for imaging changes in tumor HER2 expression associated with response to trastuzumab by PET/CT. MAbs 2017, 9, 154–164. [PubMed: 27813707]

(446). Zhou Z; Vaidyanathan G; McDougald D; Kang CM; Balyasnikova I; Devoogdt N; Ta AN; McNaughton BR; Zalutsky MR Fluorine-18 labeling of the HER2-targeting single-domain

antibody 2Rs15d using a residualizing label and preclinical evaluation. Mol. Imaging Biol 2017, 19, 867–877. [PubMed: 28409338]

(447). Gala K; Chandarlapaty S Molecular pathways: HER3 targeted therapy. Clin. Cancer Res 2014, 20, 1410–1416. [PubMed: 24520092]

(448). Pool M; Kol A; de Jong S; de Vries EGE; Lub-de Hooge MN; Terwisscha van Scheltinga AGT 89)Zr-mAb3481 PET for HER3 tumor status assessment during lapatinib treatment. MAbs 2017, 9, 1370–1378. [PubMed: 28873009]

(449). Jacob W; James I; Hasmann M; Weisser M Clinical development of HER3-targeting monoclonal antibodies: Perils and progress. Cancer Treat. Rev 2018, 68, 111–123. [PubMed: 29944978]

(450). Schaefer G; Haber L; Crocker LM; Shia S; Shao L; Dowbenko D; Totpal K; Wong A; Lee CV; Stawicki S; et al. A two-in-one antibody against HER3 and EGFR has superior inhibitory activity compared with monospecific antibodies. Cancer Cell 2011, 20, 472–486. [PubMed: 22014573]

(451). McKnight BN; Kuda-Wedagedara ANW; Sevak KK; Abdel-Atti D; Wiesend WN; Ku A; Selvakumar D; Carlin SD; Lewis JS; Viola-Villegas NT Imaging EGFR and HER3 through(89)Zr-labeled MEHD7945A (Duligotuzumab). Sci. Rep 2018, 8, 9043. [PubMed: 29899472]

(452). Sharp T; Glaus C; Fettig N; Hewig A; Ogbagabriel S; Freeman D; Beaupre D; Hwang D; Welch M Pharmacological evaluation of 64Cu - DOTA - AMG 888 (U3–1287) in control and tumor bearing mice using biodistribution and microPET imaging. Proceedings of the World Molecular Imaging Congress, 2011.

(453). Lockhart AC; Liu Y; Dehdashti F; Laforest R; Picus J; Frye J; Trull L; Belanger S; Desai M; Mahmood S; et al. Phase 1 evaluation of [(64)Cu]DOTA-patritumab to assess dosimetry, apparent receptor occupancy, and safety in subjects with advanced solid tumors. Mol. Imaging Biol 2016, 18, 446–453. [PubMed: 26567113]

(454). Alsaid H; Skedzielewski T; Rambo MV; Hunsinger K; Hoang B; Fieles W; Long ER; Tunstead J; Vugts DJ; Cleveland M; et al. Non invasive imaging assessment of the biodistribution of GSK2849330, an ADCC and CDC optimized anti HER3 mAb, and its role in tumor macrophage recruitment in human tumor-bearing mice. PLoS One 2017, 12, e0176075. [PubMed: 28448604]

(455). Menke-van der Houven van Oordt CW; McGeoch A; Bergstrom M; McSherry I; Smith DA; Cleveland M; Al-Azzam W; Chen L; Verheul H; Hoekstra OS; et al. Immuno-PET imaging to assess target engagement: experience from (89)Zr-Anti-HER3 mAb (GSK2849330) in patients with solid tumors. J. Nucl. Med 2019, 60, 902–909. [PubMed: 30733323]

(456). Mirschberger C; Schiller CB; Schraml M; Dimoudis N; Friess T; Gerdes CA; Reiff U; Lifke V; Hoelzlwimmer G; Kolm I; et al. RG7116, a therapeutic antibody that binds the inactive HER3 receptor and is optimized for immune effector activation. Cancer Res 2013, 73, 5183–5194. [PubMed: 23780344]

(457). Terwisscha van Scheltinga AG; Lub-de Hooge MN; Abiraj K; Schroder CP; Pot L; Bossenmaier B; Thomas M; Holzlwimmer G; Friess T; Kosterink JG; et al. ImmunoPET and biodistribution with human epidermal growth factor receptor 3 targeting antibody (8)(9)Zr-RG7116. MAbs 2014, 6, 1051–1058. [PubMed: 24870719]

(458). Bensch F; Lamberts LE; Smeenk MM; Jorritsma-Smit A; Lub-de Hooge MN; Terwisscha van Scheltinga AGT; de Jong JR; Gietema JA; Schroder CP; Thomas M; et al. (89)Zrlumretuzumab PET Imaging before and during HER3 antibody lumretuzumab treatment in patients with solid tumors. Clin. Cancer Res 2017, 23, 6128–6137. [PubMed: 28733442]

(459). Da Pieve C; Allott L; Martins CD; Vardon A; Ciobota DM; Kramer-Marek G; Smith G Efficient [(18)F]AlF radio-labeling of ZHER3:8698 affibody molecule for imaging of HER3 positive tumors. Bioconjugate Chem 2016, 27, 1839–1849.

(460). Maruthachalam BV; El-Sayed A; Liu J; Sutherland AR; Hill W; Alam MK; Pastushok L; Fonge H; Barreto K; Geyer CR A single-framework synthetic antibody library containing a combination of canonical and variable complementarity-determining regions. ChemBioChem 2017, 18, 2247–2259. [PubMed: 28884521]

(461). El-Sayed A; Bernhard W; Barreto K; Gonzalez C; Hill W; Pastushok L; Fonge H; Geyer CR Evaluation of antibody fragment properties for near-infrared fluorescence imaging of HER3-positive cancer xenografts. Theranostics 2018, 8, 4856–4869. [PubMed: 30279742]

(462). Martins CD; Da Pieve C; Burley TA; Smith R; Ciobota DM; Allott L; Harrington KJ; Oyen WJG; Smith G; Kramer-Marek G HER3-mediated resistance to Hsp90 inhibition detected in breast cancer xenografts by affibody-based PET imaging. Clin. Cancer Res 2018, 24, 1853–1865. [PubMed: 29437790]

(463). Orlova A; Malm M; Rosestedt M; Varasteh Z; Andersson K; Selvaraju RK; Altai M; Honarvar H; Strand J; Stahl S; et al. Imaging of HER3-expressing xenografts in mice using a (99m)Tc-(CO) 3-HEHEHE-Z HER3:08699 affibody molecule. Eur. J. Nucl. Med. Mol. Imaging 2014, 41, 1450–1459. [PubMed: 24622956]

(464). Rosestedt M; Andersson KG; Mitran B; Tolmachev V; Lofblom J; Orlova A; Stahl S Affibody-mediated PET imaging of HER3 expression in malignant tumours. Sci. Rep 2015, 5, 15226. [PubMed: 26477646]

(465). Warnders FJ; Terwisscha van Scheltinga AGT; Knuehl C; van Roy M; de Vries EFJ; Kosterink JGW; de Vries EGE; Lub-de Hooge MN Human epidermal growth factor receptor 3-specific tumor uptake and biodistribution of (89)Zr-MSB0010853 visualized by real-time and noninvasive PET imaging. J. Nucl. Med 2017, 58, 1210–1215. [PubMed: 28360206]

(466). Ferrara N; Adamis AP Ten years of anti-vascular endothelial growth factor therapy. Nat. Rev. Drug Discovery 2016, 15, 385–403. [PubMed: 26775688]

(467). Apte RS; Chen DS; Ferrara N VEGF in signaling and disease: beyond discovery and development. Cell 2019, 176, 1248–1264. [PubMed: 30849371]

(468). Ferrara N; Hillan KJ; Gerber HP; Novotny W Discovery and development of bevacizumab, an anti-VEGF antibody for treating cancer. Nat. Rev. Drug Discovery 2004, 3, 391–400. [PubMed: 15136787]

(469). Gaykema SB; Brouwers AH; Lub-de Hooge MN; Pleijhuis RG; Timmer-Bosscha H; Pot L; van Dam GM; van der Meulen SB; de Jong JR; Bart J; et al. 89Zr-bevacizumab PET imaging in primary breast cancer. J. Nucl. Med 2013, 54, 1014–1018. [PubMed: 23651946]

(470). van Asselt SJ; Oosting SF; Brouwers AH; Bongaerts AH; de Jong JR; Lub-de Hooge MN; Oude Munnink TH; Fiebrich HB; Sluiter WJ; Links TP; et al. Everolimus reduces(89)Zr-bevacizumab tumor uptake in patients with neuroendocrine tumors. J. Nucl. Med 2014, 55, 1087–1092. [PubMed: 24790218]

(471). Oosting SF; Brouwers AH; van Es SC; Nagengast WB; Oude Munnink TH; Lub-de Hooge MN; Hollema H; de Jong JR; de Jong IJ; de Haas S; et al. 89Zr-bevacizumab PET visualizes heterogeneous tracer accumulation in tumor lesions of renal cell carcinoma patients and differential effects of antiangiogenic treatment. J. Nucl. Med 2015, 56, 63–69. [PubMed: 25476536]

(472). Bahce I; Huisman MC; Verwer EE; Ooijevaar R; Boutkourt F; Vugts DJ; van Dongen GA; Boellaard R; Smit EF Pilot study of (89)Zr-bevacizumab positron emission tomography in patients with advanced non-small cell lung cancer. EJNMMI Res 2014, 4, 35. [PubMed: 26055936]

(473). Jansen MH; Veldhuijzen van Zanten SEM; van Vuurden DG; Huisman MC; Vugts DJ; Hoekstra OS; van Dongen GA; Kaspers GL Molecular drug imaging: (89)Zr-bevacizumab PET in children with diffuse intrinsic pontine glioma. J. Nucl. Med 2017, 58, 711–716. [PubMed: 27765855]

(474). Veldhuijzen van Zanten SEM; Sewing ACP; van Lingen A; Hoekstra OS; Wesseling P; Meel MH; van Vuurden DG; Kaspers GJL; Hulleman E; Bugiani M Multiregional tumor drug-uptake imaging by PET and microvascular morphology in end-stage diffuse intrinsic pontine glioma. J. Nucl. Med 2018, 59, 612–615. [PubMed: 28818988]

(475). Nagengast WB; de Korte MA; Oude Munnink TH; Timmer-Bosscha H; den Dunnen WF; Hollema H; de Jong JR; Jensen MR; Quadt C; Garcia-Echeverria C; et al. 89Zrbevacizumab PET of early antiangiogenic tumor response to treatment with HSP90 inhibitor NVP-AUY922. J. Nucl. Med 2010, 51, 761–767. [PubMed: 20395337]

(476). Gaykema SB; Schroder CP; Vitfell-Rasmussen J; Chua S; Oude Munnink TH; Brouwers AH; Bongaerts AH; Akimov M; Fernandez-Ibarra C; Lub-de Hooge MN; et al. 89Zrtrastuzumab and 89Zr-bevacizumab PET to evaluate the effect of the HSP90 inhibitor NVP-AUY922 in metastatic breast cancer patients. Clin. Cancer Res 2014, 20, 3945–3954. [PubMed: 25085789]

(477). Chakraborty S; Filippi CG; Burkhardt JK; Fralin S; Ray A; Wong T; Ortiz R; Langer DJ; Boockvar JA Durability of single dose intra-arterial bevacizumab after blood/brain barrier

disruption for recurrent glioblastoma. J. Exp. Ther. Oncol 2016, 11, 261–267. [PubMed: 27849336]

(478). Lesniak WG; Chu C; Jablonska A; Du Y; Pomper MG; Walczak P; Janowski M A Distinct advantage to intraarterial delivery of (89)Zr-bevacizumab in PET imaging of mice with and without osmotic opening of the blood-brain barrier. J. Nucl. Med 2019, 60, 617–622. [PubMed: 30315146]

(479). Nagengast WB; Lub-de Hooge MN; Oosting SF; den Dunnen WF; Warnders FJ; Brouwers AH; de Jong JR; Price PM; Hollema H; Hospers GA; et al. VEGF-PET imaging is a noninvasive biomarker showing differential changes in the tumor during sunitinib treatment. Cancer Res 2011, 71, 143–153. [PubMed: 21084271]

(480). Desar IM; Stillebroer AB; Oosterwijk E; Leenders WP; van Herpen CM; van der Graaf WT; Boerman OC; Mulders PF; Oyen WJ 111In-bevacizumab imaging of renal cell cancer and evaluation of neoadjuvant treatment with the vascular endothelial growth factor receptor inhibitor sorafenib. J. Nucl. Med 2010, 51, 1707–1715. [PubMed: 20956472]

(481). van Es SC; Brouwers AH; Mahesh SVK; Leliveld-Kors AM; de Jong IJ; Lub-de Hooge MN; de Vries EGE; Gietema JA; Oosting SF (89)Zr-bevacizumab PET: potential early indicator of everolimus efficacy in patients with metastatic renal cell carcinoma. J. Nucl. Med 2017, 58, 905–910. [PubMed: 28082434]

(482). Willett CG; Boucher Y; di Tomaso E; Duda DG; Munn LL; Tong RT; Chung DC; Sahani DV; Kalva SP; Kozin SV; et al. Direct evidence that the VEGF-specific antibody bevacizumab has antivascular effects in human rectal cancer. Nat. Med 2004, 10, 145–147. [PubMed: 14745444]

(483). Luo H; England CG; Graves SA; Sun H; Liu G; Nickles RJ; Cai W PET imaging of VEGFR-2 expression in lung cancer with 64Cu-labeled ramucirumab. J. Nucl. Med 2016, 57, 285–290. [PubMed: 26541778]

(484). Meyer JP; Edwards KJ; Kozlowski P; Backer MV; Backer JM; Lewis JS Selective imaging of VEGFR-1 and VEGFR-2 using 89Zr-labeled single-chain VEGF mutants. J. Nucl. Med 2016, 57, 1811–1816. [PubMed: 27390161]

(485). Li M; Jiang D; Barnhart TE; Cao T; Engle JW; Chen W; Cai W Immuno-PET imaging of VEGFR-2 expression in prostate cancer with (89)Zr-labeled ramucirumab. Am. J. Cancer Res 2019, 9, 2037–2046. [PubMed: 31598404]

(486). Lemmon MA; Schlessinger J Cell signaling by receptor tyrosine kinases. Cell 2010, 141, 1117–1134. [PubMed: 20602996]

(487). Bradley CA; Salto-Tellez M; Laurent-Puig P; Bardelli A; Rolfo C; Tabernero J; Khawaja HA; Lawler M; Johnston PG; Van Schaeybroeck S Targeting c-MET in gastrointestinal tumours: rationale, opportunities and challenges. Nat. Rev. Clin. Oncol 2017, 14, 562–576. [PubMed: 28374784]

(488). Wu YL; Soo RA; Locatelli G; Stammberger U; Scagliotti G; Park K Does c-Met remain a rational target for therapy in patients with EGFR TKI-resistant non-small cell lung cancer? Cancer Treat. Rev 2017, 61, 70–81. [PubMed: 29121501]

(489). Hughes VS; Siemann DW Have clinical trials properly assessed c-Met inhibitors? Trends Cancer 2018, 4, 94–97. [PubMed: 29458966]

(490). Corso S; Giordano S Cell-autonomous and non-cell-autonomous mechanisms of HGF/MET-driven resistance to targeted therapies: from basic research to a clinical perspective. Cancer Discovery 2013, 3, 978–992. [PubMed: 23901039]

(491). Spigel DR; Edelman MJ; O'Byrne K; Paz-Ares L; Mocci S; Phan S; Shames DS; Smith D; Yu W; Paton VE; et al. Results from the phase III randomized trial of onartuzumab plus erlotinib versus erlotinib in previously treated stage IIIB or IV non-small-cell lung cancer: METLung. J. Clin. Oncol 2017, 35, 412–420. [PubMed: 27937096]

(492). Catenacci DVT; Tebbutt NC; Davidenko I; Murad AM; Al-Batran SE; Ilson DH; Tjulandin S; Gotovkin E; Karaszewska B; Bondarenko I; et al. Rilotumumab plus epirubicin, cisplatin, and capecitabine as first-line therapy in advanced MET-positive gastric or gastro-oesophageal junction cancer (RILOMET-1): a randomised, double-blind, placebo-controlled, phase 3 trial. Lancet Oncol 2017, 18, 1467–1482. [PubMed: 28958504]

(493). Luo H; Hong H; Slater MR; Graves SA; Shi S; Yang Y; Nickles RJ; Fan F; Cai W PET of c-Met in cancer with (6) (4)Cu-labeled hepatocyte growth factor. J. Nucl. Med 2015, 56, 758–763. [PubMed: 25840981]

(494). Price EW; Carnazza KE; Carlin SD; Cho A; Edwards KJ; Sevak KK; Glaser JM; de Stanchina E; Janjigian YY; Lewis JS (89)Zr-DFO-AMG102 immuno-PET to determine local hepatocyte growth factor protein levels in tumors for enhanced patient selection. J. Nucl. Med 2017, 58, 1386–1394. [PubMed: 28280216]

(495). Jagoda EM; Lang L; Bhadrasetty V; Histed S; Williams M; Kramer-Marek G; Mena E; Rosenblum L; Marik J; Tinianow JN; et al. Immuno-PET of the hepatocyte growth factor receptor Met using the 1-armed antibody onartuzumab. J. Nucl. Med 2012, 53, 1592–1600. [PubMed: 22917884]

(496). Li K; Tavare R; Zettlitz KA; Mumenthaler SM; Mallick P; Zhou Y; Marks JD; Wu AM Anti-MET immunoPET for non-small cell lung cancer using novel fully human antibody fragments. Mol. Cancer Ther 2014, 13, 2607–2617. [PubMed: 25143449]

(497). Merchant M; Ma X; Maun HR; Zheng Z; Peng J; Romero M; Huang A; Yang NY; Nishimura M; Greve J; et al. Monovalent antibody design and mechanism of action of onartuzumab, a MET antagonist with anti-tumor activity as a therapeutic agent. Proc. Natl. Acad. Sci. U. S. A 2013, 110, E2987–2996. [PubMed: 23882082]

(498). Pool M; Terwisscha van Scheltinga AGT; Kol A; Giesen D; de Vries EGE; Lub-de Hooge MN 89)Zr-onartuzumab PET imaging of c-MET receptor dynamics. Eur. J. Nucl. Med. Mol. Imaging 2017, 44, 1328–1336. [PubMed: 28315949]

(499). Escorcia F; Houghton J; Abdel-Atti D; Pereira P; Cho A; Gutsche N; Baidoo K; Lewis J ImmunoPET predicts response to Met-targeted radioligand therapy in models of pancreatic cancer resistant to Met kinase inhibitors. Theranostics 2020, 10, 151–165.

(500). Klingler S; Fay R; Holland JP Light-induced radiosyn-thesis of (89)ZrDFO-azepin-onartuzumab for imaging the hepatocyte growth factor receptor. J. Nucl. Med 2020, 237180.

(501). Ostman A PDGF receptors in tumor stroma: biological effects and associations with prognosis and response to treatment. Adv. Drug Delivery Rev 2017, 121, 117–123.

(502). Heldin CH; Lennartsson J; Westermark B Involvement of platelet-derived growth factor ligands and receptors in tumorigenesis. J. Intern. Med 2018, 283, 16–44. [PubMed: 28940884]

(503). Tap WD; Jones RL; Van Tine BA; Chmielowski B; Elias AD; Adkins D; Agulnik M; Cooney MM; Livingston MB; Pennock G; et al. Olaratumab and doxorubicin versus doxorubicin alone for treatment of soft-tissue sarcoma: an open-label phase 1b and randomised phase 2 trial. Lancet 2016, 388, 488–497. [PubMed: 27291997]

(504). Lindborg M; Cortez E; Hoiden-Guthenberg I; Gunneriusson E; von Hage E; Syud F; Morrison M; Abrahmsen L; Herne N; Pietras K; et al. Engineered high-affinity affibody molecules targeting platelet-derived growth factor receptor beta in vivo. J. Mol. Biol 2011, 407, 298–315. [PubMed: 21277312]

(505). Strand J; Varasteh Z; Eriksson O; Abrahmsen L; Orlova A; Tolmachev V Gallium-68-labeled affibody molecule for PET imaging of PDGFRbeta expression in vivo. Mol. Pharmaceutics 2014, 11, 3957–3964.

(506). Tolmachev V; Varasteh Z; Honarvar H; Hosseinimehr SJ; Eriksson O; Jonasson P; Frejd FY; Abrahmsen L; Orlova A Imaging of platelet-derived growth factor receptor beta expression in glioblastoma xenografts using affibody molecule 111In-DOTAZ09591. J. Nucl. Med 2014, 55, 294–300. [PubMed: 24408895]

(507). Cai H; Shi Q; Tang Y; Chen L; Chen Y; Tao Z; Yang H; Xie F; Wu X; Liu N; et al. Positron emission tomography imaging of platelet-derived growth factor receptor beta in colorectal tumor xenograft using Zirconium-89 labeled dimeric affibody molecule. Mol. Pharmaceutics 2019, 16, 1950–1957.

(508). Zhang J; Wang P; Dykstra M; Gelebart P; Williams D; Ingham R; Adewuyi EE; Lai R; McMullen T Platelet-derived growth factor receptor-alpha promotes lymphatic metastases in papillary thyroid cancer. J. Pathol 2012, 228, 241–250. [PubMed: 22744707]

(509). Lopez-Campistrous A; Adewuyi EE; Benesch MGK; Ko YM; Lai R; Thiesen A; Dewald J; Wang P; Chu K; Ghosh S; et al. PDGFRalpha regulates follicular cell differentiation driving

treatment resistance and disease recurrence in papillary thyroid cancer. EBioMedicine 2016, 12, 86–97. [PubMed: 27682510]

(510). Ekpe-Adewuyi E; Lopez-Campistrous A; Tang X; Brindley DN; McMullen TP Platelet derived growth factor receptor alpha mediates nodal metastases in papillary thyroid cancer by driving the epithelial-mesenchymal transition. Oncotarget 2016, 7, 83684–83700. [PubMed: 27845909]

(511). Adewuyi EE; Deschenes J; Lopez-Campistrous A; Kattar MM; Ghosh S; McMullen TPW Autocrine activation of platelet-derived growth factor receptor alpha in metastatic papillary thyroid cancer. Hum. Pathol 2018, 75, 146–153. [PubMed: 29408504]

(512). Wagner M; Wuest M; Hamann I; Lopez-Campistrous A; McMullen TPW; Wuest F Molecular imaging of platelet-derived growth factor receptor-alpha (PDGFRalpha) in papillary thyroid cancer using immuno-PET. Nucl. Med. Biol 2018, 58, 51–58. [PubMed: 29367096]

(513). Mitsiades CS; Mitsiades NS; McMullan CJ; Poulaki V; Shringarpure R; Akiyama M; Hideshima T; Chauhan D; Joseph M; Libermann TA; et al. Inhibition of the insulin-like growth factor receptor-1 tyrosine kinase activity as a therapeutic strategy for multiple myeloma, other hematologic malignancies, and solid tumors. Cancer Cell 2004, 5, 221–230. [PubMed: 15050914]

(514). Belfiore A; Malaguarnera R; Vella V; Lawrence MC; Sciacca L; Frasca F; Morrione A; Vigneri R Insulin receptor isoforms in physiology and disease: an updated view. Endocr. Rev 2017, 38, 379–431. [PubMed: 28973479]

(515). Sun Y; Sun X; Shen B Molecular imaging of IGF-1R in cancer. Mol. Imaging 2017, 16, 1536012117736648. [PubMed: 29169312]

(516). Heskamp S; van Laarhoven HW; Molkenboer-Kuenen JD; Franssen GM; Versleijen-Jonkers YM; Oyen WJ; van der Graaf WT; Boerman OC ImmunoSPECT and immunoPET of IGF-1R expression with the radiolabeled antibody R1507 in a triple-negative breast cancer model. J. Nucl. Med 2010, 51, 1565–1572. [PubMed: 20847162]

(517). Hong H; Nayak TR; Shi S; Graves SA; Fliss BC; Barnhart TE; Cai W Generation and screening of monoclonal antibodies for immunoPET imaging of IGF1R in prostate cancer. Mol. Pharmaceutics 2014, 11, 3624–3630.

(518). England CG; Kamkaew A; Im HJ; Valdovinos HF; Sun H; Hernandez R; Cho SY; Dunphy EJ; Lee DS; Barnhart TE; et al. ImmunoPET imaging of insulin-Like growth factor 1 receptor in a subcutaneous mouse model of pancreatic cancer. Mol. Pharmaceutics 2016, 13, 1958–1966.

(519). Su X; Cheng K; Liu Y; Hu X; Meng S; Cheng Z PET imaging of insulin-like growth factor type 1 receptor expression with a 64Cu-labeled Affibody molecule. Amino Acids 2015, 47, 1409–1419. [PubMed: 25854877]

(520). Terwisscha van Scheltinga AG; Berghuis P; Nienhuis HH; Timmer-Bosscha H; Pot L; Gaykema SB; Lub-de Hooge MN; Kosterink JG; de Vries EG; Schroder CP Visualising dual downregulation of insulin-like growth factor receptor-1 and vascular endothelial growth factor-A by heat shock protein 90 inhibition effect in triple negative breast cancer. Eur. J. Cancer 2014, 50, 2508–2516. [PubMed: 25027745]

(521). You L; Wang X; Guo Z; Zhang D; Zhang P; Li J; Su X; Pan W; Zhang X MicroSPECT imaging of triple negative breast cancer cell tumor xenografted in athymic mice with radioiodinated anti-ICAM-1 monoclonal antibody. Appl. Radiat. Isot 2018, 139, 20–25. [PubMed: 29684714]

(522). Vugts DJ; Heuveling DA; Stigter-van Walsum M; Weigand S; Bergstrom M; van Dongen GA; Nayak TK Preclinical evaluation of 89Zr-labeled anti-CD44 monoclonal antibody RG7356 in mice and cynomolgus monkeys: Prelude to Phase 1 clinical studies. MAbs 2014, 6, 567–575. [PubMed: 24492295]

(523). Menke-van der Houven van Oordt CW; Gomez-Roca C; van Herpen C; Coveler AL; Mahalingam D; Verheul HM; van der Graaf WT; Christen R; Ruttinger D; Weigand S; et al. First-in-human phase I clinical trial of RG7356, an anti-CD44 humanized antibody, in patients with advanced, CD44-expressing solid tumors. Oncotarget 2016, 7, 80046–80058. [PubMed: 27507056]

(524). Jauw YWS; Huisman MC; Nayak TK; Vugts DJ; Christen R; Naegelen VM; Ruettinger D; Heil F; Lammertsma AA; Verheul HMW; et al. Assessment of target-mediated uptake with immuno-PET: analysis of a phase I clinical trial with an anti-CD44 antibody. EJNMMI Res 2018, 8, 6. [PubMed: 29356983]

(525). Zheleznyak A; Ikotun OF; Dimitry J; Frazier WA; Lapi SE Imaging of CD47 expression in xenograft and allograft tumor models. Mol. Imaging 2013, 12, 7290.2013.00069.

(526). Pan Y; Volkmer JP; Mach KE; Rouse RV; Liu JJ; Sahoo D; Chang TC; Metzner TJ; Kang L; van de Rijn M; et al. Endoscopic molecular imaging of human bladder cancer using a CD47 antibody. Sci. Transl. Med 2014, 6, 260ra148.

(527). Frost SH; Miller BW; Back TA; Santos EB; Hamlin DK; Knoblaugh SE; Frayo SL; Kenoyer AL; Storb R; Press OW; et al. Alpha-imaging confirmed efficient targeting of CD45-positive cells after 211At-radioimmunotherapy for hematopoietic cell transplantation. J. Nucl. Med 2015, 56, 1766–1773. [PubMed: 26338894]

(528). Bailly C; Gouard S; Lacombe M; Remaud-Le Saec P; Chalopin B; Bourgeois M; Chouin N; Tripier R; Halime Z; Haddad F; et al. Comparison of immuno-PET of CD138 and PET imaging with (64)CuCl2 and (18)F-FDG in a preclinical syngeneic model of multiple myeloma. Oncotarget 2018, 9, 9061–9072. [PubMed: 29507674]

(529). Navarro AS; Le Bihan T; Le Saec P; Bris NL; Bailly C; Sai-Maurel C; Bourgeois M; Cherel M; Tripier R; Faivre-Chauvet A TE1PA as innovating chelator for (64)Cu immuno-TEP imaging: a comparative in vivo study with DOTA/NOTA by conjugation on 9E7.4 mAb in a syngeneic multiple myeloma model. Bioconjugate Chem 2019, 30, 2393–2403.

(530). Rylova SN; Del Pozzo L; Klingeberg C; Tonnesmann R; Illert AL; Meyer PT; Maecke HR; Holland JP Immuno-PET imaging of CD30-positive lymphoma using 89Zr-desferrioxamine-labeled CD30-specific AC-10 antibody. J. Nucl. Med 2016, 57, 96–102. [PubMed: 26514172]

(531). England CG; Rui L; Cai W Lymphoma: current status of clinical and preclinical imaging with radiolabeled antibodies. Eur. J. Nucl. Med. Mol. Imaging 2017, 44, 517–532. [PubMed: 27844106]

(532). Kang L; Jiang D; Ehlerding EB; Barnhart TE; Ni D; Engle JW; Wang R; Huang P; Xu X; Cai W Noninvasive trafficking of brentuximab vedotin and PET imaging of CD30 in lung cancer murine models. Mol. Pharmaceutics 2018, 15, 1627–1634.

(533). Leget GA; Czuczman MS Use of rituximab, the new FDA-approved antibody. Curr. Opin. Oncol 1998, 10, 548–551. [PubMed: 9818234]

(534). Natarajan A; Gowrishankar G; Nielsen CH; Wang S; Iagaru A; Goris ML; Gambhir SS Positron emission tomography of 64Cu-DOTA-Rituximab in a transgenic mouse model expressing human CD20 for clinical translation to image NHL. Mol. Imaging Biol 2012, 14, 608–616. [PubMed: 22231277]

(535). Natarajan A; Gambhir SS Radiation dosimetry study of[(89)Zr]rituximab tracer for clinical translation of B cell NHL imaging using positron emission tomography. Mol. Imaging Biol 2015, 17, 539–547. [PubMed: 25500766]

(536). Muylle K; Flamen P; Vugts DJ; Guiot T; Ghanem G; Meuleman N; Bourgeois P; Vanderlinden B; van Dongen GA; Everaert H; et al. Tumour targeting and radiation dose of radioimmunotherapy with (90)Y-rituximab in CD20+ B-cell lymphoma as predicted by (89)Zr-rituximab immuno-PET: impact of preloading with unlabelled rituximab. Eur. J. Nucl. Med. Mol. Imaging 2015, 42, 1304–1314. [PubMed: 25792453]

(537). Olafsen T; Betting D; Kenanova VE; Salazar FB; Clarke P; Said J; Raubitschek AA; Timmerman JM; Wu AM Recombinant anti-CD20 antibody fragments for small-animal PET imaging of B-cell lymphomas. J. Nucl. Med 2009, 50, 1500–1508. [PubMed: 19690034]

(538). Freeman CL; Sehn LH A tale of two antibodies: obinutuzumab versus rituximab. Br. J. Haematol 2018, 182, 29–45. [PubMed: 29741753]

(539). Yoon JT; Longtine MS; Marquez-Nostra BV; Wahl RL Evaluation of next-generation anti-CD20 antibodies labeled with(89)Zr in human lymphoma xenografts. J. Nucl. Med 2018, 59, 1219–1224. [PubMed: 29348316]

(540). Zettlitz KA; Tavare R; Knowles SM; Steward KK; Timmerman JM; Wu AM ImmunoPET of malignant and normal B cells with (89)Zr- and (124)I-labeled obinutuzumab antibody fragments reveals differential CD20 internalization in vivo. Clin. Cancer Res 2017, 23, 7242–7252. [PubMed: 28928164]

(541). Tran L; Huitema AD; van Rijswijk MH; Dinant HJ; Baars JW; Beijnen JH; Vogel WV CD20 antigen imaging with (1)(2)(4)I-rituximab PET/CT in patients with rheumatoid arthritis. Hum. Antibodies 2011, 20, 29–35. [PubMed: 21558621]

(542). Bruijnen S; Tsang-A-Sjoe M; Raterman H; Ramwadhdoebe T; Vugts D; van Dongen G; Huisman M; Hoekstra O; Tak PP; Voskuyl A; van der Laken C B-cell imaging with zirconium-89 labelled rituximab PET-CT at baseline is associated with therapeutic response 24 weeks after initiation of rituximab treatment in rheumatoid arthritis patients. Arthritis Res. Ther 2016, 18, 266. [PubMed: 27863504]

(543). Laban KG; Kalmann R; Leguit RJ; de Keizer B Zirconium-89-labelled rituximab PET-CT in orbital inflammatory disease. EJNMMI Res 2019, 9, 69. [PubMed: 31363937]

(544). de Keizer B; Laban KG; Kalmann R Zirconium-89 labelled rituximab PET-CT imaging of Graves' orbitopathy. Eur. J. Nucl. Med. Mol. Imaging 2020, 47, 738–739.

(545). Adams H; van de Garde EM; van Moorsel CH; Vugts DJ; van Dongen GA; Grutters JC; Keijsers RG [(89)Zr]Zrrituximab PET/CT activity in patients with therapy refractory interstitial pneumonitis: a feasibility study. Am. J. Nucl. Med. Mol. Imaging 2019, 9, 296–308. [PubMed: 31976159]

(546). van de Donk NW; Janmaat ML; Mutis T; Lammerts van Bueren JJ; Ahmadi T; Sasser AK; Lokhorst HM; Parren PW Monoclonal antibodies targeting CD38 in hematological malignancies and beyond. Immunol. Rev 2016, 270, 95–112. [PubMed: 26864107]

(547). Morandi F; Horenstein AL; Costa F; Giuliani N; Pistoia V; Malavasi F CD38: a target for immunotherapeutic approaches in multiple myeloma. Front. Immunol 2018, 9, 2722. [PubMed: 30546360]

(548). Lokhorst HM; Plesner T; Laubach JP; Nahi H; Gimsing P; Hansson M; Minnema MC; Lassen U; Krejcik J; Palumbo A; et al. Targeting CD38 with daratumumab monotherapy in multiple myeloma. N. Engl. J. Med 2015, 373, 1207–1219. [PubMed: 26308596]

(549). Caserta E; Chea J; Minnix M; Viola D; Vonderfecht S; Yazaki P; Crow D; Khalife J; Sanchez JF; Palmer JM; et al. Copper 64-labeled daratumumab as a PET/CT imaging tracer for multiple myeloma. Blood 2018, 131, 741–745. [PubMed: 29301755]

(550). Ghai A; Maji D; Cho N; Chanswangphuwana C; Rettig M; Shen D; DiPersio J; Akers W; Dehdashti F; Achilefu S; et al. Preclinical development of CD38-targeted [(89)Zr]Zr-DFO-daratumumab for imaging multiple myeloma. J. Nucl. Med 2018, 59, 216–222. [PubMed: 29025987]

(551). Ehlerding EB; England CG; Jiang D; Graves SA; Kang L; Lacognata S; Barnhart TE; Cai W CD38 as a PET imaging target in lung cancer. Mol. Pharmaceutics 2017, 14, 2400–2406.

(552). Kang L; Jiang D; England CG; Barnhart TE; Yu B; Rosenkrans ZT; Wang R; Engle JW; Xu X; Huang P; et al. ImmunoPET imaging of CD38 in murine lymphoma models using(89)Zr-labeled daratumumab. Eur. J. Nucl. Med. Mol. Imaging 2018, 45, 1372–1381. [PubMed: 29450576]

(553). Li S; England CG; Ehlerding EB; Kutyreff CJ; Engle JW; Jiang D; Cai W ImmunoPET imaging of CD38 expression in hepatocellular carcinoma using 64Cu-labeled daratumumab. Am. J. Transl. Res 2019, 11, 6007–6015. [PubMed: 31632568]

(554). Li T; Qi S; Unger M; Hou YN; Deng QW; Liu J; Lam CMC; Wang XW; Xin D; Zhang P; et al. Immuno-targeting the multifunctional CD38 using nanobody. Sci. Rep 2016, 6, 27055. [PubMed: 27251573]

(555). Fumey W; Koenigsdorf J; Kunick V; Menzel S; Schutze K; Unger M; Schriewer L; Haag F; Adam G; Oberle A; et al. Nanobodies effectively modulate the enzymatic activity of CD38 and allow specific imaging of CD38(+) tumors in mouse models in vivo. Sci. Rep 2017, 7, 14289. [PubMed: 29084989]

(556). Oberle A; Brandt A; Alawi M; Langebrake C; Janjetovic S; Wolschke C; Schutze K; Bannas P; Kroger N; Koch-Nolte F; et al. Long-term CD38 saturation by daratumumab interferes with diagnostic myeloma cell detection. Haematologica 2017, 102, e368–e370. [PubMed: 28522580]

(557). Green DJ; Orgun NN; Jones JC; Hylarides MD; Pagel JM; Hamlin DK; Wilbur DS; Lin Y; Fisher DR; Kenoyer AL; et al. A preclinical model of CD38-pretargeted radioimmunotherapy for plasma cell malignancies. Cancer Res 2014, 74, 1179–1189. [PubMed: 24371230]

(558). Teiluf K; Seidl C; Blechert B; Gaertner FC; Gilbertz KP; Fernandez V; Bassermann F; Endell J; Boxhammer R; Leclair S; et al. alpha-Radioimmunotherapy with (2)(1)(3)Bi-anti-CD38 immunoconjugates is effective in a mouse model of human multiple myeloma. Oncotarget 2015, 6, 4692–4703. [PubMed: 25576914]

(559). O'Steen S; Comstock ML; Orozco JJ; Hamlin DK; Wilbur DS; Jones JC; Kenoyer A; Nartea ME; Lin Y; Miller BW; et al. The alpha-emitter astatine-211 targeted to CD38 can eradicate multiple myeloma in a disseminated disease model. Blood 2019, 134, 1247–1256. [PubMed: 31395601]

(560). Green DJ; O'Steen S; Lin Y; Comstock ML; Kenoyer AL; Hamlin DK; Wilbur DS; Fisher DR; Nartea M; Hylarides MD; et al. CD38-bispecific antibody pretargeted radioimmunotherapy for multiple myeloma and other B-cell malignancies. Blood 2018, 131, 611–620. [PubMed: 29158362]

(561). Jamet B; Bailly C; Carlier T; Touzeau C; Nanni C; Zamagni E; Barre L; Michaud AV; Cherel M; Moreau P; et al. Interest of PET imaging in multiple myeloma. Front. Med 2019, 6, 69.

(562). Wang Z; Yan X CD146, a multi-functional molecule beyond adhesion. Cancer Lett 2013, 330, 150–162. [PubMed: 23266426]

(563). Jiang T; Zhuang J; Duan H; Luo Y; Zeng Q; Fan K; Yan H; Lu D; Ye Z; Hao J; et al. CD146 is a coreceptor for VEGFR-2 in tumor angiogenesis. Blood 2012, 120, 2330–2339. [PubMed: 22718841]

(564). Yan X; Lin Y; Yang D; Shen Y; Yuan M; Zhang Z; Li P; Xia H; Li L; Luo D; et al. A novel anti-CD146 monoclonal antibody, AA98, inhibits angiogenesis and tumor growth. Blood 2003, 102, 184–191. [PubMed: 12609848]

(565). Bu P; Gao L; Zhuang J; Feng J; Yang D; Yan X Anti-CD146 monoclonal antibody AA98 inhibits angiogenesis via suppression of nuclear factor-kappaB activation. Mol. Cancer Ther 2006, 5, 2872–2878. [PubMed: 17121934]

(566). Ma X; Liu J; Wu J; Yan X; Wu P; Liu Y; Li S; Tian Y; Cao Y; Chen G; et al. Synergistic killing effect between vorinostat and target of CD146 in malignant cells. Clin. Cancer Res 2010, 16, 5165–5176. [PubMed: 20884621]

(567). Zeng Q; Li W; Lu D; Wu Z; Duan H; Luo Y; Feng J; Yang D; Fu L; Yan X CD146, an epithelial-mesenchymal transition inducer, is associated with triple-negative breast cancer. Proc. Natl. Acad. Sci. U. S. A 2012, 109, 1127–1132. [PubMed: 22210108]

(568). Van Cutsem E; Lambrechts D; Prenen H; Jain RK; Carmeliet P Lessons from the adjuvant bevacizumab trial on colon cancer: what next? J. Clin. Oncol 2011, 29, 1–4. [PubMed: 21115866]

(569). Yang Y; Hernandez R; Rao J; Yin L; Qu Y; Wu J; England CG; Graves SA; Lewis CM; Wang P; et al. Targeting CD146 with a 64Cu-labeled antibody enables in vivo immunoPET imaging of high-grade gliomas. Proc. Natl. Acad. Sci. U. S. A 2015, 112, E6525–6534. [PubMed: 26553993]

(570). Hernandez R; Sun H; England CG; Valdovinos HF; Barnhart TE; Yang Y; Cai W ImmunoPET imaging of CD146 expression in malignant brain tumors. Mol. Pharmaceutics 2016, 13, 2563–2570.

(571). Sun H; England CG; Hernandez R; Graves SA; Majewski RL; Kamkaew A; Jiang D; Barnhart TE; Yang Y; Cai W ImmunoPET for assessing the differential uptake of a CD146-specific monoclonal antibody in lung cancer. Eur. J. Nucl. Med. Mol. Imaging 2016, 43, 2169–2179. [PubMed: 27342417]

(572). England CG; Jiang D; Hernandez R; Sun H; Valdovinos HF; Ehlerding EB; Engle JW; Yang Y; Huang P; Cai W ImmunoPET imaging of CD146 in murine models of intrapulmonary metastasis of non-small cell lung cancer. Mol. Pharmaceutics 2017, 14, 3239–3247.

(573). Hernandez R; Sun H; England CG; Valdovinos HF; Ehlerding EB; Barnhart TE; Yang Y; Cai W CD146-targeted immunoPET and NIRF imaging of hepatocellular carcinoma with a dual-labeled monoclonal antibody. Theranostics 2016, 6, 1918–1933. [PubMed: 27570560]

(574). Seon BK; Haba A; Matsuno F; Takahashi N; Tsujie M; She X; Harada N; Uneda S; Tsujie T; Toi H; et al. Endoglin-targeted cancer therapy. Curr. Drug Delivery 2011, 8, 135–143.

(575). Dourado KMC; Baik J; Oliveira VKP; Beltrame M; Yamamoto A; Theuer CP; Figueiredo CAV; Verneris MR; Perlingeiro RCR Endoglin: a novel target for therapeutic intervention in acute leukemias revealed in xenograft mouse models. Blood 2017, 129, 2526–2536. [PubMed: 28351936]

(576). Saeednejad Zanjani L; Madjd Z; Abolhasani M; Shariftabrizi A; Rasti A; Asgari M Expression of CD105 cancer stem cell marker in three subtypes of renal cell carcinoma. Cancer Biomarkers 2018, 21, 821–837. [PubMed: 29286924]

(577). Rosen LS; Hurwitz HI; Wong MK; Goldman J; Mendelson DS; Figg WD; Spencer S; Adams BJ; Alvarez D; Seon BK; et al. A phase I first-in-human study of TRC105 (Anti-Endoglin Antibody) in patients with advanced cancer. Clin. Cancer Res 2012, 18, 4820–4829. [PubMed: 22767667]

(578). Gordon MS; Robert F; Matei D; Mendelson DS; Goldman JW; Chiorean EG; Strother RM; Seon BK; Figg WD; Peer CJ; et al. An open-label phase Ib dose-escalation study of TRC105 (anti-endoglin antibody) with bevacizumab in patients with advanced cancer. Clin. Cancer Res 2014, 20, 5918–5926. [PubMed: 25261556]

(579). Karzai FH; Apolo AB; Cao L; Madan RA; Adelberg DE; Parnes H; McLeod DG; Harold N; Peer C; Yu Y; et al. A phase I study of TRC105 anti-endoglin (CD105) antibody in metastatic castration-resistant prostate cancer. BJU Int 2015, 116, 546–555. [PubMed: 25407442]

(580). Duffy AG; Ma C; Ulahannan SV; Rahma OE; Makarova-Rusher O; Cao L; Yu Y; Kleiner DE; Trepel J; Lee MJ; et al. Phase I and preliminary phase II study of TRC105 in combination with sorafenib in hepatocellular carcinoma. Clin. Cancer Res 2017, 23, 4633–4641. [PubMed: 28465443]

(581). Dorff TB; Longmate JA; Pal SK; Stadler WM; Fishman MN; Vaishampayan UN; Rao A; Pinksi JK; Hu JS; Quinn DI; et al. Bevacizumab alone or in combination with TRC105 for patients with refractory metastatic renal cell cancer. Cancer 2017, 123, 4566–4573. [PubMed: 28832978]

(582). Hong H; Yang Y; Zhang Y; Engle JW; Barnhart TE; Nickles RJ; Leigh BR; Cai W Positron emission tomography imaging of CD105 expression during tumor angiogenesis. Eur. J. Nucl. Med. Mol. Imaging 2011, 38, 1335–1343. [PubMed: 21373764]

(583). Hong H; Severin GW; Yang Y; Engle JW; Zhang Y; Barnhart TE; Liu G; Leigh BR; Nickles RJ; Cai W Positron emission tomography imaging of CD105 expression with 89Zr-Df-TRC105. Eur. J. Nucl. Med. Mol. Imaging 2012, 39, 138–148. [PubMed: 21909753]

(584). Engle JW; Hong H; Zhang Y; Valdovinos HF; Myklejord DV; Barnhart TE; Theuer CP; Nickles RJ; Cai W Positron emission tomography imaging of tumor angiogenesis with a 66Ga-labeled monoclonal antibody. Mol. Pharmaceutics 2012, 9, 1441–1448.

(585). Hong H; Zhang Y; Severin GW; Yang Y; Engle JW; Niu G; Nickles RJ; Chen X; Leigh BR; Barnhart TE; et al. Multimodality imaging of breast cancer experimental lung metastasis with bioluminescence and a monoclonal antibody dual-labeled with 89Zr and IRDye 800CW. Mol. Pharmaceutics 2012, 9, 2339–2349.

(586). Zhang Y; Hong H; Severin GW; Engle JW; Yang Y; Goel S; Nathanson AJ; Liu G; Nickles RJ; Leigh BR; et al. ImmunoPET and near-infrared fluorescence imaging of CD105 expression using a monoclonal antibody dual-labeled with (89)Zr and IRDye 800CW. Am. J. Transl. Res 2012, 4, 333–346. [PubMed: 22937210]

(587). Zhang Y; Hong H; Nayak TR; Valdovinos HF; Myklejord DV; Theuer CP; Barnhart TE; Cai W Imaging tumor angiogenesis in breast cancer experimental lung metastasis with positron emission tomography, near-infrared fluorescence, and bioluminescence. Angiogenesis 2013, 16, 663–674. [PubMed: 23471463]

(588). Zhang Y; Hong H; Orbay H; Valdovinos HF; Nayak TR; Theuer CP; Barnhart TE; Cai W PET imaging of CD105/ endoglin expression with a (6)(1)/(6)(4)Cu-labeled Fab antibody fragment. Eur. J. Nucl. Med. Mol. Imaging 2013, 40, 759–767. [PubMed: 23344138]

(589). Hong H; Zhang Y; Orbay H; Valdovinos HF; Nayak TR; Bean J; Theuer CP; Barnhart TE; Cai W Positron emission tomography imaging of tumor angiogenesis with a (61/64)Cu-labeled F(ab′)(2) antibody fragment. Mol. Pharmaceutics 2013, 10, 709–716.

(590). Luo H; England CG; Shi S; Graves SA; Hernandez R; Liu B; Theuer CP; Wong HC; Nickles RJ; Cai W Dual targeting of tissue factor and CD105 for preclinical PET imaging of pancreatic cancer. Clin. Cancer Res 2016, 22, 3821–3830. [PubMed: 27026197]

(591). Luo H; England CG; Goel S; Graves SA; Ai F; Liu B; Theuer CP; Wong HC; Nickles RJ; Cai W ImmunoPET and near-Infrared fluorescence imaging of pancreatic cancer with a dual-labeled bispecific antibody fragment. Mol. Pharmaceutics 2017, 14, 1646–1655.

(592). Ehlerding EB; Lacognata S; Jiang D; Ferreira CA; Goel S; Hernandez R; Jeffery JJ; Theuer CP; Cai W Targeting angiogenesis for radioimmunotherapy with a (177)Lu-labeled antibody. Eur. J. Nucl. Med. Mol. Imaging 2018, 45, 123–131. [PubMed: 28821931]

(593). Bockhorn M; Tsuzuki Y; Xu L; Frilling A; Broelsch CE; Fukumura D Differential vascular and transcriptional responses to anti-vascular endothelial growth factor antibody in orthotopic human pancreatic cancer xenografts. Clin. Cancer. Res 2003, 9, 4221–4226. [PubMed: 14519649]

(594). Davis DW; Inoue K; Dinney CP; Hicklin DJ; Abbruzzese JL; McConkey DJ Regional effects of an antivascular endothelial growth factor receptor monoclonal antibody on receptor phosphorylation and apoptosis in human 253J B-V bladder cancer xenografts. Cancer Res 2004, 64, 4601–4610. [PubMed: 15231672]

(595). Sawada R; Sun SM; Wu X; Hong F; Ragupathi G; Livingston PO; Scholz WW Human monoclonal antibodies to sialyl-Lewis (CA19.9) with potent CDC, ADCC, and antitumor activity. Clin. Cancer Res 2011, 17, 1024–1032. [PubMed: 21343375]

(596). Viola-Villegas NT; Rice SL; Carlin S; Wu X; Evans MJ; Sevak KK; Drobjnak M; Ragupathi G; Sawada R; Scholz WW; et al. Applying PET to broaden the diagnostic utility of the clinically validated CA19.9 serum biomarker for oncology. J. Nucl. Med 2013, 54, 1876–1882. [PubMed: 24029655]

(597). Escorcia FE; Steckler JM; Abdel-Atti D; Price EW; Carlin SD; Scholz WW; Lewis JS; Houghton JL Tumor-specific Zr-89 immuno-PET imaging in a human bladder cancer model. Mol. Imaging Biol 2018, 20, 808–815. [PubMed: 29508263]

(598). Houghton JL; Zeglis BM; Abdel-Atti D; Aggeler R; Sawada R; Agnew BJ; Scholz WW; Lewis JS Site-specifically labeled CA19.9-targeted immunoconjugates for the PET, NIRF, and multimodal PET/NIRF imaging of pancreatic cancer. Proc. Natl. Acad. Sci. U. S. A 2015, 112, 15850–15855. [PubMed: 26668398]

(599). Houghton JL; Abdel-Atti D; Scholz WW; Lewis JS Preloading with unlabeled CA19.9 targeted human monoclonal antibody leads to improved PET imaging with (89)Zr-5B1. Mol. Pharmaceutics 2017, 14, 908–915.

(600). Houghton JL; Zeglis BM; Abdel-Atti D; Sawada R; Scholz WW; Lewis JS Pretargeted immuno-PET of pancreatic cancer: overcoming circulating antigen and internalized antibody to reduce radiation doses. J. Nucl. Med 2016, 57, 453–459. [PubMed: 26471693]

(601). Clarke-Pearson DL Clinical practice. screening for ovarian cancer. N. Engl. J. Med 2009, 361, 170–177. [PubMed: 19587342]

(602). Sharma SK; Wuest M; Wang M; Glubrecht D; Andrais B; Lapi SE; Wuest F Immuno-PET of epithelial ovarian cancer: harnessing the potential of CA125 for non-invasive imaging. EJNMMI Res 2014, 4, 60. [PubMed: 26116121]

(603). Sharma SK; Sevak KK; Monette S; Carlin SD; Knight JC; Wuest FR; Sala E; Zeglis BM; Lewis JS Preclinical 89Zr immuno-PET of high-grade serous ovarian cancer and lymph node metastasis. J. Nucl. Med 2016, 57, 771–776. [PubMed: 26837339]

(604). Crawford A; Haber L; Kelly MP; Vazzana K; Canova L; Ram P; Pawashe A; Finney J; Jalal S; Chiu D; et al. A Mucin 16 bispecific T cell-engaging antibody for the treatment of ovarian cancer. Sci. Transl. Med 2019, 11, eaau7534. [PubMed: 31217340]

(605). Bander NH Technology insight: monoclonal antibody imaging of prostate cancer. Nat. Clin. Pract. Urol 2006, 3, 216–225. [PubMed: 16607370]

(606). Maurer T; Eiber M; Schwaiger M; Gschwend JE Current use of PSMA-PET in prostate cancer management. Nat. Rev. Urol 2016, 13, 226–235. [PubMed: 26902337]

(607). Donin NM; Reiter RE Why Targeting PSMA is a game changer in the management of prostate cancer. J. Nucl. Med 2018, 59, 177–182. [PubMed: 28986509]

(608). Wustemann T; Haberkorn U; Babich J; Mier W Targeting prostate cancer: prostate-specific membrane antigen based diagnosis and therapy. Med. Res. Rev 2019, 39, 40–69. [PubMed: 29771460]

(609). Kaittanis C; Andreou C; Hieronymus H; Mao N; Foss CA; Eiber M; Weirich G; Panchal P; Gopalan A; Zurita J; et al. Prostate-specific membrane antigen cleavage of vitamin B9 stimulates oncogenic signaling through metabotropic glutamate receptors. J. Exp. Med 2018, 215, 159–175. [PubMed: 29141866]

(610). Lutje S; Heskamp S; Cornelissen AS; Poeppel TD; van den Broek SAMW; Rosenbaum-Krumme S; Bockisch A; Gotthardt M; Rijpkema M; Boerman OC PSMA ligands for radionuclide imaging and therapy of prostate cancer: clinical status. Theranostics 2015, 5, 1388–1401. [PubMed: 26681984]

(611). Afshar-Oromieh A; Babich JW; Kratochwil C; Giesel FL; Eisenhut M; Kopka K; Haberkorn U The rise of PSMA ligands for diagnosis and therapy of prostate cancer. J. Nucl. Med 2016, 57, 79S–89S. [PubMed: 27694178]

(612). Ceci F; Herrmann K; Hadaschik B; Castellucci P; Fanti S Therapy assessment in prostate cancer using choline and PSMA PET/CT. Eur. J. Nucl. Med. Mol. Imaging 2017, 44, 78–83. [PubMed: 28540419]

(613). Sheikhbahaei S; Afshar-Oromieh A; Eiber M; Solnes LB; Javadi MS; Ross AE; Pienta KJ; Allaf ME; Haberkorn U; Pomper MG; et al. Pearls and pitfalls in clinical interpretation of prostate-specific membrane antigen (PSMA)-targeted PET imaging. Eur. J. Nucl. Med. Mol. Imaging 2017, 44, 2117–2136. [PubMed: 28765998]

(614). Liu H; Moy P; Kim S; Xia Y; Rajasekaran A; Navarro V; Knudsen B; Bander NH Monoclonal antibodies to the extracellular domain of prostate-specific membrane antigen also react with tumor vascular endothelium. Cancer Res 1997, 57, 3629–3634. [PubMed: 9288760]

(615). Chang SS; Reuter VE; Heston WD; Bander NH; Grauer LS; Gaudin PB Five different anti-prostate-specific membrane antigen (PSMA) antibodies confirm PSMA expression in tumor-associated neovasculature. Cancer Res 1999, 59, 3192–3198. [PubMed: 10397265]

(616). Liu H; Rajasekaran AK; Moy P; Xia Y; Kim S; Navarro V; Rahmati R; Bander NH Constitutive and antibody-induced internalization of prostate-specific membrane antigen. Cancer Res 1998, 58, 4055–4060. [PubMed: 9751609]

(617). Milowsky MI; Nanus DM; Kostakoglu L; Vallabhajosula S; Goldsmith SJ; Bander NH Phase I trial of yttrium-90-labeled anti-prostate-specific membrane antigen monoclonal antibody J591 for androgen-independent prostate cancer. J. Clin. Oncol 2004, 22, 2522–2531. [PubMed: 15173215]

(618). Tagawa ST; Milowsky MI; Morris M; Vallabhajosula S; Christos P; Akhtar NH; Osborne J; Goldsmith SJ; Larson S; Taskar NP; et al. Phase II study of lutetium-177-labeled anti-prostate-specific membrane antigen monoclonal antibody J591 for metastatic castration-resistant prostate cancer. Clin. Cancer Res 2013, 19, 5182–5191. [PubMed: 23714732]

(619). Pandit-Taskar N; O'Donoghue JA; Beylergil V; Lyashchenko S; Ruan S; Solomon SB; Durack JC; Carrasquillo JA; Lefkowitz RA; Gonen M; et al. (8)(9)ZrhuJ591 immuno-PET imaging in patients with advanced metastatic prostate cancer. Eur. J. Nucl. Med. Mol. Imaging 2014, 41, 2093–2105. [PubMed: 25143071]

(620). Pandit-Taskar N; O'Donoghue JA; Durack JC; Lyashchenko SK; Cheal SM; Beylergil V; Lefkowitz RA; Carrasquillo JA; Martinez DF; Fung AM; et al. A phase I/II study for analytic validation of 89Zr-J591 immunoPET as a molecular imaging agent for metastatic prostate cancer. Clin. Cancer Res 2015, 21, 5277–5285. [PubMed: 26175541]

(621). Pandit-Taskar N; O'Donoghue JA; Divgi CR; Wills EA; Schwartz L; Gonen M; Smith-Jones P; Bander NH; Scher HI; Larson SM; Morris MJ Indium 111-labeled J591 anti-PSMA antibody for vascular targeted imaging in progressive solid tumors. EJNMMI Res 2015, 5, 28. [PubMed: 25984435]

(622). Fung EK; Cheal SM; Fareedy SB; Punzalan B; Beylergil V; Amir J; Chalasani S; Weber WA; Spratt DE; Veach DR; et al. Targeting of radiolabeled J591 antibody to PSMA-expressing tumors: optimization of imaging and therapy based on non-linear compartmental modeling. EJNMMI Res 2016, 6, 7. [PubMed: 26801327]

(623). Petronis JD; Regan F; Lin K Indium-111 capromab pendetide (ProstaScint) imaging to detect recurrent and metastatic prostate cancer. Clin. Nucl. Med 1998, 23, 672–677. [PubMed: 9790041]

(624). Deb N; Goris M; Trisler K; Fowler S; Saal J; Ning S; Becker M; Marquez C; Knox S Treatment of hormone-refractory prostate cancer with 90Y-CYT-356 monoclonal antibody. Clin. Cancer. Res 1996, 2, 1289–1297. [PubMed: 9816299]

(625). Tagawa ST; Beltran H; Vallabhajosula S; Goldsmith SJ; Osborne J; Matulich D; Petrillo K; Parmar S; Nanus DM; Bander NH Anti-prostate-specific membrane antigen-based radioimmunotherapy for prostate cancer. Cancer 2010, 116, 1075–1083. [PubMed: 20127956]

(626). Lutje S; Rijpkema M; Franssen GM; Fracasso G; Helfrich W; Eek A; Oyen WJ; Colombatti M; Boerman OC Dual-modality image-guided surgery of prostate cancer with a radiolabeled fluorescent anti-PSMA monoclonal antibody. J. Nucl. Med 2014, 55, 995–1001. [PubMed: 24700882]

(627). Lutje S; Gerrits D; Molkenboer-Kuenen JD; Herrmann K; Fracasso G; Colombatti M; Boerman OC; Heskamp S Characterization of site-specifically conjugated monomethyl auristatin E- and duocarmycin-based anti-PSMA antibody-drug conjugates for treatment of PSMA-expressing tumors. J. Nucl. Med 2018, 59, 494–501. [PubMed: 29146698]

(628). Novakova Z; Foss CA; Copeland BT; Morath V; Baranova P; Havlinova B; Skerra A; Pomper MG; Barinka C Novel monoclonal antibodies recognizing human prostate-specific membrane antigen (PSMA) as research and theranostic Tools. Prostate 2017, 77, 749–764. [PubMed: 28247415]

(629). Banerjee SR; Kumar V; Lisok A; Plyku D; Novakova Z; Brummet M; Wharram B; Barinka C; Hobbs R; Pomper MG Evaluation of (111)In-DOTA-5D3, a surrogate SPECT imaging agent for radioimmunotherapy of prostate-specific membrane antigen. J. Nucl. Med 2019, 60, 400–406. [PubMed: 30237212]

(630). Chatalic KL; Veldhoven-Zweistra J; Bolkestein M; Hoeben S; Koning GA; Boerman OC; de Jong M; van Weerden WM A Novel (1)(1)(1)In-labeled anti-prostate-specific membrane antigen nanobody for targeted SPECT/CT imaging of prostate cancer. J. Nucl. Med 2015, 56, 1094–1099. [PubMed: 25977460]

(631). Nawaz S; Mullen GED; Sunassee K; Bordoloi J; Blower PJ; Ballinger JR Simple, mild, one-step labelling of proteins with gallium-68 using a tris(hydroxypyridinone) bifunctional chelator: a (68)Ga-THP-scFv targeting the prostate-specific membrane antigen. EJNMMI Res 2017, 7, 86. [PubMed: 29067565]

(632). Viola-Villegas NT; Sevak KK; Carlin SD; Doran MG; Evans HW; Bartlett DW; Wu AM; Lewis JS Noninvasive Imaging of PSMA in prostate tumors with (89)Zr-Labeled huJ591 engineered antibody fragments: the faster alternatives. Mol. Pharmaceutics 2014, 11, 3965–3973.

(633). Pandit-Taskar N; O'Donoghue JA; Ruan S; Lyashchenko SK; Carrasquillo JA; Heller G; Martinez DF; Cheal SM; Lewis JS; Fleisher M; et al. First-in-human imaging with 89Zr-Df-IAB2M anti-PSMA minibody in patients with metastatic prostate cancer: pharmacokinetics, biodistribution, dosimetry, and lesion uptake. J. Nucl. Med 2016, 57, 1858–1864. [PubMed: 27516450]

(634). Joraku A; Hatano K; Kawai K; Kandori S; Kojima T; Fukumitsu N; Isobe T; Mori Y; Sakata M; Hara T; et al. Phase I/IIa PET imaging study with (89)zirconium labeled anti-PSMA minibody for urological malignancies. Ann. Nucl. Med 2019, 33, 119–127. [PubMed: 30406361]

(635). Langbein T; Chausse G; Baum RP Salivary gland toxicity of PSMA radioligand therapy: relevance and preventive strategies. J. Nucl. Med 2018, 59, 1172–1173. [PubMed: 29903929]

(636). Elsasser-Beile U; Wolf P; Gierschner D; Buhler P; Schultze-Seemann W; Wetterauer U A new generation of monoclonal and recombinant antibodies against cell-adherent prostate specific membrane antigen for diagnostic and therapeutic targeting of prostate cancer. Prostate 2006, 66, 1359–1370. [PubMed: 16894535]

(637). Elsasser-Beile U; Reischl G; Wiehr S; Buhler P; Wolf P; Alt K; Shively J; Judenhofer MS; Machulla HJ; Pichler BJ PET imaging of prostate cancer xenografts with a highly specific antibody against the prostate-specific membrane antigen. J. Nucl. Med 2009, 50, 606–611. [PubMed: 19289418]

(638). Alt K; Wiehr S; Ehrlichmann W; Reischl G; Wolf P; Pichler BJ; Elsasser-Beile U; Buhler P High-resolution animal PET imaging of prostate cancer xenografts with three different 64Cu-labeled antibodies against native cell-adherent PSMA. Prostate 2010, 70, 1413–1421. [PubMed: 20687214]

(639). Wiehr S; Buhler P; Gierschner D; Wolf P; Rolle AM; Kesenheimer C; Pichler BJ; Elsasser-Beile U Pharmacokinetics and PET imaging properties of two recombinant anti-PSMA antibody fragments in comparison to their parental antibody. Prostate 2014, 74, 743–755. [PubMed: 24610028]

(640). Rowe SP; Gorin MA; Pomper MG Imaging of prostate-specific membrane antigen with small-molecule PET radiotracers: from the bench to advanced clinical applications. Annu. Rev. Med 2019, 70, 461–477. [PubMed: 30691373]

(641). Salas Fragomeni RA; Amir T; Sheikhbahaei S; Harvey SC; Javadi MS; Solnes LB; Kiess AP; Allaf ME; Pomper MG; Gorin MA; et al. Imaging of nonprostate cancers using PSMA-targeted radiotracers: rationale, current state of the field, and a Call to Arms. J. Nucl. Med 2018, 59, 871–877. [PubMed: 29545375]

(642). Malik D; Kumar R; Mittal BR; Singh H; Bhattacharya A; Singh SK 68Ga-labeled PSMA uptake in nonprostatic malignancies: has the time come to remove “PS” From PSMA? Clin. Nucl. Med 2018, 43, 529–532. [PubMed: 29688950]

(643). Silver DA; Pellicer I; Fair WR; Heston WD; Cordon-Cardo C Prostate-specific membrane antigen expression in normal and malignant human tissues. Clin. Cancer. Res 1997, 3, 81–85. [PubMed: 9815541]

(644). Chang SS; O’Keefe DS; Bacich DJ; Reuter VE; Heston WD; Gaudin PB Prostate-specific membrane antigen is produced in tumor-associated neovasculature. Clin. Cancer. Res 1999, 5, 2674–2681. [PubMed: 10537328]

(645). Matsuda M; Ishikawa E; Yamamoto T; Hatano K; Joraku A; Iizumi Y; Masuda Y; Nishiyama H; Matsumura A Potential use of prostate specific membrane antigen (PSMA) for detecting the tumor neovasculature of brain tumors by PET imaging with (89)Zr-Df-IAB2M anti-PSMA minibody. J. Neuro-Oncol 2018, 138, 581–589.

(646). Milowsky MI; Nanus DM; Kostakoglu L; Sheehan CE; Vallabhajosula S; Goldsmith SJ; Ross JS; Bander NH Vascular targeted therapy with anti-prostate-specific membrane antigen monoclonal antibody J591 in advanced solid tumors. J. Clin. Oncol 2007, 25, 540–547. [PubMed: 17290063]

(647). Beauchemin N; Arabzadeh A Carcinoembryonic antigen-related cell adhesion molecules (CEACAMs) in cancer progression and metastasis. Cancer Metastasis Rev 2013, 32, 643–671. [PubMed: 23903773]

(648). Moffat FL Jr.; Pinsky CM; Hammershaimb L; Petrelli NJ; Patt YZ; Whaley FS; Goldenberg DM Clinical utility of external immunoscintigraphy with the IMMU-4 technetium-99m Fab′ antibody fragment in patients undergoing surgery for carcinoma of the colon and rectum: results of a pivotal, phase III trial. the immunomedics study group. J. Clin. Oncol 1996, 14, 2295–2305. [PubMed: 8708720]

(649). Sharkey RM; Cardillo TM; Rossi EA; Chang CH; Karacay H; McBride WJ; Hansen HJ; Horak ID; Goldenberg DM Signal amplification in molecular imaging by pretargeting a multivalent, bispecific antibody. Nat. Med 2005, 11, 1250–1255. [PubMed: 16258537]

(650). Schoffelen R; Sharkey RM; Goldenberg DM; Franssen G; McBride WJ; Rossi EA; Chang CH; Laverman P; Disselhorst JA; Eek A; et al. Pretargeted immuno-positron emission tomography imaging of carcinoembryonic antigen-expressing tumors with a bispecific antibody and a 68Ga- and 18F-labeled hapten peptide in mice with human tumor xenografts. Mol. Cancer Ther 2010, 9, 1019–1027. [PubMed: 20354120]

(651). Schoffelen R; van der Graaf WT; Sharkey RM; Franssen GM; McBride WJ; Chang CH; Laverman P; Goldenberg DM; Oyen WJ; Boerman OC Pretargeted immuno-PET of CEA-expressing intraperitoneal human colonic tumor xenografts: a new sensitive detection method. EJNMMI Res 2012, 2, 5. [PubMed: 22284761]

(652). Foubert F; Gouard S; Sai-Maurel C; Cherel M; Faivre-Chauvet A; Goldenberg DM; Barbet J; Bailly C; Bodet-Milin C; Carlier T; et al. Sensitivity of pretargeted immunoPET using(68)Ga-peptide to detect colonic carcinoma liver metastases in a murine xenograft model: Comparison with (18)FDG PET-CT. Oncotarget 2018, 9, 27502–27513. [PubMed: 29938001]

(653). Hall H; Velikyan I; Blom E; Ulin J; Monazzam A; Pahlman L; Micke P; Wanders A; McBride W; Goldenberg DM; et al. In vitro autoradiography of carcinoembryonic antigen in tissue from patients with colorectal cancer using multifunctional antibody TF2 and (67/68Ga)-labeled

haptens by pretargeting. Am. J. Nucl. Med. Mol. Imaging 2012, 2, 141–150. [PubMed: 23133809]

(654). Bodet-Milin C; Faivre-Chauvet A; Carlier T; Rauscher A; Bourgeois M; Cerato E; Rohmer V; Couturier O; Drui D; Goldenberg DM; et al. Immuno-PET using anticarcinoembryonic antigen bispecific antibody and 68Ga-labeled peptide in metastatic medullary thyroid carcinoma: clinical optimization of the pretargeting parameters in a first-in-human trial. J. Nucl. Med 2016, 57, 1505–1511. [PubMed: 27230928]

(655). Wu AM; Yazaki PJ; Tsai S; Nguyen K; Anderson AL; McCarthy DW; Welch MJ; Shively JE; Williams LE; Raubitschek AA; et al. High-resolution microPET imaging of carcinoembryonic antigen-positive xenografts by using a copper-64-labeled engineered antibody fragment. Proc. Natl. Acad. Sci. U. S. A 2000, 97, 8495–8500. [PubMed: 10880576]

(656). Sundaresan G; Yazaki PJ; Shively JE; Finn RD; Larson SM; Raubitschek AA; Williams LE; Chatziioannou AF; Gambhir SS; Wu AM 124I-labeled engineered anti-CEA minibodies and diabodies allow high-contrast, antigen-specific small-animal PET imaging of xenografts in athymic mice. J. Nucl. Med 2003, 44, 1962–1969. [PubMed: 14660722]

(657). Li L; Yazaki PJ; Anderson AL; Crow D; Colcher D; Wu AM; Williams LE; Wong JY; Raubitschek A; Shively JE Improved biodistribution and radioimmunoimaging with poly-(ethylene glycol)-DOTA-conjugated anti-CEA diabody. Bioconjugate Chem 2006, 17, 68–76.

(658). Kenanova V; Olafsen T; Crow DM; Sundaresan G; Subbarayan M; Carter NH; Ikle DN; Yazaki PJ; Chatziioannou AF; Gambhir SS; et al. Tailoring the pharmacokinetics and positron emission tomography imaging properties of anti-carcinoembryonic antigen single-chain Fv-Fc antibody fragments. Cancer Res 2005, 65, 622–631. [PubMed: 15695407]

(659). Girgis MD; Olafsen T; Kenanova V; McCabe KE; Wu AM; Tomlinson JS Targeting CEA in pancreas cancer xenografts with a mutated scFv-Fc antibody fragment. EJNMMI Res 2011, 1, 24. [PubMed: 22214289]

(660). Lutje S; Franssen GM; Sharkey RM; Laverman P; Rossi EA; Goldenberg DM; Oyen WJ; Boerman OC; McBride WJ Anti-CEA antibody fragments labeled with [(18)F]AlF for PET imaging of CEA-expressing tumors. Bioconjugate Chem 2014, 25, 335–341.

(661). Osada T; Hsu D; Hammond S; Hobeika A; Devi G; Clay TM; Lyerly HK; Morse MA Metastatic colorectal cancer cells from patients previously treated with chemotherapy are sensitive to T-cell killing mediated by CEA/CD3-bispecific T-cell-engaging BiTE antibody. Br. J. Cancer 2010, 102, 124–133. [PubMed: 19953093]

(662). Pishvaian M; Morse MA; McDevitt J; Norton JD; Ren S; Robbie GJ; Ryan PC; Soukharev S; Bao H; Denlinger CS Phase 1 dose escalation study of MEDI-565, a bispecific T-cell engager that targets human carcinoembryonic antigen, in patients with advanced gastrointestinal adenocarcinomas. Clin. Colorectal Cancer 2016, 15, 345–351. [PubMed: 27591895]

(663). Waaijer SJH; Warnders FJ; Stienen S; Friedrich M; Sternjak A; Cheung HK; van Scheltinga A; Schroder CP; de Vries EGE; Lub-de Hooge MN Molecular imaging of radiolabeled bispecific T-cell engager (89)Zr-AMG211 targeting CEA-positive tumors. Clin. Cancer Res 2018, 24, 4988–4996. [PubMed: 29980531]

(664). Moek KL; Waaijer SJH; Kok IC; Suurs FV; Brouwers AH; Menke-van der Houven van Oordt CW; Wind TT; Gietema JA; Schroder CP; Mahesh SVK; et al. 89)Zr-labeled bispecific T-cell engager AMG 211 PET shows AMG 211 accumulation in CD3-rich tissues and clear, heterogeneous tumor Uptake. Clin. Cancer Res 2019, 25, 3517–3527. [PubMed: 30745297]

(665). Klein C; Waldhauer I; Nicolini VG; Freimoser-Grundschober A; Nayak T; Vugts DJ; Dunn C; Bolijn M; Benz J; Stihle M; et al. Cergutuzumab amunaleukin (CEA-IL2v), a CEA-targeted IL-2 variant-based immunocytokine for combination cancer immunotherapy: Overcoming limitations of aldesleukin and conventional IL-2-based immunocytokines. Oncoimmunology 2017, 6, e1277306. [PubMed: 28405498]

(666). van Brummelen EMJ; Huisman MC; de Wit-van der Veen LJ; Nayak TK; Stokkel MPM; Mulder ER; Hoekstra OS; Vugts DJ; Van Dongen G; Verheul HM; et al. (89)Zr-labeled CEA-targeted IL-2 variant immunocytokine in patients with solid tumors: CEA-mediated tumor accumulation and role of IL-2 receptor-binding. Oncotarget 2018, 9, 24737–24749. [PubMed: 29872502]

(667). Corbet C; Feron O Tumour acidosis: from the passenger to the driver's seat. Nat. Rev. Cancer 2017, 17, 577–593. [PubMed: 28912578]

(668). Supuran CT; Alterio V; Di Fiore A; D'Ambrosio K; Carta F; Monti SM; De Simone G Inhibition of carbonic anhydrase IX targets primary tumors, metastases, and cancer stem cells: Three for the price of one. Med. Res. Rev 2018, 38, 1799–1836. [PubMed: 29635752]

(669). Oosterwijk-Wakka JC; Boerman OC; Mulders PF; Oosterwijk E Application of monoclonal antibody G250 recognizing carbonic anhydrase IX in renal cell carcinoma. Int. J. Mol. Sci 2013, 14, 11402–11423. [PubMed: 23759990]

(670). Lau J; Lin KS; Benard F Past, Present, and Future: Development of theranostic agents targeting carbonic anhydrase IX. Theranostics 2017, 7, 4322–4339. [PubMed: 29158829]

(671). Lawrentschuk N; Lee FT; Jones G; Rigopoulos A; Mountain A; O'Keefe G; Papenfuss AT; Bolton DM; Davis ID; Scott AM Investigation of hypoxia and carbonic anhydrase IX expression in a renal cell carcinoma xenograft model with oxygen tension measurements and (1)(2)(4)I-cG250 PET/CT. Urol. Oncol 2011, 29, 411–420. [PubMed: 19523858]

(672). Stillebroer AB; Franssen GM; Mulders PF; Oyen WJ; van Dongen GA; Laverman P; Oosterwijk E; Boerman OC ImmunoPET imaging of renal cell carcinoma with (124)I- and(89)Zr-labeled anti-CAIX monoclonal antibody cG250 in mice. Cancer Biother.Radiopharm 2013, 28, 510–515. [PubMed: 23697926]

(673). Cheal SM; Punzalan B; Doran MG; Evans MJ; Osborne JR; Lewis JS; Zanzonico P; Larson SM Pairwise comparison of 89Zr- and 124I-labeled cG250 based on positron emission tomography imaging and nonlinear immunokinetic modeling: in vivo carbonic anhydrase IX receptor binding and internalization in mouse xenografts of clear-cell renal cell carcinoma. Eur. J. Nucl. Med. Mol. Imaging 2014, 41, 985–994. [PubMed: 24604591]

(674). Hekman MCH; Rijpkema M; Aarntzen EH; Mulder SF; Langenhuijsen JF; Oosterwijk E; Boerman OC; Oyen WJG; Mulders PFA Positron emission tomography/computed tomography with (89)Zr-girentuximab can aid in diagnostic dilemmas of clear cell renal cell carcinoma suspicion. Eur. Urol 2018, 74, 257–260. [PubMed: 29730017]

(675). Pryma DA; O'Donoghue JA; Humm JL; Jungbluth AA; Old LJ; Larson SM; Divgi CR Correlation of in vivo and in vitro measures of carbonic anhydrase IX antigen expression in renal masses using antibody 124I-cG250. J. Nucl. Med 2011, 52, 535–540. [PubMed: 21421715]

(676). Povoski SP; Hall NC; Murrey DA Jr.; Sharp DS; Hitchcock CL; Mojzisik CM; Bahnson EE; Knopp MV; Martin EW Jr.; Bahnson RR Multimodal imaging and detection strategy with 124 I-labeled chimeric monoclonal antibody cG250 for accurate localization and confirmation of extent of disease during laparoscopic and open surgical resection of clear cell renal cell carcinoma. Surg. Innov 2013, 20, 59–69. [PubMed: 22455975]

(677). Jensen HK; Nordsmark M; Donskov F; Marcussen N; von der Maase H Immunohistochemical expression of carbonic anhydrase IX assessed over time and during treatment in renal cell carcinoma. BJU Int 2008, 101, 41–44. [PubMed: 18430123]

(678). Cepa A; Ralis J; Kral V; Paurova M; Kucka J; Humajova J; Laznicek M; Lebeda O In vitro evaluation of the monoclonal antibody (64)Cu-IgG M75 against human carbonic anhydrase IX and its in vivo imaging. Appl. Radiat. Isot 2018, 133, 9–13. [PubMed: 29272822]

(679). Cepa A; Ralis J; Maresova L; Kleinova M; Seifert D; Sieglova I; Kral V; Polasek M; Paurova M; Laznicek M; et al. Radiolabeling of the antibody IgG M75 for epitope of human carbonic anhydrase IX by (61)Cu and (64)Cu and its biological testing. Appl. Radiat. Isot 2019, 143, 87–97. [PubMed: 30391716]

(680). Ahlskog JK; Schliemann C; Marlind J; Qureshi U; Ammar A; Pedley RB; Neri D Human monoclonal antibodies targeting carbonic anhydrase IX for the molecular imaging of hypoxic regions in solid tumours. Br. J. Cancer 2009, 101, 645–657. [PubMed: 19623173]

(681). Zatovicova M; Jelenska L; Hulikova A; Csaderova L; Ditte Z; Ditte P; Goliasova T; Pastorek J; Pastorekova S Carbonic anhydrase IX as an anticancer therapy target: preclinical evaluation of internalizing monoclonal antibody directed to catalytic domain. Curr. Pharm. Des 2010, 16, 3255–3263. [PubMed: 20819068]

(682). Murri-Plesko MT; Hulikova A; Oosterwijk E; Scott AM; Zortea A; Harris AL; Ritter G; Old L; Bauer S; Swietach P; et al. Antibody inhibiting enzymatic activity of tumour-associated carbonic anhydrase isoform IX. Eur. J. Pharmacol 2011, 657, 173–183. [PubMed: 21315712]

(683). van Rij CM; Frielink C; Goldenberg DM; Sharkey RM; Lutje S; McBride WJ; Oyen WJ; Boerman OC Pretargeted radioimmunotherapy of prostate cancer with an anti-TROP-2xanti-HSG bispecific antibody and a (177)Lu-labeled peptide. Cancer Biother.Radiopharm 2014, 29, 323–329. [PubMed: 25226447]

(684). Goldenberg DM; Stein R; Sharkey RM The emergence of trophoblast cell-surface antigen 2 (TROP-2) as a novel cancer target. Oncotarget 2018, 9, 28989–29006. [PubMed: 29989029]

(685). Bardia A; Mayer IA; Vahdat LT; Tolaney SM; Isakoff SJ; Diamond JR; O'Shaughnessy J; Moroose RL; Santin AD; Abramson VG; et al. Sacituzumab Govitecan-hziy in refractory metastatic triple-negative breast cancer. N. Engl. J. Med 2019, 380, 741–751. [PubMed: 30786188]

(686). van Rij CM; Sharkey RM; Goldenberg DM; Frielink C; Molkenboer JD; Franssen GM; van Weerden WM; Oyen WJ; Boerman OC Imaging of prostate cancer with immuno-PET and immuno-SPECT using a radiolabeled anti-EGP-1 monoclonal antibody. J. Nucl. Med 2011, 52, 1601–1607. [PubMed: 21865288]

(687). Sharkey RM; van Rij CM; Karacay H; Rossi EA; Frielink C; Regino C; Cardillo TM; McBride WJ; Chang CH; Boerman OC; et al. A new Tri-Fab bispecific antibody for pretargeting Trop-2-expressing epithelial cancers. J. Nucl. Med 2012, 53, 1625–1632. [PubMed: 22952342]

(688). van Rij CM; Lutje S; Frielink C; Sharkey RM; Goldenberg DM; Franssen GM; McBride WJ; Rossi EA; Oyen WJ; Boerman OC Pretargeted immuno-PET and radioimmunotherapy of prostate cancer with an anti-TROP-2 x anti-HSG bispecific antibody. Eur. J. Nucl. Med. Mol. Imaging 2013, 40, 1377–1383. [PubMed: 23674207]

(689). Lutje S; Rijpkema M; Goldenberg DM; van Rij CM; Sharkey RM; McBride WJ; Franssen GM; Frielink C; Helfrich W; Oyen WJ; et al. Pretargeted dual-modality immuno-SPECT and near-infrared fluorescence imaging for image-guided surgery of prostate cancer. Cancer Res 2014, 74, 6216–6223. [PubMed: 25252911]

(690). van Rij CM; Frielink C; Goldenberg DM; Sharkey RM; Franssen GM; Lutje S; McBride WJ; Oyen WJ; Boerman OC Pretargeted immunoPET of prostate cancer with an anti-TROP-2 x anti-HSG bispecific antibody in mice with PC3 xenografts. Mol. Imaging Biol 2015, 17, 94–101. [PubMed: 25060065]

(691). Heist RS; Guarino MJ; Masters G; Purcell WT; Starodub AN; Horn L; Scheff RJ; Bardia A; Messersmith WA; Berlin J; et al. Therapy of advanced non-small-cell lung cancer with an SN-38-anti-Trop-2 drug conjugate, Sacituzumab Govitecan. J. Clin. Oncol 2017, 35, 2790–2797. [PubMed: 28548889]

(692). Batlle E; Clevers H Cancer stem cells revisited. Nat. Med 2017, 23, 1124–1134. [PubMed: 28985214]

(693). Medema JP Cancer stem cells: the challenges ahead. Nat. Cell Biol 2013, 15, 338–344. [PubMed: 23548926]

(694). Steinbichler TB; Dudas J; Skvortsov S; Ganswindt U; Riechelmann H; Skvortsova II. Therapy resistance mediated by cancer stem cells. Semin. Cancer Biol 2018, 53, 156–167. [PubMed: 30471331]

(695). Leung C; Tan SH; Barker N Recent advances in Lgr5(+) stem cell research. Trends Cell Biol 2018, 28, 380–391. [PubMed: 29477614]

(696). Azhdarinia A; Voss J; Ghosh SC; Simien JA; Hernandez Vargas S; Cui J; Yu WA; Liu Q; Carmon KS Evaluation of anti-LGR5 antibodies by immunoPET for imaging colorectal tumors and development of antibody-drug conjugates. Mol. Pharmaceutics 2018, 15, 2448–2454.

(697). Knowles SM; Zettlitz KA; Tavare R; Rochefort MM; Salazar FB; Stout DB; Yazaki PJ; Reiter RE; Wu AM Quantitative immunoPET of prostate cancer xenografts with 89Zrand 124I-labeled anti-PSCA A11 minibody. J. Nucl. Med 2014, 55, 452–459. [PubMed: 24504052]

(698). Knowles SM; Tavare R; Zettlitz KA; Rochefort MM; Salazar FB; Jiang ZK; Reiter RE; Wu AM Applications of immunoPET: using 124I-anti-PSCA A11 minibody for imaging disease progression and response to therapy in mouse xenograft models of prostate cancer. Clin. Cancer Res 2014, 20, 6367–6378. [PubMed: 25326233]

(699). Sonn GA; Behesnilian AS; Jiang ZK; Zettlitz KA; Lepin EJ; Bentolila LA; Knowles SM; Lawrence D; Wu AM; Reiter RE Fluorescent image-guided surgery with an anti-prostate stem

cell antigen (PSCA) diabody enables targeted resection of mouse prostate cancer xenografts in real time. Clin. Cancer Res 2016, 22, 1403–1412. [PubMed: 26490315]

(700). Tsai WK; Zettlitz KA; Tavare R; Kobayashi N; Reiter RE; Wu AM Dual-modality immunoPET/fluorescence imaging of prostate cancer with an anti-PSCA cys-minibody. Theranostics 2018, 8, 5903–5914. [PubMed: 30613270]

(701). Zettlitz KA; Tsai WK; Knowles SM; Kobayashi N; Donahue TR; Reiter RE; Wu AM Dual-modality immuno-PET and near-Infrared fluorescence imaging of pancreatic cancer using an anti-prostate stem cell antigen cys-diabody. J. Nucl. Med 2018, 59, 1398–1405. [PubMed: 29602820]

(702). Kemper K; Sprick MR; de Bree M; Scopelliti A; Vermeulen L; Hoek M; Zeilstra J; Pals ST; Mehmet H; Stassi G; et al. The AC133 epitope, but not the CD133 protein, is lost upon cancer stem cell differentiation. Cancer Res 2010, 70, 719–729. [PubMed: 20068153]

(703). Tsurumi C; Esser N; Firat E; Gaedicke S; Follo M; Behe M; Elsasser-Beile U; Grosu AL; Graeser R; Niedermann G Non-invasive in vivo imaging of tumor-associated CD133/prominin. PLoS One 2010, 5, e15605. [PubMed: 21187924]

(704). Gaedicke S; Braun F; Prasad S; Machein M; Firat E; Hettich M; Gudihal R; Zhu X; Klingner K; Schuler J; et al. Noninvasive positron emission tomography and fluorescence imaging of CD133+ tumor stem cells. Proc. Natl. Acad. Sci. U. S. A 2014, 111, E692–701. [PubMed: 24469819]

(705). Lopez-Otin C; Hunter T The regulatory crosstalk between kinases and proteases in cancer. Nat. Rev. Cancer 2010, 10, 278–292. [PubMed: 20300104]

(706). Skovgaard D; Persson M; Kjaer A PET imaging of urokinase-type plasminogen activator receptor (uPAR) in prostate cancer: current status and future perspectives. Clin Transl Imaging 2016, 4, 457–465. [PubMed: 27933281]

(707). Persson M; Skovgaard D; Brandt-Larsen M; Christensen C; Madsen J; Nielsen CH; Thurison T; Klausen TL; Holm S; Loft A; et al. First-in-human uPAR PET: imaging of cancer aggressiveness. Theranostics 2015, 5, 1303–1316. [PubMed: 26516369]

(708). Skovgaard D; Persson M; Brandt-Larsen M; Christensen C; Madsen J; Klausen TL; Holm S; Andersen FL; Loft A; Berthelsen AK; et al. Safety, dosimetry, and tumor detection ability of (68)Ga-NOTA-AE105: first-in-human study of a novel radioligand for uPAR PET imaging. J. Nucl. Med 2017, 58, 379–386. [PubMed: 27609788]

(709). Yang D; Severin GW; Dougherty CA; Lombardi R; Chen D; Van Dort ME; Barnhart TE; Ross BD; Mazar AP; Hong H Antibody-based PET of uPA/uPAR signaling with broad applicability for cancer imaging. Oncotarget 2016, 7, 73912–73924. [PubMed: 27729618]

(710). Kessenbrock K; Plaks V; Werb Z Matrix metal-loproteinases: regulators of the tumor microenvironment. Cell 2010, 141, 52–67. [PubMed: 20371345]

(711). de Lucas AG; Schuhmacher AJ; Oteo M; Romero E; Camara JA; de Martino A; Arroyo AG; Morcillo MA; Squatrito M; Martinez-Torrecuadrada JL; et al. Targeting MT1-MMP as an immunoPET-based strategy for imaging gliomas. PLoS One 2016, 11, e0158634. [PubMed: 27462980]

(712). Morcillo MA; Garcia de Lucas A; Oteo M; Romero E; Magro N; Ibanez M; Martinez A; Garaulet G; Arroyo AG; Lopez-Casas PP; et al. MT1-MMP as a PET imaging biomarker for pancreas cancer management. Contrast Media Mol. Imaging 2018, 2018, 8382148. [PubMed: 30224904]

(713). Ulmert D; Evans MJ; Holland JP; Rice SL; Wongvipat J; Pettersson K; Abrahamsson PA; Scardino PT; Larson SM; Lilja H; et al. Imaging androgen receptor signaling with a radiotracer targeting free prostate-specific antigen. Cancer Discovery 2012, 2, 320–327. [PubMed: 22576209]

(714). Thorek DL; Watson PA; Lee SG; Ku AT; Bournazos S; Braun K; Kim K; Sjostrom K; Doran MG; Lamminmaki U; et al. Internalization of secreted antigen-targeted antibodies by the neonatal Fc receptor for precision imaging of the androgen receptor axis. Sci. Transl. Med 2016, 8, 367ra167.

(715). Pastan I; Hassan R Discovery of mesothelin and exploiting it as a target for immunotherapy. Cancer Res 2014, 74, 2907–2912. [PubMed: 24824231]

(716). Hassan R; Thomas A; Alewine C; Le DT; Jaffee EM; Pastan I Mesothelin immunotherapy for cancer: ready for prime time? J. Clin. Oncol 2016, 34, 4171–4179. [PubMed: 27863199]

(717). Creaney J; Francis RJ; Dick IM; Musk AW; Robinson BW; Byrne MJ; Nowak AK Serum soluble mesothelin concentrations in malignant pleural mesothelioma: relationship to tumor volume, clinical stage and changes in tumor burden. Clin. Cancer Res 2011, 17, 1181–1189. [PubMed: 21177406]

(718). Kobayashi K; Sasaki T; Takenaka F; Yakushiji H; Fujii Y; Kishi Y; Kita S; Shen L; Kumon H; Matsuura E A novel PET imaging using (6)(4)Cu-labeled monoclonal antibody against mesothelin commonly expressed on cancer cells. J. Immunol. Res 2015, 2015, 268172. [PubMed: 25883990]

(719). Lindenberg L; Thomas A; Adler S; Mena E; Kurdziel K; Maltzman J; Wallin B; Hoffman K; Pastan I; Paik CH; et al. Safety and biodistribution of 111In-amatuximab in patients with mesothelin expressing cancers using single photon emission computed tomography-computed tomography (SPECT-CT) imaging. Oncotarget 2015, 6, 4496–4504. [PubMed: 25756664]

(720). Terwisscha van Scheltinga AG; Ogasawara A; Pacheco G; Vanderbilt AN; Tinianow JN; Gupta N; Li D; Firestein R; Marik J; Scales SJ; et al. Preclinical efficacy of an antibody-drug conjugate targeting mesothelin correlates with quantitative 89ZrimmunoPET. Mol. Cancer Ther 2017, 16, 134–142. [PubMed: 27760836]

(721). Lamberts LE; Menke-van der Houven van Oordt CW; ter Weele EJ; Bensch F; Smeenk MM; Voortman J; Hoekstra OS; Williams SP; Fine BM; Maslyar D; et al. ImmunoPET with anti-mesothelin antibody in patients with pancreatic and ovarian cancer before anti-mesothelin antibody-drug conjugate treatment. Clin. Cancer Res 2016, 22, 1642–1652. [PubMed: 26589435]

(722). Shin IS; Lee SM; Kim HS; Yao Z; Regino C; Sato N; Cheng KT; Hassan R; Campo MF; Albone EF; et al. Effect of chelator conjugation level and injection dose on tumor and organ uptake of 111In-labeled MORAb-009, an anti-mesothelin antibody. Nucl. Med. Biol 2011, 38, 1119–1127. [PubMed: 21741258]

(723). Lee JH; Kim H; Yao Z; Szajek LP; Grasso L; Kim I; Paik CH Tumor-Shed Antigen Affects Antibody Tumor Targeting: Comparison of two (89)Zr-labeled antibodies directed against shed or nonshed antigens. Contrast Media Mol. Imaging 2018, 2018, 2461257. [PubMed: 29720923]

(724). Wickstroem K; Hagemann UB; Cruciani V; Wengner AM; Kristian A; Ellingsen C; Siemeister G; Bjerke RM; Karlsson J; Ryan OB; et al. Synergistic effect of a mesothelin-targeted (227) Th conjugate in combination with DNA damage response inhibitors in ovarian cancer xenograft models. J. Nucl. Med 2019, 60, 1293–1300. [PubMed: 30850485]

(725). Sakamoto J; Kojima H; Kato J; Hamashima H; Suzuki H Organ-specific expression of the intestinal epithelium-related antigen A33, a cell surface target for antibody-based imaging and treatment in gastrointestinal cancer. Cancer Chemother. Pharmacol 2000, 46 (Suppl), S27–32. [PubMed: 10950144]

(726). Welt S; Scott AM; Divgi CR; Kemeny NE; Finn RD; Daghighian F; Germain JS; Richards EC; Larson SM; Old LJ Phase I/II study of iodine 125-labeled monoclonal antibody A33 in patients with advanced colon cancer. J. Clin. Oncol 1996, 14, 1787–1797. [PubMed: 8656247]

(727). Welt S; Divgi CR; Kemeny N; Finn RD; Scott AM; Graham M; Germain JS; Richards EC; Larson SM; Oettgen HF; et al. Phase I/II study of iodine 131-labeled monoclonal antibody A33 in patients with advanced colon cancer. J. Clin. Oncol 1994, 12, 1561–1571. [PubMed: 8040668]

(728). King DJ; Antoniw P; Owens RJ; Adair JR; Haines AM; Farnsworth AP; Finney H; Lawson AD; Lyons A; Baker TS; et al. Preparation and preclinical evaluation of humanised A33 immunoconjugates for radioimmunotherapy. Br. J. Cancer 1995, 72, 1364–1372. [PubMed: 8519646]

(729). Lee FT; Hall C; Rigopoulos A; Zweit J; Pathmaraj K; O'Keefe GJ; Smyth FE; Welt S; Old LJ; Scott AM Immuno-PET of human colon xenograft- bearing BALB/c nude mice using 124I-CDR-grafted humanized A33 monoclonal antibody. J. Nucl. Med 2001, 42, 764–769. [PubMed: 11337573]

(730). O'Donoghue JA; Smith-Jones PM; Humm JL; Ruan S; Pryma DA; Jungbluth AA; Divgi CR; Carrasquillo JA; Pandit-Taskar N; Fong Y; et al. 124I-huA33 antibody uptake is driven by A33 antigen concentration in tissues from colorectal cancer patients imaged by immuno-PET. J. Nucl. Med 2011, 52, 1878–1885. [PubMed: 22068895]

(731). Cheal SM; Fung EK; Patel M; Xu H; Guo HF; Zanzonico PB; Monette S; Wittrup KD; Cheung NV; Larson SM Curative multicycle radioimmunotherapy monitored by quantitative SPECT/CT-based theranostics, using bispecific antibody pretargeting strategy in colorectal cancer. J. Nucl. Med 2017, 58, 1735–1742. [PubMed: 28705917]

(732). Keinanen O; Brennan JM; Membreno R; Fung K; Gangangari K; Dayts EJ; Williams CJ; Zeglis BM Dual radionuclide theranostic pretargeting. Mol. Pharmaceutics 2019, 16, 4416–4421.

(733). Brand C; Sadique A; Houghton JL; Gangangari K; Ponte JF; Lewis JS; Pillarsetty NVK; Konner JA; Reiner T Leveraging PET to image folate receptor alpha therapy of an antibody-drug conjugate. EJNMMI Res 2018, 8, 87. [PubMed: 30155674]

(734). Heo GS; Detering L; Luehmann HP; Primeau T; Lee YS; Laforest R; Li S; Stec J; Lim KH; Lockhart AC; et al. Folate receptor alpha-targeted (89)Zr-M9346A immuno-PET for image-guided intervention with Mirvetuximab Soravtansine in triple-negative breast cancer. Mol. Pharmaceutics 2019, 16, 3996–4006.

(735). Cai W; Ebrahimnejad A; Chen K; Cao Q; Li ZB; Tice DA; Chen X Quantitative radioimmunoPET imaging of EphA2 in tumor-bearing mice. Eur. J. Nucl. Med. Mol. Imaging 2007, 34, 2024–2036. [PubMed: 17673999]

(736). Chacko AM; Li C; Nayak M; Mikitsh JL; Hu J; Hou C; Grasso L; Nicolaides NC; Muzykantov VR; Divgi CR; et al. Development of 124I immuno-PET targeting tumor vascular TEM1/endosialin. J. Nucl. Med 2014, 55, 500–507. [PubMed: 24525208]

(737). Li C; Chacko AM; Hu J; Hasegawa K; Swails J; Grasso L; El-Deiry WS; Nicolaides N; Muzykantov VR; Divgi CR; et al. Antibody-based tumor vascular theranostics targeting endosialin/TEM1 in a new mouse tumor vascular model. Cancer Biol. Ther 2014, 15, 443–451. [PubMed: 24553243]

(738). Burvenich IJ; Lee FT; Cartwright GA; O'Keefe GJ; Makris D; Cao D; Gong S; Chueh AC; Mariadason JM; Brechbiel MW; et al. Molecular imaging of death receptor 5 occupancy and saturation kinetics in vivo by humanized monoclonal antibody CS-1008. Clin. Cancer Res 2013, 19, 5984–5993. [PubMed: 24045184]

(739). Ciprotti M; Tebbutt NC; Lee FT; Lee ST; Gan HK; McKee DC; O'Keefe GJ; Gong SJ; Chong G; Hopkins W; et al. Phase I imaging and pharmacodynamic trial of CS-1008 in patients with metastatic colorectal cancer. J. Clin. Oncol 2015, 33, 2609–2616. [PubMed: 26124477]

(740). Burvenich IJ; Lee FT; Guo N; Gan HK; Rigopoulos A; Parslow AC; O'Keefe GJ; Gong SJ; Tochon-Danguy H; Rudd SE; et al. In vitro and in vivo evaluation of (89)Zr-DS-8273a as a theranostic for anti-death receptor 5 therapy. Theranostics 2016, 6, 2225–2234. [PubMed: 27924159]

(741). Sham JG; Kievit FM; Grierson JR; Miyaoka RS; Yeh MM; Zhang M; Yeung RS; Minoshima S; Park JO Glypican-3-targeted 89Zr PET imaging of hepatocellular carcinoma. J. Nucl. Med 2014, 55, 799–804. [PubMed: 24627434]

(742). Sham JG; Kievit FM; Grierson JR; Chiarelli PA; Miyaoka RS; Zhang M; Yeung RS; Minoshima S; Park JO Glypican-3-targeting F(ab′)2 for 89Zr PET of hepatocellular carcinoma. J. Nucl. Med 2014, 55, 2032–2037. [PubMed: 25359880]

(743). Carrasquillo JA; O'Donoghue JA; Beylergil V; Ruan S; Pandit-Taskar N; Larson SM; Smith-Jones PM; Lyashchenko SK; Ohishi N; Ohtomo T; Abou-Alfa GK I-124 codrituzumab imaging and biodistribution in patients with hepatocellular carcinoma. EJNMMI Res 2018, 8, 20. [PubMed: 29508107]

(744). Hall MA; Pinkston KL; Wilganowski N; Robinson H; Ghosh P; Azhdarinia A; Vazquez-Arreguin K; Kolonin AM; Harvey BR; Sevick-Muraca EM Comparison of mAbs targeting epithelial cell adhesion molecule for the detection of prostate cancer lymph node metastases with multimodal contrast agents: quantitative small-animal PET/CT and NIRF. J. Nucl. Med 2012, 53, 1427–1437. [PubMed: 22872743]

(745). Campbell DO; Noda A; Verlinsky A; Snyder J; Fujita Y; Murakami Y; Fushiki H; Miyoshi S; Lacayo S; Cabral E; et al. Preclinical evaluation of an anti-nectin-4 immunoPET reagent in tumor-bearing mice and biodistribution studies in cynomolgus monkeys. Mol. Imaging Biol 2016, 18, 768–775. [PubMed: 27122234]

(746). Doran MG; Watson PA; Cheal SM; Spratt DE; Wongvipat J; Steckler JM; Carrasquillo JA; Evans MJ; Lewis JS Annotating STEAP1 regulation in prostate cancer with 89Zr immuno-PET. J. Nucl. Med 2014, 55, 2045–2049. [PubMed: 25453051]

(747). Williams SP; Ogasawara A; Tinianow JN; Flores JE; Kan D; Lau J; Go M; Vanderbilt AN; Gill HS; Miao L; et al. ImmunoPET helps predicting the efficacy of antibody-drug conjugates targeting TENB2 and STEAP1. Oncotarget 2016, 7, 25103–25112. [PubMed: 27029064]

(748). O'Donoghue JA; Danila DC; Pandit-Taskar N; Beylergil V; Cheal SM; Fleming SE; Fox JJ; Ruan S; Zanzonico PB; Ragupathi G; et al. Pharmacokinetics and biodistribution of a[(89)Zr]Zr-DFO-MSTP2109A anti-STEAP1 antibody in metastatic castration-resistant prostate cancer patients. Mol. Pharmaceutics 2019, 16, 3083–3090.

(749). Carrasquillo JA; Fine BM; Pandit-Taskar N; Larson SM; Fleming SE; Fox JJ; Cheal SM; O'Donoghue JA; Ruan S; Ragupathi G; et al. Imaging patients with metastatic castration-resistant prostate cancer using 89Zr-DFO-MSTP2109A anti-STEAP1 antibody. J. Nucl. Med 2019, 60, 1517–1523. [PubMed: 31053681]

(750). Hong H; Yan Y; Shi S; Graves SA; Krasteva LK; Nickles RJ; Yang M; Cai W PET of follicle-stimulating hormone receptor: broad applicability to cancer imaging. Mol. Pharmaceutics 2015, 12, 403–410.

(751). Cheal SM; Ruan S; Veach DR; Longo VA; Punzalan BJ; Wu J; Fung EK; Kelly MP; Kirshner JR; Giurleo JT; et al. ImmunoPET imaging of endogenous and transfected prolactin receptor tumor xenografts. Mol. Pharmaceutics 2018, 15, 2133–2141.

(752). Deshayes E; Ladjohounlou R; Le Fur P; Pichard A; Lozza C; Boudousq V; Sevestre S; Jarlier M; Kashani R; Koch J; et al. Radiolabeled antibodies against mullerian-inhibiting substance receptor, type II: new tools for a theranostic approach in ovarian cancer. J. Nucl. Med 2018, 59, 1234–1242. [PubMed: 29674421]

(753). Oude Munnink TH; Arjaans ME; Timmer-Bosscha H; Schroder CP; Hesselink JW; Vedelaar SR; Walenkamp AM; Reiss M; Gregory RC; Lub-de Hooge MN; et al. PET with the 89Zr-labeled transforming growth factor-beta antibody fresolimumab in tumor models. J. Nucl. Med 2011, 52, 2001–2008. [PubMed: 22072706]

(754). den Hollander MW; Bensch F; Glaudemans AW; Oude Munnink TH; Enting RH; den Dunnen WF; Heesters MA; Kruyt FA; Lub-de Hooge MN; Cees de Groot J; et al. TGF-beta antibody uptake in recurrent high-grade glioma imaged with 89Zrfresolimumab PET. J. Nucl. Med 2015, 56, 1310–1314. [PubMed: 26135113]

(755). Rotteveel L; Poot AJ; Bogaard HJ; Ten Dijke P; Lammertsma AA; Windhorst AD In vivo imaging of TGFbeta signalling components using positron emission tomography. Drug Discovery Today 2019, 24, 2258–2272. [PubMed: 31494189]

(756). Weiss ID; Jacobson O Molecular imaging of chemokine receptor CXCR4. Theranostics 2013, 3, 76–84. [PubMed: 23382787]

(757). Azad BB; Chatterjee S; Lesniak WG; Lisok A; Pullambhatla M; Bhujwalla ZM; Pomper MG; Nimmagadda S A fully human CXCR4 antibody demonstrates diagnostic utility and therapeutic efficacy in solid tumor xenografts. Oncotarget 2016, 7, 12344–12358. [PubMed: 26848769]

(758). Yoon SO; Lee TS; Kim SJ; Jang MH; Kang YJ; Park JH; Kim KS; Lee HS; Ryu CJ; Gonzales NR; et al. Construction, affinity maturation, and biological characterization of an anti-tumor-associated glycoprotein-72 humanized antibody. J. Biol. Chem 2006, 281, 6985–6992. [PubMed: 16407221]

(759). Li L; Turatti F; Crow D; Bading JR; Anderson AL; Poku E; Yazaki PJ; Williams LE; Tamvakis D; Sanders P; et al. Monodispersed DOTA-PEG-conjugated anti-TAG-72 diabody has low kidney uptake and high tumor-to-blood ratios resulting in improved 64Cu PET. J. Nucl. Med 2010, 51, 1139–1146. [PubMed: 20554731]

(760). Li L; Crow D; Turatti F; Bading JR; Anderson AL; Poku E; Yazaki PJ; Carmichael J; Leong D; Wheatcroft D; et al. Site-specific conjugation of monodispersed DOTA-PEGn to a thiolated diabody reveals the effect of increasing peg size on kidney clearance and tumor uptake with improved 64-copper PET imaging. Bioconjugate Chem 2011, 22, 709–716.

(761). Ding H; Carlton MM; Povoski SP; Milum K; Kumar K; Kothandaraman S; Hinkle GH; Colcher D; Brody R; Davis PD; et al. Site specific discrete PEGylation of (124)I-labeled mCC49 Fab′

fragments improves tumor MicroPET/CT imaging in mice. Bioconjugate Chem 2013, 24, 1945–1954.

(762). Saunders LR; Bankovich AJ; Anderson WC; Aujay MA; Bheddah S; Black K; Desai R; Escarpe PA; Hampl J; Laysang A; et al. A DLL3-targeted antibody-drug conjugate eradicates high-grade pulmonary neuroendocrine tumor-initiating cells in vivo. Sci. Transl. Med 2015, 7, 302ra136.

(763). Rudin CM; Pietanza MC; Bauer TM; Ready N; Morgensztern D; Glisson BS; Byers LA; Johnson ML; Burris HA 3rd; Robert F; et al. Rovalpituzumab tesirine, a DLL3-targeted antibody-drug conjugate, in recurrent small-cell lung cancer: a first-inhuman, first-in-class, open-label, phase 1 study. Lancet Oncol 2017, 18, 42–51. [PubMed: 27932068]

(764). Puca L; Gavyert K; Sailer V; Conteduca V; Dardenne E; Sigouros M; Isse K; Kearney M; Vosoughi A; Fernandez L Delta-like protein 3 expression and therapeutic targeting in neuroendocrine prostate cancer. Sci. Transl. Med 2019, 11, eaav0891. [PubMed: 30894499]

(765). Sharma SK; Pourat J; Abdel-Atti D; Carlin SD; Piersigilli A; Bankovich AJ; Gardner EE; Hamdy O; Isse K; Bheddah S; et al. Noninvasive Interrogation of DLL3 Expression in Metastatic Small Cell Lung Cancer. Cancer Res 2017, 77, 3931–3941. [PubMed: 28487384]

(766). Sharma SK; Chow A; Monette S; Vivier D; Pourat J; Edwards KJ; Dilling TR; Abdel-Atti D; Zeglis BM; Poirier JT; et al. Fc-Mediated anomalous biodistribution of therapeutic antibodies in immunodeficient mouse models. Cancer Res 2018, 78, 1820–1832. [PubMed: 29363548]

(767). Vavere AL; Butch ER; Dearling JL; Packard AB; Navid F; Shulkin BL; Barfield RC; Snyder SE 64Cu-p-NH2-Bn-DOTA-hu14.18K322A, a PET radiotracer targeting neuroblastoma and melanoma. J. Nucl. Med 2012, 53, 1772–1778. [PubMed: 23064212]

(768). Maier FC; Schmitt J; Maurer A; Ehrlichmann W; Reischl G; Nikolaou K; Handgretinger R; Pichler BJ; Thaiss WM Correlation between positron emission tomography and Cerenkov luminescence imaging in vivo and ex vivo using 64Cu-labeled antibodies in a neuroblastoma mouse model. Oncotarget 2016, 7, 67403–67411. [PubMed: 27602580]

(769). Kramer K; Humm JL; Souweidane MM; Zanzonico PB; Dunkel IJ; Gerald WL; Khakoo Y; Yeh SD; Yeung HW; Finn RD; et al. Phase I study of targeted radioimmunotherapy for leptomeningeal cancers using intra-Ommaya 131-I-3F8. J. Clin. Oncol 2007, 25, 5465–5470. [PubMed: 18048828]

(770). Kramer K; Pandit-Taskar N; Humm JL; Zanzonico PB; Haque S; Dunkel IJ; Wolden SL; Donzelli M; Goldman DA; Lewis JS A phase II study of radioimmunotherapy with intraventricular (131) I-3F8 for medulloblastoma. Pediatr. Blood Cancer 2018, 65, e26754.

(771). Ladenstein R; Potschger U; Valteau-Couanet D; Luksch R; Castel V; Yaniv I; Laureys G; Brock P; Michon JM; Owens C; et al. Interleukin 2 with anti-GD2 antibody ch14.18/CHO (dinutuximab beta) in patients with high-risk neuroblastoma (HRNBL1/SIOPEN): a multicentre, randomised, phase 3 trial. Lancet Oncol 2018, 19, 1617–1629. [PubMed: 30442501]

(772). Cheal SM; Xu H; Guo HF; Zanzonico PB; Larson SM; Cheung NK Preclinical evaluation of multistep targeting of diasialoganglioside GD2 using an IgG-scFv bispecific antibody with high affinity for GD2 and DOTA metal complex. Mol. Cancer Ther 2014, 13, 1803–1812. [PubMed: 24944121]

(773). Martins F; Sofiya L; Sykiotis GP; Lamine F; Maillard M; Fraga M; Shabafrouz K; Ribi C; Cairoli A; Guex-Crosier Y; et al. Adverse effects of immune-checkpoint inhibitors: epidemiology, management and surveillance. Nat. Rev. Clin. Oncol 2019, 16, 563–580. [PubMed: 31092901]

(774). Pauken KE; Dougan M; Rose NR; Lichtman AH; Sharpe AH Adverse events following cancer immunotherapy: obstacles and opportunities. Trends Immunol 2019, 40, 511–523. [PubMed: 31053497]

(775). Wei W; Jiang D; Ehlerding EB; Luo Q; Cai W Noninvasive PET imaging of T cells. Trends Cancer 2018, 4, 359–373. [PubMed: 29709260]

(776). van der Veen EL; Bensch F; Glaudemans A; Lub-de Hooge MN; de Vries EGE Molecular imaging to enlighten cancer immunotherapies and underlying involved processes. Cancer Treat. Rev 2018, 70, 232–244. [PubMed: 30308466]

(777). Mayer AT; Gambhir SS The immunoimaging toolbox. J. Nucl. Med 2018, 59, 1174–1182. [PubMed: 29794226]

(778). Walther M; Gebhardt P; Grosse-Gehling P; Wurbach L; Irmler I; Preusche S; Khalid M; Opfermann T; Kamradt T; Steinbach J; et al. Implementation of 89Zr production and in vivo imaging of B-cells in mice with 89Zr-labeled anti-B-cell antibodies by small animal PET/CT. Appl. Radiat. Isot 2011, 69, 852–857. [PubMed: 21397511]

(779). Galli F; Rapisarda AS; Stabile H; Malviya G; Manni I; Bonanno E; Piaggio G; Gismondi A; Santoni A; Signore A In vivo imaging of natural killer cell trafficking in tumors. J. Nucl. Med 2015, 56, 1575–1580. [PubMed: 26272812]

(780). Sato N; Stringaris K; Davidson-Moncada JK; Reger R; Adler SS; Dunbar C; Choyke PL; Childs RW In-vivo tracking of adoptively transferred natural killer-cells in rhesus macaques using(89)Zirconium-oxine cell labeling and PET imaging. Clin. Cancer Res 2020, DOI: 10.1158/1078-0432.CCR-19-2897.

(781). Blykers A; Schoonooghe S; Xavier C; D'Hoe K; Laoui D; D'Huyvetter M; Vaneycken I; Cleeren F; Bormans G; Heemskerk J; et al. PET imaging of macrophage mannose receptor-expressing macrophages in tumor stroma using 18F-radiolabeled camelid single-domain antibody fragments. J. Nucl. Med 2015, 56, 1265–1271. [PubMed: 26069306]

(782). Xavier C; Blykers A; Laoui D; Bolli E; Vaneyken I; Bridoux J; Baudhuin H; Raes G; Everaert H; Movahedi K; et al. Clinical translation of [68Ga]Ga-NOTA-anti-MMR-sdAb for PET/CT imaging of protumorigenic macrophages. Mol. Imag. Biol 2019, 21, 898–906.

(783). Cao Q; Huang Q; Mohan C; Li C Small-animal PET/CT imaging of local and systemic immune response using (64)CualphaCD11b. J. Nucl. Med 2019, 60, 1317–1324. [PubMed: 30796172]

(784). Nigam S; McCarl L; Kumar R; Edinger RS; Kurland BF; Anderson CJ; Panigrahy A; Kohanbash G; Edwards WB Preclinical immunoPET imaging of glioblastoma-infiltrating myeloid cells using Zirconium-89 labeled Anti-CD11b antibody. Mol. Imag. Biol 2019, DOI: 10.1007/s11307-019-01427-1.

(785). Mall S; Yusufi N; Wagner R; Klar R; Bianchi H; Steiger K; Straub M; Audehm S; Laitinen I; Aichler M; et al. Immuno-PET imaging of engineered human T cells in tumors. Cancer Res 2016, 76, 4113–4123. [PubMed: 27354381]

(786). Keu KV; Witney TH; Yaghoubi S; Rosenberg J; Kurien A; Magnusson R; Williams J; Habte F; Wagner JR; Forman S; et al. Reporter gene imaging of targeted T cell immunotherapy in recurrent glioma. Sci. Transl. Med 2017, 9, eaag2196. [PubMed: 28100832]

(787). Yusufi N; Mall S; Bianchi HO; Steiger K; Reder S; Klar R; Audehm S; Mustafa M; Nekolla S; Peschel C; et al. In-depth characterization of a TCR-specific tracer for sensitive detection of tumor-directed transgenic T cells by immuno-PET. Theranostics 2017, 7, 2402–2416. [PubMed: 28744323]

(788). Larimer BM; Wehrenberg-Klee E; Caraballo A; Mahmood U Quantitative CD3 PET imaging predicts tumor growth response to anti-CTLA-4 therapy. J. Nucl. Med 2016, 57, 1607–1611. [PubMed: 27230929]

(789). Beckford Vera DR; Smith CC; Bixby LM; Glatt DM; Dunn SS; Saito R; Kim WY; Serody JS; Vincent BG; Parrott MC Immuno-PET imaging of tumor-infiltrating lymphocytes using zirconium-89 radiolabeled anti-CD3 antibody in immune-competent mice bearing syngeneic tumors. PLoS One 2018, 13, e0193832. [PubMed: 29513764]

(790). Gibson HM; McKnight BN; Malysa A; Dyson G; Wiesend WN; McCarthy CE; Reyes J; Wei WZ; Viola-Villegas NT IFNgamma PET imaging as a predictive tool for monitoring response to tumor immunotherapy. Cancer Res 2018, 78, 5706–5717. [PubMed: 30115693]

(791). Mayer KE; Mall S; Yusufi N; Gosmann D; Steiger K; Russelli L; Bianchi HO; Audehm S; Wagner R; Braunlein E; et al. T-cell functionality testing is highly relevant to developing novel immuno-tracers monitoring T cells in the context of immunotherapies and revealed CD7 as an attractive target. Theranostics 2018, 8, 6070–6087. [PubMed: 30613283]

(792). Tavare R; McCracken MN; Zettlitz KA; Knowles SM; Salazar FB; Olafsen T; Witte ON; Wu AM Engineered antibody fragments for immuno-PET imaging of endogenous CD8+ T cells in vivo. Proc. Natl. Acad. Sci. U. S. A 2014, 111, 1108–1113. [PubMed: 24390540]

(793). Pandit-Taskar N; Postow M; Hellmann M; Harding J; Barker C; O'Donoghue J; Ziolkowska M; Ruan S; Lyashchenko S; Tsai F; et al. First-in-human imaging with (89)Zr-Df-IAB22M2C anti-CD8 minibody in patients with solid malignancies: preliminary pharmacokinetics, biodistribution, and lesion targeting. J. Nucl. Med 2019, 59, jnumed.119.229781.

(794). Tavare R; McCracken MN; Zettlitz KA; Salazar FB; Olafsen T; Witte ON; Wu AM Immuno-PET of murine T cell reconstitution postadoptive stem cell transplantation using anti-CD4 and anti-CD8 cys-diabodies. J. Nucl. Med 2015, 56, 1258–1264. [PubMed: 25952734]

(795). Tavare R; Escuin-Ordinas H; Mok S; McCracken MN; Zettlitz KA; Salazar FB; Witte ON; Ribas A; Wu AM An effective immuno-PET imaging method to monitor CD8-dependent responses to immunotherapy. Cancer Res 2016, 76, 73–82. [PubMed: 26573799]

(796). Seo JW; Tavare R; Mahakian LM; Silvestrini MT; Tam S; Ingham ES; Salazar FB; Borowsky AD; Wu AM; Ferrara KW CD8(+) T-cell density imaging with (64)Cu-labeled cys-diabody informs immunotherapy protocols. Clin. Cancer Res 2018, 24, 4976–4987. [PubMed: 29967252]

(797). Gill H; Seipert R; Carroll VM; Gouasmat A; Yin J; Ogasawara A; de Jong I; Phan MM; Wang X; Yang J; et al. The production, quality control, and characterization of ZED8, a CD8-specific (89)Zr-labeled immuno-PET clinical imaging agent. AAPS J 2020, 22, 22. [PubMed: 31900688]

(798). Mitsuiki N; Schwab C; Grimbacher B What did we learn from CTLA-4 insufficiency on the human immune system? Immunol. Rev 2019, 287, 33–49. [PubMed: 30565239]

(799). Ehlerding EB; Lee HJ; Jiang D; Ferreira CA; Zahm CD; Huang P; Engle JW; McNeel DG; Cai W Antibody and fragment-based PET imaging of CTLA-4+ T-cells in humanized mouse models. Am. J. Cancer Res 2019, 9, 53–63. [PubMed: 30755811]

(800). Higashikawa K; Yagi K; Watanabe K; Kamino S; Ueda M; Hiromura M; Enomoto S 64Cu-DOTA-anti-CTLA-4 mAb enabled PET visualization of CTLA-4 on the T-cell infiltrating tumor tissues. PLoS One 2014, 9, e109866. [PubMed: 25365349]

(801). Ingram JR; Blomberg OS; Rashidian M; Ali L; Garforth S; Fedorov E; Fedorov AA; Bonanno JB; Le Gall C; Crowley S; et al. Anti-CTLA-4 therapy requires an Fc domain for efficacy. Proc. Natl. Acad. Sci. U. S. A 2018, 115, 3912–3917. [PubMed: 29581255]

(802). Contardi E; Palmisano GL; Tazzari PL; Martelli AM; Fala F; Fabbi M; Kato T; Lucarelli E; Donati D; Polito L; et al. CTLA-4 is constitutively expressed on tumor cells and can trigger apoptosis upon ligand interaction. Int. J. Cancer 2005, 117, 538–550. [PubMed: 15912538]

(803). Ehlerding EB; England CG; Majewski RL; Valdovinos HF; Jiang D; Liu G; McNeel DG; Nickles RJ; Cai W ImmunoPET imaging of CTLA-4 expression in mouse models of non-small cell lung cancer. Mol. Pharmaceutics 2017, 14, 1782–1789.

(804). Natarajan A; Mayer AT; Xu L; Reeves RE; Gano J; Gambhir SS Novel Radiotracer for immunoPET imaging of PD-1 checkpoint expression on tumor infiltrating lymphocytes. Bioconjugate Chem 2015, 26, 2062–2069.

(805). England CG; Ehlerding EB; Hernandez R; Rekoske BT; Graves SA; Sun H; Liu G; McNeel DG; Barnhart TE; Cai W Preclinical pharmacokinetics and biodistribution studies of 89Zr-labeled pembrolizumab. J. Nucl. Med 2017, 58, 162–168. [PubMed: 27493273]

(806). Natarajan A; Mayer AT; Reeves RE; Nagamine CM; Gambhir SS Development of novel immunoPET tracers to image human PD-1 checkpoint expression on tumor-infiltrating lymphocytes in a humanized mouse model. Mol. Imaging Biol 2017, 19, 903–914. [PubMed: 28247187]

(807). Cole EL; Kim J; Donnelly DJ; Smith RA; Cohen D; Lafont V; Morin PE; Huang RY; Chow PL; Hayes W; et al. Radiosynthesis and preclinical PET evaluation of (89)Zr-nivolumab (BMS-936558) in healthy non-human primates. Bioorg. Med. Chem 2017, 25, 5407–5414. [PubMed: 28803798]

(808). England CG; Jiang D; Ehlerding EB; Rekoske BT; Ellison PA; Hernandez R; Barnhart TE; McNeel DG; Huang P; Cai W (89)Zr-labeled nivolumab for imaging of T-cell infiltration in a humanized murine model of lung cancer. Eur. J. Nucl. Med. Mol. Imaging 2018, 45, 110–120. [PubMed: 28821924]

(809). Niemeijer AN; Leung D; Huisman MC; Bahce I; Hoekstra OS; van Dongen G; Boellaard R; Du S; Hayes W; Smith R; et al. Whole body PD-1 and PD-L1 positron emission tomography in patients with non-small-cell lung cancer. Nat. Commun 2018, 9, 4664. [PubMed: 30405135]

(810). Lesniak WG; Chatterjee S; Gabrielson M; Lisok A; Wharram B; Pomper MG; Nimmagadda S PD-L1 detection in tumors using [(64)Cu]atezolizumab with PET. Bioconjugate Chem 2016, 27, 2103–2110.

(811). Truillet C; Oh HLJ; Yeo SP; Lee CY; Huynh LT; Wei J; Parker MFL; Blakely C; Sevillano N; Wang YH; et al. Imaging PD-L1 expression with immunoPET. Bioconjugate Chem 2018, 29, 96–103.

(812). Moroz A; Lee CY; Wang YH; Hsiao JC; Sevillano N; Truillet C; Craik CS; Fong L; Wang CI; Evans MJ A preclinical assessment of (89)Zr-atezolizumab identifies a requirement for carrier added formulations not observed with (89)Zr-C4. Bioconjugate Chem 2018, 29, 3476–3482.

(813). Xu M; Han Y; Liu G; Xu Y; Duan D; Liu H; Du F; Luo P; Liu Z Preclinical study of a fully human anti-PD-L1 antibody as a theranostic agent for cancer immunotherapy. Mol. Pharmaceutics 2018, 15, 4426–4433.

(814). Vento J; Mulgaonkar A; Woolford L; Nham K; Christie A; Bagrodia A; de Leon AD; Hannan R; Bowman I; McKay RM; et al. PD-L1 detection using Zr-atezolizumab immuno-PET in renal cell carcinoma tumorgrafts from a patient with favorable nivolumab response. J. Immunother Cancer 2019, 7, 144. [PubMed: 31155004]

(815). Natarajan A; Patel CB; Ramakrishnan S; Panesar PS; Long SR; Gambhir SS A novel engineered small protein for positron emission tomography imaging of human programmed death ligand-1: validation in mouse models and human cancer tissues. Clin. Cancer Res 2019, 25, 1774–1785. [PubMed: 30373750]

(816). Donnelly DJ; Smith RA; Morin P; Lipovsek D; Gokemeijer J; Cohen D; Lafont V; Tran T; Cole EL; Wright M; et al. Synthesis and biologic evaluation of a novel (18)F-labeled adnectin as a PET radioligand for imaging PD-L1 expression. J. Nucl. Med 2018, 59, 529–535. [PubMed: 29025984]

(817). Maute RL; Gordon SR; Mayer AT; McCracken MN; Natarajan A; Ring NG; Kimura R; Tsai JM; Manglik A; Kruse AC; et al. Engineering high-affinity PD-1 variants for optimized immunotherapy and immuno-PET imaging. Proc. Natl. Acad. Sci. U. S.A 2015, 112, E6506–6514. [PubMed: 26604307]

(818). Mayer AT; Natarajan A; Gordon SR; Maute RL; McCracken MN; Ring AM; Weissman IL; Gambhir SS Practical immuno-PET radiotracer design considerations for human immune checkpoint imaging. J. Nucl. Med 2017, 58, 538–546. [PubMed: 27980047]

(819). Gonzalez Trotter DE; Meng X; McQuade P; Rubins D; Klimas M; Zeng Z; Connolly BM; Miller PJ; O'Malley SS; Lin SA; et al. In vivo imaging of the programmed death ligand 1 by (18)F PET. J. Nucl. Med 2017, 58, 1852–1857. [PubMed: 28588151]

(820). Li D; Cheng S; Zou S; Zhu D; Zhu T; Wang P; Zhu X Immuno-PET imaging of (89)Zr labeled anti-PD-L1 domain antibody. Mol. Pharmaceutics 2018, 15, 1674–1681.

(821). Lv G; Sun X; Qiu L; Sun Y; Li K; Liu Q; Zhao Q; Qin S; Lin J PET imaging of tumor PD-L1 expression with a highly specific non-blocking nanobody. J. Nucl. Med 2020, 61, 117–122.

(822). Broos K; Lecocq Q; Xavier C; Bridoux J; Nguyen TT; Corthals J; Schoonooghe S; Lion E; Raes G; Keyaerts M; et al. Evaluating a single domain antibody targeting human PD-L1 as a nuclear imaging and therapeutic agent. Cancers 2019, 11, 872.

(823). Wissler HL; Ehlerding EB; Lyu Z; Zhao Y; Zhang S; Eshraghi A; Buuh ZY; McGuth JC; Guan Y; Engle JW; et al. Site-specific immuno-PET tracer to image PD-L1. Mol. Pharmaceutics 2019, 16, 2028–2036.

(824). Kikuchi M; Clump DA; Srivastava RM; Sun L; Zeng D; Diaz-Perez JA; Anderson CJ; Edwards WB; Ferris RL Preclinical immunoPET/CT imaging using Zr-89-labeled anti-PD-L1 monoclonal antibody for assessing radiation-induced PD-L1 upregulation in head and neck cancer and melanoma. Oncoimmunology 2017, 6, e1329071. [PubMed: 28811971]

(825). Ehlerding EB; Lee HJ; Barnhart TE; Jiang D; Kang L; McNeel DG; Engle JW; Cai W Noninvasive imaging and quantification of radiotherapy-induced PD-L1 upregulation with(89)Zr-Df-atezolizumab. Bioconjugate Chem 2019, 30, 1434–1441.

(826). Li D; Zou S; Cheng S; Song S; Wang P; Zhu X Monitoring the response of PD-L1 expression to epidermal growth factor receptor tyrosine kinase inhibitors in nonsmall-cell lung cancer xenografts by immuno-PET imaging. Mol. Pharmaceutics 2019, 16, 3469–3476.

(827). Gong B; Kiyotani K; Sakata S; Nagano S; Kumehara S; Baba S; Besse B; Yanagitani N; Friboulet L; Nishio M; et al. Secreted PD-L1 variants mediate resistance to PD-L1 blockade therapy in non-small cell lung cancer. J. Exp. Med 2019, 216, 982–1000. [PubMed: 30872362]

(828). Josefsson A; Nedrow JR; Park S; Banerjee SR; Rittenbach A; Jammes F; Tsui B; Sgouros G Imaging, biodistribution, and dosimetry of radionuclide-labeled PD-L1 antibody in an immunocompetent mouse model of breast cancer. Cancer Res 2016, 76, 472–479. [PubMed: 26554829]

(829). Hettich M; Braun F; Bartholoma MD; Schirmbeck R; Niedermann G High-resolution PET imaging with therapeutic antibody-based PD-1/PD-L1 checkpoint tracers. Theranostics 2016, 6, 1629–1640. [PubMed: 27446497]

(830). Ingram JR; Dougan M; Rashidian M; Knoll M; Keliher EJ; Garrett S; Garforth S; Blomberg OS; Espinosa C; Bhan A; et al. PD-L1 is an activation-independent marker of brown adipocytes. Nat. Commun 2017, 8, 647. [PubMed: 28935898]

(831). Willoughby J; Griffiths J; Tews I; Cragg MS OX40: structure and function - what questions remain? Mol. Immunol 2017, 83, 13–22. [PubMed: 28092803]

(832). Alam IS; Mayer AT; Sagiv-Barfi I; Wang K; Vermesh O; Czerwinski DK; Johnson EM; James ML; Levy R; Gambhir SS Imaging activated T cells predicts response to cancer vaccines. J. Clin. Invest 2018, 128, 2569–2580. [PubMed: 29596062]

(833). Burke JD; Young HA IFN-gamma: A cytokine at the right time, is in the right place. Semin. Immunol 2019, 43, 101280. [PubMed: 31221552]

(834). Larimer BM; Wehrenberg-Klee E; Dubois F; Mehta A; Kalomeris T; Flaherty K; Boland G; Mahmood U Granzyme B PET imaging as a predictive biomarker of immunotherapy response. Cancer Res 2017, 77, 2318–2327. [PubMed: 28461564]

(835). Larimer BM; Bloch E; Nesti S; Austin EE; Wehrenberg-Klee E; Boland G; Mahmood U The effectiveness of checkpoint inhibitor combinations and administration timing can be measured by granzyme B PET imaging. Clin. Cancer Res 2019, 25, 1196–1205. [PubMed: 30327313]

(836). van der Veen EL; Antunes IF; Maarsingh P; Hessels-Scheper J; Zijlma R; Boersma HH; Jorritsma-Smit A; Hospers GAP; de Vries EGE; Lub-de Hooge MN; de Vries EFJ Clinical-grade N-(4-[18F]fluorobenzoyl)-interleukin-2 for PET imaging of activated T-cells in humans. EJNMMI Radiopharm. Chem 2019, 4, 15. [PubMed: 31659562]

(837). Grivennikov SI; Greten FR; Karin M Immunity, inflammation, and cancer. Cell 2010, 140, 883–899. [PubMed: 20303878]

(838). Lee HJ; Ehlerding EB; Cai W Antibody-based tracers for PET/SPECT imaging of chronic inflammatory diseases. ChemBio-Chem 2019, 20, 422–436.

(839). Smolen JS; Aletaha D; Barton A; Burmester GR; Emery P; Firestein GS; Kavanaugh A; McInnes IB; Solomon DH; Strand V; Yamamoto K Rheumatoid arthritis. Nat. Rev. Dis Primers 2018, 4, 18001. [PubMed: 29417936]

(840). Aletaha D; Smolen JS Diagnosis and management of rheumatoid arthritis: a review. JAMA 2018, 320, 1360–1372. [PubMed: 30285183]

(841). Wipke BT; Wang Z; Kim J; McCarthy TJ; Allen PM Dynamic visualization of a joint-specific autoimmune response through positron emission tomography. Nat. Immunol 2002, 3, 366–372. [PubMed: 11896393]

(842). Schwager K; Kaspar M; Bootz F; Marcolongo R; Paresce E; Neri D; Trachsel E Preclinical characterization of DEKAVIL (F8-IL10), a novel clinical-stage immunocytokine which inhibits the progression of collagen-induced arthritis. Arthritis Res. Ther 2009, 11, R142. [PubMed: 19781067]

(843). Bruijnen STG; Chandrupatla D; Giovanonni L; Neri D; Vugts DJ; Huisman MC; Hoekstra OS; Musters RJP; Lammertsma AA; van Dongen G; et al. F8-IL10: a new potential antirheumatic drug evaluated by a PET-guided translational approach. Mol. Pharmaceutics 2019, 16, 273–281.

(844). Beckford-Vera DR; Gonzalez-Junca A; Janneck JS; Huynh TL; Blecha JE; Seo Y; Li X; VanBrocklin HF; Franc BL PET/CT imaging of human TNFalpha using [(89)Zr]-certolizumab pegol in a transgenic preclinical model of rheumatoid arthritis. Mol. Imaging Biol 2020, 22, 105–114.

(845). Loktev A; Lindner T; Burger EM; Altmann A; Giesel F; Kratochwil C; Debus J; Marme F; Jager D; Mier W; et al. Development of fibroblast activation protein-targeted radiotracers with improved tumor retention. J. Nucl. Med 2019, 60, 1421–1429. [PubMed: 30850501]

(846). Giesel FL; Kratochwil C; Lindner T; Marschalek MM; Loktev A; Lehnert W; Debus J; Jager D; Flechsig P; Altmann A; et al. 68)Ga-FAPI PET/CT: biodistribution and preliminary dosimetry estimate of 2 DOTA-containing FAP-targeting agents in patients with various cancers. J. Nucl. Med 2019, 60, 386–392. [PubMed: 30072500]

(847). Lindner T; Loktev A; Giesel F; Kratochwil C; Altmann A; Haberkorn U Targeting of activated fibroblasts for imaging and therapy. EJNMMI Radiopharm Chem 2019, 4, 16. [PubMed: 31659499]

(848). Bacac M; Freimoser-Grundschober A; Hosse R; Klein C; Moessner E; Nicolini VG; Umaña P Anti-FAP antibodies and methods of use US US9011847B2, 2015.

(849). Laverman P; van der Geest T; Terry SY; Gerrits D; Walgreen B; Helsen MM; Nayak TK; Freimoser-Grundschober A; Waldhauer I; Hosse RJ; et al. Immuno-PET and immuno-SPECT of rheumatoid arthritis with radiolabeled anti-fibroblast activation protein antibody correlates with severity of arthritis. J. Nucl. Med 2015, 56, 778–783. [PubMed: 25858044]

(850). Terry SY; Koenders MI; Franssen GM; Nayak TK; Freimoser-Grundschober A; Klein C; Oyen WJ; Boerman OC; Laverman P Monitoring therapy response of experimental arthritis with radiolabeled tracers targeting fibroblasts, macrophages, or integrin alphavbeta3. J. Nucl. Med 2016, 57, 467–472. [PubMed: 26635344]

(851). van der Geest T; Laverman P; Gerrits D; Walgreen B; Helsen MM; Klein C; Nayak TK; Storm G; Metselaar JM; Koenders MI; et al. Liposomal treatment of experimental arthritis can be monitored noninvasively with a radiolabeled anti-fibroblast activation protein antibody. J. Nucl. Med 2017, 58, 151–155. [PubMed: 27493266]

(852). van der Geest T; Roeleveld DM; Walgreen B; Helsen MM; Nayak TK; Klein C; Hegen M; Storm G; Metselaar JM; van den Berg WB; et al. Imaging fibroblast activation protein to monitor therapeutic effects of neutralizing interleukin-22 in collagen-induced arthritis. Rheumatology (Oxford, U. K.) 2018, 57, 737–747.

(853). Liu TC; Stappenbeck TS Genetics and pathogenesis of inflammatory bowel disease. Annu. Rev. Pathol.: Mech. Dis 2016, 11, 127–148.

(854). Dmochowska N; Wardill HR; Hughes PA Advances in imaging specific mediators of inflammatory bowel disease. Int. J. Mol. Sci 2018, 19, 2471.

(855). Dearling JL; Park EJ; Dunning P; Baker A; Fahey F; Treves ST; Soriano SG; Shimaoka M; Packard AB; Peer D Detection of intestinal inflammation by MicroPET imaging using a(64)Cu-labeled anti-beta(7) integrin antibody. Inflamm. Bowel Dis 2010, 16, 1458–1466. [PubMed: 20186943]

(856). Dearling JL; Daka A; Veiga N; Peer D; Packard AB Colitis immunoPET: defining target cell populations and optimizing pharmacokinetics. Inflamm. Bowel Dis 2016, 22, 529–538. [PubMed: 26841223]

(857). Dmochowska N; Tieu W; Keller MD; Wardill HR; Mavrangelos C; Campaniello MA; Takhar P; Hughes PA Immuno-PET of innate immune markers CD11b and IL-1beta detects inflammation in murine colitis. J. Nucl. Med 2019, 60, 858–863. [PubMed: 30413657]

(858). Freise AC; Zettlitz KA; Salazar FB; Tavare R; Tsai WK; Chatziioannou AF; Rozengurt N; Braun J; Wu AM Immuno-PET in inflammatory bowel disease: imaging CD4-positive T cells in a murine model of colitis. J. Nucl. Med 2018, 59, 980–985. [PubMed: 29326360]

(859). Van Elssen C; Rashidian M; Vrbanac V; Wucherpfennig KW; Habre ZE; Sticht J; Freund C; Jacobsen JT; Cragnolini J; Ingram J; et al. Noninvasive imaging of human immune responses in a human xenograft model of graft-versus-host disease. J. Nucl. Med 2017, 58, 1003–1008. [PubMed: 28209904]

(860). Pektor S; Schloder J; Klasen B; Bausbacher N; Wagner DC; Schreckenberger M; Grabbe S; Jonuleit H; Miederer M Using immuno-PET imaging to monitor kinetics of T cell-mediated inflammation and treatment efficiency in a humanized mouse model for GvHD. Eur. J. Nucl. Med. Mol. Imaging 2019, DOI: 10.1007/s00259-019-04507-0.

(861). De Vos J; Mathijs I; Xavier C; Massa S; Wernery U; Bouwens L; Lahoutte T; Muyldermans S; Devoogdt N Specific targeting of atherosclerotic plaques in ApoE(−/−) mice using a new Camelid sdAb binding the vulnerable plaque marker LOX-1. Mol. Imaging Biol 2014, 16, 690–698. [PubMed: 24687730]

(862). Senders ML; Que X; Cho YS; Yeang C; Groenen H; Fay F; Calcagno C; Meerwaldt AE; Green S; Miu P; et al. PET/MR imaging of malondialdehyde-acetaldehyde epitopes with a human antibody detects clinically relevant atherothrombosis. J. Am. Coll. Cardiol 2018, 71, 321–335. [PubMed: 29348025]

(863). Senders ML; Hernot S; Carlucci G; van de Voort JC; Fay F; Calcagno C; Tang J; Alaarg A; Zhao Y; Ishino S; et al. Nanobody-facilitated multiparametric PET/MRI phenotyping of atherosclerosis. JACC Cardiovasc. Imaging 2019, 12, 2015–2026. [PubMed: 30343086]

(864). Mumprecht V; Honer M; Vigl B; Proulx ST; Trachsel E; Kaspar M; Banziger-Tobler NE; Schibli R; Neri D; Detmar M In vivo imaging of inflammation- and tumor-induced lymph node lymphangiogenesis by immuno-positron emission tomography. Cancer Res 2010, 70, 8842–8851. [PubMed: 20978206]

(865). Mumprecht V; Roudnicky F; Detmar M Inflammation-induced lymph node lymphangiogenesis is reversible. Am. J. Pathol 2012, 180, 874–879. [PubMed: 22200615]

(866). Santangelo PJ; Rogers KA; Zurla C; Blanchard EL; Gumber S; Strait K; Connor-Stroud F; Schuster DM; Amancha PK; Hong JJ; et al. Whole-body immunoPET reveals active SIV dynamics in viremic and antiretroviral therapy-treated macaques. Nat. Methods 2015, 12, 427–432. [PubMed: 25751144]

(867). Morad HOJ; Wild AM; Wiehr S; Davies G; Maurer A; Pichler BJ; Thornton CR Pre-clinical imaging of invasive candidiasis using immunoPET/MR. Front. Microbiol 2018, 9, 1996. [PubMed: 30190717]

(868). Pickett JE; Thompson JM; Sadowska A; Tkaczyk C; Sellman BR; Minola A; Corti D; Lanzavecchia A; Miller LS; Thorek DL Molecularly specific detection of bacterial lipoteichoic acid for diagnosis of prosthetic joint infection of the bone. Bone Res 2018, 6, 13. [PubMed: 29707402]

(869). Santangelo PJ; Cicala C; Byrareddy SN; Ortiz KT; Little D; Lindsay KE; Gumber S; Hong JJ; Jelicic K; Rogers KA; et al. Early treatment of SIV+ macaques with an alpha4beta7 mAb alters virus distribution and preserves CD4(+) T cells in later stages of infection. Mucosal Immunol 2018, 11, 932–946. [PubMed: 29346349]

(870). Duvenhage J; Ebenhan T; Garny S; Hernandez Gonzalez I; Leyva Montana R; Price R; Birkholtz LM; Zeevaart JR Molecular imaging of a Zirconium-89 labeled antibody targeting plasmodium falciparum-infected human erythrocytes. Mol. Imaging Biol 2020, 22, 115–123.

(871). Rolle AM; Hasenberg M; Thornton CR; Solouk-Saran D; Mann L; Weski J; Maurer A; Fischer E; Spycher PR; Schibli R; et al. ImmunoPET/MR imaging allows specific detection of Aspergillus fumigatus lung infection in vivo. Proc. Natl. Acad. Sci. U.S. A 2016, 113, E1026–1033. [PubMed: 26787852]

(872). Davies G; Rolle AM; Maurer A; Spycher PR; Schillinger C; Solouk-Saran D; Hasenberg M; Weski J; Fonslet J; Dubois A; et al. Towards translational immunoPET/MR imaging of invasive pulmonary aspergillosis: the humanised monoclonal antibody JF5 detects aspergillus lung infections in vivo. Theranostics 2017, 7, 3398–3414. [PubMed: 28912884]

(873). Thornton CR Molecular imaging of invasive pulmonary aspergillosis using immunoPET/MRI: the future looks bright. Front. Microbiol 2018, 9, 691. [PubMed: 29686661]

(874). Whiting DR; Guariguata L; Weil C; Shaw J IDF diabetes atlas: global estimates of the prevalence of diabetes for 2011 and 2030. Diabetes Res. Clin. Pract 2011, 94, 311–321. [PubMed: 22079683]

(875). Wei W; Ehlerding EB; Lan X; Luo QY; Cai W Molecular imaging of beta-cells: diabetes and beyond. Adv. Drug Delivery Rev 2019, 139, 16–31.

(876). Vats D; Wang H; Esterhazy D; Dikaiou K; Danzer C; Honer M; Stuker F; Matile H; Migliorini C; Fischer E; et al. Multimodal imaging of pancreatic beta cells in vivo by targeting transmembrane protein 27 (TMEM27). Diabetologia 2012, 55, 2407–2416. [PubMed: 22790173]

(877). Balhuizen A; Massa S; Mathijs I; Turatsinze JV; De Vos J; Demine S; Xavier C; Villate O; Millard I; Egrise D; et al. A nanobody-based tracer targeting DPP6 for non-invasive imaging of human pancreatic endocrine cells. Sci. Rep 2017, 7, 15130. [PubMed: 29123178]

(878). Demine S; Garcia Ribeiro R; Thevenet J; Marselli L; Marchetti P; Pattou F; Kerr-Conte J; Devoogdt N; Eizirik DL A nanobody-based nuclear imaging tracer targeting dipeptidyl peptidase 6 to determine the mass of human beta cell grafts in mice. Diabetologia 2020, 63, 825–836.

(879). Graves SA; Hernandez R; Valdovinos HF; Ellison PA; Engle JW; Barnhart TE; Cai W; Nickles RJ Preparation and in vivo characterization of 51MnCl2 as PET tracer of Ca2+ channel-mediated transport. Sci. Rep 2017, 7, 3033. [PubMed: 28596540]

(880). Hernandez R; Graves SA; Gregg T; VanDeusen HR; Fenske RJ; Wienkes HN; England CG; Valdovinos HF; Jeffery JJ; Barnhart TE; et al. Radiomanganese PET detects changes in functional beta-cell mass in mouse models of diabetes. Diabetes 2017, 66, 2163–2174. [PubMed: 28515126]

(881). Kolbert KS; Pentlow KS; Pearson JR; Sheikh A; Finn RD; Humm JL; Larson SM Prediction of absorbed dose to normal organs in thyroid cancer patients treated with 131I by use of 124I PET and 3-dimensional internal dosimetry software. J. Nucl. Med 2007, 48, 143–149. [PubMed: 17204711]

(882). Ho AL; Grewal RK; Leboeuf R; Sherman EJ; Pfister DG; Deandreis D; Pentlow KS; Zanzonico PB; Haque S; Gavane S; et al. Selumetinib-enhanced radioiodine uptake in advanced thyroid cancer. N. Engl. J. Med 2013, 368, 623–632. [PubMed: 23406027]

(883). Werner RA; Weich A; Kircher M; Solnes LB; Javadi MS; Higuchi T; Buck AK; Pomper MG; Rowe SP; Lapa C The theranostic promise for Neuroendocrine Tumors in the late 2010s -Where do we stand, where do we go? Theranostics 2018, 8, 6088–6100. [PubMed: 30613284]

(884). Ahmadzadehfar H; Rahbar K; Essler M; Biersack HJ PSMA-based theranostics: a step-by-step practical approach to diagnosis and therapy for mCRPC patients. Semin. Nucl. Med 2020, 50, 98–109.

(885). Langbein T; Weber WA; Eiber M Future of theranostics: an outlook on precision oncology in nuclear medicine. J. Nucl. Med 2019, 60, 13S–19S. [PubMed: 31481583]

(886). Liersch T; Meller J; Kulle B; Behr TM; Markus P; Langer C; Ghadimi BM; Wegener WA; Kovacs J; Horak ID; et al. Phase II trial of carcinoembryonic antigen radioimmunotherapy with 131I-labetuzumab after salvage resection of colorectal metastases in the liver: five-year safety and efficacy results. J. Clin. Oncol 2005, 23, 6763–6770. [PubMed: 16170184]

(887). Liersch T; Meller J; Bittrich M; Kulle B; Becker H; Goldenberg DM Update of carcinoembryonic antigen radio-immunotherapy with (131)I-labetuzumab after salvage resection of colorectal liver metastases: comparison of outcome to a contemporaneous control group. Ann. Surg. Oncol 2007, 14, 2577–2590. [PubMed: 17570017]

(888). Morschhauser F; Radford J; Van Hoof A; Vitolo U; Soubeyran P; Tilly H; Huijgens PC; Kolstad A; d'Amore F; Gonzalez Diaz M; et al. Phase III trial of consolidation therapy with yttrium-90-ibritumomab tiuxetan compared with no additional therapy after first remission in advanced follicular lymphoma. J. Clin. Oncol 2008, 26, 5156–5164. [PubMed: 18854568]

(889). Flem-Karlsen K; Fodstad O; Tan M; Nunes-Xavier CE B7-H3 in cancer - beyond immune regulation. Trends Cancer 2018, 4, 401–404. [PubMed: 29860983]

(890). Bao R; Wang Y; Lai J; Zhu H; Zhao Y; Li S; Li N; Huang J; Yang Z; Wang F; et al. Enhancing anti-PD-1/PD-L1 immune checkpoint inhibitory cancer therapy by CD276-targeted photodynamic ablation of tumor cells and tumor vasculature. Mol. Pharmaceutics 2019, 16, 339–348.

(891). Burvenich IJG; Parakh S; Lee FT; Guo N; Liu Z; Gan HK; Rigopoulos A; O'Keefe GJ; Gong SJ; Goh YW; et al. Molecular imaging of T cell co-regulator factor B7-H3 with(89)Zr-DS-5573a. Theranostics 2018, 8, 4199–4209. [PubMed: 30128047]

(892). Modak S; Kramer K; Gultekin SH; Guo HF; Cheung NK Monoclonal antibody 8H9 targets a novel cell surface antigen expressed by a wide spectrum of human solid tumors. Cancer Res 2001, 61, 4048–4054. [PubMed: 11358824]

(893). Kramer K; Kushner BH; Modak S; Pandit-Taskar N; Smith-Jones P; Zanzonico P; Humm JL; Xu H; Wolden SL; Souweidane MM; et al. Compartmental intrathecal radio-immunotherapy: results for treatment for metastatic CNS neuroblastoma. J. Neuro-Oncol 2010, 97, 409–418.

(894). Bailey K; Pandit-Taskar N; Humm JL; Zanzonico P; Gilheeney S; Cheung NV; Kramer K Targeted radioimmuno-therapy for embryonal tumor with multilayered rosettes. J. Neuro-Oncol 2019, 143, 101–106.

(895). Pandit-Taskar N; Zanzonico PB; Kramer K; Grkovski M; Fung EK; Shi W; Zhang Z; Lyashchenko SK; Fung AM; Pentlow KS; et al. Biodistribution and dosimetry of intraventricularly administered (124)I-omburtamab in patients with metastatic leptomeningeal tumors. J. Nucl. Med 2019, 60, 1794–1801. [PubMed: 31405921]

(896). Souweidane MM; Kramer K; Pandit-Taskar N; Zhou Z; Haque S; Zanzonico P; Carrasquillo JA; Lyashchenko SK; Thakur SB; Donzelli M; et al. Convection-enhanced delivery for diffuse intrinsic pontine glioma: a single-centre, dose-escalation, phase 1 trial. Lancet Oncol 2018, 19, 1040–1050. [PubMed: 29914796]

(897). Le Doussal JM; Chetanneau A; Gruaz-Guyon A; Martin M; Gautherot E; Lehur PA; Chatal JF; Delaage M; Barbet J Bispecific monoclonal antibody-mediated targeting of an indium-111-labeled DTPA dimer to primary colorectal tumors: pharmacokinetics, biodistribution, scintigraphy and immune response. J. Nucl. Med 1993, 34, 1662–1671. [PubMed: 8410279]

(898). Schoffelen R; van der Graaf WT; Franssen G; Sharkey RM; Goldenberg DM; McBride WJ; Rossi EA; Eek A; Oyen WJ; Boerman OC Pretargeted 177Lu radioimmunotherapy of carcinoembryonic antigen-expressing human colonic tumors in mice.J. Nucl. Med 2010, 51, 1780–1787. [PubMed: 21051650]

(899). Schoffelen R; Boerman OC; Goldenberg DM; Sharkey RM; van Herpen CM; Franssen GM; McBride WJ; Chang CH; Rossi EA; van der Graaf WT; et al. Development of an imaging-guided CEA-pretargeted radionuclide treatment of advanced colorectal cancer: first clinical results. Br. J. Cancer 2013, 109, 934–942. [PubMed: 23860529]

(900). Schoffelen R; Woliner-van der Weg W; Visser EP; Goldenberg DM; Sharkey RM; McBride WJ; Chang CH; Rossi EA; van der Graaf WT; Oyen WJ; Boerman OC Predictive patient-specific dosimetry and individualized dosing of pretargeted radioimmunotherapy in patients with advanced colorectal cancer. Eur. J. Nucl. Med. Mol. Imaging 2014, 41, 1593–1602. [PubMed: 24643780]

(901). Heskamp S; Hernandez R; Molkenboer-Kuenen JDM; Essler M; Bruchertseifer F; Morgenstern A; Steenbergen EJ; Cai W; Seidl C; McBride WJ; et al. Alpha- versus beta-emitting radionuclides for pretargeted radioimmunotherapy of carcinoembryonic antigen-expressing human colon cancer xenografts. J. Nucl. Med 2017, 58, 926–933. [PubMed: 28232604]

(902). Nittka S; Krueger MA; Shively JE; Boll H; Brockmann MA; Doyon F; Pichler BJ; Neumaier M Radioimmunoimaging of liver metastases with PET using a 64Cu-labeled CEA antibody in transgenic mice. PLoS One 2014, 9, e106921. [PubMed: 25226518]

(903). Lu Z; Pham TT; Rajkumar V; Yu Z; Pedley RB; Arstad E; Maher J; Yan R A dual reporter Iodinated labeling reagent for cancer positron emission tomography imaging and fluorescence-guided surgery. J. Med. Chem 2018, 61, 1636–1645. [PubMed: 29388770]

(904). Bodet-Milin C; Ferrer L; Rauscher A; Masson D; Rbah-Vidal L; Faivre-Chauvet A; Cerato E; Rousseau C; Hureaux J; Couturier O; et al. Pharmacokinetics and dosimetry studies for optimization of pretargeted radioimmunotherapy in CEA-expressing advanced lung cancer patients. Front. Med 2015, 2, 84.

(905). Houghton JL; Membreno R; Abdel-Atti D; Cunanan KM; Carlin S; Scholz WW; Zanzonico PB; Lewis JS; Zeglis BM Establishment of the in vivo efficacy of pretargeted radio-immunotherapy utilizing inverse electron demand diels-alder click chemistry. Mol. Cancer Ther 2017, 16, 124–133. [PubMed: 28062708]

(906). Witzig TE; Gordon LI; Cabanillas F; Czuczman MS; Emmanouilides C; Joyce R; Pohlman BL; Bartlett NL; Wiseman GA; Padre N; et al. Randomized controlled trial of yttrium-90-labeled ibritumomab tiuxetan radioimmunotherapy versus rituximab immunotherapy for patients with relapsed or refractory low-grade, follicular, or transformed B-cell non-Hodgkin's lymphoma. J. Clin. Oncol 2002, 20, 2453–2463. [PubMed: 12011122]

(907). Kaminski MS; Tuck M; Estes J; Kolstad A; Ross CW; Zasadny K; Regan D; Kison P; Fisher S; Kroll S; et al. 131I-tositumomab therapy as initial treatment for follicular lymphoma. N. Engl. J. Med 2005, 352, 441–449. [PubMed: 15689582]

(908). Tennvall J; Fischer M; Bischof Delaloye A; Bombardieri E; Bodei L; Giammarile F; Lassmann M; Oyen W; Brans BE; et al. EANM procedure guideline for radio-immunotherapy for B-cell lymphoma with 90Y-radiolabelled ibritumomab tiuxetan (Zevalin). Eur. J. Nucl. Med. Mol. Imaging 2007, 34, 616–622. [PubMed: 17323056]

(909). Thakral P; Singla S; Vashist A; Yadav MP; Gupta SK; Tyagi JS; Sharma A; Bal CS; Snehlata EY; Malhotra A Preliminary experience with yttrium-90-labelled rituximab (chimeric anti CD-20 antibody) in patients with relapsed and refractory B cell non-Hodgkins lymphoma. Curr. Radiopharm 2016, 9, 160–168. [PubMed: 27593256]

(910). Vaes M; Bron D; Vugts D; Paesmans M; Meuleman M; Ghanem G; Guiot T; Vanderlinden B; Thielemans K; van Dongen G Safety and efficacy of radioimmunotherapy with 90Yttrium-rituximab in patients with relapsed CD20+ B cell lymphoma: a feasibility study. J. Cancer Sci. Ther 2012, 4, 394–400.

(911). Green DJ; Frayo SL; Lin Y; Hamlin DK; Fisher DR; Frost SH; Kenoyer AL; Hylarides MD; Gopal AK; Gooley TA; et al. Comparative analysis of bispecific antibody and streptavidin-targeted radioimmunotherapy for B-cell cancers. Cancer Res 2016, 76, 6669–6679. [PubMed: 27590740]

(912). Park SI; Shenoi J; Frayo SM; Hamlin DK; Lin Y; Wilbur DS; Stayton PS; Orgun N; Hylarides M; Buchegger F; et al. Pretargeted radioimmunotherapy using genetically engineered antibody-streptavidin fusion proteins for treatment of non-hodgkin lymphoma. Clin. Cancer Res 2011, 17, 7373–7382. [PubMed: 21976541]

(913). Cassaday RD; Press OW; Pagel JM; Rajendran JG; Gooley TA; Fisher DR; Holmberg LA; Miyaoka RS; Sandmaier BM; Green DJ; et al. Phase I study of a CD45-targeted antibody–radionuclide conjugate for high-risk lymphoma. Clin. Cancer Res 2019, 25, 6932–6938. [PubMed: 31481510]

(914). Petrich T; Korkmaz Z; Krull D; Fromke C; Meyer GJ; Knapp WH In vitro experimental (211)At-anti-CD33 antibody therapy of leukaemia cells overcomes cellular resistance seen in vivo against gemtuzumab ozogamicin. Eur. J. Nucl. Med. Mol. Imaging 2010, 37, 851–861. [PubMed: 20107790]

(915). Hagemann UB; Wickstroem K; Wang E; Shea AO; Sponheim K; Karlsson J; Bjerke RM; Ryan OB; Cuthbertson AS In vitro and in vivo efficacy of a novel CD33-targeted thorium-227 conjugate for the treatment of acute myeloid leukemia. Mol. Cancer Ther 2016, 15, 2422–2431. [PubMed: 27535972]

(916). Srideshikan SM; Brooks J; Zuro D; Kumar B; Sanchez J; Echavarria Parra L; Orellana M; Vishwasrao P; Nair I; Chea J; et al. ImmunoPET, [(64)Cu]Cu-DOTA-Anti-CD33 PET-CT, imaging of an AML xenograft model. Clin. Cancer Res 2019, 25, 7463–7474. [PubMed: 31548348]

(917). de Vries EG; de Jong S; Gietema JA Molecular imaging as a tool for drug development and trial design. J. Clin. Oncol 2015, 33, 2585–2587. [PubMed: 26169612]

(918). Willmann JK; van Bruggen N; Dinkelborg LM; Gambhir SS Molecular imaging in drug development. Nat. Rev. Drug Discovery 2008, 7, 591–607. [PubMed: 18591980]

(919). Larson SM Cancer drug development with the help of radiopharmaceuticals: academic experience. Curr. Pharm. Des 2009, 15, 950–956. [PubMed: 19275659]

(920). Miller MA; Weissleder R Imaging of anticancer drug action in single cells. Nat. Rev. Cancer 2017, 17, 399–414. [PubMed: 28642603]

(921). Cai W; Rao J; Gambhir SS; Chen X How molecular imaging is speeding up antiangiogenic drug development. Mol. Cancer Ther 2006, 5, 2624–2633. [PubMed: 17121909]

(922). Lamberts LE; Williams SP; Terwisscha van Scheltinga AG; Lub-de Hooge MN; Schroder CP; Gietema JA; Brouwers AH; de Vries EG Antibody positron emission tomography imaging in anticancer drug development. J. Clin. Oncol 2015, 33, 1491–1504. [PubMed: 25779566]

(923). Berg E; Zhang X; Bec J; Judenhofer MS; Patel B; Peng Q; Kapusta M; Schmand M; Casey ME; Tarantal AF; et al. Development and evaluation of mini-EXPLORER: a long axial field-of-view PET scanner for nonhuman primate imaging. J. Nucl. Med 2018, 59, 993–998. [PubMed: 29419483]

(924). Berg E; Gill H; Marik J; Ogasawara A; Williams SP; van Dongen G; Vugts DJ; Cherry SR; Tarantal AF Total-body PET and highly stable chelators together enable meaningful (89)Zr-antibody-PET studies up to 30 days post-injection. J. Nucl. Med 2020, 61, 453–460.

(925). Rosenkrans ZT; Cai W Total-body PET imaging for up to 30 days after injection of (89)Zr-labeled antibodies. J. Nucl. Med 2020, 61, 451–452.

(926). Jauw YWS; O'Donoghue JA; Zijlstra JM; Hoekstra OS; Menke-van der Houven van Oordt CW; Morschhauser F; Carrasquillo JA; Zweegman S; Pandit-Taskar N; Lammertsma AA; et al. 89)Zr-Immuno-PET: toward a noninvasive clinical tool to measure target engagement of therapeutic antibodies in vivo. J. Nucl. Med 2019, 60, 1825–1832. [PubMed: 31147401]

(927). Oude Munnink TH; Dijkers EC; Netters SJ; Lub-de Hooge MN; Brouwers AH; Haasjes JG; Schroder CP; de Vries EG Trastuzumab pharmacokinetics influenced by extent human epidermal growth factor receptor 2-positive tumor load. J. Clin. Oncol 2010, 28, e355–356 author reply e357.. [PubMed: 20458048]

(928). Beck A; Goetsch L; Dumontet C; Corvaia N Strategies and challenges for the next generation of antibody-drug conjugates. Nat. Rev. Drug Discovery 2017, 16, 315–337. [PubMed: 28303026]

(929). Sijbrandi NJ; Merkul E; Muns JA; Waalboer DC; Adamzek K; Bolijn M; Montserrat V; Somsen GW; Haselberg R; Steverink PJ; et al. A novel platinum(II)-based bifunctional ADC linker benchmarked using 89Zr-desferal and auristatin F-conjugated trastuzumab. Cancer Res 2017, 77, 257–267. [PubMed: 27872093]

(930). Muns JA; Montserrat V; Houthoff HJ; Codee-van der Schilden K; Zwaagstra O; Sijbrandi NJ; Merkul E; van Dongen G In vivo characterization of platinum (II)-based linker technology for the development of antibody-drug conjugates: taking advantage of dual labeling with (195m)Pt and (89)Zr. J. Nucl. Med 2018, 59, 1146–1151. [PubMed: 29496986]

(931). Jacobson O; Li Q; Chen H; Niu G; Kiesewetter DO; Xu L; Cook K; Yang G; Dall'Acqua W; Tsui P; et al. PET-guided evaluation and optimization of internalized antibody-drug conjugates targeting erythropoietin-producing hepatoma A2 receptor.J. Nucl. Med 2017, 58, 1838–1844. [PubMed: 28546337]

(932). Adumeau P; Vivier D; Sharma SK; Wang J; Zhang T; Chen A; Agnew BJ; Zeglis BM Site-specifically labeled antibody-drug conjugate for simultaneous therapy and immunoPET. Mol. Pharmaceutics 2018, 15, 892–898.

(933). Teicher BA; Chari RV Antibody conjugate therapeutics: challenges and potential. Clin. Cancer Res 2011, 17, 6389–6397. [PubMed: 22003066]

(934). Rizvi SN; Visser OJ; Vosjan MJ; van Lingen A; Hoekstra OS; Zijlstra JM; Huijgens PC; van Dongen GA; Lubberink M Biodistribution, radiation dosimetry and scouting of 90Y-ibritumomab tiuxetan therapy in patients with relapsed B-cell non-Hodgkin's lymphoma using 89Zr-ibritumomab tiuxetan and PET. Eur. J. Nucl. Med. Mol. Imaging 2012, 39, 512–520. [PubMed: 22218876]

(935). Moek KL; Giesen D; Kok IC; de Groot DJA; Jalving M; Fehrmann RSN; Lub-de Hooge MN; Brouwers AH; de Vries EGE Theranostics using antibodies and antibody-related therapeutics. J. Nucl. Med 2017, 58, 83S–90S. [PubMed: 28864618]

(936). Schwarz SW; Decristoforo C; Goodbody AE; Singhal N; Saliba S; Ruddock P; Zukotynski K; Ross AA Harmonization of United States, European Union and Canadian first-in-human regulatory requirements for radiopharmaceuticals-is this possible? J. Nucl. Med 2019, 60, 158.

(937). Wright BD; Whittenberg J; Desai A; DiFelice C; Kenis PJ; Lapi SE; Reichert DE Microfluidic preparation of a 89Zr-labeled trastuzumab single-patient dose. J. Nucl. Med 2016, 57, 747–752. [PubMed: 26769862]

(938). Poot AJ; Adamzek KWA; Windhorst AD; Vosjan M; Kropf S; Wester HJ; van Dongen G; Vugts DJ Fully automated(89)Zr labeling and purification of antibodies. J. Nucl. Med 2019, 60, 691–695. [PubMed: 30530830]

(939). Cherry SR; Badawi RD; Karp JS; Moses WW; Price P; Jones T Total-body imaging: Transforming the role of positron emission tomography. Sci. Transl. Med 2017, 9, eaaf6169. [PubMed: 28298419]

(940). Karp JS; Viswanath V; Geagan MJ; Muehllehner G; Pantel AR; Parma MJ; Perkins AE; Schmall JP; Werner ME; Daube-Witherspoon ME PennPET explorer: design and preliminary performance of a whole-body imager. J. Nucl. Med 2020, 61, 136–143.

(941). Badawi RD; Shi H; Hu P; Chen S; Xu T; Price PM; Ding Y; Spencer BA; Nardo L; Liu W; et al. First human imaging studies with the EXPLORER total-body PET scanner. J. Nucl. Med 2019, 60, 299–303. [PubMed: 30733314]

(942). Zaidi H; Alavi A; Naqa IE Novel quantitative PET techniques for clinical decision support in oncology. Semin. Nucl. Med 2018, 48, 548–564. [PubMed: 30322481]

(943). Haberkorn U; Mier W; Kopka K; Herold-Mende C; Altmann A; Babich J Identification of ligands and translation to clinical applications. J. Nucl. Med 2017, 58, 27S–33S. [PubMed: 28864609]

(944). Lee ST; Burvenich I; Scott AM Novel target selection for nuclear medicine studies. Semin. Nucl. Med 2019, 49, 357–368. [PubMed: 31470931]

(945). Jefferis R Antibody therapeutics: isotype and glycoform selection. Expert Opin. Biol. Ther 2007, 7, 1401–1413. [PubMed: 17727329]

(946). Jefferis R Isotype and glycoform selection for antibody therapeutics. Arch. Biochem. Biophys 2012, 526, 159–166. [PubMed: 22465822]

(947). Bournazos S; Ravetch JV Fcgamma receptor function and the design of vaccination strategies. Immunity 2017, 47, 224–233. [PubMed: 28813656]

(948). Warnders FJ; Lub-de Hooge MN; de Vries EGE; Kosterink JGW Influence of protein properties and protein modification on biodistribution and tumor uptake of anticancer antibodies, antibody derivatives, and non-Ig scaffolds. Med. Res. Rev 2018, 38, 1837–1873. [PubMed: 29635825]

(949). Zhang T; Song X; Xu L; Ma J; Zhang Y; Gong W; Zhang Y; Zhou X; Wang Z; Wang Y; et al. The binding of an anti-PD-1 antibody to FcgammaRIota has a profound impact on its biological functions. Cancer Immunol. Immunother 2018, 67, 1079–1090. [PubMed: 29687231]

(950). Ingram JR; Blomberg OS; Sockolosky JT; Ali L; Schmidt FI; Pishesha N; Espinosa C; Dougan SK; Garcia KC; Ploegh HL; et al. Localized CD47 blockade enhances immunotherapy for murine melanoma. Proc. Natl. Acad. Sci. U. S. A 2017, 114, 10184–10189. [PubMed: 28874561]

(951). Vivier D; Sharma SK; Adumeau P; Rodriguez C; Fung K; Zeglis BM The impact of FcgammaRI binding on immuno-PET.J. Nucl. Med 2019, 60, 1174–1182. [PubMed: 30733320]

(952). Vivier D; Fung K; Rodriguez C; Adumeau P; Ulaner GA; Lewis JS; Sharma SK; Zeglis BM The influence of glycans-specific bioconjugation on the FcγRI binding and in vivo performance of 89Zr-DFO-pertuzumab. Theranostics 2020, 10, 1746–1757.

(953). Ehlerding EB; Sun L; Lan X; Zeng D; Cai W Dual-targeted molecular imaging of cancer. J. Nucl. Med 2018, 59, 390–395. [PubMed: 29301927]

(954). Kraeber-Bodere F; Rousseau C; Bodet-Milin C; Frampas E; Faivre-Chauvet A; Rauscher A; Sharkey RM; Goldenberg DM; Chatal JF; Barbet J A pretargeting system for tumor PET imaging and radioimmunotherapy. Front. Pharmacol 2015, 6, 54. [PubMed: 25873896]

(955). Keinanen O; Fung K; Pourat J; Jallinoja V; Vivier D; Pillarsetty NK; Airaksinen AJ; Lewis JS; Zeglis BM; Sarparanta M Pretargeting of internalizing trastuzumab and cetuximab with a (18)F-tetrazine tracer in xenograft models. EJNMMI Res 2017, 7, 95. [PubMed: 29198065]

(956). Stefan N; Gebleux R; Waldmeier L; Hell T; Escher M; Wolter FI; Grawunder U; Beerli RR Highly potent, anthracycline-based antibody-drug conjugates generated by enzymatic, site-specific conjugation. Mol. Cancer Ther 2017, 16, 879–892. [PubMed: 28258164]

(957). De La Rochere P; Guil-Luna S; Decaudin D; Azar G; Sidhu SS; Piaggio E Humanized mice for the study of immunooncology. Trends Immunol 2018, 39, 748–763. [PubMed: 30077656]

(958). Fernandes SRG; Fernandes R; Sarmento B; Pereira PMR; Tome JPC Photoimmunoconjugates: novel synthetic strategies to target and treat cancer by photodynamic therapy. Org. Biomol. Chem 2019, 17, 2579–2593. [PubMed: 30648722]

(959). Kobayashi H; Choyke PL Near-infrared photoimmuno-therapy of cancer. Acc. Chem. Res 2019, 52, 2332–2339. [PubMed: 31335117]

(960). Green DJ; Press OW Whither radioimmunotherapy: to be or not to be? Cancer Res 2017, 77, 2191–2196. [PubMed: 28428282]

(961). Patra M; Zarschler K; Pietzsch HJ; Stephan H; Gasser G New insights into the pretargeting approach to image and treat tumours. Chem. Soc. Rev 2016, 45, 6415–6431. [PubMed: 27722526]

(962). Levy A; Nigro G; Sansonetti PJ; Deutsch E Candidate immune biomarkers for radioimmunotherapy. Biochim. Biophys. Acta, Rev. Cancer 2017, 1868, 58–68. [PubMed: 28254528]

(963). Cheal SM; Xu H; Guo HF; Patel M; Punzalan B; Fung EK; Lee SG; Bell M; Singh M; Jungbluth AA; et al. Theranostic pretargeted radioimmunotherapy of internalizing solid tumor antigens in human tumor xenografts in mice: curative treatment of HER2-positive breast carcinoma. Theranostics 2018, 8, 5106–5125. [PubMed: 30429889]

(964). Kraeber-Bodere F; Bodet-Milin C; Rousseau C; Eugene T; Pallardy A; Frampas E; Carlier T; Ferrer L; Gaschet J; Davodeau F; et al. Radioimmunoconjugates for the treatment of cancer. Semin. Oncol 2014, 41, 613–622. [PubMed: 25440606]

(965). Ehlerding EB; Lan X; Cai W "Albumin Hitchhiking" with an evans blue analog for cancer theranostics. Theranostics 2018, 8, 812–814. [PubMed: 29344308]

(966). Kratochwil C; Bruchertseifer F; Giesel FL; Weis M; Verburg FA; Mottaghy F; Kopka K; Apostolidis C; Haberkorn U; Morgenstern A 225Ac-PSMA-617 for PSMA-targeted alpha-radiation therapy of metastatic castration-resistant prostate cancer. J. Nucl. Med 2016, 57, 1941–1944. [PubMed: 27390158]

(967). Kratochwil C; Schmidt K; Afshar-Oromieh A; Bruchertseifer F; Rathke H; Morgenstern A; Haberkorn U; Giesel FL Targeted alpha therapy of mCRPC: dosimetry estimate of (213)Bismuth-PSMA-617. Eur. J. Nucl. Med. Mol. Imaging 2018, 45, 31–37. [PubMed: 28891033]

(968). Vahrmeijer AL; Hutteman M; van der Vorst JR; van de Velde CJ; Frangioni JV Image-guided cancer surgery using near-infrared fluorescence. Nat. Rev. Clin. Oncol 2013, 10, 507–518. [PubMed: 23881033]

(969). Linssen MD; Ter Weele EJ; Allersma DP; Lub-de Hooge MN; van Dam GM; Jorritsma-Smit A; Nagengast WB Roadmap for the development and clinical translation of optical tracers cetuximab-800CW and trastuzumab-800CW. J. Nucl. Med 2019, 60, 418–423. [PubMed: 30630938]

(970). Zettlitz KA; Waldmann CM; Tsai WK; Tavare R; Collins J; Murphy JM; Wu AM A dual-modality linker enables site-specific conjugation of antibody fragments for (18)F-immuno-PET and fluorescence imaging. J. Nucl. Med 2019, 60, 1467–1473. [PubMed: 30877181]

(971). Cohen R; Vugts DJ; Stigter-van Walsum M; Visser GW; van Dongen GA Inert coupling of IRDye800CW and zirconium-89 to monoclonal antibodies for single- or dual-mode fluorescence and PET imaging. Nat. Protoc 2013, 8, 1010–1018. [PubMed: 23619892]

(972). Lee HJ; Ehlerding EB; Jiang D; Barnhart TE; Cao T; Wei W; Ferreira CA; Huang P; Engle JW; Cai W Dual-labeled pertuzumab for multimodality image-guided ovarian tumor resection. Am. J. Cancer Res 2019, 9, 1454–1468. [PubMed: 31392081]

(973). Shaffer TM; Pratt EC; Grimm J Utilizing the power of Cerenkov light with nanotechnology. Nat. Nanotechnol 2017, 12, 106–117. [PubMed: 28167827]

(974). Ferreira CA; Ni D; Rosenkrans ZT; Cai W Radionuclide-activated nanomaterials and their biomedical applications. Angew. Chem., Int. Ed 2019, 58, 13232–13252.

(975). Kotagiri N; Sudlow GP; Akers WJ; Achilefu S Breaking the depth dependency of phototherapy with Cerenkov radiation and low-radiance-responsive nanophotosensitizers. Nat. Nanotechnol 2015, 10, 370–379. [PubMed: 25751304]

(976). Maier FC; Wild AM; Kirchen N; Holm F; Fuchs K; Schwenck J; Maurer A; Wiehr S Comparative immuno-Cerenkov luminescence and -PET imaging enables detection of PSMA(+) tumors in mice using (64)Cu-radiolabeled monoclonal antibodies. Appl. Radiat. Isot 2019, 143, 149–155. [PubMed: 30445280]

(977). Ni D; Ferreira CA; Barnhart TE; Quach V; Yu B; Jiang D; Wei W; Liu H; Engle JW; Hu P; et al. Magnetic targeting of nanotheranostics enhances Cerenkov radiation-induced photodynamic therapy. J. Am. Chem. Soc 2018, 140, 14971–14979. [PubMed: 30336003]

(978). Yu B; Wei H; He Q; Ferreira CA; Kutyreff CJ; Ni D; Rosenkrans ZT; Cheng L; Yu F; Engle JW; et al. Efficient uptake of (177) Lu-porphyrin-PEG nanocomplexes by tumor mitochondria for multimodal-imaging-guided combination therapy. Angew. Chem., Int. Ed 2018, 57, 218–222.

(979). Xing Y; Chand G; Liu C; Cook GJR; O'Doherty J; Zhao L; Wong NCL; Meszaros LK; Ting HH; Zhao J Early phase I study of a (99m)Tc-labeled anti-programmed death ligand-1 (PD-L1) single-domain antibody in SPECT/CT assessment of PD-L1 expression in non-small cell lung cancer. J. Nucl. Med 2019, 60, 1213–1220. [PubMed: 30796165]

(980). Zhang P; Zhuang R; Guo Z; Su X; Chen X; Zhang X A highly efficient copper-mediated radioiodination approach using aryl boronic acids. Chem. - Eur. J 2016, 22, 16783–16786. [PubMed: 27730680]

(981). Pruszynski M; Loktionova NS; Filosofov DV; Rosch F Post-elution processing of (44)Ti/(44)Sc generator-derived (44)Sc for clinical application. Appl. Radiat. Isot 2010, 68, 1636–1641. [PubMed: 20434351]

(982). Alliot C; Kerdjoudj R; Michel N; Haddad F; Huclier-Markai S Cyclotron production of high purity (44m,44)Sc with deuterons from (44)CaCO3 targets. Nucl. Med. Biol 2015, 42, 524–529. [PubMed: 25794463]

(983). van der Meulen NP; Bunka M; Domnanich KA; Muller C; Haller S; Vermeulen C; Turler A; Schibli R Cyclotron production of (44)Sc: From bench to bedside. Nucl. Med. Biol 2015, 42, 745–751. [PubMed: 26093495]

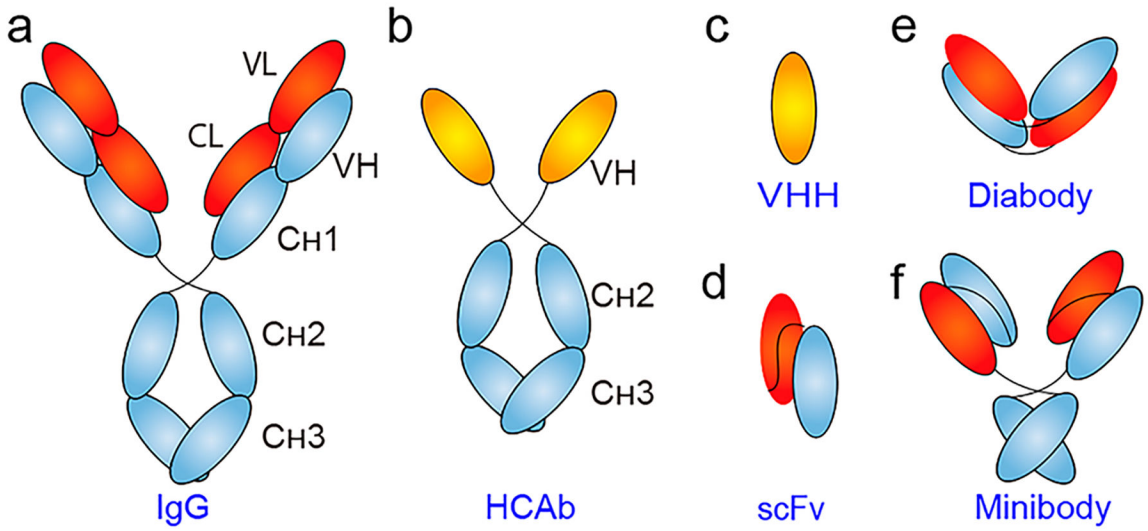

Figure 1.

Schematic of representative antibody and antibody fragments. (a) Conventional IgG is composed of two identical heavy chains and two identical light chains. While each heavy chain consists of three constant domains (i.e., C_H1, C_H2, and C_H3) and a variable domain (VH), an IgG light chain has one constant domain (CL) and one variable domain (VL). (b) Heavy-chain-only antibody (HCAb) lacks the light chains and the typical C_H1 domain. (c) The antigen-binding specificity of a HCAb is due to the single VHH domain. (d) Single-chain variable fragment (scFv) is the smallest unit of the IgG molecule that retains antigen-binding capacity. Using scFv as the building block, (e) diabody (dimers of scFv), and (f) minibody (dimers of scFv–C_H3) can be constructed.

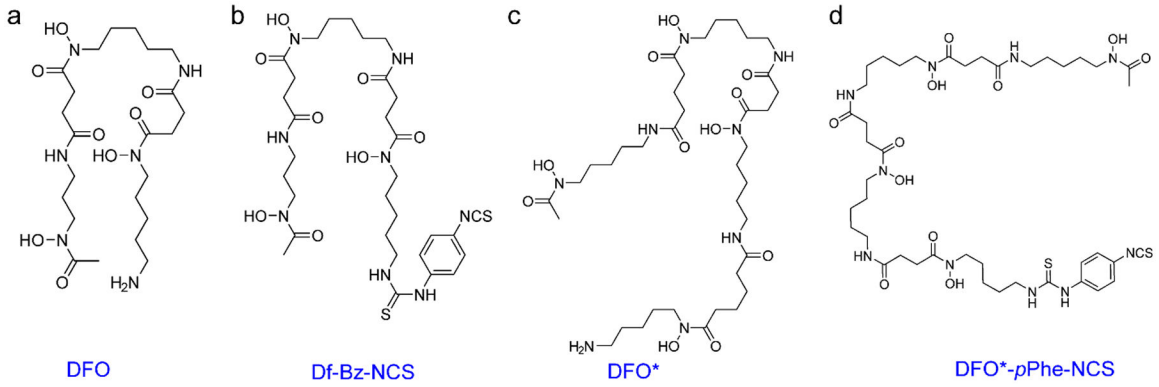

Figure 2.
Chemical structures of chelators used in ^{89}Zr-labeling of antibody vectors.

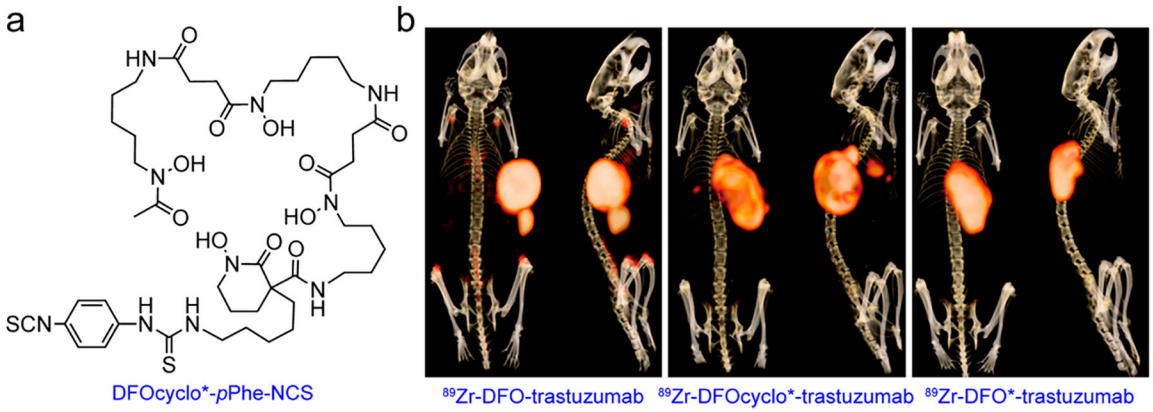

Figure 3.

Comparison DFO, DFO*, and DFOcyclo* in immunoPET imaging. (a) Chemical structure of DFOcyclo*-*p*Phe-NCS. (b) ImmunoPET imaging with ^{89}Zr-DFO-trastuzumab (left), ^{89}Zr-DFOcyclo*-trastuzumab (middle), and ^{89}Zr-DFO*-trastuzumab (right) in HER2^{+} SKOV-3 models. The results showed bone uptake in mice injected with ^{89}Zr-DFO-trastuzumab but not with ^{89}Zr-DFOcyclo*-trastuzumab or ^{89}Zr-DFO*-trastuzumab at 168 h after injection of the radiotracers. Reproduced with permission from ref 126. Copyright 2019 Springer Berlin Heidelberg under [CC LICENSE] [http://creativecommons.org/licenses/by/4.0/].

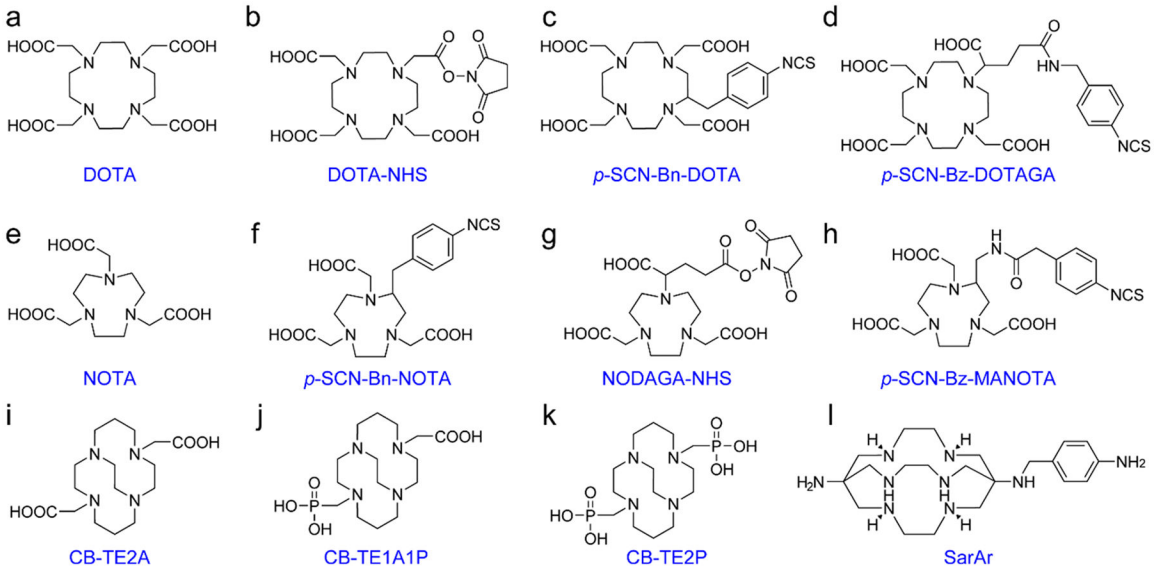

Figure 4.

Chemical structures of chelators used in ^{64}Cu-labeling of antibody vectors.

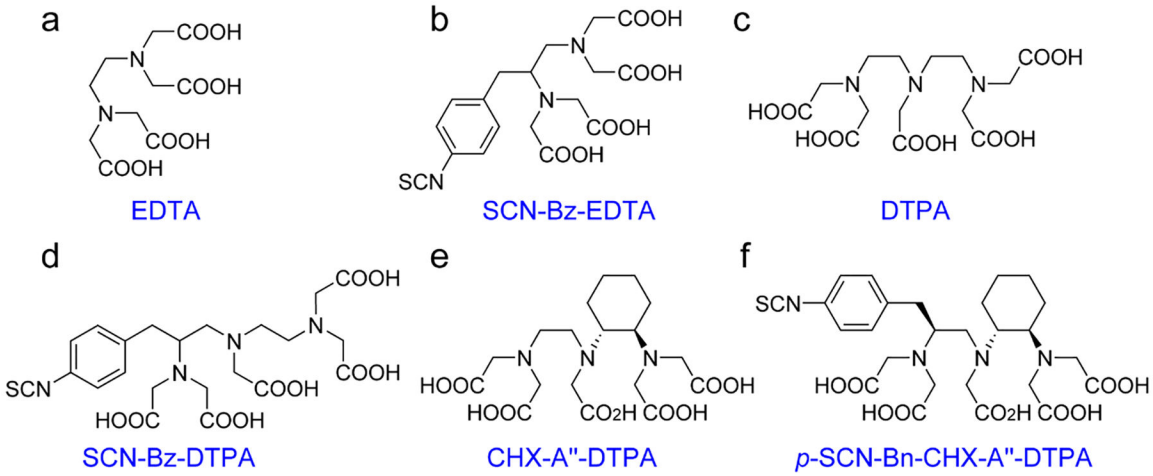

Figure 5.
Chemical structures of chelators used in ^{86}Y-labeling of antibody vectors.

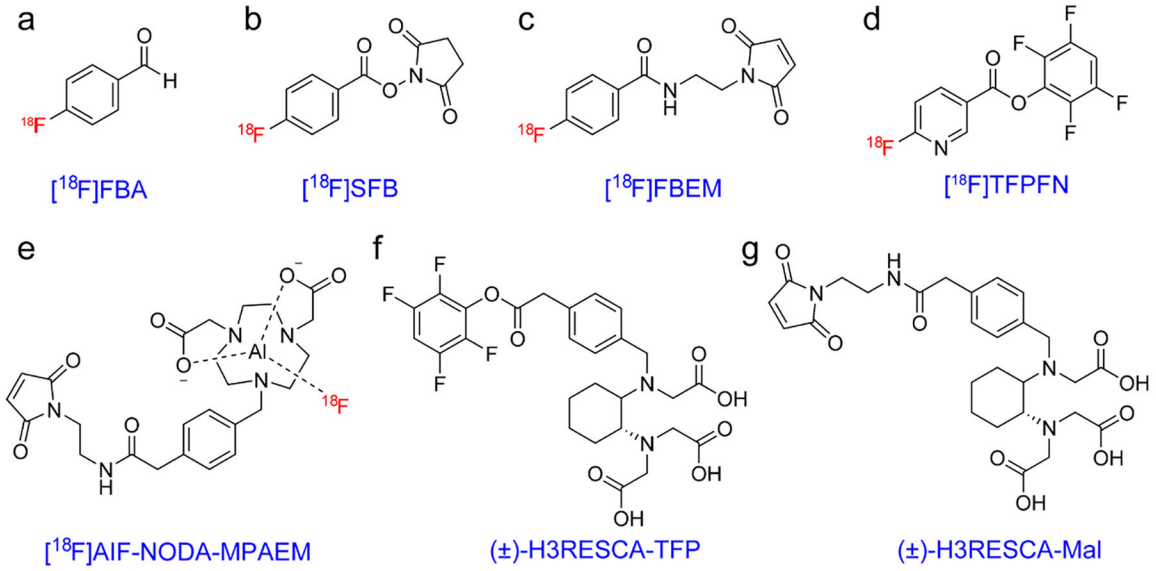

Figure 6.
Chemical structures of prosthetic groups and chelators in ^{18}F-labeling of antibody vectors.

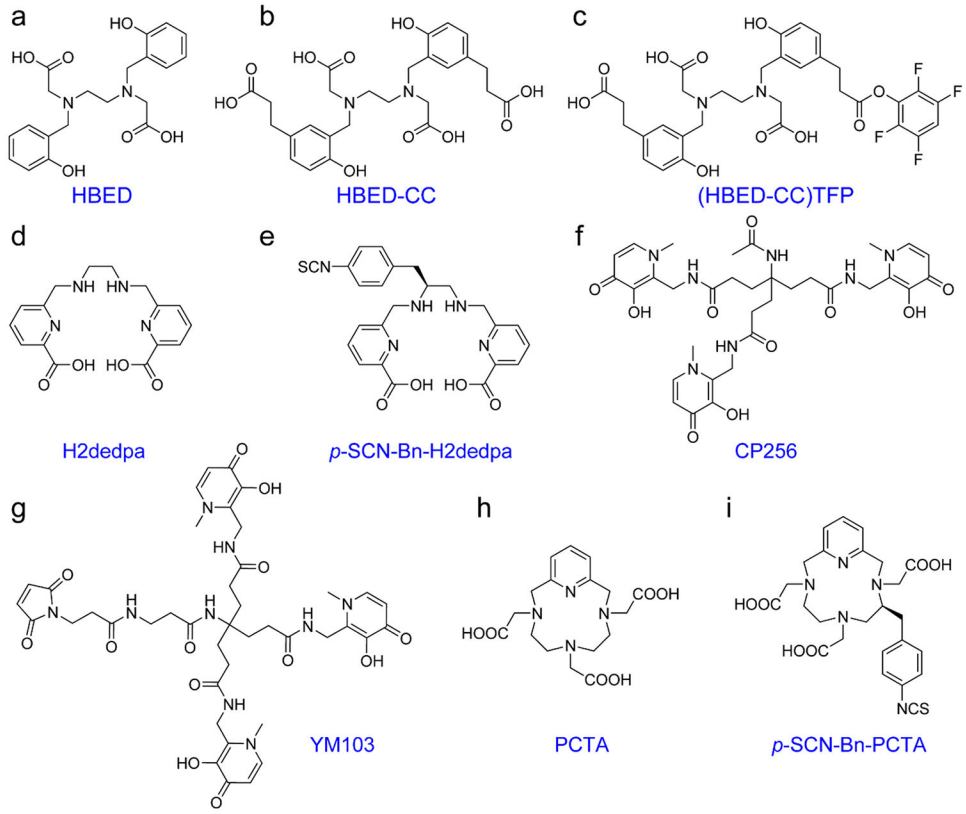

Figure 7.
Chemical structures of chelators used in ^{68}Ga-labeling of antibody vectors.

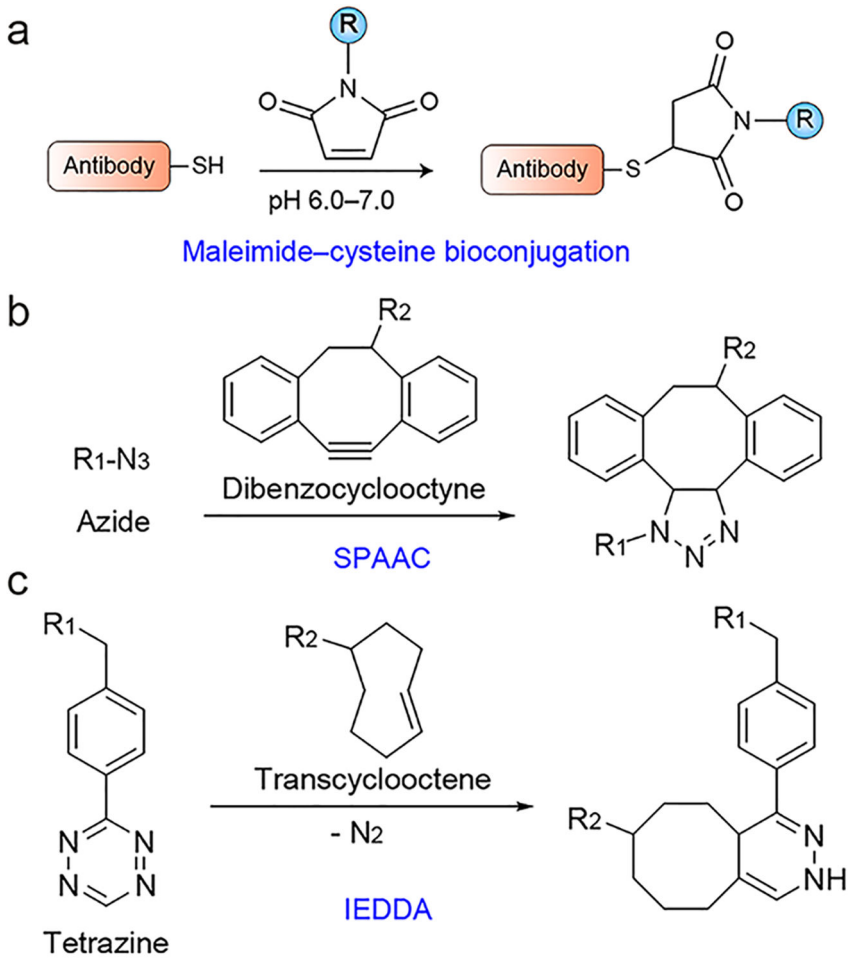

Figure 8.

Site-specific radiolabeling strategies. (a) The maleimide–cysteine reaction is among the most commonly used strategies for site-specific radiolabeling of antibody vectors. R = chelator of interest. (b) The strain-promoted azide–alkyne cycloaddition (SPAAC) reaction. R1 = antibody of interest, R2 = chelator of interest. (c) The inverse electron demand Diels–Alder (IEDDA) cycloaddition reaction. R1 = chelator of interest, R2 = antibody of interest. It is worth noting that radiolabeling via the click chemistry reaction goes both ways.

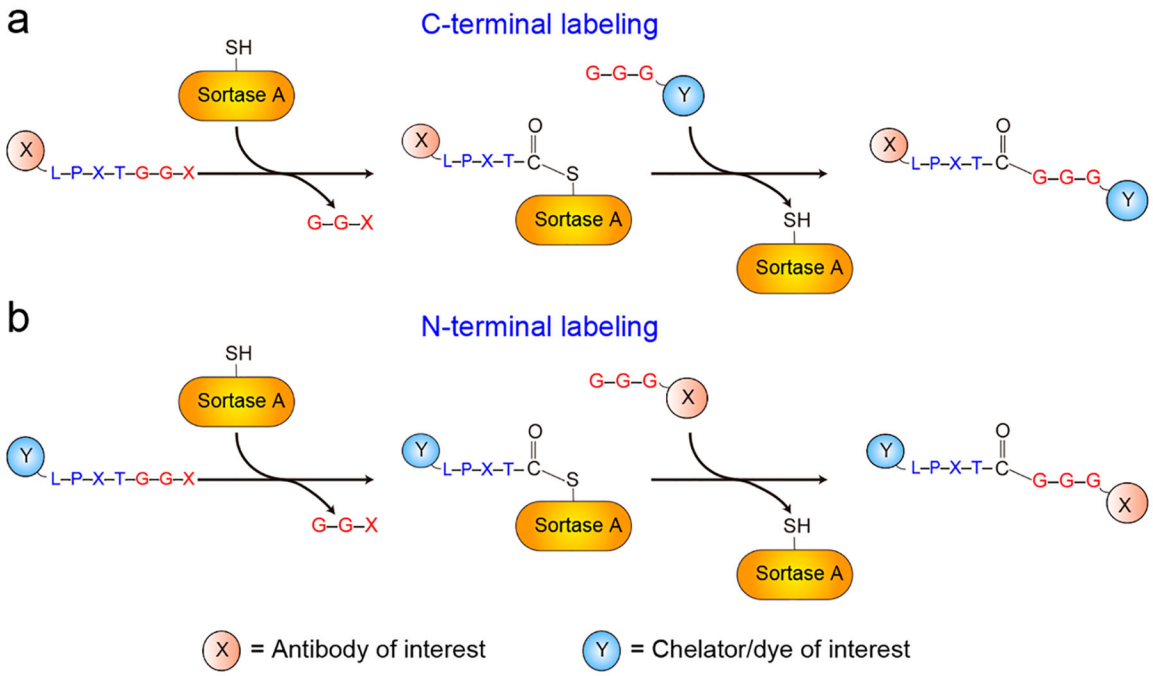

Figure 9.

Sortase-catalyzed site-specific labeling of antibody moieties. (a) For C-terminal labeling, the LP*X*TG motif is expressed at the C-terminus of the targeting vector (e.g., VHH and antibody fragment). (b) For N-terminal labeling, sortase recognition tag (i.e., LP*X*TG) is positioned at the C-terminus of the modification (e.g., chelator and dye) with the oligoglycine nucleophile inserted at the N-terminus of the targeting vector.

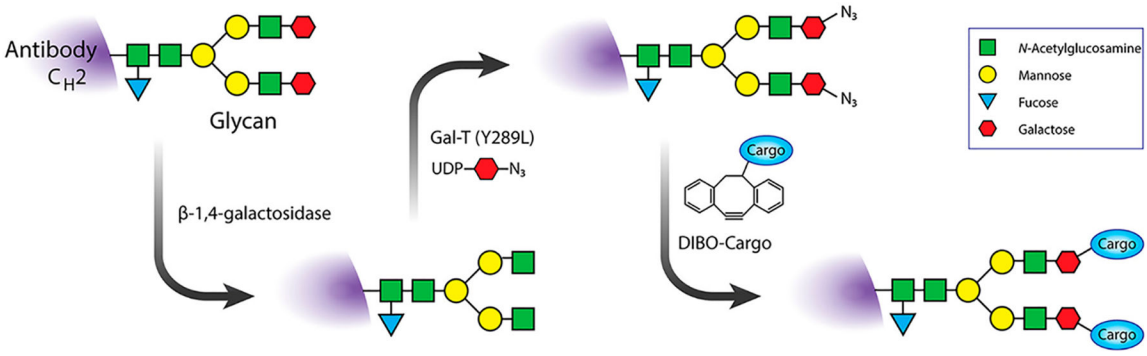

Figure 10.

Schematic of a chemoenzymatic methodology for site-specifically grafting cargoes (e.g., chelator) to the heavy-chain glycans of an antibody of interest. Reproduced with permission from ref 261. Copyright 2016 American Chemical Society.

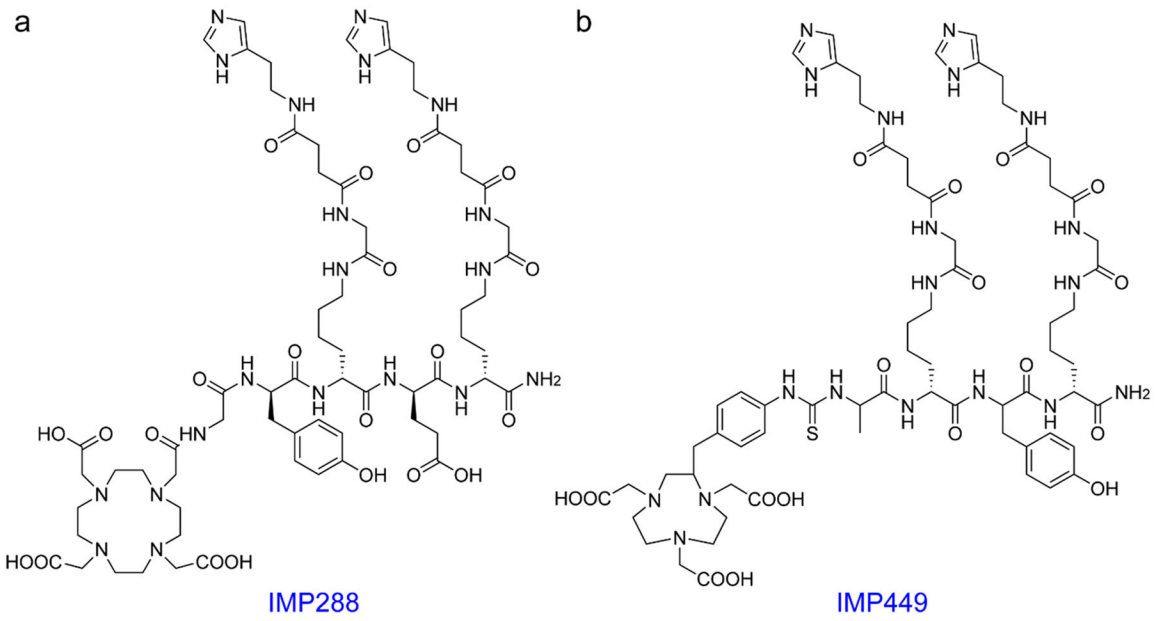

Figure 11.

Chemical structures of DOTA-HSG and NOTA-HSG hapten peptides used in pretargeted immunoPET imaging.

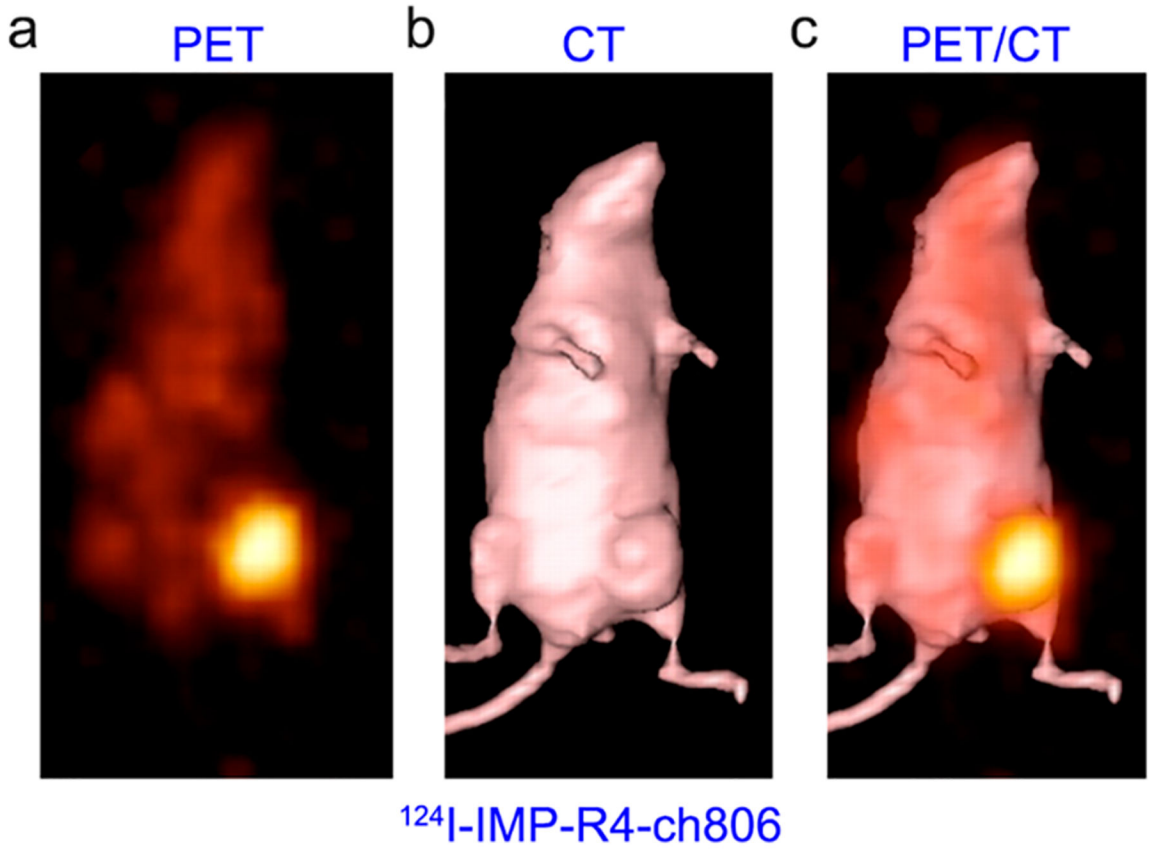

Figure 12.

ImmunoPET imaging of EGFR expression using ^{124}I-labeled residualizing radiotracer. (a–c) ^{124}I-IMP-R4-ch806 immuno-PET imaging clearly delineated EGFR-positive gliomas with negligible uptake in normal tissues. Reproduced with permission from ref 373. Copyright 2010 SNMMI.

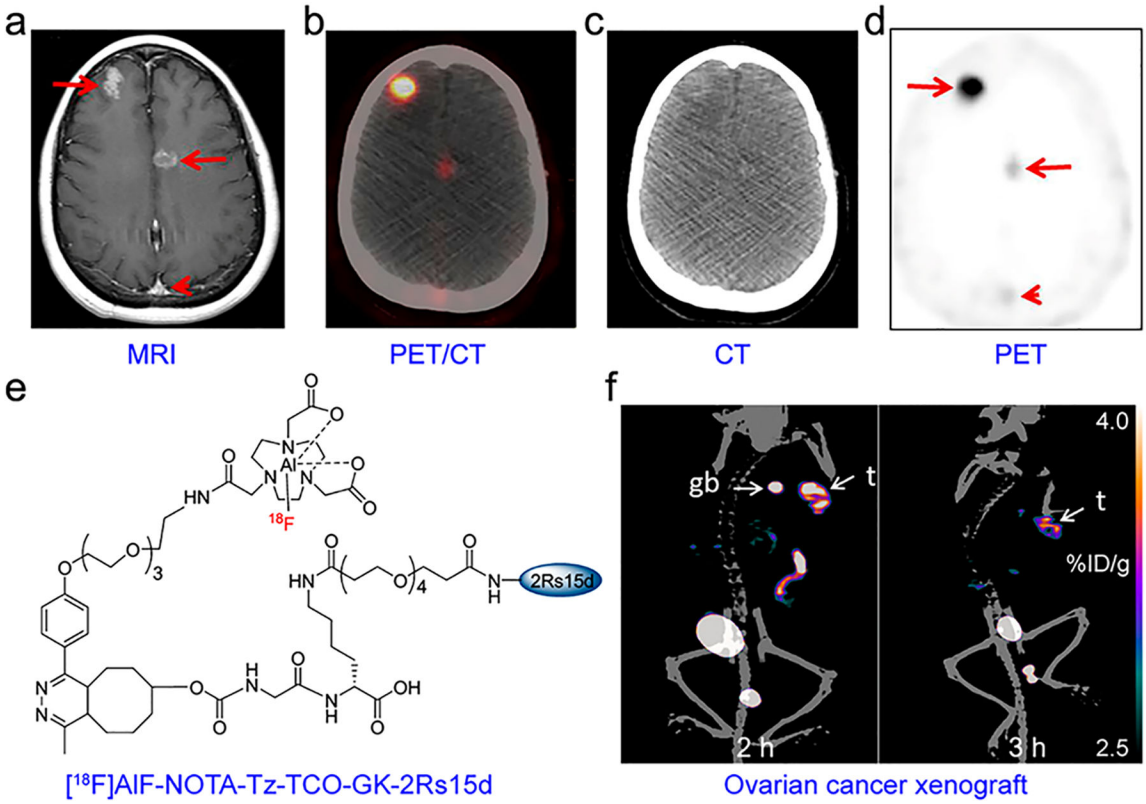

Figure 13.

ImmunoPET imaging of HER2 expression. (a) T1-weighed MR imaging of a 46-year-old woman showed brain metastases from breast cancer (red arrows). (b–d) ^{89}Zr-Dfpertuzumab immunoPET/CT imaging of the same patient demonstrated varying uptake of the radiotracer in brain metastases (red arrows) and minimal uptake in the superior sagittal sinus (red arrowhead). Reproduced with permission from ref 396. Copyright 2018 SNMMI. (e) Chemical structure of [^{18}F]AlF-NOTA-Tz-TCOGK-2Rs15d. (f) ImmunoPET/CT imaging of a human ovarian cancer xenograft at 2 and 3 h after injection of [^{18}F]AlF-NOTA-Tz-TCOGK-2Rs15d. Reproduced with permission from ref 416. Copyright 2018 American Chemical Society.

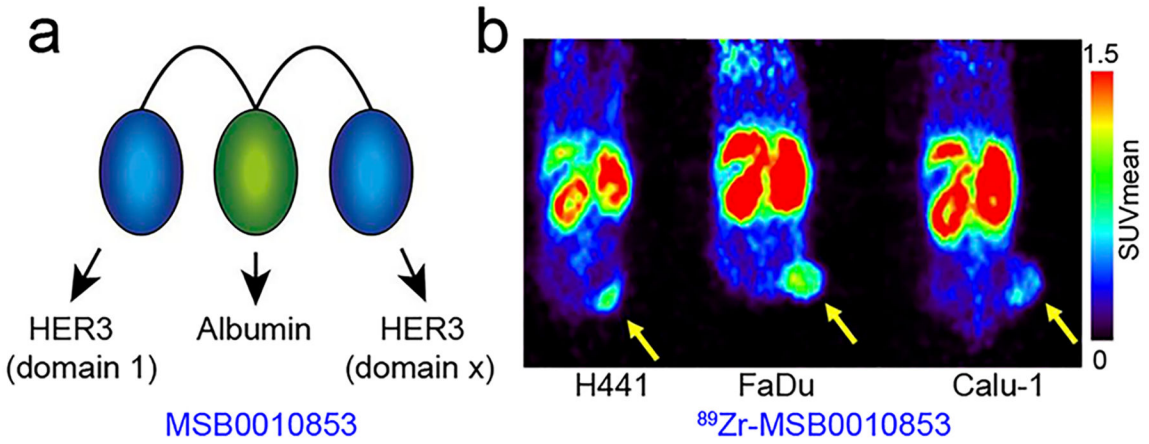

Figure 14.

ImmunoPET imaging of HER3 expression. (a) MSB0010853 is composed of two Nanobodies targeting two different epitopes of HER3 and an additional Nanobody targeting albumin. (b) ^{89}Zr-MSB0010853 immunoPET imaging of HER3-positive mouse xenografts (H441 and FaDu) and HER3-negative mouse xenograft (Calu-1) demonstrated the ability of this imaging approach to reveal varying HER3 expression levels. Reproduced with permission from ref 465. Copyright 2017 SNMMI.

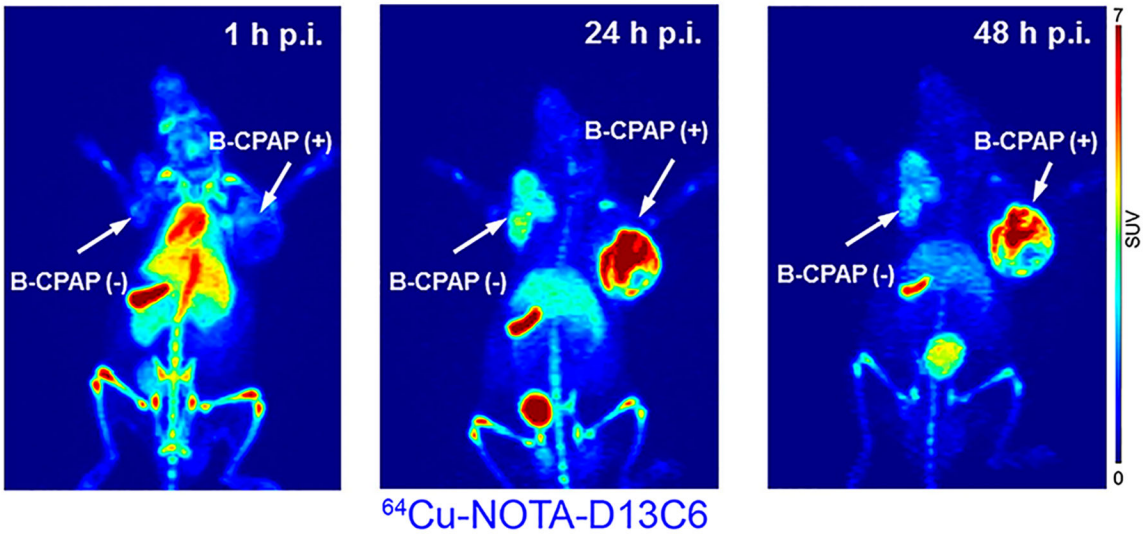

Figure 15.

ImmunoPET imaging of PDGFRa expression using ^{64}Cu-NOTA-D13C6. While lower uptake of ^{64}Cu-NOTA-D13C6 was seen in the PDGFRα-negative B-CPAP tumor (left flank), higher accumulation of the radiotracer was observed in the transfected PDGFRα-positive B-CPAP tumor (right flank) at late time-points. Reproduced with permission from ref 512. Copyright 2018 Elsevier Inc.

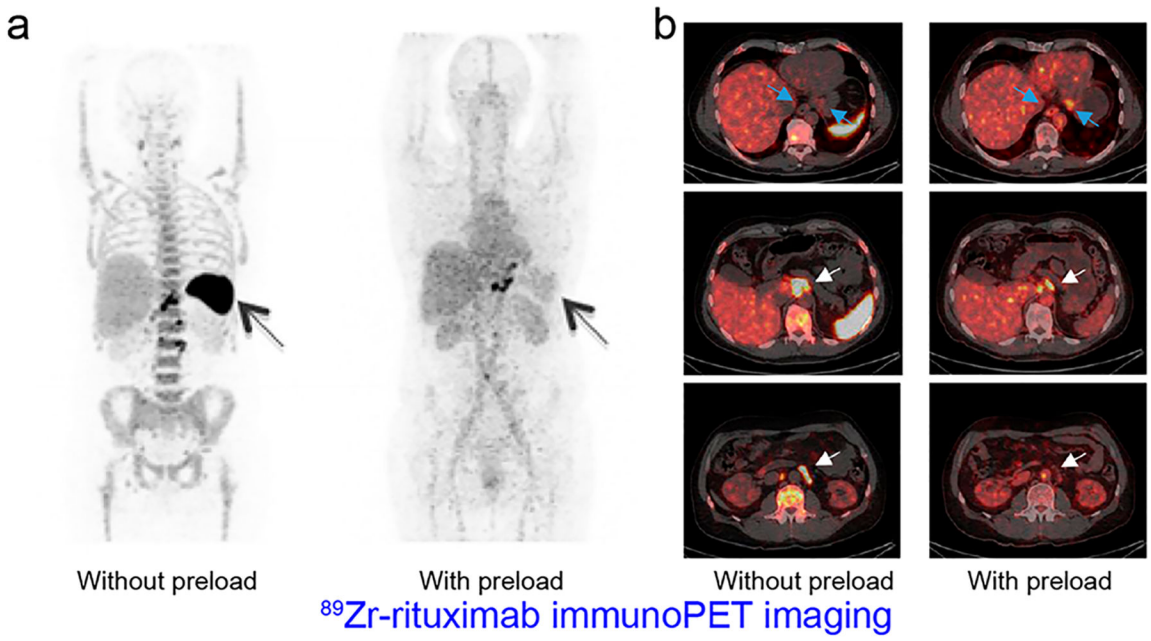

Figure 16.

ImmunoPET imaging of non-Hodgkin's lymphomas. (a) In a patient with circulating $CD20^{+}$ lymphocytes, significant uptake of ^{89}Zr-rituximab was observed in the spleen, which was blocked by preloading with unlabeled rituximab (250 mg/m^2) prior to injection of ^{89}Zr-rituximab. The spleen is indicated with black arrows. (b) In the same patient, preloading reduced ^{89}Zr-rituximab uptake in the involved lymph nodes (white arrows), but enhanced uptake of the radiotracer in the visceral lesions (blue arrows). Reproduced with permission from ref 536. Copyright 2015 Springer Berlin Heidelberg.

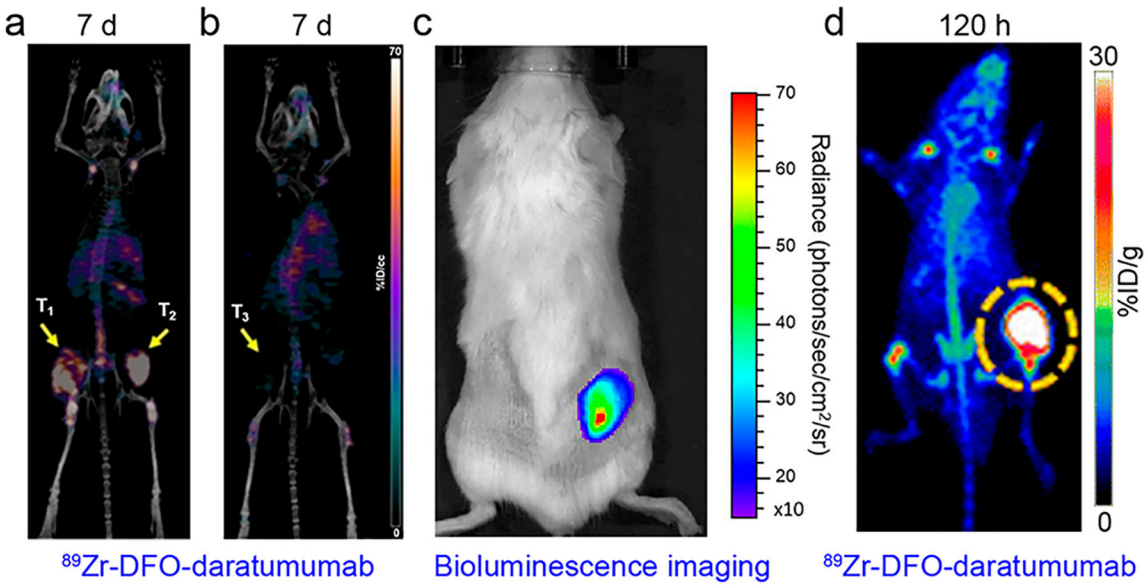

Figure 17.

ImmunoPET imaging of CD38 expression. (a) ^{89}Zr-DFO-daratumumab immunoPET/CT imaging of a mouse bearing bilateral MM1.S tumors (T_1 and T_2). (b) ^{89}Zr-DFO-daratumumab immuno-PET/CT imaging of a mouse bearing a unilateral MM1.S tumor (T_3) in the presence of unlabeled daratumumab as a blocking agent. (c) Representative bioluminescence imaging of the mice in the blocking group receiving an injection of cold daratumumab. The bioluminescent signal indicates the successful establishment of the tumor on the right flank of the mouse. Reproduced with permission from ref 550. Copyright 2018 SNMMI. (d) ^{89}Zr-DFO-daratumumab immunoPET imaging of lymphoma (Ramos tumor) at 120 h after administration of the tracer. Reproduced with permission from ref 552. Copyright 2018 Springer Berlin Heidelberg.

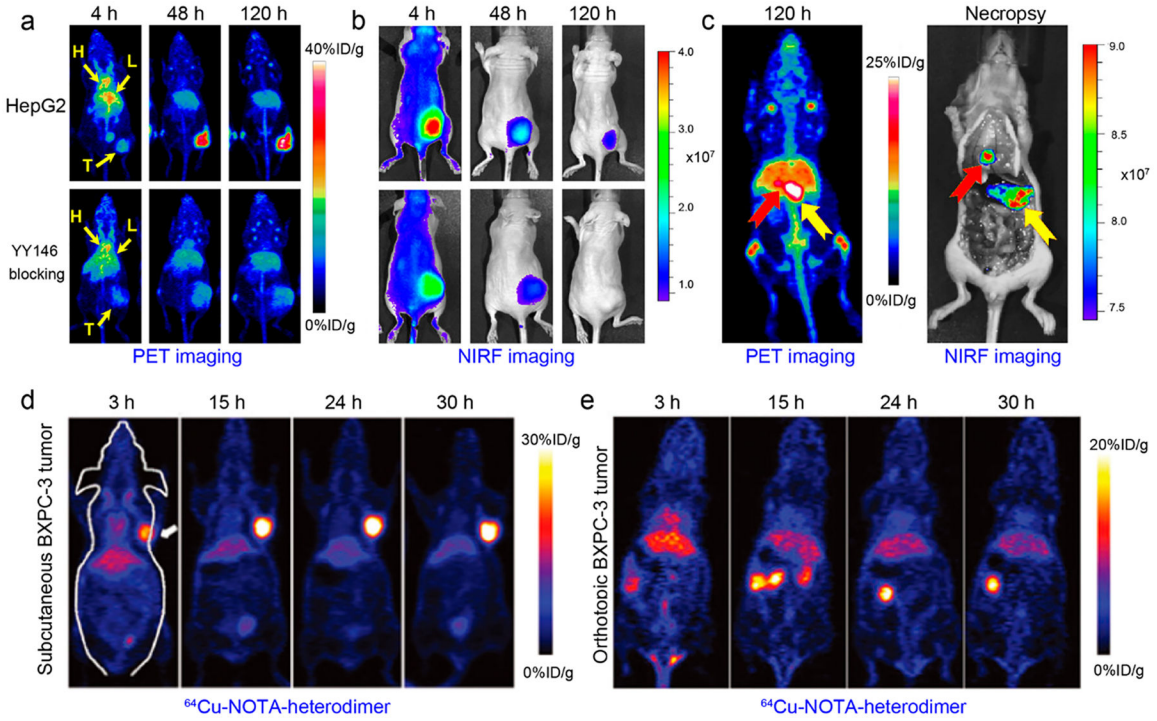

Figure 18.

ImmunoPET probes targeting CD146 and CD105. (a) ImmunoPET and (b) near-infrared fluorescence (NIRF) imaging performed at different time-points after intravenous injection of ^{89}Zr-Df-YY146-ZW800 demonstrated prominent and persistent uptake of the tracer in HepG2 tumors but not in the YY146 blocking group. H (heart), L (liver), and T (tumor). (c) Clear delineation of orthotopic HepG2 tumors by both PET and NIRF imaging was enabled through ^{89}Zr-Df-YY146-ZW800, which further facilitated image-guided resection of the multiple tumors (red and yellow arrows). Reproduced with permission from ref 573. Copyright 2016 Ivyspring International Publisher. (d) Serial coronal immunoPET imaging using a tissue factor and CD105 dual-targeting ^{64}Cu-NOTA-heterodimer at 3, 15, 24, and 30 h postinjection of the tracer clearly detected the BxPC-3 tumor. (e) Coronal PET images of mice bearing an orthotopic BxPC-3 tumor at 3, 15, 24, and 30 h following injection of ^{64}Cu-NOTA-heterodimer. This imaging technique realized an easy diagnosis of the orthotopic BxPC-3 tumor with negligible radioactivity around the surrounding tissues. Reproduced with permission from ref 590. Copyright 2016 American Association for Cancer Research.

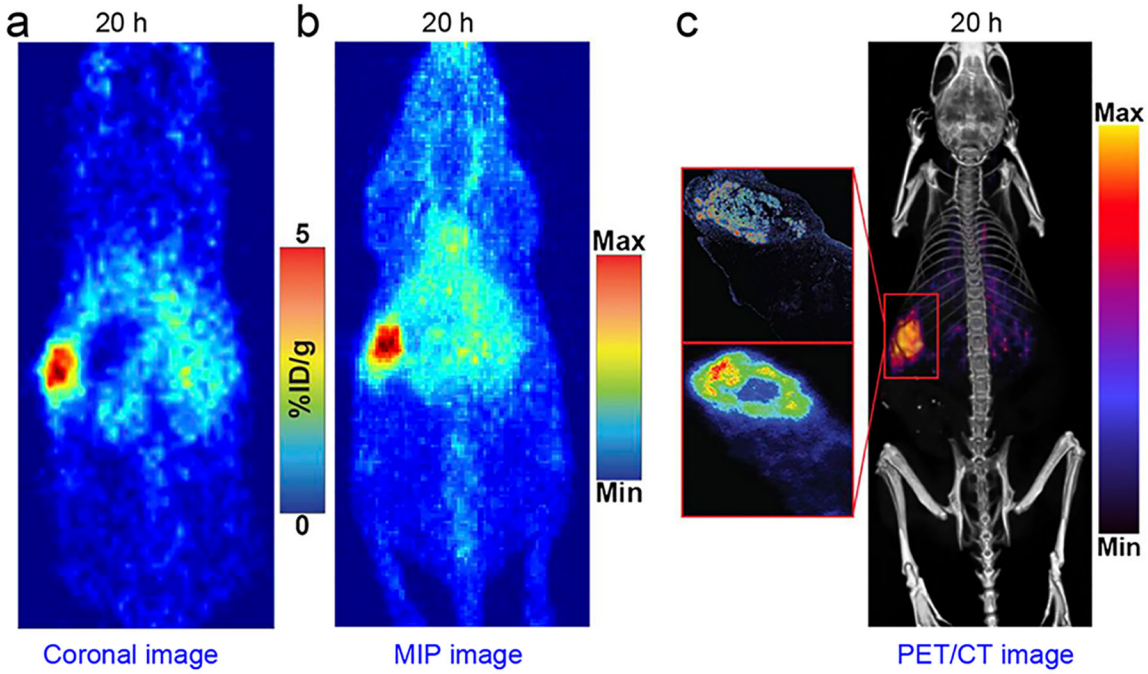

Figure 19.

Pretargeted immunoPET imaging of pancreatic cancer. 5B1-TCO was first administered to target CA19.9-expressing orthotopic Capan-2 xenograft followed by injection of ^{64}Cu-NOTAPEG$_7$-Tz 3 days after the previous injection. (a) Coronal and (b) maximum-intensity projection (MIP) images demonstrated that this pretargeted imaging approach clearly delineated the Capan-2 tumor.(c) Immunohistochemistry (top left), autoradiography (bottom left), and fused PET/CT image (right) from the same mouse further showed precise colocalization of CA19.9-expressing tumor cells and ^{64}Cu-NOTA-PEG$_7$-Tz. Reproduced with permission from ref 600. Copyright 2016 SNMMI.

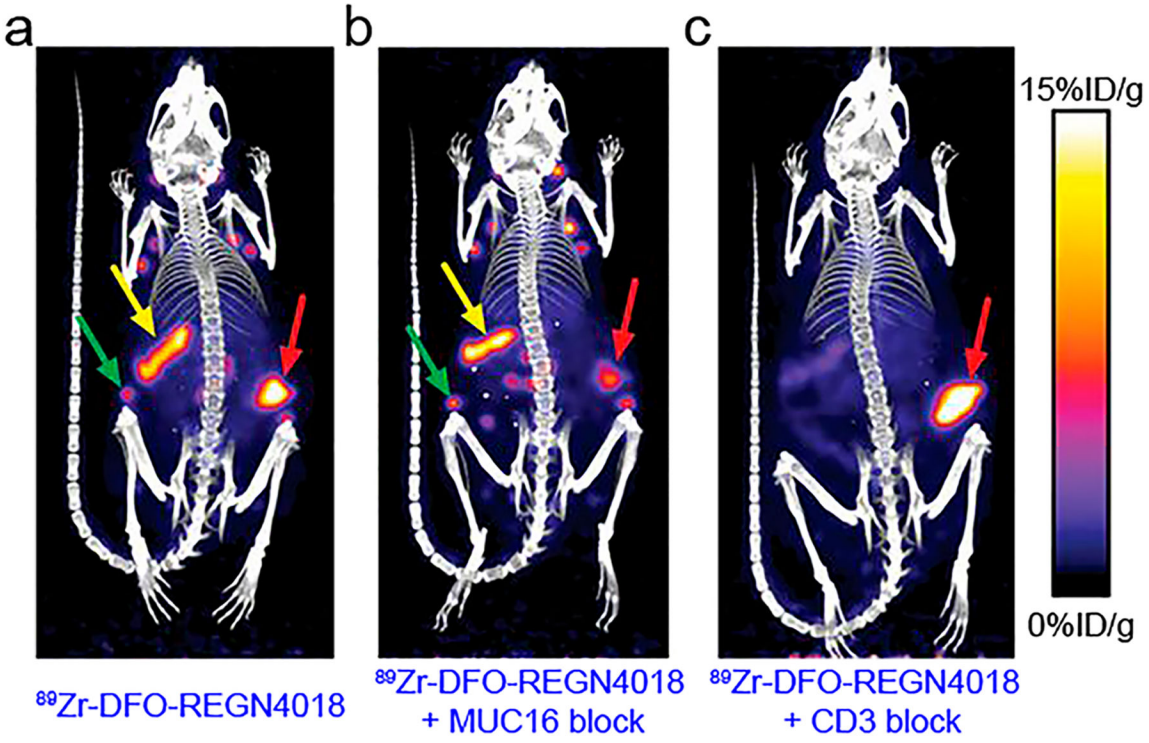

Figure 20.

ImmunoPET imaging of ovarian cancers with a bispecific radiotracer ^{89}Zr-DFO-REGN4018. (a) ^{89}Zr-DFO-REGN4018 immunoPET/CT imaging of humanized tumor-bearing mice showed the distribution of the tracer to the spleen (yellow arrow), lymph nodes (green arrow), and tumor (red arrow). (b) Blocking with a MUC16 parental antibody reduced the tumor uptake of ^{89}Zr-DFO-REGN4018 without influencing the spleen and lymph node uptake. (c) Blocking with an anti-CD3 antibody substantially reduced the spleen and lymph node uptake of ^{89}Zr-DFO-REGN4018 without influencing the tumor uptake. Reproduced with permission from ref 604. Copyright 2019 American Association for the Advancement of Science.

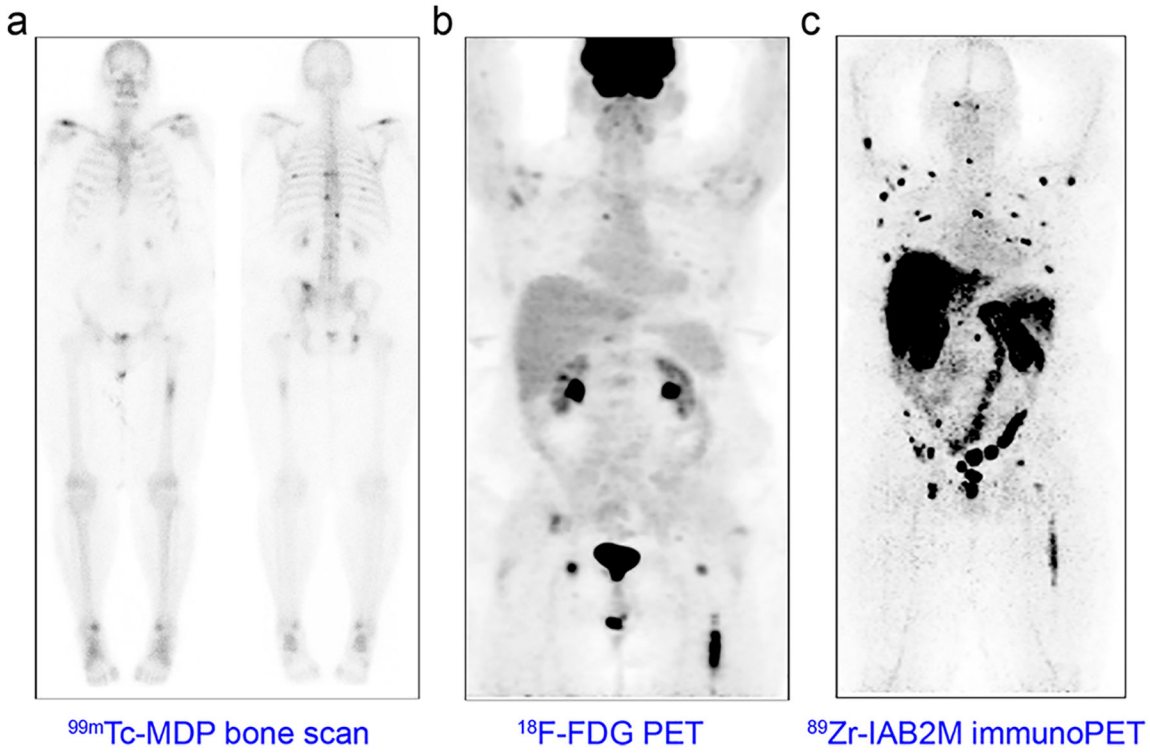

Figure 21.

ImmunoPET imaging of prostate cancers with the minibody-based ^{89}Zr-IAB2M. (a) ^{99m}Tc-MDP bone scan of a PCa patient showed multiple metastatic lesions in ribs, vertebrae, and left femur. (b) An ^{18}F-FDG PET scanning showed the lesion in the left femur but failed to clearly detect the vertebral lesions. (c) ^{89}Zr-IAB2M immunoPET imaging of the same patient detected more lesions than either conventional imaging modalities. Reproduced with permission from ref 633. Copyright 2016 SNMMI.

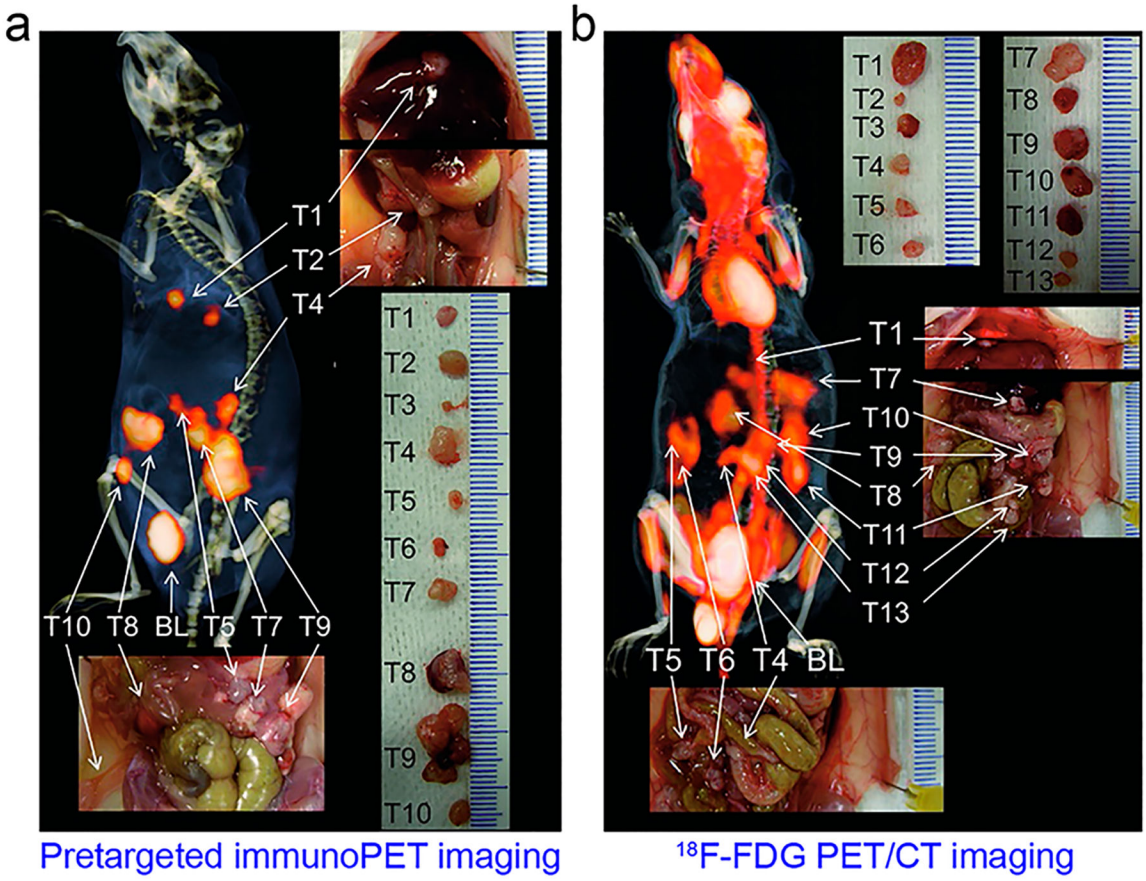

Figure 22.

Pretargeted immunoPET imaging of metastatic colorectal cancers. (a) In this approach, CEA- and HSG-targeting BsAb TF2 was given first to saturate the LS174T tumors, followed by administration of DOTA- and HSG-containing 68Ga-IMP288 16 h later. This imaging approach clearly delineated tumors, except for two small tumor lesions (T3 and T6). Bladder (BL) uptake indicates excellent excretion of the ^{68}Ga-IMP288 through the urinary system. (b) ^{18}FFDG PET/CT imaging of the same mouse showed less optimal image contrast due to uptake in the intestines. Reproduced with permission from ref 651. Copyright 2012 Springer Nature.

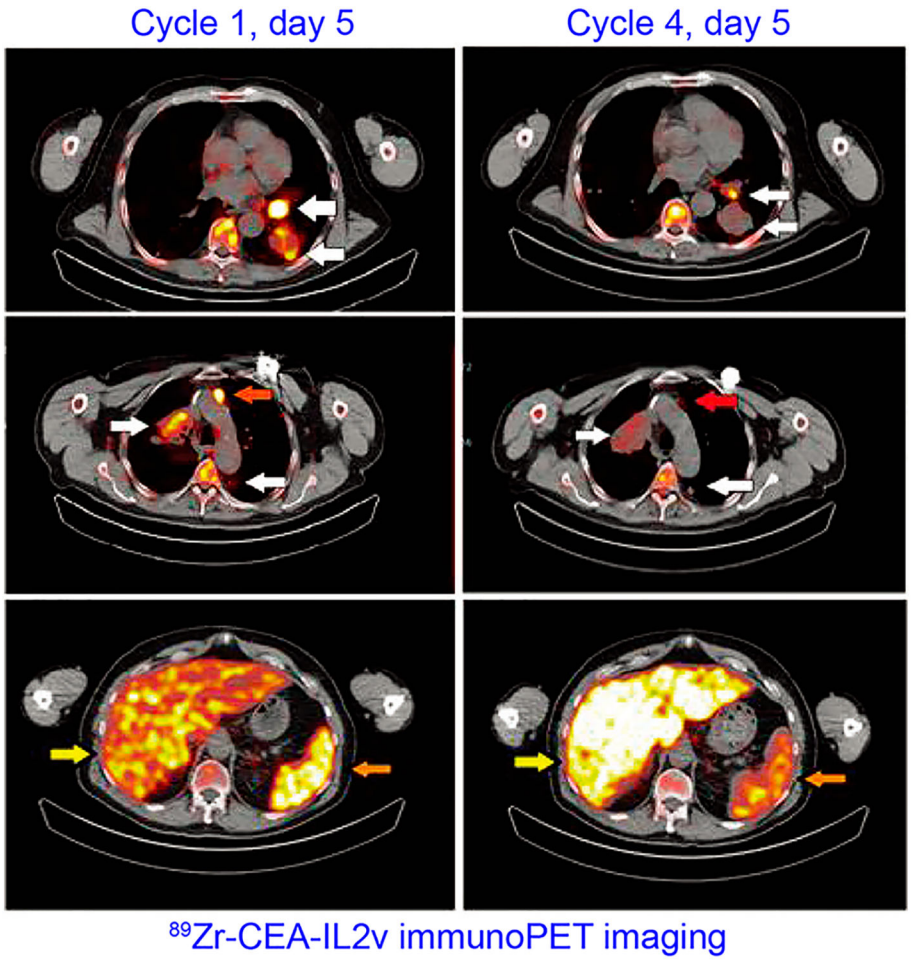

Figure 23.

ImmunoPET imaging of solid tumors using ^{89}Zr-CEAIL2v. ^{89}Zr-CEA-IL2v immunoPET imaging of a patient with CEA^{+} colorectal cancer at cycle 1, day 5 (left) showed uptake of the radiotracer in the bilateral hilar lymph nodes and the left dorsal lung metastasis (white arrows). The uptake in these malignant lesions and a nonpathological lymph node (red arrows) decreased after the fourth cycle of CEA-IL2v treatment (right). Notably, uptake in the liver (yellow arrows) increased and uptake in the spleens (orange arrows) decreased following the treatments. Reproduced with permission from ref 666. Copyright 2018 Impact Journals, LLC.

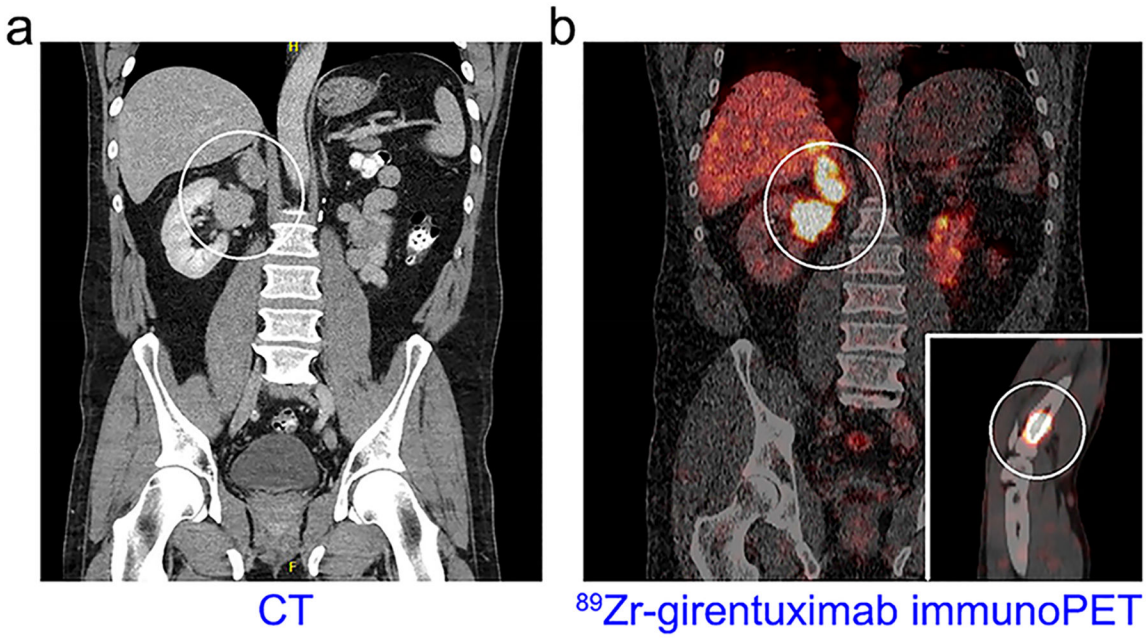

Figure 24.

ImmunoPET imaging of clear cell renal cell carcinoma (ccRCC) with ^{89}Zr-girentuximab. (a) A patient with ccRCC who previously had undergone nephrectomy was subjected to a CT scan that showed neoplasms in the right kidney and the adjacent adrenal (white circle). (b) ^{89}Zr-girentuximab immunoPET/CT imaging of the same patient showed that both the lesions had an uptake of the tracer. Additional uptake in the proximal radius was seen (insert), which changed the management strategy of the patient from a futile radical nephrectomy to radiotherapy. Reproduced with permission from ref 674. Copyright 2018 European Association of Urology.

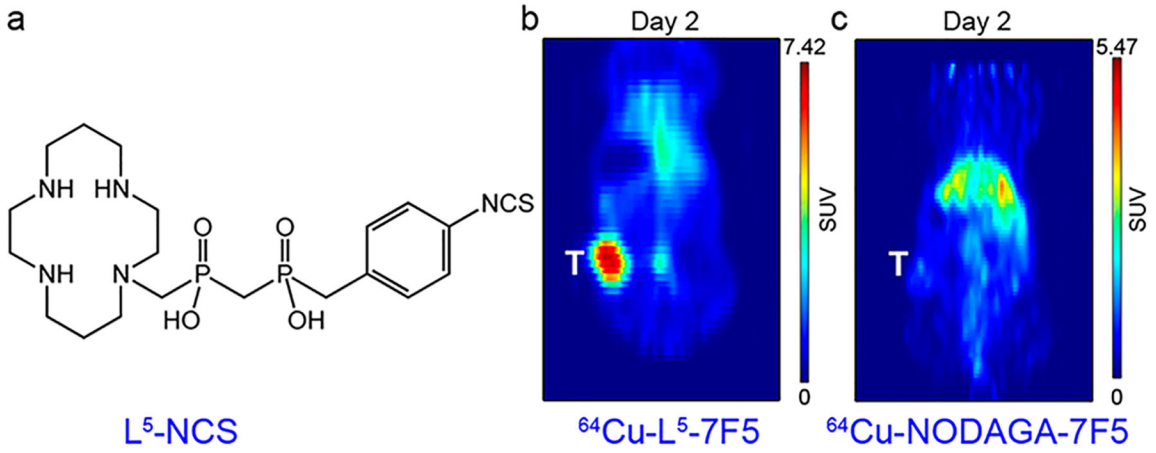

Figure 25.

ImmunoPET imaging of cancer stem cell markers. (a) Chemical structure of a novel chelator L^5-NCS. (b) ^{64}Cu-L^5-7F5 immunoPET imaging clearly detected PSCA-expressing PC3 tumor 2 days after injection of the tracer. (c) In comparison, ^{64}Cu-NODAGA-7F5 showed much lower tumor uptake and higher liver uptake. Reproduced with permission from ref 158. Copyright 2018 American Chemical Society.

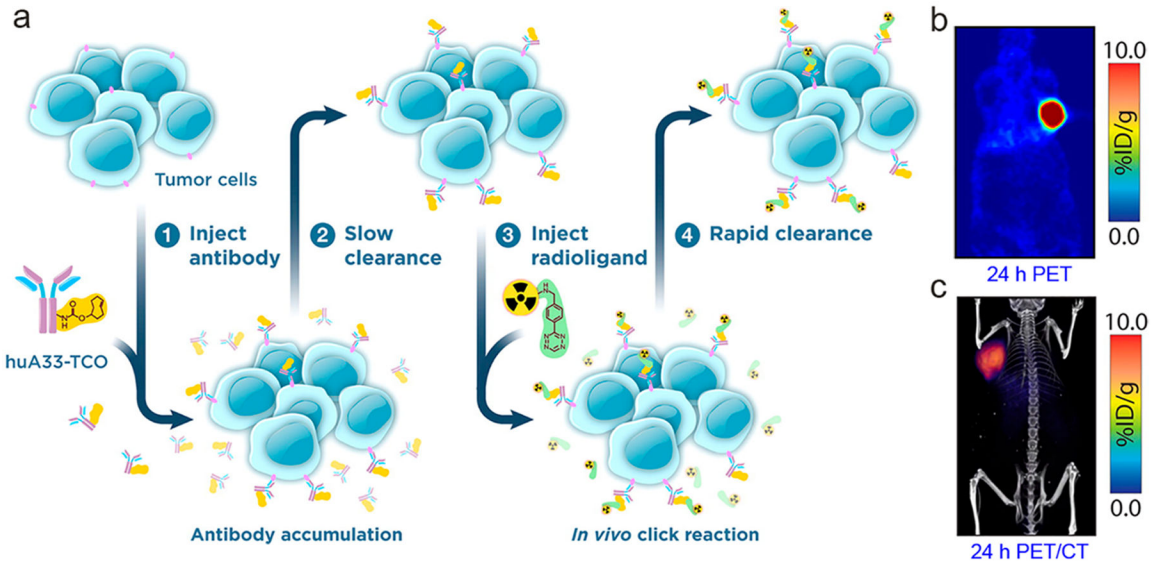

Figure 26.

Pretargeted immunoPET imaging of colorectal cancers. (a) Schematic of the imaging strategy, in which huA33-TCO was first administered to accumulate in the tumor followed by injection of ^{64}Cu-Tz-SarAr 24 h later. (b) Coronal image and (c) fused PET/CT images 24 h postinjection of the radioligand showed the effective delineation of the subcutaneous SW1222 xenografts. Reproduced with permission from ref 339. Copyright 2015 American Chemical Society.

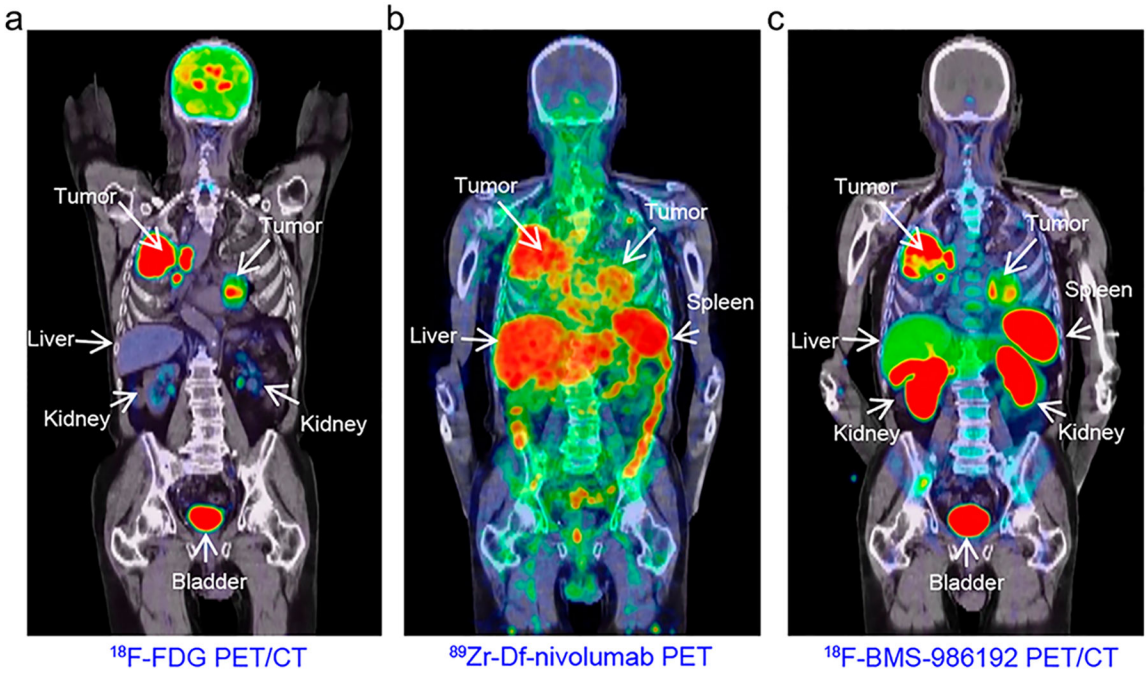

Figure 27.

ImmunoPET imaging of immune checkpoints in nonsmall-cell lung cancer (NSCLC). (a) ^{18}F-FDG PET/CT scan of a patient with NSCLC showed lung tumors and mediastinal lymph node metastases with high glucose metabolism. (b) PD-1-specific ^{89}Zr-Dfnivolumab immunoPET/CT imaging demonstrated heterogeneous uptake of the radiotracer within and between the tumor lesions. (c) Similarly, heterogeneous uptake of PD-L1-specific ^{18}F-BMS-986192, a ^{18}F-labeled adnectin protein, was seen within and between the tumor lesions. Reproduced with permission from ref 809. Copyright 2018 Springer Nature.

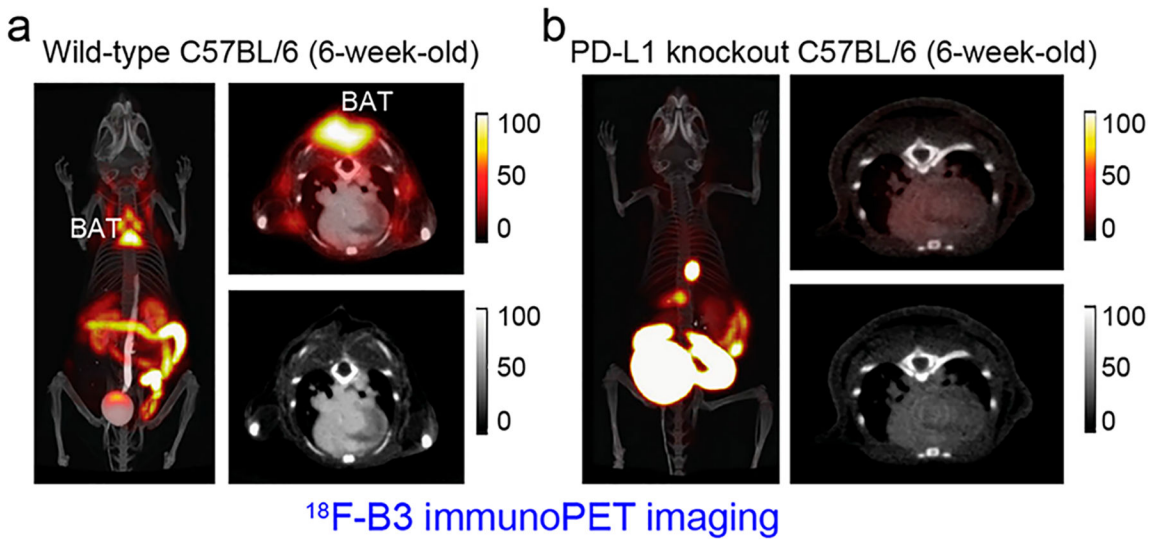

Figure 28.

ImmunoPET imaging of programmed death-ligand 1 (PDL1) in brown adipose tissue (BAT). B3 is a single domain antibody specific for mouse PD-L1 and (a) ^{18}F-B3 immunoPET/CT imaging of a 6-week-old wild-type C57BL/6 mouse showed deposition of the radiotracer in the BAT. (b) ^{18}F-B3 immunoPET/CT imaging of an age-matched PD-L1 knockout mouse showed the absence of PD-L1 signal in the BAT, confirming the specificity of the developed radiotracer. Reproduced with permission from ref 830. Copyright 2017 Springer Nature.

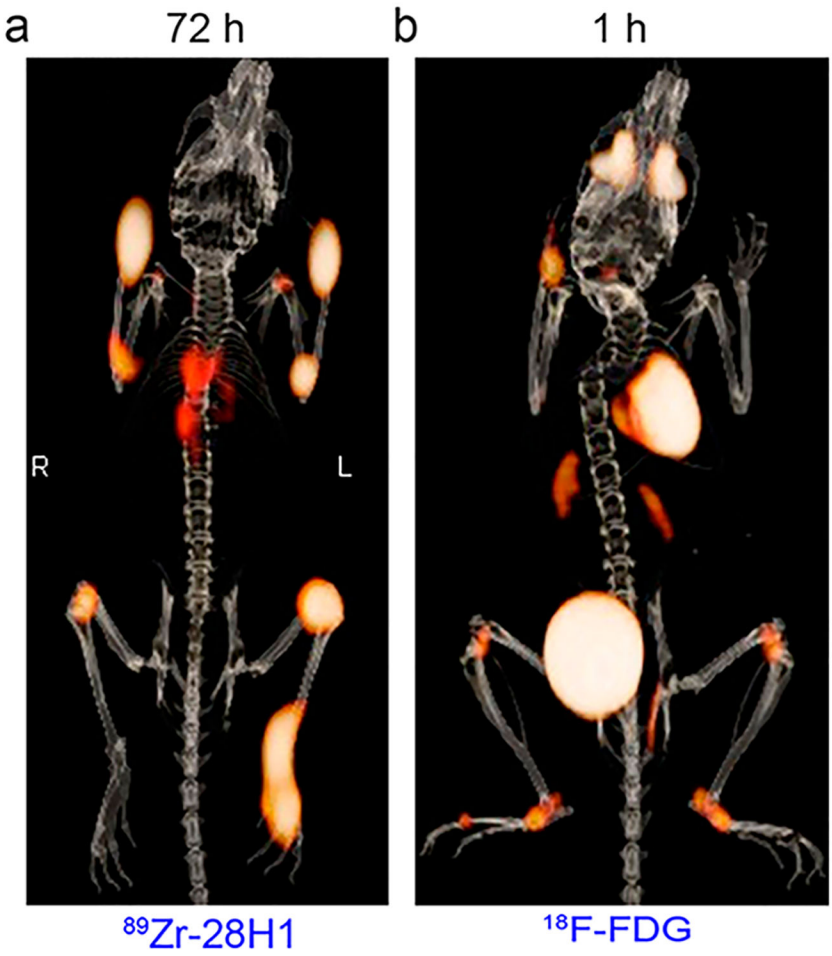

Figure 29.

ImmunoPET imaging of rheumatoid arthritis (RA). (a) ^{89}Zr-28H1 immunoPET/CT imaging of a mouse with collagen-II-induced arthritis 72 h after injection of the radiotracer. ^{89}Zr-28H1 accumulated in the inflamed joints with high contrast. (b) ^{18}F-FDG PET/CT imaging also showed uptake in the inflamed joints but the uptake was lower than that of ^{89}Zr-28H1. Reproduced with permission from ref 849. Copyright 2015 SNMMI.

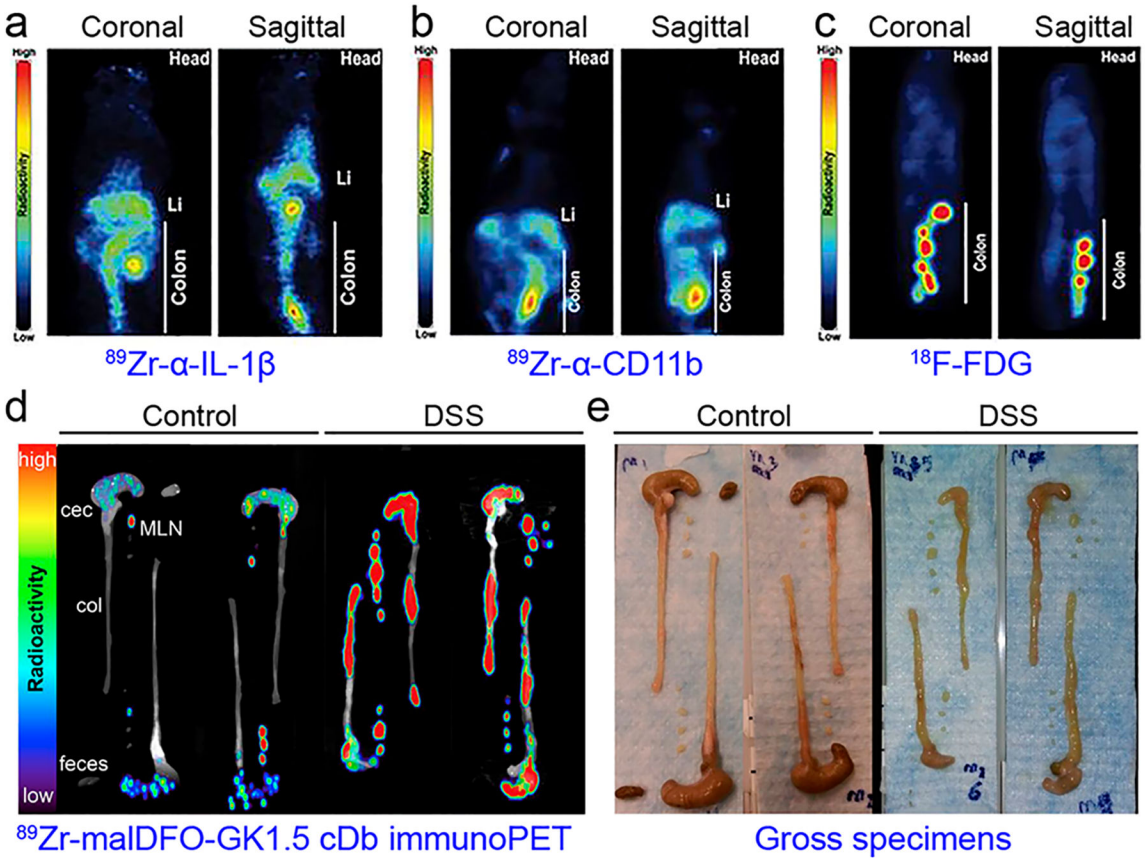

Figure 30.

ImmunoPET imaging of inflammatory bowel disease (IBD). (a) ^{89}Zr-a-IL-1b, (b) ^{89}Zr-α-CD11b immunoPET imaging, and (c) conventional ^{18}F-FDG PET imaging all detected dextran sulfate sodium (DSS)-induced colonic inflammations, which was indicated by uptake in the colons. Reproduced with permission from ref 857. Copyright 2019 SNMMI. (d) ^{89}Zr-malDFO-GK1.5 cDb, an immunoPET probe targeting mouse CD4, was used to image IBD by capturing CD4^{+} T cells. Ex vivo 89Zr-malDFO-GK1.5 cDb immunoPET imaging showed increased radiotracer concentration in the DSS-treated colons, ceca, and mesenteric lymph nodes (MLNs).(e) Corresponding gross specimens obtained from the normal mice and from the colitic mice. Note that colons of the DSS-treated mice were shorter than that of the control mice. Reproduced with permission from ref 858. Copyright 2018 SNMMI.

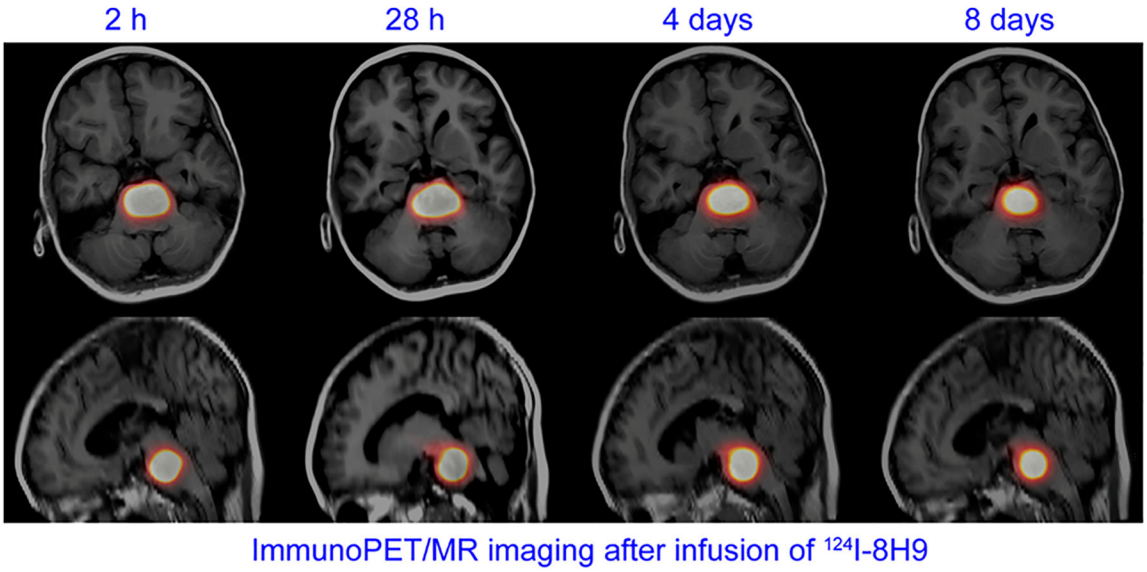

Figure 31.

Representative immunoPET/MR imaging of a patient with diffuse intrinsic pontine glioma after convection-enhanced delivery of ^{124}I-8H9. The axial (upper sections) and sagittal (lower sections) fused PET/MR images showed predominant retention of ^{124}I-8H9 in the brainstem. In this case, ^{124}I-8H9 servers as a theranostic agent allowing for concurrent imaging, dosimetry, and therapy. Reproduced with permission from ref 896. Copyright 2018 Elsevier Inc.

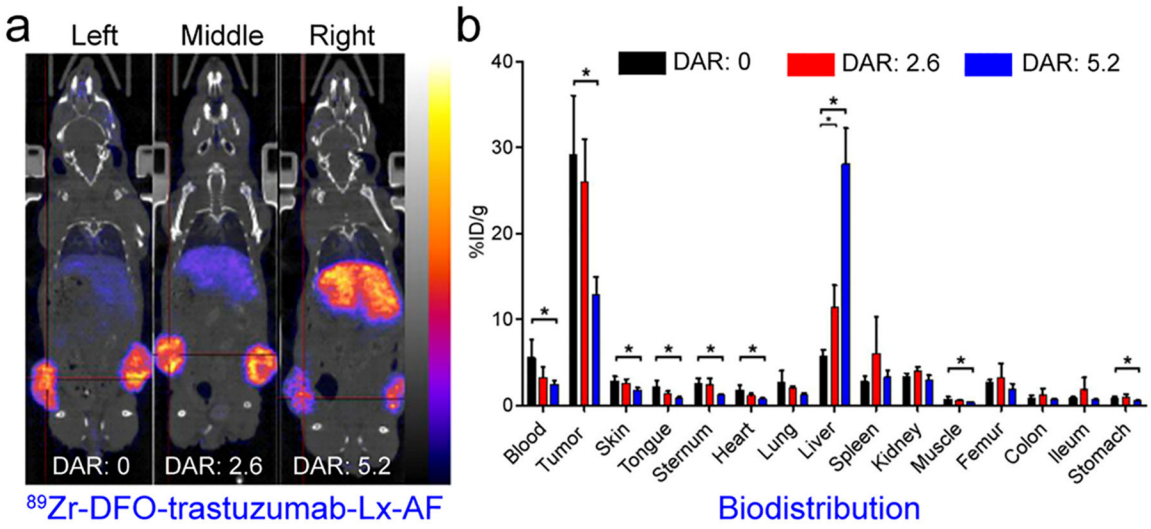

Figure 32.

ImmunoPET imaging guides antibody drug development. (a) Trastuzumab-*Lx*-AF is an antibody–drug conjugate developed by linking trastuzumab with auristatin F (AF) via the linker *Lx*. To evaluate the influence of drug-to-antibody ratios (DARs), ^{89}Zr-DFO-trastuzumab-*Lx*-AF immunoPET/CT imaging was carried out at 96 h postinjection of the radiotracer. The imaging results demonstrated the varying stabilities of the *Lx*-based ADCs. Importantly, a DAR of 2.6 did compromise the tumor targeting. (b) Biodistribution studies further confirmed the immunoPET imaging results (black bars, DAR of 0; red bars, DAR of 2.6; blue bars, DAR of 5.2; *, $P < 0.05$). Reproduced with permission from ref 930. Copyright 2018 SNMMI.

Table 1.

Representative Radionuclides Used in Developing ImmunoPET Imaging Probes[a]

isotope	$T_{1/2}$	emission profiles	production methods	ref
^{89}Zr	78.4 h	β^+: 22.8%, $E_{\beta+max}$ = 901 keV; EC: 77%, E_γ = 909 keV	^{89}Y(d,2n)^{89}Zr, ^{89}Y(p,n)^{89}Zr, ^{nat}Sr(α,xn)^{89}Zr, etc.	111,120
^{64}Cu	12.7 h	β^+: 19%, $E_{\beta+max}$ = 656 keV; EC 41%, E_γ = 1346 keV; β^-: 40%, $E_{\beta-max}$ = 579 keV	^{64}Ni(p,n)^{64}Cu ^{64}Ni(d, 2n)^{64}Cu ^{68}Zn(p,α)^{64}Cu	141
^{124}I	4.18 d	β^+: 22%, $E_{\beta+max}$ = 2.13 MeV	^{124}Te(p,n)^{124}I	180
^{86}Y	14.7 h	β^+: 34%, $E_{\beta+max}$ = 3.153 MeV; EC: 66%, E_γ = 1043 keV	^{86}Sr(p,n)^{86}Y ^{86}Sr(d,2n)^{86}Y	163,164
^{68}Ga	1.1 h	β^+: 89%, $E_{\beta+max}$ = 1899 keV; EC: 11%, E_γ = 1077 keV	^{68}Ge/^{68}Ga generator ^{68}Zn(p,n)^{68}Ga	225,226
^{44}Sc	3.9 h	β^+: 94%, $E_{\beta+max}$ = 1474 keV; EC: 6%, E_γ = 1157 keV	^{44}Ti/^{44}Sc generator ^{nat}Ca(p,n)^{44}Sc ^{44}Ca(p,n)^{44}Sc	981–983
^{18}F	109.8 min	β^+: 97%, $E_{\beta+max}$ = 635 keV	^{18}O(p,n)^{18}F	196
^{52}Mn	5.591 d	β^+: 29.4%, $E_{\beta+max}$ = 575 keV; E_γ = 1434	^{52}Cr(p,n)^{52} Mn ^{nat}Cr(p,x)^{52} Mn	246

[a]Abbreviations: $T_{1/2}$, half-life; EC, electron capture (e.c.). The methods given in this Table are commonly used approaches to produce radionuclides. The readers are recommended to refer to the cited references for production details.

Table 2.

Representative Clinical-Stage ImmunoPET Imaging Probes[a]

probe	target	targeting moiety	cancer types	ref
^{89}Zr-Df-cetuximab	EGFR	mAb	solid tumors	356,358
^{89}Zr-panitumumab	EGFR	mAb	colorectal cancer	368
^{89}Zr-Df-trastuzumab	HER2	mAb	breast cancer, EGA	41,391,399
^{64}Cu-DOTA-trastuzumab	HER2	mAb	breast cancer	394,395
^{89}Zr-Df-pertuzumab	HER2	mAb	breast cancer	396
^{124}I-trastuzumab	HER2	mAb	GC, GEC	400
^{68}Ga-HER2-Nanobody	HER2	Nanobody	breast cancer	412
^{68}Ga-ABY-025	HER2	Affibody	breast cancer	430,433
^{64}Cu-DOTA-patritumab	HER3	mAb	solid tumors	453
^{89}Zr-GSK2849330	HER3	mAb	solid tumors	455
^{89}Zr-lumretuzumab	HER3	mAb	solid tumors	458
^{89}Zr-Df-bevacizumab	VEGF	mAb	solid tumors	469,471,474
^{124}I-huA33	A33	mAb	colorectal cancer	185
^{89}Zr-cmAb U36	CD44v6	mAb	HNSCC	118
^{89}Zr-RG7356	CD44	mAb	solid tumors	523,524
^{89}Zr-rituximab	CD20	mAb	lymphoma	536
^{89}Zr-DFO-5B1	CA19.9	mAb	pancreatic cancer	39
^{89}Zr-huJ591	PSMA	mAb	prostate cancer	619,620
^{89}Zr-Df-IAB2M	PSMA	Mb	prostate cancer	633,634
^{68}Ga-IMP288	CEA	BsAb	medullary thyroid cancer	654
^{89}Zr-AMG 211	CEA/CD3	BiTE	gastrointestinal adenocarcinomas	664
^{89}Zr-CEA-IL2	CEA	immunocytokine	solid tumors	
^{89}Zr-girentuximab	CAIX	mAb	renal cell carcinoma	674
^{124}I-cG250	CAIX	mAb	renal cell carcinoma	675
^{89}Zr-DF0-MSTP2109A	STEAP1	mAb	prostate cancer	748,749
^{89}Zr-fresolimumab	TGF-β	mAb	glioma	754
^{89}Zr-Df-IAB22M2C	CD8	Mb	solid tumors	793

probe	target	targeting moiety	cancer types	ref
^{89}Zr-atezolizumab	PD-L1	mAb	NSCLC, TNBC, bladder cancer	21
^{18}F-BMS-986192	PD-L1	adnectin	lung cancer	809
^{89}Zr-nivolumab	PD1	mAb	lung cancer	809
[^{124}I]I-F8-IL10	fibronectin	Fv fragment	rheumatoid arthritis	843

[a]Abbreviations: mAb, monoclonal antibody; EGA, esophagogastric adenocarcinoma; GC, gastric cancer; GEC, gastroesophageal junction cancer; HNSCC, squamous cell carcinoma of the head and neck; Mb, minibody; Fv fragment, single-chain antibody variable domain (Fv) fragment; BsAb, bispecific antibody; BiTE, bispecific T-cell engager; PSMA, prostate-specific membrane antigen; CEA, carcinoembryonic antigen; CAIX, carbonic anhydrase IX; STEAP1, six-transmembrane epithelial antigen of prostate-1; TGF-*β*, transforming growth factor-*β*; NSCLC, nonsmall cell lung cancer; TNBC, triple-negative breast cancer; PD-L1, programmed death ligand-1; PD1, programmed death receptor 1.